The study on short elastin-like peptides: sequence, condition of solution, and structures influenced self-assembly of the peptide

田坪, 大来

The study on short elastin-like peptides: sequence, condition of solution, and structures influenced self-assembly of the peptide

田 坪 大 来

The study on short elastin-like peptides: sequence, condition of solution, and structures influenced self-assembly of the peptide

Daiki Tatsubo

Laboratory of Biomolecular Chemistry
Department of Chemistry
Graduate School of Science
Kyushu University

March 2019

CONTENTS

ABBREVIATIONS

The abbreviations according to biochemical nomenclature by IUPAC-IUB Joint Commission, *Eur. J. Biochem*., **138**, 9-37 (1984), are used throughout. Unless otherwise specified, the amino acids are L-stereoisomers. Additional abbreviations are follows, but generally accepted abbreviations and symbols were used without definition.

1,8-ANS	8-anilino-1-naphthalenesulfonic acid
(CW3)2	$(H\text{-}C(WPGVG)_3\text{-}NH_2)_2$
AA	All atom
Boc	*tert*-butyloxycarbonyl
C(Cys)W6	$H\text{-}Cys(H\text{-}Cys\text{-}NH_2)(WPGVG)_6\text{-}NH_2$
CD	Circular dichloism
CG	Coarse grained
CHARMm	Chemistry at harvard macromolecular mechanics
CLP	Collagen-like peptide
DLS	Dynamic light scattering
DMF	Dimethylformamide
DMSO	Dimethyl sulfoxide
DSC	Differential scanning calorimetry
ECM	Extracellular Matrix
EDT	1,2-ethanedithiol
ELPs	Elastin like peptide
ESI	Electrospray ionization
Fmoc	9-fluorenylmethyloxycarbonyl chloride
Fn	$(FPGVG)_n$
GBSW	Generalized born with simple switching
GROMACS	Groningen machine for chemical simulations
HBTU	2-(1*H*-benzotriazole-1-yl)-1,1,3,3tetramethyluronium hexafluorophosphate
HOBt	1-hydroxybenzotriazole
HPLC	High performance liquid chromatography
IDPs	Intrinsic disordered proteins
LCST	Lower critical solution temperature
MALDI	Matrix Assisted Laser Desorption/Ionization

MD	Molecular dynamics
MS	Mass spectrometry
ODS	Octadecylsilyl
pNIPAM	Poly(*N*-isopropylacrylamide)
R_g	Radius of gyration
RGM	Repulsive guidance molecule
RMS	Root mean square
RMSD	Root mean square deviation
RMSF	Root mean square fluctuation
RP	Reverse phase
SASA	Solvent-accessible surface area
TFA	Trifluoroacetic acid
TIS	Triisopropylsilane
TOF	Time of flight
T_t	Phase transition temperature
UPLC	Ultra performance liquid chromatography
UV	Ultraviolet
Wn	$(WPGVG)_n$

CHAPTER 1

Elastin and elastin-like peptides, an introduction of the study on self-assembling property of ELPs

Abstract

Elastin imparts the resiliency and robustness of the connective tissue in the body. Its distribution determines the characteristics of the tissue. It plays essential roles in enlarging and sophisticating the architectures of connective tissues in vertebrates, such as arteries, tendons, and lungs. In other words, vertebrates have evolved with the distribution and differentiation of elastin. Elastin is known to exhibit temperature-dependent reversible self-assembling property during its maturation process. Its unique properties that self-assembly occurs at high temperatures and re-dissociation does at low temperature are expected to be applied as biomaterials. Therefore, in addition to the studies on the biological function of elastin itself, the development of functional elastin-like peptides (ELPs), and the studies elucidating the molecular mechanism of the reversible self-assembly nature have been actively conducted in recent years. The application studies gave variety of functional and biocompatible materials such as vehicles of drug delivery system or scaffolds of tissue engineering. However, the peptides available for these applications were often required polypeptides chains longer than 200 amino acid residues, although such long polypeptides could be expensive for bulk application. In the studies on ELP, there have been various arguments to solve particularly the relationship between the structure and function in the self-assembly mechanism. In view of this, this thesis aimed at not only developing short ELPs that are easier to be synthesized and handled, but also exploring into self-assembling mechanism by using the ELPs. As a background of these researches, this chapter reviews the origin, the molecular evolution, and the function of elastin and ELPs. In addition, this section also describes the fundamental understandings of presumed molecular mechanism and stimuli-responsiveness of the self-assembly that was often investigated by using ELPs, and the application of ELPs as biomaterials in recent years.

1. Understandings of elastin and studies on ELPs

Appearance of elastin and its composition

Elastin is not found in invertebrates but exists in all vertebrates except for cyclostomata which is most primitive one [1-3]. Instead of the elastin, there is a protein called lamprin in cartilage tissues of lamprey eel which belongs to cyclostomata. The lamprin has high homology with elastin. It was suggested that molecular evolution from lamprin into elastin was happened along with the evolution between cyclostomata and gnathostomata [4].

According to a phylogeny, it was also suggested that elastin appeared around the times when the closed circulatory system in animals was formed. It was also analyzed that emergence of elastin was adaptive response to blood pressure [5]. As higher vertebrate, the amino acid composition of elastin become more hydrophobic than that of rumpling and elastic fibers become denser [2, 6]. These changes in composition and morphology might be related to the temperature conditions where the vertebrate grows, because elasticity and self-assembling properties have temperature dependence [7, 8].

Elastin has many repetitions of a unique sequence composed of several amino acids. Due to the large number of the repetitions and low diversity of the amino acid composition, it was considered difficult to analyze the relationship between evolution of the amino acid sequences and function of elastins observed among species. He *et al*. reported the paper comparing the elastin sequences of mammals, chicken, xenopus, zebrafish, describing the dipeptide sequence of PG is commonly found in all species, although repetitive motifs in hydrophobic domains have some differences among species. They also found that GXV tripeptide sequence was frequently adjacent to PGX. It was mentioned that this order of the sequences would serve as a backbone of elastic function of elastin [9]. They also analyzed that the exons of the elastin gene shared several sites among species and unique sites to the species acquired by gene replication during phylogenesis. The authors emphasized that gene duplication played an important role in molecular evolution of elastin. On the other hand, it was reported that the hydrophobic domain of mammalian elastin was moderately preserved, that is, a mutation rate of amino acid composition of the domains was 1% in 5.8 million years [10]. This was because that most of mutations which did not impair hydrophobicity (single nucleotide polymorphism, recombination between repetitive elements, insertion / deletion) could be tolerated. In addition, Piontkivska *et al*. reported that sequence of the hydrophobic domains was poor conserved [11]. Such a low selective pressure in the hydrophobic domain is thought to drive interspecific diversity of the elastin gene. However, the hydrophilic domain and the junction of hydrophilic / hydrophobic domain in primary structure is highly conserved [10, 11]. The hydrophilic domains were involved in the site of cross-linking on the precursors, called tropoelastin, linking together themselves by formation of desmosine and isodesmosine. Such a sequence specificity of elastin is important to keep the morphogenic function. As a summary of characteristic feature of elastin, compared to hydrophilic regions involved in cross-linking sites, the sequence requirements are low in hydrophobic regions involved in elasticity and self-assembly properties, except for conserved PG sequence.

Functions of elastin, tropoelastin, and ELPs

Elastin imparts elasticity to tissue. This property is derived from hydrophobic repetitive sequences in elastin. Compared with other elastic proteins (e.g. collagen and spider dragline silk), elastin possesses high resilience, large strains, and low stiffness [12]. To explain the mechanism of the elastic property, some structural models have been proposed. Many of them suggested that stretching reduced the entropy of the system and contraction was driven by recovery to maximum entropy [13-15]. It was reported that the relaxed structure of elastin is in dynamic equilibrium of folded structures (β-turns) and elongated ones (PPII or β-strand), and this structural ensemble was considered to provide high entropy in relaxed state of elastin [16]. Other study also reported that the secondary structure of elastin becomes ordered with elongation, and this structural change causes fluctuation of entropy that can drive the resilience of elastin. [17]. On the other hand, in ELP that was artificially synthesized by mimicking repeat sequences in elastin, it was reported that specific secondary structure was not required for the expression of its mechanical properties [18]. It was also claimed by another researchers that the expression of elastic properties requires hydrophobic hydration rather than construction of a specific secondary structure [19]. Although it is plausible that the elastic properties of elastin require fluctuation of entropy [20], its molecular mechanism remains controversial.

A precursor of elastin, tropoelastin that is a main component of elastin fiber, exhibits temperature dependent reversible self-assembly. Although tropoelastin dissolves in water at a temperature of 20°C or lower, the solution shows turbidity at a temperature near body temperature (*ca.* 36°C) that causes two phase separation with progress of the time [21]. This self-assembly is reversible structural alteration depending on the temperature. In some papers the property was considered as lower critical separation temperature (LCST) behavior in physicochemical terms [22, 23]. This assembly of homologous molecules is thought to be an essential process for maturation of elastin *in vivo* [24]. It was thought that the property was provided by the hydrophobic domain of tropoelastin and was driven by hydrophobic effect. Thus, the hydrophobic domain of elastin was prevented from aggregating by hydrophobic hydration of neighboring water clusters at low temperatures [7], however, an increase in temperature destabilizes the water clusters, thereby exposing hydrophobic domains, and inducing hydrophobic effects to construct aggregates [25]. Although this process was disadvantageous for the exothermic van der Waals interactions caused by the association of tropoelastin, collapse of the water clusters greatly increased the entropy of the system at the same time [26, 27]. A differential scanning calorimetry and a van't Hoff plot showed the positive entropy changes associated with the phase transition of ELPs and tropoelastin, respectively [27, 28]. It is certainly that the self-assembly reaction is entropy driven behavior [19, 20].

Similar to the elasticity, it was also reported that structural changes obtained with increasing temperature significantly contributed to the self-assembling properties. It was shown that hydrophobic domains 3, 7, 18, 20, 24, and 30 of tropoelastin acquired β-strands and domain 26 acquired β-structures with increasing temperature [29, 30]. Tropoelastin and ELPs were often reported to change their structures from the disordered conformations to the ordered β-structures including β-strands, β-turn, and β-spiral with increasing temperature. It was suggested that these β-structures in hydrophobic regions played an important role in intermolecular interaction between tropoelastins or ELPs [31, 32]. On the other hand, in a structural comparison among some ELP analogs, the existence of specific β-structures and self-assembling property did not correlate in the coacervate behavior. [18]. Other computational study gave a knowledge about the structural change of the short-length elastin sequence : Self-assembling property was provided by the change in distributions of neighboring waters around elastin rather than the specific structural change of elastin itself [22, 23]. Additionally, it was also said that the folding property of elastin would depend on the chain length [23]. There are many reports on the relationship between self-assembly and structures of elastin and ELP, but the details still remain unclear [33].

Features of elastin-like peptides

As a characteristic feature, ELPs possess repetitive sequences derived from tropoelastin. ELPs containing the repetitive sequences could also maintain elastic properties or self-assembly properties similar to tropoelastin. Therefore, elucidation of the molecular mechanism of their agglutinative properties was often performed by using ELPs as model compounds. In addition to the investigation of entropy driven processes [7, 15, 18, 19, 22, 23, 25-27], studies of ELPs revealed that the reversible self-assembling property was affected by molecular weight [22, 23, 34], amino acid sequence [34-38], and concentration of ELP [39] of ELP. Pressure [40, 41], salt [40, 42], and pH [43] conditions were also important for the self-assembly. These characteristics of ELP and assay conditions have been effective approaches to study the self-assembling property. ELPs are also expected to be applied as biomaterials due to their reversible self-assembling property, biodegradability, and biocompatibility. For example, ELPs were used as a backbone or temperature sensitive domains of novel biopolymers [44, 45]. Some researches demonstrated that ELPs could construct higher order structures such as gels [46, 47], membranes [48, 49], liquid crystals [50], and fibers [51] by molecular designs of ELPs and precise controls of assembling conditions. Temperature-dependent self-assembly have also been applied as depots to the localization or the retention of drugs [52-54]. Furthermore, ELPs were applied as base-materials of drug delivery system targeting cancer tissues by conjugating with a cancer cell specific ligand [55, 56] or by pH change [57-59] as stimulus that induced self-assembly

instead of temperature. Such promising properties of ELPs would prompt to explore into novel physical properties of ELPs and its industrial and pharmaceutical applications. Moreover, insights into their self-assembling mechanism would be helpful for rational design of novel ELPs with the reversible-temperature dependent coacervation character. Focusing on these points of contention, this study developed novel ELPs with unique characteristics, and gave some insights into self-assembling mechanism.

2. Stimulus responsiveness of ELPs and molecular design controlling the self-assembly

Some macromolecules such as nucleic acids, proteins, and saccharides that are present *in vivo*, have specific responsiveness to external stimulation. Such responsiveness is corresponded to structural changes of the macromolecules because of the alteration of intra/inter molecular noncovalent bonds resulting from temperature changes or the formation of typical conformation that required for signal transduction system. In recent years, studies to apply such stimulus responsiveness to artificial macromolecules which are called smart polymers has been on the rise in medical and bioengineering fields [60]. Among them, researches on ELPs seems to be attractive due to the points that (1) they can show reversible self-assembly in a thermostimulatory manner and (2) the self-assembly can be induced and controlled rigorously with other stimulants such as salt, pH, pressure, and light [61]. This thesis intends for developing novel ELPs to elucidate their self-assembling mechanism. Therefore, this section focused on how the stimulus responsiveness of self-assembling property was obtained. In addition, various methodologies to control the self-assembly of ELPs were introduced.

Control of the self-assembling property by sequence design

As mentioned above, ELPs have typical repetitive sequences such as $(VPGXG)_n$ or $(XPGVG)_n$ (X is a guest residue excluding proline) derived from hydrophobic domain of tropoelastin and exhibit self-assembling property due to entropy-driven hydrophobic effect accompanying temperature rise. The self-assembling ability was often discussed by its inverse phase transition temperature, T_t. The self-assembling property and T_t depends on the sequence length, molecular weight, molecular hydrophobicity, and concentration of ELP. In many cases, the self-assembling property was controlled by varying these factors. A previous study investigated the dependence of T_t on the sequence length and the alanine content at guest residues by using $(VPGXG)_n$ (X =A or V). As a result, linear decreases in T_t was shown by the substitution of Ala residues with relatively hydrophobic Val residues, and nonlinear decreases was observed by the elongation of sequence [34]. Using synthetic short ELPs containing X = L, I, and F, it was revealed that self-assembling properties could be obtained even with short chain length by using hydrophobic amino acids [35]. The dependence of the

self-assembling property against amino acid sequence or amino acid content of ELP was also analyzed by measuring T_t of C(VPGXG)$_{10}$ (X = A, V, L, and I). In the study, T_t of C((VPGIG)$_3$(VPGLG)$_2$)$_2$ was lower than that of C(VPGIG)$_{10}$. Thus, the stereochemical structure of side chain on Ile was thought to affect self-assembling property [62]. In regards to this result, it was shown that the local hydration state of the residues, which has an influence on the self-assembling property, was different depending on the bulkiness and hydrophobicity of the side chain. It was suggested that this difference was involved in the change of macroscopic phase transition behavior of the ELP [63]. Recently, a method to control T_t artificially by changing the hydrophobicity via oxidation or alkylation of methionine residues at guest position was devised. It was indicated that chemical modification of the residues could also be a control technique of self-assembling property of ELP [64, 65]. From these investigations, designing of the sequence have been popular approach to obtain favorable self-assembling property of ELPs. It can be said that differences in sequence of ELPs have a strong influence on their self-assembly behavior.

Control of the self-assembling property by multimerization

Methods for controlling self-assembling property of ELPs by molecular structure design have been studied, e.g. dimers conjugated via disulfide bond between cysteine residues [62], dimers that chemically induced dimerization of receptor protein and its ligand [66], trimers conjugated via the fibrin trimer domain (foldon) of T4 phage [67-69], dendrimers in which peptide bonds were branched via lysine residues [70-72], and so far. Although these multimer and branched dendrimers showed relatively lower T_t than monomer due to increase of molecular weight, they tended to show higher T_t than linear one that elongated its sequence to the corresponding molecular weight [67, 71]. This tendency might be derived from an increase of the degree of freedom in the structure due to the relatively flexible binding site for the multimerization. In the study on dendrimers, the influence was well analyzed. By the comparison between dendrimers and corresponding linear peptides, it was revealed that the contribution against T_t change by the branching to form dendrimers was larger than that by simply induced free lysine residues, which were originally used as branching points, on the linear ELP analog [71]. As mentioned above, these multimerization techniques can easily increase the molecular weight of ELPs. Therefore, they would be one of the effective methods to control temperature responsiveness of ELPs.

Dependence of the self-assembling property on peptide concentration and pressure

Among various physical factors affecting the T_t, T_t value of ELPs are influenced by its concentration and pressure. The sequence length and the hydrophobicity of the residues determined the degree of the dependence of T_t on concentration and pressure [39]. In the

coexistence curve of LCST phase transition, the relationship between T_t and peptide concentration appeared as follows: T_t was determined with respect to concentration: critical concentration was determined with respect to temperature. Although dependence on peptide concentration was discussed together with T_t as an indicator of the ability of self-assembling properties, it has been scarcely discussed as a subject to date. The pressure dependence of the phase transition was also analyzed by using $(VPGVG)_{40}$ [40]. It was observed that T_t increased at the pressure between 0.1 and 100 MPa, but T_t decreased at the pressure exceeding 100 MPa. The effect of the pressure was further analyzed, that is, Tamura *et al*. reported that the temperature-pressure phase diagram of ELPs indicating the similarity to that of thermo-responsive polymers such as poly(*N*-isopropylacrylamide), pNIPAM, which also showed LCST behavior [41]. It was suggested that ELP and pNIPAM commonly underwent the self-assembling process accompanying hydrophobic collapse. In summary, self-assembly of ELPs showed pressure dependence. However, the pressure dependence is generally rarely discussed as a main subject similar to the peptide concentration dependence, since it seems difficult to change the pressure in the experiment of self-assembly.

Dependence of the self-assembling property on salt

The temperature responsiveness of elastin and ELPs is known to depend on the concentration of coexisting salt [40, 42]. Using this dependency, the T_t values of several ELPs that did not exhibit self-assembly in pure water were estimated by the extrapolation from the T_t values determined in high salt concentrations [35]. Self-assembly of ELPs are also affected by the type of salt. Increase and decrease of T_t were often reported by associating with salting in and out effects depending on the salt type, respectively [40]. Cho *et al*. reported that the anions exhibited the salting in and out effects on an ELP, $(VPGVG)_{120}$ according to the Hofmeister series [73]. It was further analyzed how the interaction between the anions and peptides differed among anions [74]. It was indicated that kosmotropic anions, Cl^- and SO_4^{2-}, approached only the vicinity of the nitrogen atom of the peptide. However, the more chaotropic anion, SCN^- widely adsorbed electron withdrawing atoms including weakly positively charged hydrocarbon groups. Such absorption was thought to cause salting in effect in a way that prevents hydrophobic collapse. On the other hand, the effect of cations is not clear as compared to anions. In the previous studies, it was reported that their salting in and out effects did not follow the Hofmeister series. It was also reported that these effects of cations varied dependent on salt concentrations [62, 75]. In recent years, it has been shown that cations interact with carbonyl oxygens in the peptide backbone [76]. The difference in interaction between cations and ELP was thought to derive the difference in the self-assembling property depending cation types.

Responsiveness of ELPs to salt in the self-assembly can becontrolled by selection of guest residues on ELPs. Addition of salt binding motif or molecule on ELPs is an exemplary method that can regulate the responsiveness. The effect of carboxyl group on hydrophobic collapse and salt responsiveness was analyzed by using ELPs with aspartic acids as the guest residues [77]. Kherb *et al.* reported that the interaction between monovalent cations and the peptide ($NH_4^+ > Li^+ > Na^+ > NMe_4^+ > K^+ > Rb^+ \geq Cs^+$, K_D = 78 ~ 345 mM) was weaker than that between divalent cations and the peptide ($Zn^{2+} > Ca^{2+} > Ba^{2+} > Sr^{2+} > Mg^{2+}$, K_D = 1 ~ 10 mM) in the basic conditions (pH = 9.76). It was also indicated that very strong chaotropic cations tended to decrease T_t via interaction with the carboxy groups [77]. However, Aladini *et al.* reported different results as mentions above, that is, the substitution of leucine with glutamic acid at the guest residue position of ELP did not change the responsiveness to salt (in neutral conditions at pH = 7.8). In addition, the influence of cation on T_t decreasing followed an order, $Ca^{2+} > K^+ > Na^+ \approx Mg^{2+}$, at 3 M of salt [62]. Even there is difference in the reports regarding the influence of cation on T_t decreasing [62, 77], it seems that the effect of cations on T_t decrease tends to significantly depend on their concentration rather than the cation types. The effect of salts on decreasing T_t in the ELP with glutamic acid was further measured and found the effectiveness as Na_2SO_4 >> NaCl and $(NH_4)_2SO_4$ >> NH_4Cl [62]. It was also shown that the difference in types of anion significantly influenced to the negatively charged ELPs.

The influences of salts on ELPs with basic guest residues were also reported. The effects on T_t decreasing in ELP with lysine guest residue were in the order of $K^+ \approx Na^+ < NH_4^+$ for cations, and Na_2SO_4 >> NaCl and $(NH_4)_2SO_4$ >> NH_4Cl for anions [62]. This study showed that the effects by monovalent cations were in agreement with Hofmeister series of cations and the divalent cations did not induce self-assembly. In addition, SO_4^{2-} was shown to decrease T_t more effectively compared to Cl^-. The influence of distribution and ratio of basic residues on ELPs against the salt responsiveness was also analyzed. Comparison between ELPs which possessed biased and alternate arrangements of lysine and isoleucine residues at the guest residue positions in the repetitive sequences indicated that the distribution of positive charges in the sequence did not influence salt responsiveness in T_t. However, comparison between ELPs with single lysine as a guest residue and different molecular weight indicated that a high ratio of positive charges against molecular weight might improve the sensitivity of T_t to NaCl [78].

In addition to findings mentioned above, methods to control salt sensitivity by addition of functional motifs or molecules that act as salt-specific binding sites have also been developed. In an attempt to addition of the Ca^{2+} binding domain of calmodulin on ELPs, it was found that a phase transition was induced by charge neutralization via Ca^{2+} binding [79, 80]. Likewise, ELP with Zn^{2+} binding motif was also examined [81]. They are good

examples of the fusion ELPs showing specific binding to ions that induce evident self-assembling properties of the ELPs. Besides the addition of Ca^{2+} and Zn^{2+} binding sites, ELPs were fused with transition metal binding motifs such as the polyhistidine-tag (His tag) with a high affinity for Cd^{2+} [82] and the metalloregulatory protein MerR with a high affinity for Hg^{2+} [83]. They showed specific binding to target ions, respectively, while maintaining self-assembling properties of the based-ELPs. These findings indicated the possibility of utilizing these ELP analogs as scavengers of heavy metals. In summary, many insights have been obtained how ELPs respond to types and concentration of the salt. The responsiveness of self-assembly to salt can be rationally controlled by appropriate introduction of guest residues and additional metal-binding motifs on ELPs.

Dependence of the self-assembling property on pH

T_t values greatly depend on ionized state of ELPs and the pH, because the self-assembly properties are dependent on molecular hydrophobicity [84]. In α-elastin, which is solubilized form of elastin, the T_t value was the lowest at weakly acidic conditions (pH = 5.0 - 5.3), and the T_t value increased as the pH was departed from the acidic condition [85]. On the other hand, tropoelastin tended to have lower T_t as pH became higher [28]. Although these trends did not seem consistent, they commonly possessed the lowest T_t near the isoelectric point of them. It was indicated that ionized state of molecule prevented the self-assembling property. Incidentally, influence of ionized state on T_t was thought to be small compared with the concentration of salt and protein [28]. Lower T_t was also observed in the ELPs containing many basic guest residues at high pH or in the ELPs with many acidic guest residues at low pH [43]. However, there is no influence of pH on T_t in the ELPs when the ELPs do not have charged amino acids [74]. The pH condition is thought to be a factor that can control the self-assembly by affecting only the ionized state of the chargeable amino acid residues. Although consideration on the influence of the pH against the hydrophobic sequence of ELPs is still insufficient, the pH, which is one of the experimental conditions, is very easy to operate artificially. Therefore, some ELPs that contained charged amino acid residues as the guest residues were applied as a sensor of pH using the self-assembling property [86, 87].

3. Review of recent studies on ELPs

As shown in figure 1, the number of studies related to ELPs have been increasing in recent years. In order to compare the overall position and importance of this study with other researches, this section exhaustively outlined recent researches on ELPs including application examples. In Elsevier's abstract and citation database “Scopus”, 175 papers were found as of June 2018 by searching in "elastin like peptide" in region of “Article title,

Abstract, Keywords" with limitation of publication period as "2015 ~ 2018" and document type as "Article" [23, 44-49, 50-59, 62, 64, 65, 70-72, 88-239]. Then, the contents of the 4 papers seemed to be review of ELPs [236-239] and 18 papers were not related to ELPs [218-235]. This section roughly categorized rest 153 articles into four groups, (1) theoretical study, (2) process study, (3) application to functionalized material, and (4) application of ELPs as drug carrier. The number of papers in these four categories is also shown in the figure 1. Recent trends of researches on ELPs, new discoveries and noteworthy application would be helpful to recognize importance of this theme.

(Figure 1)

(1) Theoretical study

Effect of sequence and multimerization

The mechanisms in the self-assembly of ELPs have been studied widely. As shown in section 2 in this chapter, it was mentioned that the sequence length and the hydrophobicity of the residues controlled the self-assembling property and T_t value [23, 62, 64, 65]. With regard to branching ELPs, a multimeric ELP consisting of streptavidin and biotin-ELP have been developed. The stoichiometry in the phase transition behavior were discussed [5]. Other concepts of multimeric ELPs, such as dendrimer, was introduced in the section 2 in this chapter and following chapter 2 [71, 72, 89, 91, 92].

Functions of elastin, ELPs and peptide fragments from elastin degradation, in vivo

As for *in vivo* behavior and physiological activities of elastin, ELPs and other peptides derived from the decomposition of elastin have been reported. Recently, new physiological activities were reported for ELPs. It was shown that ELPs that possessed either hydrophobic residues or positively charged residues as a guest residue induced proliferation of fibroblasts via interaction of ELPs with heparan sulfate proteoglycans on the cell surface [92]. Studies on sequence dependence of elastin behavior *in vivo* have been also reported with keyword of "Elastin like peptide". The β-sheet motif formed by the proline-poor domain 30 of tropoelastin has been shown to contribute to the stiffness and viscoelasticity of crosslinked tropoelastin [93]. In relation to this, it has been shown that some ELPs modeled single nucleotide polymorphisms and splice variants in tropoelastin present different properties in T_t, hydrodynamic radius, and elasticity, after crosslinking [94]. Through these studies, it gradually becomes clear that physical properties of elastin and its degradates are controlled by the primary structure and the domain structure, although elastin is poor in compositional complexity. Physiological activities of decomposition products of elastin have been reported in recent years. Sequence of VGVTAG was identified in the insulin-like growth factor-1-binding protein-1 and VGVAPG, IGVAPG was found in the rice bran, and both induced

elastogenesis. It was shown that these peptides up-regulated elastin mRNA and expression of tropoelastin in human dermal fibroblasts via activation of insulin-like growth factor-1 receptors [95]. On the other hand, degradation of elastin in temporomandibular joint dysfunction was reported to enhance the production of inflammation-inducing peptides [96]. It was also reported that AGVPGLGVG in the domain 26 of elastin had a property as a matrikine and promoted tumor progression factor [97]. These studies suggested that peptide fragments provided by elastin degradation may adversely affect on the human body. Thus, it is necessary to examine the physiological activities of fragments of elastin and ELPs.

The influence of domain sequences and conjugation of additional molecule on ELPs

With regard to block copolymers having an artificial domain structure, the dependence of self-assembly on the domain sequence has been confirmed. A study using 11 different domain sequence variants composed of a hydrophobic pentapeptide (VPGVG) and a hydrophilic pentapeptide (VPGSG), showed that the size and morphology of polypeptide micelles was controlled by the block structure [98]. In addition, there is another report aimed at constructing a general theory on the self-assembly of diblock copolymers composed of hydrophilic and hydrophobic motifs. It was demonstrated that diblock copolymers self-assembled into weak micelles with dense core and nearly unstretched corona [99]. It has also been reported that sequences generated by fusion of other molecules to ELPs influence the self-assembly of ELPs. When ELPs were fused to red fluorescent protein mCherry, it was clarified that the presence or absence of phase transition behavior varied depending on whether the ELP existed at the N-terminus or the C-terminus [100]. In summary, the domain structure occurring in ELP composed of two or more components seemed to have some influences on the self-assembling property.

As a model of phase transition behavior when ELPs were conjugated with different molecules, ELPs conjugated with collagen-like peptide (CLP) have been analyzed by computational method. The behavior of the fusion of CLP and multiple ELPs was reproduced by two molecular dynamics (MD) methods: all atoms (AA) MD and coarse grained (CG) MD [101]. In this report, the thermodynamic indexes showed that local crowding and self-assembly state of ELPs were more advantageous than free and dispersed state of ELPs in the simulation condition. Interestingly, it was experimentally revealed that the fusion of ELP-CLP exhibited a marked decrease in T_t due to formation of CLP triple helix [102]. It was thought that crowding of the ELPs associated with the triple helix formation promoted the self-assembling of the ELPs. In addition, self-assembly of asymmetric telechelic polymers that separated by a random coil polypeptide block connecting the two end groups, silk-like polypeptide and ELP blocks or silk-like polypeptide and CLP, was reported. It was demonstrated that the morphology of the self-assembly was

controlled by the chain length of the random coil connector and the strength of the interaction between the asymmetric peptide parts (silk-like polypeptides and one of the CLP or ELP) [103]. Not only the influence of polypeptide itself on self-assembly, but also the influence of the linker was also considered by computational method. It was also reported that CG constructed to reproduce the melting behavior (dissociation of triple helix) of the CLP conjugate, could satisfactorily reproduce the self-assembly of CLP-ELP [104]. Optimization of the MD platform to reproduce and to predict the behavior of ELP conjugates has been in progress.

Structure of ELPs

There is still room for discussion about the structure of ELPs. The present structural analysis of ELPs has been greatly aided by computational methods, because of the difficulty in experimental observation of the disordered structure obtained by Gly and Pro rich ELP sequence. By using computational methods, it was calculated that no apparent temperature-dependent structural transition was shown in short ELPs, $(VPGVG)_n$ at $n < 10$ [23]. It was indicated that the structure transition of ELPs was controlled by the chain length. On the contrary, a calculation result indicated that a short ELP $(GVGVP)_6$ showed the structural transformation under the condition of 1 M NaCl [105]. The calculation of each study showed different results in structural transition of ELPs. To provide a certain insight in the discussion, a large-scale simulation of 200 μs using 27 molecules of $(GVPGV)_7$ was performed [106]. This calculation showed that ELPs formed a triplet of association by contact of nonpolar residues, while maintaining a constant hydration state. It was also indicated that individual ELP chains formed transient hydrogen bonded turns, but took on a maximally disordered structure which also called solution state. Contrary to these analyses using AA-MD, analyses using CG handling more macro systems have also been carried out. In a CG system developed by adding oppositely charged dummy particles inside protein backbone beads, it was suggested that dipole interaction plays a more important role in the structure transition of $(GV)_4$ from disordered aggregation to fibril-like ordered aggregation [107]. Several studies providing a bridge between computational analysis and experimental results have been advanced recently. A structural analysis method was developed by combining MD simulation and isotope-labeled Amide I vibration spectroscopy which was able to identify individual peptide bond [108]. In this method, both of computational and experimental results showed that V and A residue following GPG in GVGVPVVG peptide were likely to take extended structure. Although structure analysis on ELPs have been significantly supported by development in computational study, it is thought that combination of experimental and computational studies are still needed and are believed to provide more reliable results and discussion on the disordered structure of ELPs.

The influence of surrounding environment on self-assembly

In addition to structure analysis of ELPs, analysis on water surrounding ELPs in solution have also been conducted. In a measurement using differential scanning calorimetry (DSC), there was a correlation between the formation temperature of water clathrate surrounding ELPs and the T_t of the ELPs [109]. In addition to this DSC measurement, ELPs; $(XGGZG)_3$ were analyzed by thermally stimulated currents [110]. As a result, $(VGGVG)_3$ and $(LGGVG)_3$ exhibited the rapid exchange between clathrate water and bulk water in the phase transition. At the same time, $(VGGVG)_3$ and $(LGGVG)_3$ possessed abundant β-sheet and β-turn structures that made molecular motion more rigidly. It was suggested that a simple substitution of one amino acid (V to L) strongly influenced peptide hydration and movement.

It has been discussed that the influence of salt on the self-assembly of ELPs in section 2 of this chapter. In addition to the influence of salt, the effect of osmolytes has been investigated in recent years. It was shown that T_t of ELPs linearly changed with respect to properties of solvent, the dipole / polarizability, and the acidity as the hydrogen bond donor, which depended on the solute [111]. At the same time, salt and osmolytes were shown to have different quantitative relationships with respect to the T_t change. It was mentioned that these results reflected the direct interactions with the main chain which mainly caused by salt, and indirect interaction via a change in the water property which mainly caused by osmolytes. On the other hand, the property of ELP-water interfaces seemed to vary depending on the type of osmolytes [112]. This report also proposed that the influence of osmolytes on the structure of water and ELP varied depending on the presence or absence of surface activity in the osmolyte molecule. Osmolytes have been recently studied as an external factor affecting self-assembling property of ELPs. Since there are few papers that discussed the influence on the self-assembly, it was thought that knowledge in this region seemed to be still insufficient.

Theory based development of biomaterial including ELPs

Regarding the development of functionalized materials, theoretical based researches for structure design were introduced in this section. As an example of such research, there was a study that designed a fusion of ELP and spherical domain of laminin as a bioadhesive molecule, in order to provide a physiologically active ECM scaffold [45]. A lot of cost is expected to carry out experimental analyses on the physical properties of the ECM mimetic protein, but this research intended to avoid the cost by starting the molecular design with MD-based structure construction. As a result, fused proteins showed structural phase transition by physiological temperature. The phase transition behavior was controlled by selection of ELP domains, but it was revealed that no interaction was observed between ELP

and laminin domains. Such a research would give insight into the rational design of ECM mimetic proteins. Such bottom-up structure design via computational supports was also used in a study on network formation of a complex of ELP and a coiled-coil motif [44]. This research succeeded in constructing a stimuli responsive two-dimensional plane network by optimally designing a helix that mediates noncovalent crosslinking, using computationally evaluation of intermolecular coiled-coil interactions. As a highly advanced theoretical molecular design, a dynamic system controlling the non-equilibrium morphological change of superstructure was constructed using the conformational change of ELP that caused by peptide amphiphiles, such as PAK3 (Palmitoyl-$V_3A_3K_3$-NH_2) [113]. Although almost all of the construction of superstructure using ELPs has been done in an equilibrium system, a spatially free structure construction with a time scale was performed in this report. As seen in these studies, the construction of superstructure using ELPs has dramatically advanced by using the theory based method.

(2) Process study

Application as purification tags and improvement of expression methods

When proteins and peptides are used experimentally or industrially, their efficient and economical preparations still remain one of challenging tasks. Here, the self-assembling ELPs have been prepared by the method using purification tags [114-125], which are usually removed after purification. In some papers, ELP tags were used in purification and cleaved after purification [119-123]. In addition, purification tags combining ELP and intein that causes protein splicing have recently been devised. This combining tag can be cleaved without using enzymatic or chemical treatment and easily removed from purified ELPs. The optimization and practical use of the ELP tags have been reported [122, 123, 126]. On the other hand, several studies were performed to evaluate the physiological activity of proteins without removing purification tag of ELP. Interestingly, in these reports, the ELP might behave as a depot, and physiological activity of protein was improved [124, 125]. Methods for efficient expression of proteins including ELP tags have also been developed [126-132]. Hydrophobic ELPs and ELP tags, including leucine and isoleucine and having relatively low T_t, were enabled to expression [129-131]. A methodology for expressing high molecular weight ELPs that has a premise of functionalization by enzyme-mediated posttranslational modification, has also been developed [132]. These studies would imply that expectations are increasing for the applications of ELPs as the purification tags and the support proteins with functionalized modification.

Synthesis of long ELPs in flask

In addition to genetically engineering techniques of ELPs, methods for synthesizing long-length ELPs have been developed. In the study using microwave irradiation, it was shown that high molecular weight (exceeding 7,000 Da) poly(GVGVP) was synthesized via condensation of H-GVGVP-OH on a gram scale in high yield [133]. Moreover, long-length ELPs were also synthesized enzymatically by using papain known as a cysteine protease, which possesses an activity of catalyzing the polymerization reaction of amino acid esters [134]. In this report, poly (VPG-co-VG) was synthesized by condensation of H-VPG-OEt tripeptide and H-VG-OEt dipeptide, and the reaction was proceeded under the mild condition, although the method required the preparation of a large amount of starting materials such as dipeptide, tripeptide, and tetrapeptide by conventional synthetic methods. As shown in these studies, development of an efficient and economical ELP synthesis method has been attempted in recent years..

(3) Application to functionalized material

Outline of functional polymers including ELPs

ELPs have been used in functional polymers having new physical properties. The development in novel ELP polymers is summarized in Table 1. Briefly, since ELPs consist of repetitive peptide sequences, successfully expressed in genetically engineering method and is tolerant to substitution of residues, they were often used as a backbone of polymer [135] and temperature-sensitive functional motif(s) [136-143]. ELPs are also used in various forms, such as relative short peptides [136, 137], polypeptides [138-141], dimer polypeptides [135], branched polypeptides [142], and cyclic peptides [143]. As described above, ELPs have been applied as various functional polymers.

(Table 1)

Superstructure and device built by ELPs

ELPs have often been used as a scaffold of polymers forming superstructure, due to its stiffness, elasticity, and stimuli-responsiveness. Higher order structures such as hydrogels, films, liquid crystals, fibers, and mats were produced by using ELPs. These higher order structures were often highly functionalized by various chemical modifications. It was reported that highly elastic hydrogel was provided by crosslinking ELPs with 4-arm PEG [46]. Additionally, ELPs telechelically crosslinked via cysteine residues at both termini, and they showed excellent elasticity and stiffness in addition to erosion resistance, diffusion, and release of encapsulated particles [47]. On the other hand, a concentrated solution of $(XPAVG)_n$ (n = 50 - 120), a subclass of ELPs, was shown to form an irreversible phase

transition upon heating, and finally became an elastic gel [144]. Interestingly it spontaneously forms hydrogels without using crosslinking agents.

Application of ELPs is not limited to hydrogel only. The GFP-fused supercharged polypeptide, GFP-$(VPGEG)_n$ (n = 9 - 144) formed liquid crystal which was stable in nonaqueous systems, by mixing the ELP and two cationic surfactants in water at an arbitrary ratio [50]. It was known that ELP solution formed a film at a liquid-liquid interface with peptide amphiphiles (PAs) solution. The dynamics in the formation of the self-assembled monolayer film was observed in real time by a newly developed fluid device [48]. The stability of such self-assembled monolayer consisted of ELP-PA was also known to be improved by crosslinking between ELP and amine in PA molecule with crosslinking reagents. Differences in stability of the membrane and in its biocompatibility that were responsible for selection of crosslinking agents have been compared by assessing the metabolic activity and morphology of adipose-derived stem cells cultured on the different membranes [49]. As a result, membranes cross-linked with genipin exhibited better resistance in physiological environments, stability against enzymatic degradation, *in vitro* cytocompatibility compared to the other synthetic cross-linking agents, such as succinimidyl carboxymethyl ester. As a similar example of film-like structure, it was reported that layered superstructure of a protein obtained by conjugation of ELP and spidroin, a constituent protein of spider silk, exhibited cell compatibility in addition to high elasticity [145]. The production method of the ELP and spidroin conjugate using tobacco leaves expression system was also optimized by combination of purification techniques including inverse transition cycling [146]. Furthermore, cast film consisted of conjugate of $(VPAVG)_{200}$ and antimicrobial peptide CM4 exhibited antibacterial activity and cell affinity [147].

Because elastin works as elastic fiber *in vivo*, several studies applied ELPs as functionalized fibers. Some ELPs constructed moniliform nanofibers in a single composition by being controlled its block sequence [51]. In this study, it was also reported that fibers having cell proliferation activity could be prepared by adding an RGD sequence to the ELP which formed moniliform fibers. In addition, RGD-ELP fibers with cell compatibility were obtained by electrospinning and *in situ* crosslinking using click reaction [148]. Likewise, electrospun CM4-$(VPAVG)_{200}$ fiber showed stability in water and higher thermal degradation activation. It was also reported that the highly antimicrobial fiber mats were fabricated using the electrospun CM4-$(VPAVG)_{200}$ fiber [149]. In this way, a lot of superstructures highly functionalized have been constructed by using ELPs. These knowledges would help further advance of ELP applications.

ELP application as matrix and culture medium

ELPs have often been used in application for extra cellular matrix (ECM) mimetics and culture medium of cells and tissues. In recent years, it has been investigated how the cooperation of novel ELP conjugates and physiologically active substances, that is, heparan sulfates, cell-binding epitope (Arg-Gly-Asp-Ser sequence), and cell-stimulating "RGD" peptide motifs [150-152]. In addition, cultivation of induced pluripotent stem cells and induction of tissue differentiation were tested in a system including ELPs [153-157]. Many of these systems were composed of ELPs conjugating RGD motif which showed cell adhesion activity [151-156] and/or collagen domain which is similar to elastin as an ECM protein [156, 157]. In these reports, desired properties would be obtained by addition of various molecule species cooperatively. Additionally, ELPs were also applied as a three-dimensional medium [158] and bioinks in 3D-bioprinting [159]. A lot of applications of ELPs has been developed by devising its molecular design and morphology. Outline of these applications was summarized in Table 2.

(Table 2)

Application of ELP related to inorganic materials

Recently, a series of studies on conjugations of ELPs and a peptide derived from statherin, which is a saliva protein promoting precipitation of calcium phosphate, has been reported [160-163]. These studies showed that biomineralization was promoted by the statherin-ELP conjugates [160] and hydrogel of statherin-ELP crosslinked by Huisgen cyclization [161]. In addition, these studies also developed molecular bilayer of statherin-ELP-chitosan exhibiting biomineralization and antimicrobial activities [162]. As an application of ELPs in firmer material, hydroxyapatite functionalized its surface by ELP-RGD and statherin-ELP-RGD was shown to promote differentiation of osteoblasts and bone regeneration [163]. Additionally, it was also reported that the addition of ELP to calcium phosphate cement that worked as a substitute for bone, influenced the physical properties and biocompatibility of the cement [164]. As shown in these studies, ELPs have been drawing attention even in the field of dentistry.

As other inorganic-organic hybrid materials, conjugate polymers consisting of ELPs and silica-binding peptide, which derived from silaffin and exhibits bonding to silicic acid, have been developed. The conjugate was shown to absorb on the silica surface in the form of micelles, and its kinetics have been studied [165]. Additionally, the conjugate was possible to fabricate a monodisperse hybrid ELP-silica particles due to localized condensation of silica by the silaffin peptide presented on the outside of micelle [166]. This system was also applied as a DDS confirming that the drug could be encapsulated in the silica matrix [167]. This study pointed out that the form of the matrix can be controlled by

copolymerization of silica localized on the surface. The system showed sustained release of drugs depending on pH. Although hybrid applications with inorganic materials are still under development, these studies have shown that conjugation of ELP and inorganic materials could bring preferable properties as applications for functional biomaterials.

Other advanced applications and applications in analytical materials

In this paragraph, the outline of the application method in advanced concepts different from the above mentioned is briefly described. As an interesting report, there is a technique incorporating ELPs into cells and constructing nanostructures inside the cells by enzyme-catalyzed polymerization [168]. Moreover, it was thought that this *in situ* superstructure can be used as a high performance bioimaging agent or a drug depot because of its high accumulation and retention time in living cells. On the other hand, ELPs were often applied as a material related to various analyses. Development of a methodology using ELPs as a linker instead of PEG in a single molecule atomic force microscope [169], development of ionomer-ELP conjugate as a new material in the field of electrode materials [170], and development of ELP-based immunoassay [171, 172] have been reported. Additionally, on-chip degradation assay of drug depot constructed with silk-ELP [173], application of ELP conjugated with cell penetrating peptides, named penetratin and LAEL, as a non-viral vector [174], and creation of 3D model for analysis on pathogenic elastin hydrolyzate [175] have been also developed. As a most complicated example, conjugate of ELPs, organophosphate hydrolase, bovine serum albumin, titanium dioxide nanofibers, and carboxylic acid functionalized multi-walled carbon nanotubes were reported [176]. The conjugate was designed as a biosensor for sensitive and selective monitoring of p-nitrophenyl substituted organophosphate pesticides in aqueous system. As shown in here, various ideas on application of ELPs have been provided by many researchers.

(4) Application of ELPs as a drug carrier

Potential for pharmaceutical application

As described above, the advantage of applying ELPs as a drug carrier is that ELPs can localize or maintain the agent using the temperature-dependent self-assembling property of ELPs. In addition, it is a remarkable advantage that amino acid sequence of ELPs are tolerant to immunity [177]. By taking these advantages as a basic principle, a lot of ELPs with different shapes and efficacies have been developed in the field of pharmaceutical application. Control of morphology, size, and polydispersity are significant factors in order to effectively use ELPs as a carrier of drug transport. In a previous review [236], the shape of ELPs are classified into 4 groups, ELP-hybrid (covalent fusion with other physiologically active molecule), ELP-ELP (Agent-encapsulated aggregation, micelles and nanoparticles,

built by noncovalent interaction of ELPs) and crosslinked ELP-ELP (crosslinked ELP containing drug in its structure). Recent studies of ELPs in pharmaceutical application were outlined below.

Shapes and morphologies of the ELPs in the pharmaceutical application

Among the above three classes, ELP-hybrid, ELP-ELP, and crosslinked ELP-ELP, ELP-ELP did not find in literatures between 2015 and 2018. On the other hand, few example of Crosslinked ELP-ELP has been reported in recent years. They seem to be designed for carriers with characteristics of long-term drug release. There is a method of administering a crosslinked ELP gel as a drug depot by injection [178]. Moreover, it was also reported that the methods for gradual drug release from *in situ* ELP hydrogel formation were developed by using a relatively mild crosslinking agent such as enzyme or hydrogen peroxide [179, 180]. Compared to ELP-ELP and crosslinked ELP-ELP, studies on ELP-hybrid have grown in number of reports. Various kind of physiologically active molecules were conjugated with ELPs. In most of them, it has been expected that the function of ELPs as a drug depot, which prevents diffusion and excretion of physiologically active molecules, and enhances the therapeutic effects [52-54, 181-190]. Besides this, an ELP conjugate was developed to possess inclusion sites for capturing hydrophobic drugs. It carried a physiologically active molecule in a noncovalent manner [191].

Methods for adding cell or tissue specificity to ELPs

There are some methods to impart specificity to adsorption and uptake of ELPs in specific cells and tissues. It was often achieved by conjugating a ligand that can bind to a specific receptor on ELPs [192-195]. This additional specificity was emphasized in applications to deliver drugs to target cancer cells [55, 56, 196-201] by applying the following strategies; adding of cancer cell-specific ligand to ELPs [55, 56], fusing a ligand and a cytotoxic peptide to ELPs [55, 56], fusing ligand and a cytotoxic peptide together to ELPs [56, 197-199], and forming nanoparticles obtained by mixing ELP-ligand with ELP-cytotoxic peptide or ELP-anticancer drug at an arbitrary ratio [200, 201]. In case that the conjugates possessed a linker, it was reported that its specificity was impaired by improper length, hydrophobicity, and charge of the linker [202]. Thus, careful design of the linker is necessary for optimization of the cell specificity. Regarding the design of linker, there are some ELPs targeting a specific acidic environment around cancer cells by adding pH responsiveness functions to the linker. These ELPs were designed to release anticancer drugs by dissociation of the pH responsive linker from the conjugates [57], or to show adhesion to cancer cells due to the pH-triggered conformational change of the ELP linker [58]. More complicated ELP having a combination of cancer-specific ligands and pH-responsive linkers

was also reported [59]. In these applications, some targeting ELPs possessed cell penetrating or fusogenic peptides in the molecule [199, 203]. These peptides promoted the uptake of ELPs into cell, and improved accumulation of ELPs in the stroma [204-206]. As shown in the studies mentioned above, there seems to be almost no restriction on the combination of ELPs and bioactive molecules. Numerous molecular designs have been studied to elicit more effective antitumor activity and will continue in the future.

Pharmaceutical application of ELP in combination with external stimuli

ELPs show pharmacological activity in response to external stimuli. Such characteristic activities of ELPs have also been developed to strengthen the advantages for drug development. The apparent temperature responsiveness of the ELPs was applied for anti-cancer therapies and tissue regeneration therapy via hyperthermia [203, 207, 208]. These self-assembling ELPs show localization to target tissue, where they penetrate into cell and release drug by collapse of their self-assembling motifs. On the other hand, because such hyperthermia directly caused thermal damage to tissues, non-thermal acoustic treatment was also devised. It was reported that liposomes composed of synthetic conjugate of the fatty acid-ELP and surfactant was successfully localized to cancer cells, by nonthermic acoustic treatment that does not generate heat [209]. In addition to the heat responsive ELPs, ELPs which responds light as an external stimulus have also been developed. Thermally reactive ELP dendrimers carrying photothermogenic gold nanoparticles exhibited photocytotoxicity [70, 210]. The gold nano particle-loaded ELP dendrimers that exhibited both photothermal and thermosensitive properties readily associated with cells and induced efficient photocytotoxicity. It was suggested that ELP dendrimers behaved as potent carriers of AuNPs for photothermal therapy. Furthermore, triple-functional ELP nanoparticle consisting of diblock ELP-recombinant llama heavy-chain antibody fragments and diblock ELP- photosensitizer was reported [211]. This system reversibly self-assembled into nanoparticles, specifically bound to cancer cell, and brought cancer cell-specific light-induced killing. As shown in this study, further selectivity was given to the expression of efficacy by efficiently using external stimuli. In these studies, ELP has been often used as an important part for temperature-dependent construction of nanostructure.

Other advanced pharmaceutical applications of elastin

As other interesting applications of ELPs, studies using radiolabeled ELP for brachytherapy have been reported. ^{131}I-labeled ELP was used to liver tumor model rabbits in the form of concentrated solution [212] and to prostate tumor model mice in the form of *in situ* gel [213], respectively. They showed effectiveness as a relatively stable source depot. ELPs were also applied as a carrier for vaccines. A series of study aiming to deliver antigens

to dendritic cells using ELPs have been reported [214-217]. These studies showed that uptake of conjugates of ELP and a peptide vaccine into dendritic cells activated cytotoxic T lymphocytes [214, 215]. It was suggested that the conjugate could be used as a vaccine. In order to further increase the efficiency of this ELP vaccine, a method of conjugating an antigen and an adjuvant was developed to make an immune-tolerant elastin-like polypeptide-based nanoparticle as an effective and unique cytotoxic T lymphocyte vaccine carrier [216]. Moreover, a method loading antigens directory to antigen presentation site was also devised by placing a protease sensitive peptide that produced by dendritic cells, on the antigenic sequence. Subsequently, cleaving the antigen occurred near the dendritic cell [217]. Optimization of peptide vaccine function is being achieved by improvement of molecular design.

4. Conclusion

This chapter outlined and reviewed the origin of elastin, the properties of elastin and ELPs, molecular designs to control the function of ELPs, stimulus responsiveness, and latest studies on ELPs. ELPs possess biocompatibility, biodegradability, immune tolerance, stiffness, elasticity, and stimulus responsive self-assembling properties. These properties are very promising as application seeds. In addition, these properties can be controlled by molecular designs and are not impaired even in fusion with other molecules. Therefore, the ranges of application of ELPs have been expanding. As representative application examples, ELPs have been used as a stimuli responsive site and as a backbone of a polymer or a molecular scaffold of superstructures. On the other hand, these applications were often constructed by using long ELPs provided genetically engineering techniques. They would be more expensive than the application of chemically synthesized peptides and polymers. Thus, this theme was interested in exploring the design of chemically synthesizable short ELPs and investigating their physical properties for future applications.

Theoretical researches on ELPs have also been actively carried out in recent years. The reversible and stimuli responsive self-assembling property are very unique as a characteristic of peptide. Analysis on the influence of the environment surrounding ELPs on the self-assembling property and analysis on flexible and inordered structure of ELPs have been progressed. However, the relationship between its structure and functions, such as self-assembling properties, is still obscure, and there is room for discussion. Therefore, this theme was also interested in elucidating the mechanism of the self-assembling property of short ELPs. Furthermore, this study set a question as to why the ELPs constructed with hydrophobic residues could dissolve in water. This theme investigated these questions using short ELPs that are easier to analyze than long ELPs. The findings from this study would

help the efficient design of ELPs in applications and understanding in physical properties of hydrophobic and structure disordered peptides.

5. References

[1] Vrhovski B., Weiss A. S., Biochemistry of tropoelastin, *Eur. J. Biochem.*, **258**, 1-18 (1998).

[2] Sage H., Gray W. R., Studies on the evolution of elastin-I. Phylogenetic distribution, *Comp. Biochem. Physiol.*, **64B**, 313-327 (1979).

[3] Davison I. G., Wright G. M., DeMont M. E., The structure and physical properties of invertebrate and primitive vertebrate arteries, *J. Exp. Biol*, **198**, 2185-2196 (1995).

[4] Robson P., Wright G. M., Sitarz E., Maiti A., Rawat M., Youson J. H., Keeley F. W., Characterization of lamprin, an unusual matrix protein from lamprey cartilage, *J. Biol. Chem.*, **268**, 1440-1447 (1993).

[5] Sage H., Gray, W. R., Evolution of elastin structure, *Adv. Exp. Med. Biol.*, **79**, 291-309 (1977).

[6] Sage H., Gray W. R., Studies on the evolution of elastin-II. Histology, *Comp. Biochem. Physiol.*, **66B**, 13-22 (1980).

[7] Miao M., Bellingham C. M., Stahl R. J., Sitarz E. E., Lane C. J., Keeley F. W., Sequence and structure determinants for the self-aggregation of recombinant polypeptides modeled after human elastin, *J. Biol. Chem.*, **278**, 48553–48562 (2003).

[8] Sage H., Structure–function relationship in the evolution of elastin, *J. Invest. Dermatol.*, **79**, 146–153, (1982).

[9] He D., Chung M., Chan E., Alleyne T., Ha K. C., Miao M., Stahl R. J., Keeley F. W., Parkinson J., Comparative genomics of elastin: Sequence analysis of a highly repetitive protein. *Matrix Biol.*, **26**, 524-540 (2007).

[10] Boyd, C. C., Christiano, A. M., Pierce, R. A., Stolle, C. A., Deak, S. B., Mammalian tropoelastin: multiple domains of the protein define an evolutionarily divergent amino acid sequence, *Matrix*, **11**, 235-241 (1991).

[11] Piontkivska H., Zhang Y., Green E. D., NISC Comparative Sequencing Program, Elnitski L., Multi-species sequence comparison reveals dynamic evolution of the elastin gene that has involved purifying selection and lineage-specific insertions/deletions. *BMC Genomics*, **5** (2004).

[12] Gosline J., Lillie M., Carrington E., Guerette P., Ortlepp C., Savage K., Elastic proteins: biological roles and mechanical properties, *Philos. Trans. R. Soc. Lond. B. Biol. Sci.*, **357**, 121-132 (2002).

[13] Weis-Fogh T., Andersen S. O., New molecular model for the long-range elasticity of elastin, *Nature*, **227**, 718-721 (1970).

[14] Dorrington K. L., McCrum N. G., Elastin as a rubber, *Biopolymers*, **16**, 1201-1222 (1977).

[15] Gosline J. M., Hydrophobic interaction and a model for the elasticity of elastin, *Biopolymers*, **17**, 677-695 (1978).

[16] Bochicchio B., Pepe A., Tamburro A. M., Investigating by CD the Molecular Mechanism of Elasticity of Elastomeric Proteins, *Chirality*, **20**, 985-994 (2008).

[17] Debelle L., Tamburro A. M., Elastin: molecular description and function, *Int. J. Biochem. Cell Biol.*, **31**, 261-272 (1999).

[18] Chen Y., Guan Z., Bioinspired modular synthesis of elastin-mimic polymers to probe the mechanism of elastin elasticity, *J. Am. Chem. Soc.*, **132**, 4577-4579 (2010).

[19] Rauscher S., Baud S., Miao M., Keeley F. W., Pomès R., Proline and Glycine Control Protein Self-Organization into Elastomeric or Amyloid Fibrils, *Structure*, **14**, 1667-1676 (2006).

[20] Perticaroli S., Ehlers G., Jalarvo N., Katsaras J., Nickels J. D., Elasticity and Inverse Temperature Transition in Elastin, *J. Phy.s Chem. Lett.,* **6**, 4018-4025 (2015).

[21] Urry, D. W., Entropic elastic processes in protein mechanisms I. Elastic structure due to an inverse temperature transition and elasticity due to internal chain dynamics, *J. Protein. Chem.*, **7**, 1-34 (1988)

[22] Li N. K., García Quiroz F., Hall C. K., Chilkoti A., Yingling Y. G., Molecular Description of the LCST Behavior of an Elastin-Like Polypeptide, *Biomacromolecules*, **15**, 3522-3530 (2014).

[23] Zhao B., Li N. K., Yingling Y. G., Hall C. K., LCST Behavior is Manifested in a Single Molecule: Elastin-Like polypeptide $(VPGVG)_n$, *Biomacromolecules*, **17**, 111-118 (2016).

[24] Patel D., Menon R., Taite L. J., Self-assembly of elastin-based peptides into the ECM: the importance of integrins and the elastin binding protein in elastic fiber assembly, *Biomacromolecules*, **12**, 432-440 (2011).

[25] Luan C. H., Parker T. M., Prasad K. U., Urry D. W., Differential scanning calorimetry studies of NaCl effect on the inverse temperature transition of some elastin-based polytetrapeptides, polypentapeptides, and polynonapeptides, *Biopolymers*, **31**, 465-475 (1991).

[26] Urry D. W., The change in Gibbs free energy for hydrophobic association - derivation and evaluation by means of inverse temperature transitions, *Chem. Phys. Lett.*, **399**, 177-183 (2004).

[27] Luan C. H., Harris R. D., Prasad K. U., Urry D. W., Differential scanning calorimetry studies of the inverse temperature transition of the polypentapeptide of elastin and its analogs, *Biopolymers*, **29**, 1699–1706 (1990).

[28] Vrhovski B., Jensen S., Weiss A. S., Coacervation characteristics of recombinant human tropoelastin, *Eur. J. Biochem.*, **250**, 92–98 (1997).

[29] Toonkool P., Regan D. G., Kuchel P. W., Morris M. B., Weiss A. S., Thermodynamic and hydrodynamic properties of human tropoelastin - analytical ultracentrifuge and pulsed field-gradient spin-echo NMR studies, *J. Biol. Chem.*, **276**, 28042–28050 (2001).

[30] Bochicchio B., Ait-Ali A., Tamburro A. M,, Alix A. J. P., Spectroscopic evidence revealing polyproline II structure in hydrophobic, putatively elastomeric sequences encoded by specific exons of human tropoelastin, *Biopolymers*, **73**, 484–493 (2004).

[31] Tamburro A. M., Guantieri V., Gordini D. D., Synthesis and structural studies of a pentapeptide sequence of elastin. Poly (Val-Gly-Gly-Leu-Gly), *J. Biomol. Struct. Dyn.*, **10**, 441–454 (1992).

[32] Rapaka R. S., Urry D. W., Coacervation of sequential polypeptide models of tropoelastin-synthesis of H-(Val-Ala-Pro-Gly)$_n$-Val-Me and H-(Val-Pro-Gly-Gly)$_n$-Val-OMe, *Int. J. Pept. Protein Res.*, **11**, 97–108 (1978).

[33] Cirulis J., Keeley F. W., Kinetics and morphology of self-assembly of an elastin-like polypeptide based on the alternating domain arrangement of human tropoelastin. *Biochemistry*, **49**, 5726-5733 (2010).

[34] McDaniel J. R., Radford D. C., Chilkoti A., A unified model for de novo design of elastin-like polypeptides with tunable inverse transition temperatures, *Biomacromolecules*, **14**, 2866-2872 (2013).

[35] Nuhn H., Klok H. A., Secondary structure formation and LCST behavior of short elastin-like peptides, *Biomacromolecules*, **9**, 2755-2763 (2008).

[36] Maeda I., Taniguchi S., Ebina J., Watanabe N., Hattori T., Nose T., Comparison between coacervation property and secondary structure of synthetic peptides, Ile-containing elastin derived pentapeptide repeats, *Protein Pept. Lett.*, **20**, 905-910 (2013).

[37] Maeda I., Taniguchi S., Watanabe N., Inoue A., Yamasaki Y., Nose T, Design of Phenylalanine-Containing Elastin-Derived Peptides Exhibiting Highly Potent Self-Assembling Capability, *Protein Pept. Lett.*, **22**, 934-939 (2015).

[38] Taniguchi S., Watanabe N., Nose T., Maeda I, Development of short and highly potent self-assembling elastin derived pentapeptide repeats containing aromatic amino acid residues, *J. Pept. Sci.*, **22**, 36-42 (2016).

[39] Meyer D. E., Chilkoti A., Quantification of the effects of chain length and concentration on the thermal behavior of elastin-like polypeptides, *Biomacromolecules*, **5**, 846-851 (2004),

[40] Yamaoka T., Tamura T., Seto Y., Tada T., Kunugi S., Tirrell D. A., Mechanism for the phase transition of a genetically engineered elastin model peptide (VPGIG)$_{40}$ in

aqueous solution, *Biomacromolecules*, **4**, 1680-1685 (2003).

[41] Tamura T., Yamaoka T., Kunugi S., Panitch A., Tirrell D. A., Effects of temperature and pressure on the aggregation properties of an engineered elastin model polypeptide in aqueous solution. *Biomacromolecules*, **1**, 552-555 (2000).

[42] Reguera J., Urry D. W., Parker T. M., McPherson D. T., Rodríguez-Cabello J. C., Effect of NaCl on the exothermic and endothermic components of the inverse temperature transition of a model elastin-like polymer. *Biomacromolecules*, **8**, 354-358. (2007).

[43] Mackay J. A., Callahan D. J., Fitzgerald K. N., Chilkoti A., Quantitative model of the phase behavior of recombinant pH-responsive elastin-like polypeptides, *Biomacromolecules*, **11**, 2873-2879 (2010).

[44] Fazelinia H., Balog E. R. M., Desireddy A., Chakraborty S., Sheehan C. J., Strauss C. E. M., Martinez J. S., Genetically Engineered Elastomeric Polymer Network through Protein Zipper Assembly, *ChemistrySelect*, **2**, 5008-5012 (2017).

[45] Tang J. D., McAnany C. E., Mura C., Lampe K. J., Toward a Designable Extracellular Matrix: Molecular Dynamics Simulations of an Engineered Laminin-Mimetic, Elastin-Like Fusion Protein, *Biomacromolecules*, **17**, 3222-3233 (2016).

[46] Desai M. S., Wang E., Joyner K., Chung T. W., Jin H. E., Lee S. W., Elastin-Based Rubber-Like Hydrogels, *Biomacromolecules*, **17**, 2409-2416 (2016).

[47] Glassman M. J., Avery R. K., Khademhosseini A., Olsen B. D., Toughening of Thermoresponsive Arrested Networks of Elastin-Like Polypeptides to Engineer Cytocompatible Tissue Scaffolds, *Biomacromolecules*, **17**, 415-426 (2016).

[48] Mendoza-Meinhardt A., Botto L., Mata A., A fluidic device for the controlled formation and real-time monitoring of soft membranes self-assembled at liquid interfaces, *Sci. Rep.*, **8** (2018).

[49] Inostroza-Brito K. E., Collin E. C., Majkowska A., Elsharkawy S., Rice A., del Río Hernández A. E., Xiao X., Rodríguez-Cabello J., Mata A., Cross-linking of a biopolymer-peptide co-assembling system, *Acta Biomater.*, **58**, 80-89 (2017).

[50] Liu K., Pesce D., Ma C., Tuchband M., Shuai M., Chen D., Su J., Liu Q., Gerasimov J. Y., Kolbe A., Zajaczkowski W., Pisula W., Müllen K., Clark N. A., Herrmann A., Solvent-free liquid crystals and liquids based on genetically engineered supercharged polypeptides with high elasticity, *Adv. Mater.*, **27**, 2459-65 (2015).

[51] Le D. H. T., Tsutsui Y., Sugawara-Narutaki A., Yukawa H., Baba Y., Ohtsuki C., Double-hydrophobic elastin-like polypeptides with added functional motifs: Self-assembly and cytocompatibility, *J. Biomed. Mater. Res. A.*, **105**, 2475-2484 (2017).

[52] Sreekumar P. G., Li Z., Wang W., Spee C., Hinton D. R., Kannan R., MacKay J. A., Intra-vitreal αB crystallin fused to elastin-like polypeptide provides neuroprotection in a mouse model of age-related macular degeneration, *J. Control. Release*, **10**, 94-104 (2018).

[53] Gilroy C. A., Roberts S., Chilkoti A., Fusion of fibroblast growth factor 21 to a thermally responsive biopolymer forms an injectable depot with sustained anti-diabetic action, *J. Control. Release*, **277**, 154-164 (2018).

[54] Yang S., Wei S., Mao Y., Zheng H., Feng J., Cui J., Xie X., Chen F., Li H., Novel hemostatic biomolecules based on elastin-like polypeptides and the self-assembling peptide RADA-16, *BMC Biotechnol.*, **18** (2018).

[55] Zhang W., Garg S., Eldi P., Zhou F. H. H., Johnson I. R. D., Brooks D. A., Lam F., Rychkov G., Hayball J., Albrecht H., Targeting prostate cancer cells with genetically engineered polypeptide-based micelles displaying gastrin-releasing peptide, *Int. J. Pharm.*, **513**, 270-279 (2016)

[56] Assal Y., Mizuguchi Y., Mie M., Kobatake E., Growth Factor Tethering to Protein Nanoparticles via Coiled-Coil Formation for Targeted Drug Delivery, *Bioconjug. Chem.*, **29**, 1672-1677 (2015).

[57] Zhao P., Xia G., Dong S., Jiang Z. X., Chen M., An iTEP-salinomycin nanoparticle that specifically and effectively inhibits metastases of 4T1 orthotopic breast tumors, *Biomaterials*, 93, 1-9 (2016).

[58] Veneti E., Tu R. S., Auguste D. T., RGD-Targeted Liposome Binding and Uptake on Breast Cancer Cells Is Dependent on Elastin Linker Secondary Structure, *Bioconjug. Chem.*, **27**, 1813-1821 (2016).

[59] Hu J., Xie L., Zhao W., Sun M., Liu X., Gao W., Design of tumor-homing and pH-responsive polypeptide-doxorubicin nanoparticles with enhanced anticancer efficacy and reduced side effects, *Chem. Commun. (Camb).*, **51**, 11405-11408 (2015).

[60] Kumar A., Srivastava A., Galaev I. Y., Mattiasson B., Smart polymers: Physical forms and bioengineering applications, *Prog. Polym. Sci.*, **32**, 1205-1237 (2007).

[61] MacEwan S. R., Chilkoti A., Elastin-like polypeptides: biomedical applications of tunable biopolymers, *Biopolymers*, **94**, 60-77 (2010).

[62] Aladini F., Araman C., Becker C. F., Chemical synthesis and characterization of elastin-like polypeptides (ELPs) with variable guest residues, *J. Pept. Sci.*, **22**, 334-342 (2016).

[63] Kurzbach D., Hassouneh W., McDaniel J. R., Jaumann E. A., Chilkoti A., Hinderberger D., Hydration layer coupling and cooperativity in phase behavior of stimulus responsive peptide polymers, *J. Am. Chem. Soc.*, **135**, 11299-11308 (2013).

[64] Petitdemange R., Garanger E., Bataille L., Dieryck W., Bathany K., Garbay B., Deming T. J., Lecommandoux S., Selective Tuning of Elastin-like Polypeptide Properties via Methionine Oxidation, *Biomacromolecules*, **18**, 544-550 (2017).

[65] Petitdemange R., Garanger E., Bataille L., Bathany K., Garbay B., Deming T. J., Lecommandoux S., Tuning Thermoresponsive Properties of Cationic Elastin-like Polypeptides by Varying Counterions and Side-Chains, *Bioconjug. Chem.*, **28**, 1403-1412 (2017).

[66] Dhandhukia J., Weitzhandler I., Wang W., MacKay J. A., Switchable elastin-like polypeptides that respond to chemical inducers of dimerization, *Biomacromolecules*, **14**, 976-985 (2013).

[67] Ghoorchian A., Cole J. T., Holland N. B., Thermoreversible Micelle Formation Using a Three-Armed Star Elastin-like Polypeptide, *Macromolecules*, **43**, 4340–4345 (2010).

[68] Ghoorchian A., Holland N. B., Molecular architecture influences the thermally induced aggregation behavior of elastin-like polypeptides, *Biomacromolecules*, **12**, 4022-4029 (2011).

[69] Ghoorchian A., Vandemark K., Freeman K., Kambow S., Holland N. B., Streletzky K. A., Size and shape characterization of thermoreversible micelles of three-armed star elastin-like polypeptides, *J. Phys. Chem. B.*, **117**, 8865-8874 (2013).

[70] Fukushima D., Sk U. H., Sakamoto Y., Nakase I., Kojima C., Dual stimuli-sensitive dendrimers: Photothermogenic gold nanoparticle-loaded thermo-responsive elastin-mimetic dendrimers, *Colloids Surf. B. Biointerfaces*, **132**, 155-160 (2015).

[71] Navon Y., Zhou M., Matson J. B., Bitton R., Dendritic Elastin-like Peptides: The Effect of Branching on Thermoresponsiveness, *Biomacromolecules*, **17**, 262-270 (2016).

[72] Zhou M., Shmidov Y., Matson J. B., Bitton R., Multi-scale characterization of thermoresponsive dendritic elastin-like peptides, *Colloids Surf. B.*, **153**, 141-151 (2017).

[73] Cho Y., Zhang Y., Christensen T., Sagle L. B., Chilkoti A., Cremer P. S., Effects of Hofmeister anions on the phase transition temperature of elastin-like polypeptides, *J. Phys. Chem. B*, **112**, 13765-13771 (2008).

[74] Rembert K. B., Paterová J., Heyda J., Hilty C., Jungwirth P., Cremer P. S., Molecular mechanisms of ion-specific effects on proteins, *J. Am. Chem. Soc.*, **134**, 10039-10046 (2012).

[75] Kondo M., Nakashima Y., Kodama H., Okamoto K., Study on coacervation of the repeat pentapeptide model of tropoelastin: effect of cations, *J. Biochem.*, **101**, 89-94 (1987).

[76] Vrbka L., Vondrásek J., Jagoda-Cwiklik B., Vácha R., Jungwirth P., Quantification and rationalization of the higher affinity of sodium over potassium to protein surfaces, *Proc. Natl. Acad. Sci. USA*, **103**, 15440-15444 (2006).

[77] Kherb J., Flores S. C., Cremer P. S., Role of carboxylate side chains in the cation Hofmeister series, *J. Phys. Chem. B*, **116**, 7389-7397 (2012).

[78] Lim D. W., Trabbic-Carlson K., Mackay J. A., Chilkoti A., Improved non-chromatographic purification of a recombinant protein by cationic elastin-like polypeptides, *Biomacromolecules*, **8**, 1417-1424 (2007).

[79] Kim B., Chilkoti A., Allosteric actuation of inverse phase transition of a stimulus-

responsive fusion polypeptide by ligand binding, *J. Am. Chem. Soc.*, **130**, 17867-17873 (2008).

[80] Hassouneh W., Nunalee M. L., Shelton M. C., Chilkoti A., Calcium binding peptide motifs from calmodulin confer divalent ion selectivity to elastin-like polypeptides, *Biomacromolecules*, **14**, 2347-2353 (2013).

[81] Gonzalez M. A., Simon J. R., Ghoorchian A., Scholl Z., Lin S., Rubinstein M., Marszalek P., Chilkoti A., López G. P., Zhao X., Strong, Tough, Stretchable, and Self-Adhesive Hydrogels from Intrinsically Unstructured Proteins, *Adv. Mater.*, **29**, 1604743 (2017).

[82] Prabhukumar G., Matsumoto M., Mulchandani A., Chen W., Cadmium removal from contaminated soil by tunable biopolymers., *Environ Sci Technol.*, **38**, 3148-3152 (2004).

[83] Kostal J., Mulchandani A., Gropp K. E., Chen W., A temperature responsive biopolymer for mercury remediation, *Environ. Sci. Technol.*, **37**, 4457-4462 (2003).

[84] Urry D. W., Physical Chemistry of Biological Free Energy Transduction As Demonstrated by Elastic Protein-Based Polymers, *J. Phys. Chem. B*, **101**, 11007–11028 (1997).

[85] Kaibara K., Sakai K., Okamoto K., Uemura Y., Miyakawa K., Kondo M., Alpha-elastin coacervate as a protein liquid membrane: effect of pH on transmembrane potential responses. *Biopolymers*, **32**, 1173-1180 (1992).

[86] Callahan D. J., Liu W., Li X., Dreher M. R., Hassouneh W., Kim M., Marszalek P., Chilkoti A., Triple stimulus-responsive polypeptide nanoparticles that enhance intratumoral spatial distribution., *Nano Lett.*, **12**, 2165-2170 (2012).

[87] Valiaev A., Abu-Lail N. I., Lim D. W., Chilkoti A., Zauscher S., Microcantilever sensing and actuation with end-grafted stimulus-responsive elastin-like polypeptides, *Langmuir*, **23**, 339-344 (2007).

[88] Dhandhukia J. P., Brill D. A., Kouhi A., Pastuszka M. K., MacKay J. A., Elastin-like polypeptide switches: A design strategy to detect multimeric proteins, *Protein Sci.*, **26**, 1785-1795 (2017).

[89] Kojima C., Biomaterials using linear and dendritic polylysines, *Kobunshi Ronbunshu*, **75**, 137-142 (2018).

[90] Tatsubo D., Suyama K., Miyazaki M., Maeda I., Nose T., Stepwise Mechanism of Temperature-Dependent Coacervation of the Elastin-like Peptide Analogue Dimer, $(C(WPGVG)_3)_2$, *Biochemistry-US*, **57**, 1582-1590 (2018).

[91] Suyama K., Taniguchi S., Tatsubo D., Maeda I., Nose T., Dimerization effects on coacervation property of an elastin-derived synthetic peptide $(FPGVG)_5$, *J. Pept. Sci.*, **22**, 236-243 (2016).

[92] Yuan Y., Koria P., Proliferative activity of elastin-like-peptides depends on charge

and phase transition, *J. Biomed. Mater. Res. A*, **104**, 697-706 (2016).

[93] Muiznieks L. D., Miao M., Sitarz E. E., Keeley F. W., Contribution of domain 30 of tropoelastin to elastic fiber formation and material elasticity, *Biopolymers*, **105**, 267-275 (2016).

[94] Miao M., Reichheld S. E., Muiznieks L. D., Sitarz E. E., Sharpe S., Keeley F. W., Single nucleotide polymorphisms and domain/splice variants modulate assembly and elastomeric properties of human elastin. Implications for tissue specificity and durability of elastic tissue, *Biopolymers*, **107**, 5 (2017).

[95] Qa'aty N., Vincent M., Wang Y., Wang A., Mitts T. F., Hinek A., Synthetic ligands of the elastin receptor induce elastogenesis in human dermal fibroblasts via activation of their IGF-1 receptors, *J. Dermatol. Sci.*, **80**, 175-185 (2015).

[96] Kobayashi K., Jokaji R., Miyazawa-Hira M., Takatsuka S., Tanaka A., Ooi K., Nakamura H., Kawashiri S., Elastin-derived peptides are involved in the processes of human temporomandibular disorder by inducing inflammatory responses in synovial cells, *Mol. Med. Rep.*, **16**, 3147-3154 (2017).

[97] Da Silva J., Lameiras P., Beljebbar A., Berquand A., Villemin M., Ramont L., Dukic S., Nuzillard J. -M., Molinari M., Gautier M., Brassart-Pasco S., Brassart B., Structural characterization and *in vivo* pro-tumor properties of a highly conserved matrikine, *Oncotarget*, **9**, 17839-17857 (2018).

[98] MacEwan S. R., Weitzhandler I., Hoffmann I., Genzer J., Gradzielski M., Chilkoti A., Phase behavior and self-assembly of perfectly sequence-defined and monodisperse multiblock copolypeptides, *Biomacromolecules*, **18**, 599-609 (2017).

[99] Hassouneh W., Zhulina E. B., Chilkoti A., Rubinstein M., Elastin-like polypeptide diblock copolymers self-assemble into weak micelles, *Macromolecules*, **48**, 4183-4195 (2015).

[100] Qin G., Perez P. M., Mills C. E., Olsen B. D., Effect of ELP sequence and fusion protein design on concentrated solution self-assembly, *Biomacromolecules*, **17**, 928-934 (2016).

[101] Condon J. E., Martin T. B., Jayaraman A., Effect of conjugation on phase transitions in thermoresponsive polymers: An atomistic and coarse-grained simulation study, *Soft Matter*, **13**, 2907-2918 (2017).

[102] Luo T., Kiick K. L., Noncovalent modulation of the inverse temperature transition and self-assembly of elastin-b-collagen-like peptide bioconjugates, *J. Am. Chem. Soc.*, **137**, 15362-15365 (2015).

[103] Kumar A., Lowe C. P., Cohen Stuart M. A., Bolhuis P. G., Trigger sequence can influence final morphology in the self-assembly of asymmetric telechelic polymers, *Soft Matter*, **12**, 2095-2107 (2016).

[104] Condon J. E., Jayaraman A., Development of a coarse-grained model of collagen-like peptide (CLP) for studies of CLP triple helix melting, *J. Phys. Chem. B*, **122**, 1929-1939 (2018).

[105] Tarakanova A., Huang W., Weiss A. S., Kaplan D. L., Buehler M. J., Computational smart polymer design based on elastin protein mutability, *Biomaterials*, **127**, 49-60 (2017).

[106] Rauscher S., Pomès R., The liquid structure of elastin, *eLife*, **6**, e26526 (2017).

[107] Ganesan S. J., Matysiak S., Interplay between the hydrophobic effect and dipole interactions in peptide aggregation at interfaces, *Phys. Chem. Chem. Phys.*, **18**, 2449-2458 (2016).

[108] Reppert M., Roy A. R., Tempkin J. O. B., Dinner A. R., Tokmakoff A., Refining disordered peptide ensembles with computational amide I spectroscopy: Application to elastin-like peptides, *J. Phys. Chem. B*, **120**, 11395-11404 (2016).

[109] Dandurand J., Samouillan V., Lacabanne C., Pepe A., Bochicchio B., Water structure and elastin-like peptide aggregation: A differential calorimetric approach, *J. Therm. Anal. Calorim.*, **120**, 419-426 (2015).

[110] Dandurand J., Samouillan V., Lacabanne C., Pepe A., Bochicchio B., Phase behavior and chain dynamics of elastin-like peptides versus amino acid sequences, *J. Therm. Anal. Calorim.*, **131**, 1323-1332 (2018).

[111] Ferreira L. A., Cole J. T., Reichardt C., Holland N. B., Uversky V. N., Zaslavsky B. Y., Solvent properties of water in aqueous solutions of elastin-like polypeptide, *Int. J. Mol. Sci.*, **16**, 13528-13547 (2015).

[112] Liao Y. -T., Manson A. C., DeLyser M. R., Noid W. G., Cremer P. S., Trimethylamine N-oxide stabilizes proteins via a distinct mechanism compared with betaine and glycine, *P. Natl. Acad. Sci. USA*, **114**, 2479-2484 (2017).

[113] Inostroza-Brito K. E., Collin E., Siton-Mendelson O., Smith K. H., Monge-Marcet A., Ferreira D. S., Rodríguez R. P., Alonso M., Rodríguez-Cabello J. C., Reis R. L., Sagués F., Botto L., Bitton R., Azevedo H. S., Mata A., Co-Assembly, spatiotemporal control and morphogenesis of a hybrid protein-peptide system, *Nat. Chem.*, **7**, 897-904 (2015).

[114] Kim H., Chen W., A non-chromatographic protein purification strategy using Src 3 homology domains as generalized capture domains, *J. Biotechnol.*, **234**, 27-34 (2016).

[115] Xia W., Lu H., Li Y., Cao J., Zhou X., Zhang X., Xia X., Sun H., Purification of chicken IgY by binding capture using elastin-like polypeptide-tagged immunoglobulin-binding domain of streptococcal protein G, *Vet. Immunol. Immunop.*, **192**, 13-19 (2017).

[116] Wang J., Wang Y., Wang X., Zhang D., Wu S., Zhang G., Enhanced thermal stability

of lichenase from Bacillus subtilis 168 by SpyTag/SpyCatcher-mediated spontaneous cyclization, *Biotechnol. Biofuels.*, **9**, 79 (2016).

[117] Swartz A. R., Sun Q., Chen W., ligand-induced cross-linking of Z-elastin-like polypeptide-functionalized E2 protein nanoparticles for enhanced affinity precipitation of antibodies, *Biomacromolecules*, **18**, 1654-1659 (2017).

[118] Chen Q., Sun Q., Molino N. M., Wang S. -W., Boder E. T., Chen W., Sortase A-mediated multi-functionalization of protein nanoparticles, *Chem. Commun.*, **51**, 12107-12110 (2015).

[119] Li Z., Wang P., Jiang C., Cui P., Zhang S., Antibacterial activity and modes of action of phosvitin-derived peptide Pt5e against clinical multi-drug resistance bacteria, *Fish Shellfish Immunol.*, **58**, 370-379 (2016).

[120] Pang Y., Liu J., Qi Y., Li X., Chilkoti A., A modular method for the high-yield synthesis of site-specific protein–polymer therapeutics, *Angew. Chem. Int. Ed. Engl.*, **55**, 10296-10300 (2016).

[121] Rao S., Zang X., Yang Z., Gao L., Yin Y., Fang W., Soluble expression and purification of the recombinant bioactive peptide precursor BPP-1 in *Escherichia coli* using a cELP-SUMO dual fusion system, *Protein Expres. Purif.*, **118**, 113-119 (2016).

[122] Müller H., Salzig D., Czermak P., Considerations for the process development of insect-derived antimicrobial peptide production, *Biotechnol. Progr.*, **31**, 1-11 (2015).

[123] Sousa D. A., Mulder K. C. L., Nobre K. S., Parachin N. S., Franco O. L., Production of a polar fish antimicrobial peptide in *Escherichia coli* using an ELP-intein tag, *J. Biotechnol.*, **234**, 83-89 (2016).

[124] Huang K., Duan N., Zou W., Zhang C., Lai Y., Shen P., Hua Z., Fused hydrophobic elastin-like-peptides (ELP) enhance biological activity of tumor necrosis factor-related apoptosis-inducing ligand (TRAIL), *Protein Peptide Lett.*, **22**, 1000-1006 (2015).

[125] Du K., Sun J., Song X., Song C., Feng W., Enhancement of the solubility and stability of D-amino acid oxidase by fusion to an elastin like polypeptide, *J. Biotechnol.*, **212**, 50-55 (2015).

[126] Shi C., Han T.-C., Wood D. W., Purification of microbially expressed recombinant proteins via a dual ELP split intein system, *Methods Mol Biol.*, **1495**, 13-25 (2017).

[127] Soleyman M. R., Khalili M., Meigoni A. S., Ghasghaii H. M., Zendedel A., Baazm M., Gene cassette design, cloning and expression of recombinant elastin like polypeptide to produce a functional biomaterial in tissue engineering, *Koomesh*, **17**, 2006-2016 (2016).

[128] Azam A., Li C., Metcalf K. J., Tullman-Ercek D., Type III secretion as a generalizable strategy for the production of full-length biopolymer-forming proteins, *Biotechnol.*

Bioeng., **113**, 2313-2320 (2016).

[129] Bahniuk M. S., Alshememry A. K., Unsworth L. D., High-yield recombinant expression and purification of marginally soluble, short elastin-like polypeptides, *Biotechniques*, **61**, 297-304 (2016).

[130] Bataille L., Dieryck W., Hocquellet A., Cabanne C., Bathany K., Lecommandoux S., Garbay B., Garanger E., Recombinant production and purification of short hydrophobic Elastin-like polypeptides with low transition temperatures, *Protein Expres. Purif.*, **121**, 81-87 (2016).

[131] Bataille L., Dieryck W., Hocquellet A., Cabanne C., Bathany K., Lecommandoux S., Garbay B., Garanger E., Expression and purification of short hydrophobic elastin-like polypeptides with maltose-binding protein as a solubility tag, *Protein Expres. Purif.*, **110**, 165-171 (2015).

[132] Ott W., Nicolaus T., Gaub H. E., Nash M. A., Sequence-independent cloning and post-translational modification of repetitive protein polymers through sortase and Sfp-mediated enzymatic ligation, *Biomacromolecules*, **17**, 1330-1338 (2016).

[133] Goto M., Endo T., High-molecular-weight poly(Gly-Val-Gly-Val-Pro) synthesis through microwave irradiation, *J. Pept. Sci.*, **22**, 452-460 (2016).

[134] Gudeangadi P. G., Tsuchiya K., Sakai T., Numata K., Chemoenzymatic synthesis of polypeptides consisting of periodic di- and tri-peptide motifs similar to elastin, *Polym. Chem.*, **9**, 2336-2344 (2018).

[135] Seifried, B. M., Cao, J., Olsen, B. D., Multifunctional, High Molecular Weight, Post-Translationally Modified Proteins through Oxidative Cysteine Coupling and Tyrosine Modification, *Bioconjugate Chem.*, **29**, 1876-1884 (2018).

[136] Kojima C., Sk U. H., Fukushima D., Irie K., Akazawa N., Umeda M., Niidome T., Effect of main chain conformation on thermosensitivity in elastin-like peptide-grafted polylysine, *RSC Adv.*, **5**, 104900-104906 (2015).

[137] Paik B. A., Blanco M. A., Jia X., Roberts C. J., Kiick K. L., Aggregation of poly(acrylic acid)-containing elastin-mimetic copolymers, *Soft Matter*, **11**, 1839-1850 (2015).

[138] Le Fer G., Portes D., Goudounet G., Guigner J. -M., Garanger E., Lecommandoux S., Design and self-assembly of PBLG-: B -ELP hybrid diblock copolymers based on synthetic and elastin-like polypeptides, *Org. Biomol. Chem.*, **15**, 10095-10104 (2017).

[139] Malho, J., Brand, J., Pecastaings, G., Ruokolainen, J., Gröschel, A., Sèbe, G., Garanger, E., Lecommandoux, S., Multifunctional stimuli-responsive cellulose nanocrystals via dual surface modification with genetically engineered elastin-like polypeptides and poly(acrylic acid), *ACS Macro Lett.*, **7**, 646-650 (2018).

[140] Mozhdehi D., Luginbuhl K. M., Simon J. R., Dzuricky M., Berger R., Varol H. S.,

Huang F. C., Buehne K. L., Mayne N. R., Weitzhandler I., Bonn M., Parekh S. H., Chilkoti A., Genetically encoded lipid-polypeptide hybrid biomaterials that exhibit temperature-triggered hierarchical self-assembly, *Nat. Chem.*, **10**, 496-505 (2018).

[141] Le D. H., Okubo T., Sugawara-Narutaki A., Beaded nanofibers assembled from double-hydrophobic elastin-like block polypeptides: Effects of trifluoroethanol, *Biopolymers*, **103**, 175-185 (2015).

[142] Bo J., Wang L., Li W., Zhang X., Zhang A., Comb-like polymers pendanted with elastin-like peptides showing sharp and tunable thermoresponsiveness through dynamic covalent chemistry, *J. Polym. Sci. A1*, **54**, 3379-3387 (2016).

[143] Wang Z., Li Y., Huang Y., Thompson M. P., Leguyader C. L. M., Sahu S., Gianneschi N. C., Enzyme-regulated topology of a cyclic peptide brush polymer for tuning assembly, *Chem. Commun.*, **51**, 17108-17111 (2015).

[144] Glassman M. J., Olsen B. D., Arrested phase separation of elastin-like polypeptide solutions yields stiff, thermoresponsive gels, *Biomacromolecules*, **16**, 3762-3773 (2015).

[145] Hauptmann V., Menzel M., Weichert N., Reimers K., Spohn U., Conrad U., In planta production of ELPylated spidroin-based proteins results in non-cytotoxic biopolymers, *Bmc. Biotechnol.*, **15**, 9 (2015).

[146] Heppner R., Weichert N., Schierhorn A., Conrad U., Pietzsch M., Low-tech, pilot scale purification of a recombinant spider silk protein analog from tobacco leaves, *Int. J. Mol. Sci.*, **17**, 1687 (2016).

[147] Da Costa A., Machado R., Ribeiro A., Collins T., Thiagarajan V., Neves-Petersen M. T., Rodriguez-Cabello J. C., Gomes A. C., Casal M., Development of elastin-like recombinamer films with antimicrobial activity, *Biomacromolecules*, **16**, 625-635 2015).

[148] González de Torre I., Ibáñez-Fonseca A., Quintanilla L., Alonso M., Rodríguez-Cabello J. -C., Random and oriented electrospun fibers based on a multicomponent, *in situ* clickable elastin-like recombinamer system for dermal tissue engineering, *Acta Biomater.*, **72**, 137-149 (2018).

[149] Da Costa A., Pereira A. M., Gomes A. C., Rodriguez-Cabello J. C., Sencadas V., Casal M., MacHado R., Single step fabrication of antimicrobial fibre mats from a bioengineered protein-based polymer, *Biomed Mater.*, **12**, 045011 (2017).

[150] Boraldi F., Moscarelli P., Bochicchio B., Pepe A., Salvi A. M., Quaglino D., Heparan sulfates facilitate harmless amyloidogenic fibril formation interacting with elastin-like peptides, *Sci. Rep.,* **8**, 3115 (2018).

[151] Koga T., Nakamoto K., Odawara K., Matsuoka T., Higashi N., Fabrication of thermo-responsive molecular layers from self-assembling elastin-like oligopeptides

containing cell-binding domain for tissue engineering, *Polymers*, **7**, 134-146 (2015).

[152] Zeng Q., Desai M. S., Jin H. -E., Lee J. H., Chang J., Lee S.- W., Self-healing elastin-bioglass hydrogels, *Biomacromolecules*, **17**, 2619-2625 (2016).

[153] Adnan N., Mie M., Haque A., Hossain S., Mashimo Y., Akaike T., Kobatake E., Construction of a defined biomimetic matrix for long-term maintenance of mouse induced pluripotent stem cells, *Bioconjugate Chem.*, **27**, 1599-1605 (2016).

[154] Romano N. H., Madl C. M., Heilshorn S. C., Matrix RGD ligand density and L1CAM-mediated Schwann cell interactions synergistically enhance neurite outgrowth, *Acta Biomater.*, **11**, 48-57 (2015).

[155] Mahara A., Kiick K. L., Yamaoka T., *In vivo* guided vascular regeneration with a non-porous elastin-like polypeptide hydrogel tubular scaffold, *J. Biomed. Mater. Res. A* , **105**, 1746-1755 (2017).

[156] D'Andrea P., Scaini D., Severino L. U., Borelli V., Passamonti S., Lorenzon P., Bandiera A., *In vitro* myogenesis induced by human recombinant elastin-like proteins, *Biomaterials*, **67**, 240-253 (2015).

[157] Gurumurthy B., Bierdeman P. C., Janorkar A. V., Composition of elastin like polypeptide–collagen composite scaffold influences *in vitro* osteogenic activity of human adipose derived stem cells, *Dent. Mater.*, **32**, 1270-1280 (2016).

[158] Turner P. A., Tang Y., Weiss S. J., Janorkar A. V., Three-dimensional spheroid cell model of *in vitro* adipocyte inflammation, *Tissue Eng. Pt. A*, **21**, 1837-1847 (2015).

[159] Hedegaard C. L., Collin E. C., Redondo-Gómez C., Nguyen L. T. H., Ng K. W., Castrejón-Pita A. A., Castrejón-Pita J. R., Mata A., Hydrodynamically guided hierarchical self-assembly of peptide–protein bioinks, *Adv. Funct. Mater.*, **28**, 1703716 (2018).

[160] Shuturminska K., Tarakina N. V., Azevedo H. S., Bushby A. J., Mata A., Anderson P., Al-Jawad M., Elastin-like protein, with statherin derived peptide, controls fluorapatite formation and morphology, *Frontiers in Physiology*, **8**, 368 (2017).

[161] Vila M., García A., Girotti A., Alonso M., Rodríguez-Cabello J. C., González-Vázquez A., Planell J. A., Engel E., Buján J., García-Honduvilla N., Vallet-Regí M., 3D silicon doped hydroxyapatite scaffolds decorated with elastin-like recombinamers for bone regenerative medicine, *Acta Biomater.*, **45**, 349-356 (2016).

[162] Misbah M. H., Santos M., Quintanilla L., Günter C., Alonso M., Taubert A., Rodríguez-Cabello J. C., Recombinant DNA technology and click chemistry: A powerful combination for generating a hybrid elastin-like-statherin hydrogel to control calcium phosphate mineralization, *Beilstein J. Nanotechnol.*, **8**, 772-783 (2017).

[163] Govindharajulu J. P., Chen X., Li Y., Rodriguez-Cabello J. C., Battacharya M.,

Aparicio C., Chitosan-recombinamer layer-by-layer coatings for multifunctional implants, *Int. J. Mol. Sci.*, **18**, 369 (2017).

[164] Jang J. -H., Shin S., Kim H. -J., Jeong J., Jin H. -E., Desai M. S., Lee S. -W., Kim S. -Y., Improvement of physical properties of calcium phosphate cement by elastin-like polypeptide supplementation, *Scientific Reports*, **8**, 5216 (2018).

[165] Li L., Li N. K., Tu Q., Im O., Mo C. -K., Han W., Fuss W. H., Carroll N. J., Chilkoti A., Yingling Y. G., Zauscher S., López G. P., Functional modification of silica through enhanced adsorption of elastin-like polypeptide block copolymers, *Biomacromolecules*, **19**, 298-306 (2018).

[166] Han W., MacEwan S. R., Chilkoti A., López G. P., Bio-inspired synthesis of hybrid silica nanoparticles templated from elastin-like polypeptide micelles, *Nanoscale*, **7**, 12038-12044 (2015).

[167] Han W., Chilkoti A., López G. P., Self-assembled hybrid elastin-like polypeptide/silica nanoparticles enable triggered drug release, *Nanoscale*, **9**, 6178-6186 (2017).

[168] Li L. -L., Qiao S. -L., Liu W. -J., Ma Y., Wan D., Pan J., Wang H., Intracellular construction of topology-controlled polypeptide nanostructures with diverse biological functions, *Nature Communications*, **8**, 1276 (2017).

[169] Ott W., Jobst M. A., Bauer M. S., Durner E., Milles L. F., Nash M. A., Gaub H. E., Elastin-like polypeptide linkers for single-molecule force spectroscopy, *ACS Nano*, **11**, 6346-6354 (2017).

[170] Su Z., Pramounmat N., Watson S. T., Renner J. N., Engineered interaction between short elastin-like peptides and perfluorinated sulfonic-acid ionomer, *Soft Matter*, **14**, 3528-3535 (2018).

[171] Sugihara T., Mie M., Kobatake E., Application of elastin-based nanoparticles displaying antibody binding domains for a homogeneous immunoassay, *Anal. Biochem.*, **544**, 72-79 (2018).

[172] Ikeda Y., Mashimo Y., Mie M., Kobatake E., Design of luciferase-displaying protein nanoparticles for use as highly sensitive immunoassay detection probes, *Analyst*, **141**, 6557-6563 (2016).

[173] Jeon H. -Y., Jung S. -H., Jung Y. M., Kim Y. -M., Ghandehari H., Ha K. -S., Array-Based high-throughput analysis of silk-elastinlike protein polymer degradation and c-peptide release by proteases, *Anal. Chem.*, **88**, 5398-5405 (2016).

[174] Piña M. J., Alex S. M., Arias F. J., Santos M., Rodríguez-Cabello J. C., Ramesan R. M., Sharma C. P., Elastin-like recombinamers with acquired functionalities for gene-delivery applications, *J. Biomed. Mater. Res. A*, **103**, 3166-3178 (2015).

[175] Corich L., Busetti M., Petix V., Passamonti S., Bandiera A., Evaluation of a

biomimetic 3D substrate based on the human elastin-like polypeptides (HELPs) model system for elastolytic activity detection, *J. Biotechnol.*, **255**, 57-65 (2017).

[176] Bao J., Hou C., Dong Q., Ma X., Chen J., Huo D., Yang M., Galil K. H. A. E., Chen W., Lei Y., ELP-OPH/BSA/TiO2 nanofibers/c-MWCNTs based biosensor for sensitive and selective determination of p-nitrophenyl substituted organophosphate pesticides in aqueous system, *Biosens. Bioelectron.*, **85**, 935-942 (2016).

[177] Nouri F. S., Wang X., Chen X., Hatefi A., Reducing the visibility of the vector/DNA nanocomplexes to the immune system by elastin-like peptides, *Pharm. Res.*, **32**, 3018-3028 (2015).

[178] Kimmerling K. A., Furman B. D., Mangiapani D. S., Moverman M. A., Sinclair S. M., Huebner J. L., Chilkoti A., Kraus V. B., Setton L. A., Guilak F., Olson S. A., Sustained intra-articular delivery of IL-1Ra from a thermally-responsive elastin-like polypeptide as a therapy for post-traumatic arthritis, *Eur. Cells. Mater.*, **29**, 124-140 (2015).

[179] Dash B. C., Thomas D., Monaghan M., Carroll O., Chen X., Woodhouse K., O'Brien T., Pandit A., An injectable elastin-based gene delivery platform for dose-dependent modulation of angiogenesis and inflammation for critical limb ischemia, *Biomaterials*, **65**, 126-139 (2015).

[180] Asai D., Kanamoto T., Takenaga M., Nakashima H., *In situ* depot formation of anti-HIV fusion-inhibitor peptide in recombinant protein polymer hydrogel, *Acta Biomater.*, **64**, 116-125 (2017).

[181] Zhang W., Song Y., Eldi P., Guo X., Hayball J. D., Garg S., Albrecht H., Targeting prostate cancer cells with hybrid elastin-like polypeptide/liposome nanoparticles, *Int. J. Nanomed.*, **13**, 293-305 (2018).

[182] Luginbuhl, K. M., Mozhdehi, D., Dzuricky, M., Yousefpour, P, Huang, F. C., Mayne, N. R., Buehne, K. L., Chilkoti, A., Recombinant synthesis of hybrid lipid–peptide polymer fusions that self-assemble and encapsulate hydrophobic drugs, *Angew. Chem. Int. Edit.*, **56**, 13979-13984 (2017).

[183] Leonard A., Koria P., Growth factor functionalized biomaterial for drug delivery and tissue regeneration, *J. Bioact. Compat. Pol.*, **32**, 568-581 (2017).

[184] Devalliere J., Dooley K., Yu Y., Kelangi S. S., Uygun B. E., Yarmush M. L., Co-delivery of a growth factor and a tissue-protective molecule using elastin biopolymers accelerates wound healing in diabetic mice, *Biomaterials*, **141**, 149-160 (2017).

[185] Park, J., Kim, J. Y, Choi, S. -K., Kim, J. Y., Kim, J. H., Jeon, W. B., Lee, J. E., Thermo-sensitive assembly of the biomaterial REP reduces hematoma volume following collagenase-induced intracerebral hemorrhage in rats, *Nanomed-Nanotechnol.*, **13**, 1853-1862 (2017).

[186] Luginbuhl K. M., Schaal J. L., Umstead B., Mastria E. M., Li X., Banskota S., Arnold S., Feinglos M., D'Alessio D., Chilkoti A., One-week glucose control via zero-order release kinetics from an injectable depot of glucagon-like peptide-1 fused to a thermosensitive biopolymer, *Nature Biomedical Engineering*, **1**, 0078 (2017).

[187] Dooley K., Devalliere J., Uygun B. E., Yarmush M. L., Functionalized biopolymer particles enhance performance of a tissue-protective peptide under proteolytic and thermal stress, *Biomacromolecules*, **17**, 2073-2079 (2016).

[188] Chade A. R., Tullos N. A., Harvey T. W., Mahdi F., Bidwell G. L., III, Renal therapeutic angiogenesis using a bioengineered polymer-stabilized vascular endothelial growth factor construct, *J. Am. Soc. Nephrol.*, **27**, 1741-1752 (2016).

[189] Johnson T., Koria P., Expression and purification of neurotrophin-elastin-like peptide fusion proteins for neural regeneration, *BioDrugs*, **30**, 117-127 (2016).

[190] Yeboah A., Cohen R. I., Faulknor R., Schloss R., Yarmush M. L., Berthiaume F., The development and characterization of SDF1α-elastin-like-peptide nanoparticles for wound healing, *J. Control. Release*, **232**, 238-247 (2016).

[191] Nawroth J. F., McDaniel J. R., Chilkoti A., Jordan R., Luxenhofer R., Maleimide-functionalized poly(2-oxazoline)s and their conjugation to elastin-like polypeptides, *Macromol. Biosci.*, **16**, 322-333 (2016).

[192] Hsueh P. -Y., Edman M. C., Sun G., Shi P., Xu S., Lin Y. -A., Cui H., Hamm-Alvarez S. F., Mackay J. A., Tear-mediated delivery of nanoparticles through transcytosis of the lacrimal gland, *J. Control. Release*, **208**, 2-13 (2015).

[193] McCarthy B., Yuan Y., Koria P., Elastin-like-polypeptide based fusion proteins for osteogenic factor delivery in bone healing, *Biotechnol. Progr.*, **32**, 1029-1037 (2016).

[194] Luo T., David M. A., Dunshee L. C., Scott R. A., Urello M. A., Price C., Kiick K. L., Thermoresponsive elastin-b-collagen-like peptide bioconjugate nanovesicles for targeted drug delivery to collagen-containing matrices, *Biomacromolecules*, **18**, 2539-2551 (2017).

[195] Bidwell G. L., III, Mahdi F., Shao Q., Logue O. C., Waller J. P., Reese C., Chade A. R., A kidney-selective biopolymer for targeted drug delivery, *Am. J. Physiol. -Renal*, **312**, F54-F64 (2017).

[196] Sarangthem V., Cho E. A., Yi A., Kim S. K., Lee B. -H., Park R. -W., Application of bld-1-embedded elastin-like polypeptides in tumor targeting, *Scientific Reports*, **8**, 3892 (2018).

[197] Hu J., Wang G., Liu X., Gao W., Enhancing pharmacokinetics, tumor accumulation, and antitumor efficacy by elastin-like polypeptide fusion of interferon alpha, *Adv. Mater.*, **27**, 7320-7324 (2015).

[198] Sarangthem V., Kim Y., Singh T. D., Seo B. -Y., Cheon S. -H., Lee Y. -J., Lee B. -H.,

Park R. -W., Multivalent targeting based delivery of therapeutic peptide using AP1-ELP carrier for effective cancer therapy, *Theranostics*, **6**, 2235-2249 (2016).

[199] Hatefi A., Karjoo Z., Nomani A., Development of a recombinant multifunctional biomacromolecule for targeted gene transfer to prostate cancer cells, *Biomacromolecules*, **18**, 2799-2807 (2017).

[200] Dhandhukia J. P., Shi P., Peddi S., Li Z., Aluri S., Ju Y., Brill D., Wang W., Janib S. M., Lin Y. -A., Liu S., Cui H., Mackay J. A., Bifunctional elastin-like polypeptide nanoparticles bind rapamycin and integrins and suppress tumor growth *in vivo*, *Bioconjugate Chem.*, **28**, 2715-2728 (2017).

[201] Iglesias R., Koria P., Leveraging growth factor induced macropinocytosis for targeted treatment of lung cancer, *Med. Oncol.*, **32**, 259 (2015).

[202] Wang J., Dzuricky M., Chilkoti A., The weak link: optimization of the ligand-nanoparticle interface to enhance cancer cell targeting by polymer micelles, *Nano Lett.*, **17**, 5995-6005 (2017).

[203] Opačak-Bernardi T., Ryu J. S., Raucher D., Effects of cell penetrating Notch inhibitory peptide conjugated to elastin-like polypeptide on glioblastoma cells, *J. Drug Target.*, **25**, 523-531 (2017).

[204] Weinberger A., Walter V., MacEwan S. R., Schmatko T., Muller P., Schroder A. P., Chilkoti A., Marques C. M., Cargo self-assembly rescues affinity of cell-penetrating peptides to lipid membranes, *Scientific Reports*, **7**, 43963 (2017).

[205] George E. M., Mahdi F., Logue O. C., Robinson G. G., Bidwell G. L., III, Corneal penetrating elastin-like polypeptide carriers, *J. Ocul. Pharmacol. Th.*, **32**, 163-171 (2016).

[206] McGowan J. W. D., Shao Q., Vig P. J. S., Bidwell G. L., III, Intranasal administration of elastin-like polypeptide for therapeutic delivery to the central nervous system, *Drug. Des. Devel. Ther.*, **10**, 2803-2813 (2016).

[207] Kim H. R., You D. G., Park S. -J., Choi K. -S., Um W., Kim J. -H., Park J. H., Kim Y. -S., MRI monitoring of tumor-selective anticancer drug delivery with stable thermosensitive liposomes triggered by high-intensity focused ultrasound, *Mol. Pharm.*, **13**, 1528-1539 (2016).

[208] Meikle S. T., Piñeiro Y., Bañobre López M., Rivas J., Santin M., Surface functionalization superparamagnetic nanoparticles conjugated with thermoresponsive poly(epsilon-lysine) dendrons tethered with carboxybetaine for the mild hyperthermia-controlled delivery of VEGF, *Acta Biomater.*, **40**, 235-242 (2016).

[209] Um W., Kwon S., You D. G., Cha J. M., Kim H. R., Park J. H., Non-thermal acoustic treatment as a safe alternative to thermosensitive liposome-involved hyperthermia for cancer therapy, *RSC Advances*, **7**, 29618-29625 (2017).

[210] Kojima C., Fukushima D., Applications of gold nanoparticle-loaded thermosensitive elastin-mimetic dendrimer to photothermal therapy, *J. Photopolym. Sci. Tec.*, **29**, 519-523 (2016).

[211] Pille J., Van Lith S. A. M., Van Hest J. C. M., Leenders W. P. J., Self-assembling VHH-elastin-like peptides for photodynamic nanomedicine, *Biomacromolecules*, **18**, 1302-1310 (2017).

[212] Liu X., Shen Y., Zhang X., Lin R., Jia Q., Chang Y., Liu W., Liu W., Brachytherapy using elastin-like polypeptides with ^{131}I inhibit tumor growth in rabbits with VX2 liver tumor, *Digest. Dis. Sci.*, **61**, 2921-2927 (2016).

[213] Schaal J. L., Li X., Mastria E., Bhattacharyya J., Zalutsky M. R., Chilkoti A., Liu W., Injectable polypeptide micelles that form radiation crosslinked hydrogels *in situ* for intratumoral radiotherapy, *J. Control. Release*, **228**, 58-66 (2016).

[214] Dong S., Xu T., Zhao P., Parent K., Chen M., A comparison study of iTEP nanoparticle-based CTL vaccine carriers revealed a surprise relationship between the stability and efficiency of the carriers, *Theranostics*, **6**, 666-678 (2016).

[215] Cho S., Dong S., Parent K. N., Chen M., Immune-tolerant elastin-like polypeptides (iTEPs) and their application as CTL vaccine carriers, *J. Drug Target.*, **24**, 328-339 (2016).

[216] Dong S., Xu T., Wang P., Zhao P., Chen M., Engineering of a self-adjuvanted iTEP-delivered CTL vaccine, *Acta Pharm. Sinic.*, **38**, 914-923 (2017).

[217] Dong S., Wang P., Zhao P., Chen M., Direct loading of iTEP-delivered CTL epitope onto MHC class I complexes on the dendritic cell surface, *Mol. Pharm.*, **14**, 3312-3321 (2017).

[218] Lee J. -K., Luchian T., Park Y., New antimicrobial peptide kills drug-resistant pathogens without detectable resistance, *Oncotarget*, **9**, 15616-15634 (2018).

[219] Lu H. -Y., Huang C. -Y., Shih C. -M., Lin Y. -W., Tsai C. -S., Lin F. -Y., Shih C. -C., A potential contribution of dipeptidyl peptidase-4 by the mediation of monocyte differentiation in the development and progression of abdominal aortic aneurysms, *J. Vasc. Surg.*, **66**, 1217-12260 (2017).

[220] Lei Y., Yang G., Hu L., Piao L., Inoue A., Jiang H., Sasaki T., Zhao G., Yisireyili M., Yu C., Xu W., Takeshita K., Okumura K., Kuzuya M., Cheng X. -W., Increased dipeptidyl peptidase-4 accelerates diet-related vascular aging and atherosclerosis in ApoE-deficient mice under chronic stress, *Int. J. Cardiol.*, **243**, 413-420 (2017).

[221] Yang G., Lei Y., Inoue A., Piao L., Hu L., Jiang H., Sasaki T., Wu H., Xu W., Yu C., Zhao G., Ogasawara S., Okumura K., Kuzuya M., Cheng X. -W., Exenatide mitigated diet-induced vascular aging and atherosclerotic plaque growth in ApoE-deficient mice under chronic stress, *Atherosclerosis*, **264**, 1-10 (2017).

[222] George L., Mitra A., Thimraj T. A., Irmler M., Vishweswaraiah S., Lunding L., Hühn D., Madurga A., Beckers J., Fehrenbach H., Upadhyay S., Schulz H., Leikauf G. D., Ganguly K., Transcriptomic analysis comparing mouse strains with extreme total lung capacities identifies novel candidate genes for pulmonary function, *Resp. Res.*, **18**, 152 (2017).

[223] Chouhan D., Chakraborty B., Nandi S. K., Mandal B. B., Role of non-mulberry silk fibroin in deposition and regulation of extracellular matrix towards accelerated wound healing, *Acta Biomater.*, **48**, 157-174 (2017).

[224] Schmidt S. R., Production challenges for complex biologics: Fusion proteins, *American Pharmaceutical Review*, **20**, 1 (2017).

[225] Pastel E., Joshi S., Knight B., Liversedge N., Ward R., Kos K., Effects of Exendin-4 on human adipose tissue inflammation and ECM remodelling, *Nutrition and Diabetes*, **6**, e235 (2016).

[226] Li J., Bao X., Li Y., Wang Y., Zhao Z., Jin X., Study of the functional mechanisms of osteopontin and chemokine-like factor 1 in the development and progression of abdominal aortic aneurysms in rats, *Experimental and Therapeutic Medicine*, **12**, 4007-4011 (2016).

[227] Lu W. -W., Jia L. -X., Ni X. -Q., Zhao L., Chang J. -R., Zhang J. -S., Hou Y. -L., Zhu Y., Guan Y. -F., Yu Y. -R., Du J., Tang C. -S., Qi Y. -F., Intermedin1- 53 attenuates abdominal aortic aneurysm by inhibiting oxidative stress, *Arterioscl. Throm. Vas.*, **36**, 2176-2190 (2016).

[228] Swanson J. P., Martinez M. R., Cruz M. A., Mankoci S. G., Costanzo P. J., Joy A., A coacervate-forming biodegradable polyester with elevated LCST based on bis-(2-methoxyethyl)amine, *Polymer Chemistry*, **7**, 4693-4702 (2016).

[229] McGann C. L., Akins R. E., Kiick K. L., Resilin-PEG hybrid hydrogels yield degradable elastomeric scaffolds with heterogeneous microstructure, *Biomacromolecules*, **17**, 128-140 (2016).

[230] Krishna S. M., Seto S. W., Jose R. J., Biros E., Moran C. S., Wang Y., Clancy P., Golledge J., A peptide antagonist of thrombospondin-1 promotes abdominal aortic aneurysm progression in the angiotensin II-infused apolipoprotein-E-deficient mouse, *Arterioscl. Throm. Vas.*, **35**, 389-398 (2016).

[231] Kosinski A. M., Sivasankar M. P., Panitch A., Varying RGD concentration and cell phenotype alters the expression of extracellular matrix genes in vocal fold fibroblasts, *J. Biomed. Mater. Res. A*, **103**, 3094-3100 (2015).

[232] Wang X., Zhou B., Hu W., Zhao Q., Lin Z., Formation of active inclusion bodies induced by hydrophobic self-assembling peptide GFIL8, *Microb. Cell Fact.*, **14**, 88 (2015).

[233] Lu H. Y., Huang C. Y., Shih C. M., Chang W. H., Tsai C. S., Lin F. Y., Shih C. C., Dipeptidyl peptidase-4 inhibitor decreases abdominal aortic aneurysm formation through GLP-1-dependent monocytic activity in mice, *PLoS ONE*, **10**, e0121077 (2015).

[234] Qa'Aty N., Wang Y., Wang A., Mao S., Vincent M., Husain M., Hinek A., The antidiabetic hormone glucagon-like peptide-1 induces formation of new elastic fibers in human cardiac fibroblasts after cross-Activation of IGF-IR, *Endocrinology*, **156**, 90-102 (2015).

[235] Tsuchiya T., Osaki T., Minamino N., Sasaki K., Peptidomics for studying limited proteolysis, *J. Proteome. Res*., **14**, 4921-4931 (2015).

[236] Smits F. C. M., Buddingh B. C., Van Eldijk M. B., Van Hest J. C. M., Elastin-like polypeptide based nanoparticles: Design rationale toward nanomedicine, *Macromol. Biosci*., **15**, 36-51 (2015).

[237] Despanie J., Dhandhukia J. P., Hamm-Alvarez S. F., MacKay J. A., Elastin-like polypeptides: Therapeutic applications for an emerging class of nanomedicines, *J. Control. Release*, **240**, 93-108 (2016).

[238] Yeo G. C., Aghaei-Ghareh-Bolagh B., Brackenreg E. P., Hiob M. A., Lee P., Weiss A. S., Fabricated Elastin, *Adv. Healthc. Mater.*, **4**, 2530-2556 (2015).

[239] Loo Y., Goktas M., Tekinay A. B., Guler M. O., Hauser C. A. E., Mitraki A., Self-assembled proteins and peptides as scaffolds for tissue regeneration, *Adv. Healthc. Mater.*, **4**, 2557-2586 (2015).

Table 1. An outline of ELPs used in various forms.

Reference number	content	Commentary
[135]	Production of bioconjugates mimicking glycoproteins that are difficult to produce.	The conjugate was expressed with ELPs as a backbone. In order to mimic glycoproteins, sugars or other functional moieties were added to the tyrosine residues introduced as guest residue.
[136]	Grafting of short chain ELPs to polylysine dendrimer added thermal response to the dendrimer.	The conformation of the grafted polypeptide depended on the type of dendrimer. It was suggested that this change influenced T_t of the dendrimer.
[137]	Evaluation on physical properties of diblock and triblock conjugates of polyacrylic acid and an ELP.	Polydisperse aggregates were formed by dropping PBS into the DMSO solution of this conjugate. Interaction of poly(acrylic acid) with the peptide and itself seemed to be a driving force of the aggregation.
[138]	Synthesis of amphipathic polypeptides containing ELP blocks by ring-opening polymerization of γ-benzyl-L-glutamate.	Resulting conjugates showed formation of spherical micelles. The self-assembling property was depending on the molecular weight and the hydrophobicity of the ELPs.
[139]	Preparation of dual functional cellulose nanocrystals modified with polyacrylic acid and an ELP.	The cellulose nanocrystals acquired temperature responsiveness of ELP and pH sensitivity of polyacrylic acid.
[140]	Development of stimuli-responsive hybrid material consisting of C_{14}-β-sheet motif-ELP.	Due to coexpression of N-myristoyl transferase, post-translational modification of β-sheet motif-ELP became possible in one pot.
[141]	The effect of trifluoroethanol on ELPs mimicking the hydrophobic domain localization of elastin.	The nanostructures of triblock polypeptides consisting of (VGGVG) and (VPGXG) were controlled by concentration of trifluoroethanol.
[142]	Evaluation of physical properties of comb-like polymers which obtained by addition of branched ELPs to poly(methyl methacrylate).	By covalently adding oligoethylene glycol, the T_t could be further controlled.
[143]	Synthesis of brush-like polymer with cyclic ELPs by norbornene ring opening polymerization.	The self-assembling properties of the polymer could be controlled by opening of ELP by enzyme.

Table 2. An outline of ELP applications as matrix and culture medium.

Reference number	Content	Commentary
[150]	Analysis on the effect of cooperation of synthetic ELPs $(VGGVG)_n$ and heparin sulfate on fibroblasts.	Heparin sulfate possessed physiological activity on ECM. Heparin sulfate promoted the amyloid-like fibril formation of ELPs, but there was no difference in cell survival level, resulting in a change in cell adhesion properties.
[151]	Structure analysis, morphological analysis and cell adhesion test of RGD-diethylene glycol-ELP using diethylene glycol as a spacer.	Self-assembled membranes that RGD-diethylene glycol-ELP formed on hydrophobic plates showed effective cell adhesion.
[152]	*In situ* formation of hydrogel via crosslinking of ELP-Bioglass complex triggered by pH change due to bioglass.	ELP-Bioglass had composition-dependent and concentration-dependent gelation behavior and change in mechanical property. Moreover, cell proliferation and adhesion activity was added by conjugation with RGD sequence.
[153]	Coating of ELPs conjugated with RGD motif and cadherin binding sequence, on tissue culture medium.	The resulting cell culture medium supported long-term maintains of mouse induced pluripotent stem cells.
[154]	Neurite outgrowth and culture of Schwann cells supporting it in artificial ECM using ELPs.	Nerve fiber elongation was controlled by the density of RGD ligand added to ELPs and the concentration of nerve growth factor.
[155]	*In vivo* guided vascular regeneration with a non-porous elastin-like polypeptide $(VPGIG)_n$ hydrogel tubular scaffold.	RGD sequence was added to ELPs which showed excellent elasticity and antithrombogenicity, for the regeneration of connective tissue .
[156]	Fusion of ELPs, A2 chain domain of type IV collagen and two RGD domains, as adhesion matrix of myoblasts.	Adherence of cells on the fusion ELPs induced cell proliferation and differentiation, expression of myosin heavy chain and fusion of myosin fibers to multinucleated myotubes.
[157]	Evaluation on the effectiveness of ELP-collagen complex that cultured human adipose-derived stem cells and enabled them to undergo osteogenic differentiation.	ELP-collagen complex applied as scaffolds for guided bone regeneration, and evaluation of its physical properties and cell culture test were conducted.
[158]	Development of three dimensional *in vitro* model of adipose tissue showing lipid accumulation.	By culturing mouse adipocytes on the ELP-polyethyleneimine coating, spheroidal cell aggregates showing a good phenotype to reproduce the obesity state were obtained.
[159]	Development of bioprinting method using ELPs as components of bioink.	A matrix with dispersed hepatocytes was constructed by control in formation of higher order molecular self-assembly.

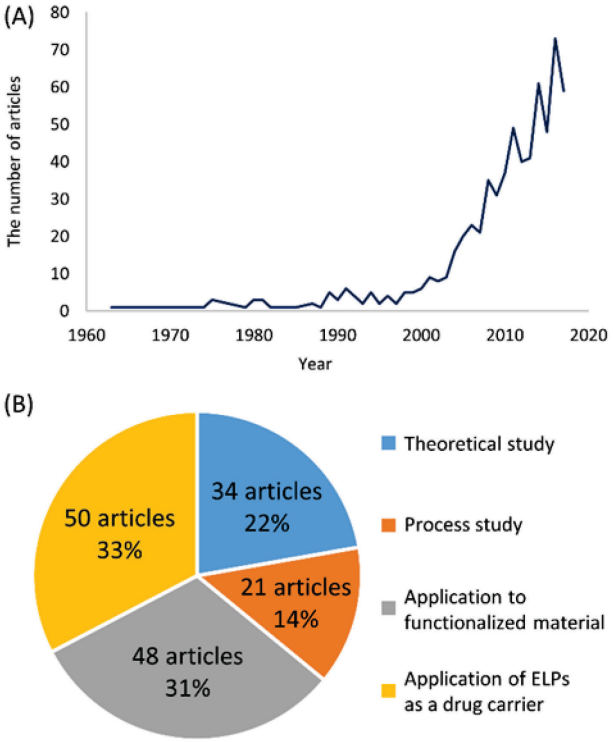

Figure 1. Recent trends of studies on ELPs.

(A) The number of articles found in “Scopus” by searching in "elastin like peptide" in region of “Article title, Abstract, Keywords”. The data between 1963 and 2017 were shown here. (B) Contents of 153 articles introduced in this section. They were classified into 4 groups, and the number of articles in each group was shown here.

CHAPTER 2

Investigation of self-assembling mechanism in dimerized short elastin-like peptide analog and the influence of dimerization on coacervation property

Abstract

Elastin-like peptides (ELPs) possess characteristic hydrophobic repetitive sequences and exhibit a temperature-dependent reversible self-association and dissociation, so-called coacervation. Typical repetitive sequence of ELPs can be found in elastin. Taking advantage of the characteristic responding to temperature change, ELPs have been developed as base materials for new functional biomaterials. For development of new biomaterials using ELPs as base materials, it is necessary to know the detailed relationship between their amino acid sequences and coacervation properties. Due to the structural flexibility of ELPs, precise mechanisms underlying coacervation of ELPs remain obscure. In this study, we synthesized a novel dimeric ELP analog (H-C(WPGVG)$_3$-NH_2)$_2$, henceforth abbreviated (CW3)2, and its analogs to analyze self-assembling properties and structural features as indicators of coacervation. In the turbidity measurements, (CW3)2 exhibited strong coacervation at a lower concentration than the monomeric form and other ELPs. In addition, it was observed in the optical microscopy that the coacervate of (CW3)2 held water-soluble dye molecules in its internal space. Furthermore, fluorescence microscopy, dynamic light scattering, and the microscopy revealed that the self-assembly of (CW3)2 occurs in a stepwise process. To analyze the structural factors of (CW3)2, molecular dynamics simulations and circular dichroism spectroscopic analysis were performed. These measurements indicated that initial helical structures consisting of proline and glycine residues became more disordered at high temperatures, causing significant exposure of their hydrophobic surfaces. This change in the hydrophobic surface was attributed to the potent self-assembling property of (CW3)2. These findings provide important insights into more efficient applications of ELPs and their analogs, as well as the coacervation mechanisms of ELPs and elastin.

1. Introduction

In addition to elucidating the molecular mechanisms of biomacromolecules, controlling their various functions is one of the important issues in biochemistry. The functions of intrinsically disordered proteins (IDPs) have recently gained attention. [1, 2] These proteins serve significant roles in cellular and extracellular functions, particularly by participating in molecular recognition and providing mechanical properties [3, 4]. Among IDPs, tropoelastin, a precursor of elastic protein, elastin, in the extracellular matrix, provides extensibility and condensability to connective tissues in arterial walls, lungs, and skin [5, 6].

Tropoelastin and purified soluble elastin also exhibits temperature-dependent, reversible association and dissociation that results in a phase transition characterized by lower-critical solution temperature (LCST) behavior [7]. This characteristic self-assembly is known as coacervation and it is considered to be important for elastin maturation *in vivo* [8]. Because of this temperature-responsive property, elastin-like peptides (ELPs), which contain elastin-derived hydrophobic repetitive sequence(s), have recently been considered to be useful in the design of new scaffold materials for developing biomedical products related to drug delivery systems and tissue engineering [9, 10]. Furthermore, as the biophysical properties of ELPs are similar to those of many other IDPs, ELPs have also been studied as a model peptide [11]. Thus, elucidating the mechanism of coacervation of elastin using artificial ELPs is important for its efficient use in applications and for understanding the behaviors of other complex IDPs.

The hydrophobic, repetitive sequences of elastin, such as $(GGVP)_n$, $(VPGVG)_n$, and $(GVGVAP)_n$, are essential to regulate the coacervating property elastin [8, 12]. Previous studies have examined the relationships between peptide sequences and the coacervation properties of various ELPs based on the $(VPGVG)_n$ sequence by altering its length or substituting the amino acid residues [9, 13]. The introduction of hydrophobic residues (Ile and Leu > Val > Ala), larger numbers of hydrophobic amino acids, and longer chain lengths resulted in more potent coacervation properties [14-18]. In this trend, few studies have focused on ELPs that contain aromatic amino acids, though the hydrophobicity of the aromatic amino acids would make a significant contribution coacervation behavior. On the other hand, conformation of ELPs are disordered, because their repetitive sequences contain many secondary structure breakers, such as glycine and proline residues [19]. Self-assembly of ELPs was assumed to be related to their disordered conformations in solution [6, 20]. Because of the difficulties in analyzing flexible and disordered secondary structures in solution, the relationship between the structure and coacervation properties of ELPs has not been completely elucidated.

The self-assembly of ELPs is mainly attributed to the hydrophobic effect. ELPs are thought to be hydrated in clathrate-like water molecules in solution [8, 17, 21]. It has been hypothesized that ELPs assemble by hydrophobic interaction after the collapse of the clathrate-like structures of water at high temperatures [8, 22-24]. On the other hand, the hydrophobic domains of ELPs are presumed to be dominated by recurring β-turns [25-29]. It has been also suggested that the β-structures are important for intermolecular interactions of the peptides [30, 31]. Unlike the reports discussing β-structures, previous studies have revealed that the structures of ELPs fluctuate between folded and disordered structures depending on the temperature [25, 26]. Due to such confusion of discussion, the essential structural factors for regulating the coacervation of ELPs have not been clarified. Thus,

further structural analyses of ELPs in conjunction with self-assembly measurements to detect interpeptide interactions are required for elucidating the general mechanism of coacervation.

Short-length ELPs with self-assembling properties would be useful in the structural and mechanistic analyses of the coacervation, because of the simplified structures and their easy preparations. Previous studies indicated that one of the representative ELPs, $(VPGVG)_n$ required a significantly large repetition number ($n > 40$) for coacervation [32, 33]. In general, it is difficult to investigate the structure in solution of such a long-length peptide chain (> 200 amino acid residues) without having a fixed conformation. On the contrary, previous studies have also demonstrated that synthetic hydrophobic ELP analogs, H-$(IPGVG)_n$-NH_2, H-$(FPGVG)_n$-NH_2 (abbreviated as Fn), and H-$(WPGVG)_n$-NH_2 (abbreviated as Wn) [33-35] exhibit coacervating property at significantly smaller repetition numbers ($n = 7$, 5, and 3, respectively). It was indicated that the increased hydrophobicity enhanced their self-assembling property. Furthermore, it was recently reported that dimeric analogs of F5, which were synthesized by introduction of disulfide bonds at N-terminal of F5 via additional Cys residues, showed strong coacervating properties. The coacervating temperatures and concentrations of the F5-dimers were (much) lower than that of F5-monomer [36]. Short ELPs synthesized by disulfide bond-mediated dimerization enabled structural analyses and simultaneous measurements of coacervation. Thus, the dimeric elastin-derived peptides were assumed to be useful models for elucidating the mechanism of coacervation because of their short peptide length with strong coacervation activity. Additionally, the related multimerization technique has recently become popular to control the self-assembling property of ELPs [37-44]. Knowledge of how the multimerization affects the ELPs may be useful for controlling characteristics of ELPs and for future application using ELPs.

In this study, we synthesized the novel, dimeric elastin-derived peptide analog (H-$C(WPGVG)_3$-$NH_2)_2$, abbreviated as (CW3)2, and investigated its self-assembly properties, dye uptake ability, and elucidate the structural features that are important for coacervation. The short elastin-derived peptide analog did not show specific, ordered secondary structures with increasing temperature in solution. Moreover, the increase in the exposed hydrophobic surface area associated with the structural change induced interpeptide interactions. This study revealed the relationship between the structure and function of short ELPs, in particular, suggested the stepwise mechanism of coacervation of ELPs.

2. Materials and methods

Chemicals

Fmoc-amino acids and Rink Amide MBHA resin LL (100–200 mesh) were purchased from Merck KGaA (Darmstadt, Germany). 2-(1H-Benzotriazol-1-yl)-1,1,3,3-tetramethyluronium hexafluorophosphate (HBTU) and 1-hydroxybenzotriazole (HOBt)

were purchased from Kokusan Chemical Co., Ltd. (Tokyo, Japan). 8-Anilino-1-naphthalenesulfonic acid (1,8-ANS) was purchased from Sigma-Aldrich Co. (St. Louis, MO). Water for sample preparation was purified by Milli-Q Integral 3 (Merck Millipore, Billerica, MA). Other reagents for peptide synthesis were purchased from Watanabe Chemical Industries Ltd. (Hiroshima, Japan). Solvents for peptide synthesis and other reagents for analyses were also obtained from commercial suppliers and used without further purification.

Synthesis of the Monomer Peptide

A building block of the dimer H-C(WPGVG)$_3$-NH_2 (abbreviated as CW3) was synthesized by following the synthesis method described in our previous study [36]. Briefly, CW3 was synthesized by ABI 433A peptide synthesizer with the FastMoc™ protocol (Applied Biosystems, Foster city, CA) which consists of a solid-phase method with the Fmoc-chemistry. 0.45 M HBTU and HOBt mixed solution in DMF was used for coupling reaction in FastMoc 0.10 mmol program included in SynthAssist™ 2.0 software (Applied Biosystems). After the elongation of peptides chain, the peptide was cleaved from the resin with the reagents cocktails containing 94% trifluoroacetic acid (TFA), 2.5% 1,2-ethanedithiol, 2.5% H_2O and 1% triisopropylsilane. The peptide was pre-purified by Sep-pak Vac 35cc C18 (Waters Co., Milford, MA) column. Subsequently, further purification was performed by RP-HPLC (The Breeze™ 2 HPLC System, Waters Co.) equipped with a ODS column (LiChrospher® RP-18 (20 x 250 mm), Merck KGaA, Darmstadt, Germany) with a solvent system consisting of 0.1% TFA aqueous solution (v/v) and 80% acetonitrile solution diluted with 0.1% TFA aqueous solution (v/v). The peptide was obtained as a colorless powder (40.5 mg, 25.2 μmol, 25.2%). Purity and molecular weights of the peptide were analyzed by ACQUITY UPLC H-Class (Waters Co.) equipped with an ACQUITY UPLC BEH C-18 column (100 mm, flow rate 0.6 mL/min) (Waters Co.) at 49 ˚C and the eluting product was detected by UV at 225 nm and a quadrupole mass spectrometer, ACQUITY QDa (Waters Co.). The solvent system for UPLC consisted of 0.1% formic acid aqueous solution (v/v, solvent A) and 0.1% formic acid in acetonitrile (v/v, solvent B). The peptide was monitored in a linear gradient of solvent A in solvent B, 24% to 56% over 4.23 min.

CW3 : H-C(WPGVG)$_3$-NH_2

Retention time = 1.907 min. MS (ESI) m/z: calculated for $C_{78}H_{104}N_{20}O_{16}S$ 805.94 ($[M + 2H]^{2+}$), found 805.96.

Synthesis of the Dimeric Peptide

Dimeric peptide (CW3)2 was synthesized by aerobic oxidation of purified CW3. CW3 (6.49 mg, 4.03 μmol) was dissolved in a 1 mg/mL ammonium bicarbonate/60% acetonitrile aqueous solution (649 μL) [37]. This solution was stirred overnight at 5°C by a rotator (ACR-100, AS ONE Co., Osaka, Japan), in shake mode. The resulting mixture was purified by the RP-HPLC. The peptide was obtained as a colorless powder (5.88 mg, 1.82 μmol, 90.3%). The purity and molecular weight were confirmed by UPLC–MS in the method described above. The molecular weight of the dimeric peptide was also strictly determined by matrix-assisted laser desorption ionization (MALDI) time-of-flight (TOF) MS using a mass spectrometer (Voyager DE-PRO, PerSeptive Biosystems Inc., Framingham, MA).

(CW3)2 : (H-C(WPGVG)$_3$-NH$_2$)$_2$

Retention time = 2.438 min. MS (ESI) m/z: calculated for $C_{156}H_{206}N_{40}O_{32}S_2$ 1073.59 ($[M + 3H]^{3+}$), found 1073.46. MS (MALDI-TOF) m/z: calculated 3218.75 ($[M + H]^{+}$), found 3218.58.

Synthesis of linear peptides corresponding to chain length of (CW3)2

H-C(H-Cys-NH$_2$)(WPGVG)$_6$-NH$_2$ (abbreviated as C(Cys)W6) was synthesized by solid-phase method with the Fmoc-chemistry and the aerobic oxidation. H-C(WPGVG)$_6$-NH$_2$ (abbreviated as CW6) was synthesized and purified in the same manner as CW3. The peptide was obtained as a colorless powder (10.9 mg, 3.37 μmol, 3.39%). The purity and molecular weight were confirmed by UPLC–MS in the condition described above. Disulfide bond formation between CW6 (2.43 mg, 0.755 μmol) and H-Cys-NH$_2$ (28.5 mg, 0.237 mmol) was performed by aerobic oxidation in 10 mg/ml ammonium bicarbonate/60% acetonitrile aqueous solution (2.43 ml). The solution was stirred for 2 hour at 5°C by the rotator, in shake mode. The resulting mixture was purified by RP-HPLC. The peptide was obtained as a colorless powder (1.03 mg, 0.320 μmol, 42.4%). The purity and molecular weight were confirmed by UPLC–MS in the described condition. The molecular weight of the peptide was also strictly determined by matrix-assisted laser desorption ionization MALDI-TOF MS using a mass spectrometer, Bruker Autoflex II (Bruker Daltonics Inc., Billerica, MA).

CW6 : H-C(WPGVG)$_6$-NH$_2$

Retention time = 3.002 min. MS (ESI) m/z, calculated for $C_{153}H_{197}N_{37}O_{31}S$ 1034.20 ($[M + 3H]^{3+}$), found 1034.38.

C(Cys)W6 : H-C(H-Cys-NH_2)(WPGVG)$_6$-NH_2

Retention time = 2.650 min. MS (ESI) m/z, calculated for $C_{156}H_{206}N_{40}O_{32}S_2$: 1073.59 ($[M + 3H]^{3+}$), found 1073.67. MS (MALDI-TOF) m/z, calculated 3240.73 ($[M + Na]^+$), found 3241.09.

Turbidity Measurement

The temperature-dependent coacervation of (CW3)2 and C(Cys)W6 was evaluated using a JASCO V-660 spectral photometer, (JASCO Co., Tokyo, Japan). Solutions of (CW3)2 were prepared at concentrations of 0.050, 0.50, and 1.0 mg/mL in pure water. C(Cys)6 was prepared at concentration of 0.05 mg/ml. In addition, supernatant of 0.5 mg/ml C(Cys)6 was also prepared by centrifugation. Turbidity measurements were performed at 400 nm while the temperature was being increased or decreased at a rate of 0.2 °C/min (for the 0.50 and 1.0 mg/mL (CW3)2 and supernatant of 0.5 mg/ml C(Cys)W6) or 0.5 °C/min (for the 0.05 mg/mL samples) from 5°C. Each concentration was measured at least three times. Coacervation was determined by the phase transition temperature (T_t), which is the temperature at which the turbidity of the solution reaches half the maximum value [36]. Reversibility was defined as the percent decrease in solution turbidity after cooling to 5°C (which took at least 8 h) to the increase in absorbance after increasing the temperature [45].

Fluorescence Measurement

The fluorescence of (CW3)2 was measured using 1,8-ANS and was determined on a model FP-8500 fluorescence spectrometer (JASCO Co.). The fluorescence intensity of the peptide solution was measured between 400 and 700 nm with an excitation wavelength of 370 nm. The emission of the peptide solution was measured at various concentration of 0.003–0.5 mg/mL in pure water containing 50 μM 1,8-ANS [46], with increasing the temperature in intervals 10°C from 5 to 25°C. The measurement of each concentration was performed at least three times.

Dynamic Light Scattering (DLS) Analysis

The distribution of the particle size in the (CW3)2 solution was analyzed by DLS measurement using Zetasizer nano ZS (Malvern Instruments Ltd., Worcestershire, U.K.) in a measurement cell (ZEN0112, Malvern Instruments Ltd.). The peptide sample solution was diluted to a concentration of 1.0 mg/mL in pure water and filtered using the Millex-LG (Cat. NO. SLLGH04NL, Merck Millipore) 0.20 μm syringe driven filter unit before measurement. DLS analysis was performed by increasing the temperature in 10°C intervals from 5 to 65°C. The measurement duration was selected automatically. Protein (refractive index, 1.450; absorption, 0.001) was used as the material, and water (refractive index, 1.330; viscosity,

0.8872) was chosen as the dispersant. Attenuation was selected automatically. The measurement of each concentration was performed at least three times.

Optical Microscopy

The morphologies of the coacervates of (CW3)2 in the presence and absence of a water-soluble dye, Ponceau S (Sigma-Aldrich Co.), were observed. The morphology without dye was by bright-field microscopy at 180× magnification using a BIOREVO BZ-9000 instrument (KEYENCE Co., Osaka, Japan) equipped with a PlanApo VC 60× oil objective (3× digital zoom; Nikon Co., Tokyo, Japan). The peptide solution was diluted to 1 mg/mL in pure water and applied to a glass slide. Sample imaging was performed at 25°C or after heating to 60°C on a hot plate for 30 s.

Coacervates containing dye were prepared as follows. 1.0 mg/mL (CW3)2 solution was prepared with 25 mM Ponceau S at 4°C. The mixture was heated to 60°C for 1 h and then centrifuged (14,000 rpm for 2 min). The resulting precipitate was washed with hot water (60°C). Bright-field microscopy was performed at 400× magnification using a Leica DM IL LED instrument (Leica Microsystems CMS GmbH, Wetzlar, Germany) equipped with a HI PLAN 40× oil objective (Leica Microsystems CMS GmbH) and an HC PLAN 10× eyepiece (Leica Microsystems CMS GmbH).

Molecular Dynamics (MD) Simulation

MD simulations of (CW3)2 and H-(WPGVG)$_3$-NH_2 (W3) were performed by using a DELL PRECISION T3610 Workstation (Dell Inc., Round Rock, TX) and a software package of the Discovery Studio 4.0 (Accelrys, Inc., San Diego, CA). The trajectories of these peptide were obtained at simulation temperature of 278, 294, 310, 326, and 343 K. The simulation parameters were set as described in a previous study [36]. The structure of each peptide were constructed as an "extended" conformation. The models were applied to "Standard Dynamics Cascade" protocol, which contains a series of energy minimization and molecular dynamics steps with the CHARMm force field and generalized born with simple switching (GBSW) implicit solvent model. A first step of minimization using steepest descent algorithm, using a maximum of 10,000 steps, repulsive guidance molecule (RGM) gradient of 1.0, and no constraints; followed by a second step of minimization using Conjugate Gradient algorithm, using a maximum of 20,000 steps, root mean square (RMS) gradient of 0.1, and no constraints; heating step: parameters were 400 steps, time step 2 fs, initial temperature 50.0 K, target temperature 278.0 K, 310.0 K, or 343.0 K, and no constraints; an equilibration step: parameters were 1,000 steps with a time step of 2 fs, target temperature 278.0 K, 310.0K, or 343.0 K, no constraints, constant pressure; and finally, a production step consisting of 50,000 steps, time step 2 fs, target temperature 278.0 K, 310.0 K, or 343.0 K,

temperature coupling decay time=5.0 ps, no constraints, type=constant volume constant temperature ensemble (NVT), TMass=1,000.0, nonbond list radius=14, nonbond higher cutoff distance=12, nonbond lower cutoff distance=10, electrostatics=spherical cutoff, Kappa=0.34, order=4, dynamics integrator=leapfrog verlet, apply SHAKE constraint=true.

Circular Dichroism (CD) Measurement

CD measurement was performed in a 1.0 mm path-length cuvette using a JASCO J-725 spectropolarimeter (JASCO Co.). (CW3)2 was dissolved in pure water at a concentration of 0.1 mg/mL. Spectra of the sample solution were measured from 260 to 190 nm at various cell temperatures between 5 and 65°C. All spectra of the peptide solution were obtained by subtracting the solvent spectra obtained under the same conditions and smoothing with Savitzky–Golay smoothing filters. The measurement was performed twice.

3. Results and discussion

Synthesis of the peptides

(CW3)2 and C(Cys)W6 were successfully synthesized by the conventional solid phase peptide synthesis procedure and the aerobic oxidation. These structure was shown in figure 1. The resulting monomeric peptide CW3 and C(Cys)W6 were then dimerized by aerobic oxidation in a 60% acetonitrile aqueous solution with ammonium bicarbonate. The dimerization was not successful in pure water because of the production of an insoluble precipitate of monomeric peptide. Therefore, an acetonitrile aqueous solution was used to dissolve the peptide deposition. The purity and molecular weight of each peptide were confirmed by RP-UPLC–MS and MALDI-TOF MS. These results were shown in figures 2 and 3. The synthetic yield of the (CW3)2 was approximately 90%. In summary, we found that the reaction conditions were suitable for obtaining a dimeric short elastin-like peptide with a high yield.

(Figures 1, 2, and 3)

Coacervation of the dimeric peptide

The temperature-dependent coacervation of the synthetic peptide, (CW3)2, was evaluated by measuring the turbidity of aqueous (CW3)2 solutions at various concentrations. To quantitatively evaluate coacervation, T_t and reversibility were calculated from the change in turbidity (Table 1) [36, 45]. Our previous study showed that at least 30 mg/mL W3 monomer was required to demonstrate turbidity [35]. In comparison with the W3 monomer, (CW3)2 showed coacervation at significantly lower concentrations of 0.50 and 1.0 mg/mL, indicating that dimerization significantly enhanced the coacervation of the W3 monomer. These data were shown in figure 4A. Similarly, this trend has been observed in dimeric

peptides of F5 [36]. However, F5 dimers required higher concentration (at least 10 mg/mL) and longer chain length than W3 dimer to exhibit coacervation. Thus, it was confirmed that (CW3)2 possessed a coacervation propensity that was stronger than the F5 dimer did. Short chain peptides that exhibit various functional properties at low concentrations can be advantageous for analytical experiments and applied researches [33−36] Thus, we hypothesized that (CW3)2 could be used to elucidate the mechanism of the self-assembly. We concluded that dimeric peptides demonstrate characteristics distinct from those of their linear peptide analogs that have longer peptide chains. Specifically, (CW3)2 showed enhanced coacervation with maintaining high water solubility, whereas the linear 6-mer analog of (WPGVG), C(Cys)W6, showed low water solubility and irreversible self-assembly (Figure 4B). Thus, dimerization of ELPs is an effective method for obtaining peptide analogs that possess strong coacervation abilities and are easy to handle.

(Table 1)

(Figure 4)

In this study, we found that (CW3)2 showed hysteresis during coacervation. In the turbidity assay profile, the two turbidity curves of (CW3)2 during heating were slightly different from those during cooling. This disagreement between the heating and cooling processes would indicate that aggregates formed during heating retained their structures at temperatures below the T_t. However, the turbidity of the dimer solution gradually decreased when the temperature reached < 10°C with some additional time. Finally, almost complete reversibility of the turbidity was observed after maintaining a low temperature for several hours (5°C for at least 8 h). This hysteresis was also observed for the F5 dimer [36] and other ELPs, such as $(APGVGV)_n$, $(VPAVG)_n$, and ($EP20–24^4$) that contains four repeating of exons 20–24 from the human aortic elastin gene [46-48]. These previous studies determined that the aggregation and dissociation rates of the ELPs disagreed with each other. Similar to these reports, the dissociation of (CW3)2 progressed more slowly than the aggregation. These results suggested that hysteresis during coacervation of (CW3)2 was caused by the differences in the association and dissociation rates.

Existence of invisible initial microcoacervates

The self-assembly behavior of (CW3)2 was examined by the use of the fluorescent probe 1,8-ANS [49]. The results were shown in figure 5. Fluorescence spectra of 1,8-ANS maximized at near 480 nm. The fluorescence intensity became increased when the concentration of the (CW3)2 solution was >0.03 mg/mL (Figure 5A). This increase in the fluorescence intensity indicated that 1,8-ANS was incorporated into the hydrophobic peptide assemblies. These results showed that the peptides required a critical concentration to form

assemblies, and that the initial microaggregates may be generated above the boundary concentration.

(Figure 5)

The effect of temperature on the critical concentration of (CW3)2 was also investigated by the fluorescence measurement. The analysis was performed only at relatively low temperatures (5, 15, and 25°C), because the fluorescence intensity was significantly decreased at higher temperatures where (CW3)2 formed aggregates. The critical concentrations were analyzed by the two-line method [49] and were calculated as 0.031 ± 0.05, 0.032 ± 0.05, and 0.033 ± 0.05 mg/mL at 5, 15, and 25°C, respectively. These results were ahown in figure 5. The determined critical concentrations were significantly lower than the concentrations at which the peptide solution became turbid, suggesting that the formation of initial invisible microaggregates occurred at a low temperature and at a concentration where coacervation was apparently not observed. Consequently, fluorescence analysis has revealed a novel morphology of (CW3)2, that is, invisible microaggregates were initially formed in peptide solution below the temperature of T_t, although they could not be observed by conventional turbidity measurements.

Size distribution of the microaggregates

The coacervation behavior of (CW3)2 was also analyzed by DLS analysis at various temperatures in the range from 5 to 65°C. The observed distribution of the hydrodynamic diameter of the peptide aggregates is shown in figure 6. At between 5 and 25°C, (CW3)2 showed a broad distribution around approximately 100 nm. Thus, at low temperature, (CW3)2 showed submicrometer aggregates that did not induced apparent turbidity in visible light region. In addition, the size of the aggregates increased with an increase in temperature. Because light scattering and turbidity are dependent on particle size, the growth of the aggregates would imply coacervation. On the basis of the DLS analysis, we suggested that the coacervation of (CW3)2 probably follows a stepwise process in which the generation of microaggregates is followed by coacervate maturation triggered by the increase in temperature.

(Figure 6)

Observation of the coacervate morphology

Optical microscopy analysis of the (CW3)2 solution was performed to study the morphology of the aggregates at different temperatures. Microscopic images of the peptide solution were captured at 25°C and after heating to 60°C. These data were shown in figure 7. At 25°C, dozens of distorted and nonspherical microaggregates were observed (Figure 7A). This results indicated that microaggregates of (CW3)2 were formed below the phase

transition temperature. Although small microaggregates between 0.2 and 0.8 μm in diameter were hardly observed in solution, microaggregates between 0.8 and 1.0 μm in diameter, which were also observed in the DLS measurement, were commonly identified in the observation at 25°C (Figure 7C). After heating to 60°C, the number of spherical coacervates was significantly increased. In the observation at 60°C, microaggregates between 0.8 and 1.0 μm in diameter were also predominantly observed (Figure 7B and 7D). Because of the limited resolution of the optical microscope, small microaggregates (approximately less than 200 nm) were hardly observed; therefore, results of the microscopic measurements were not as specific as those of the DLS, and the size distribution also did not necessarily agree with that determined by the DLS. In the optical microscope study, the increase in the distribution of large aggregates was similar to that observed in the DLS measurement (Figure 6). However, the change in the dominant distribution found in the DLS, that is, the distribution trend changed in temperature alteration was not clearly observed by the optical microscopy. Consequently, it was suggested that the increment in turbidity during coacervation was derived from the proliferation of the aggregates observed during microscopy and the increase in the distribution of large aggregates, which also could be observed by DLS. The morphological changes in the peptide aggregates were thought to affect the coacervation behavior directly. Because these results were consistent between fluorescence and DLS analyses, the hypothesis of the stepwise coacervation process was strongly supported.

(Figure 7)

Furthermore, the ability to hold a water-soluble dye in the coacervate of (CW3)2 was observed by optical microscopy. As shown in figure 8, dye uptake of sub-micro meter coacervates of the (CW3)2 was observed at 60°C and the co-mixtures were stable during observation at 25°C. The uptake ability of exogenous molecules such as drugs and the stability of the coacervate at low temperatures might be useful for the development of ELP-derived biomaterials possessing temperature-sensing capabilities, such as matrices for drug delivery systems or tissue engineering.

(Figure 8)

Estimation of the structural properties of the dimeric peptide by MD simulation

The analysis of the structural properties of the dimeric peptide was valuable for estimation of the intermolecular events of self-assembly. Thus, the conformational behavior of W3 and (CW3)2 in the solution was estimated by MD simulation at various target temperatures. In addition, the structural parameters of these peptides were analyzed from the trajectories of the MD simulation.

A proportion of the representative secondary structures in the peptides was calculated

from the trajectory. The representative structures of W3 and (CW3)2 at varying temperatures are shown in figure 9. The secondary structures were determined by using the method of Kabsch and Sander [50]. The peptides primarily showed turns, sheets, and random-coil structures. The ratios of each secondary structure on a residue were also estimated and shown in table 2, figures 10, and 11. The turn structure frequently appeared in each PGV sequence and was present in the middle of the building block. The sheet structures were formed frequently in VG and WP sequences, that were present at either side of the turns (Figure 10). These peptides exhibited a well-folded structure and a smaller R_g between 278 and 310 K (Table 2). As shown in figures 9 and 10, accumulated turn structures were frequently observed in the dimer at 273 K. In addition, the consecutive secondary structure sheet–turn–sheet motif was frequently observed at 294 and 310 K. However, the proportion of these secondary structures decreased with an increased simulation temperature. A random-coil structure was predominantly observed at 326 and 343 K. These results suggested that the dimeric peptide possessed a tendency to alter the ordered structure observed at low temperatures to a disordered structure at higher temperatures.

(Table 2)

(Figures 9, 10, and 11)

The R_g and total solvent-accessible surface area (SASA) values were calculated to describe the manner in which the structural changes of the peptide chain were associated with the change in temperature (Table 2). These values increased gradually with an increase in temperature. Notably, the changes in the R_g and SASA values of the dimeric peptide were greatly larger than those of the monomer, which suggested that the dimeric peptide experienced a remarkable change in structure with an increase in temperature. The SASA value of the side chain on each residue was also calculated in the trajectory at various simulation temperatures (Figure 11). Although the SASA value of each residue tended to increase with an increase in temperature, the change in the dimer was more significant than that in the monomer. In particular, the SASA values of hydrophobic residues, such as valine and tryptophan, were markedly altered in the dimeric peptide. As the SASA value of the monomer did not change drastically, it was plausible that the molecular surface of the monomeric peptide was exposed in both ordered and disordered states. In contrast, it has been suggested that the hydrophobic surface of the dimeric peptide would be embedded when the peptide is dissolved in water, which implied that the estimated molecular structure of the dimeric peptide preserved its water solubility by effectively embedding hydrophobic residues into the interface between single peptide chains. The increase in the SASA value with a corresponding increase in temperature indicated that the secondary structures could collapse and the folded structure of the dimeric peptide shifted to an extended structure.

Because the extended structure of (CW3)2 was not dispersible in water, the molecules of (CW3)2 could assemble via hydrophobic effect. This drastic change in the hydrophobic surface may contribute to the potent coacervation property of (CW3)2. Furthermore, these results may indicate that coacervation occurred primarily as a result of the exposure of the hydrophobic surface of the peptides and not as a result of the formation of a particular conformation.

Temperature-dependent structural transitions of the dimeric peptide

Because the conformational change in (CW3)2 was temperature-dependent, its structure was further analyzed by circular dichroism spectroscopy. A reversible spectrum shift was observed during heating and cooling processes. This result was shown in figure 12. The spectrum showed a slightly negative band at 242 nm, a positive peak at 225 nm, and a prominent negative peak at 198 nm. As the temperature increased, the intensity of these bands decreased; this result was similar to the CD spectra of the W5 monomer observed in our previous study [35]. Thus, the dimeric peptide exhibited conformational changes similar to those of the monomer. Conversely, it was considered that the structural features of the peptide were not altered by dimerization, because of high similarity in spectra between W5 and (CW3)2. In addition, this spectral change was similar to that observed during disordering of collagen helices or polyproline helix II structures [51-53]. Thus, it was suggested that the dimeric peptide formed an ordered structure based on proline residues at low temperatures and was converted to a disordered structure while being heated.

(Figure 12)

Mechanism of the stepwise coacervation of ELP

The stepwise coacervation process of dimeric peptide (CW3)2, with detailed analyses of the morphology after coacervation, is shown in figure 13. As shown in figure 5, (CW3)2 exhibited a critical concentration for the generation of initial microaggregates. Then, these aggregates matured at higher temperatures, showing the increase in size and proliferation. To the best of our knowledge, we report the first demonstration of these characteristic properties of the ELP analog using the tryptophan residue in the repetitive sequence. Previous studies showed that the hydrophobicity of the residue enhanced the coacervation property of ELP [14-18, 33, 34]. In addition to these preceding studies, this study reveals that the hydrophobicity of the residue affected the morphology of the coacervates. Hydrophobic amino acids are abundantly contained in tandem repeats of elastin. Therefore, the morphology of elastin could be regulated by an ingenious combination of hydrophobic amino acid residues.

(Figure 13)

Insights into the mechanism of coacervation of the dimeric peptide

In this study, we demonstrated novel insight into the relationship between the structure and coacervation property of ELPs. The hydrophobicity of (CW3)2 was extremely high; the peptide formed microaggregates, even at low concentrations and temperatures. Previous studies suggested that ELPs exhibit coacervation via collapse of the clathrate water [8, 17, 21-24]. Therefore, it was considered that the strong hydrophobicity of the dimeric peptide effectively destabilized the hydrating water. Consequently, the potent coacervation property of (CW3)2 that resulted from the hydrophobic interpeptide interaction occurred during the early stages of aggregate formation (Figure 13). Previous studies suggested that the manner of the structural shift of ELP was dependent on the peptide chain length [29, 40, 54]. Moreover, it was considered that longer ELPs exhibited stronger coacervation properties and were likely to show ordered structures at high temperatures [40, 54]. However, the results of this study clearly indicated that the short dimeric elastin-like peptide (CW3)2 possessed a potent coacervation property and its structure was disordered at high temperatures where the aggregation occurred. Thus, this study showed that the expression of coacervation property did not necessarily require for a long peptide chain length or a specific ordered structure at high temperatures but required potent hydrophobicity and soluble structures at low temperatures. Therefore, we believe that this study offered new insights into the self-assembly mechanism of ELPs, based on the results of hydration, dispersion, and conformational analyses of the hydrophobic molecule. The study of IDPs, including ELPs, has gained momentum in recent years [1-4, 6, 11] and the applications of ELPs have been fervently studied [9, 10, 13]. The study of ELPs presented here appears to provide insights with respect to its structure and coacervation properties that would assist the design of more efficient ELPs for industrial applications and support future researches on IDPs.

4. Conclusion

In this study, novel elastin-derived dimeric peptide (CW3)2 was assayed in turbidity measurements, fluorescence microscopy, DLS, MD simulation, and CD spectroscopy, as a model-peptide for ELPs studies. The results revealed that the hydrophobicity of the residues regulated the morphology of the aggregates. Moreover, it was shown that the dimeric peptide exhibited strong coacervation and the ability to take up dye, despite its low molecular weight and disordered structure at high temperatures. It was also suggested that the coacervation was dependent on the hydrophobicity and structural solubility at low temperatures rather than the high-molecular weight or formation of any specific ordered structures at high temperatures. In conclusion, these findings elucidated the coacervation mechanism of the short-length ELP dimer and demonstrated the potential for the future development of short coacervatable peptide-based biomaterials.

5. References

[1] Tompa P., Unstructural biology coming of age, *Curr. Opin. Struct. Biol.*, **21**, 419-425 (2011).

[2] Chouard T., Structural biology: Breaking the protein rules, *Nature*, **471**, 151-153 (2011).

[3] Mittag T., Kay L. E., Forman-Kay J. D., Protein dynamics and conformational disorder in molecular recognition, *J. Mol. Recognit.*, **23**, 105-116 (2010).

[4] Peysselon F., Xue B., Uversky V. N., Ricard-Blum S., Intrinsic disorder of the extracellular matrix, *Mol. Biosyst.*, **7**, 3353-3365 (2011).

[5] Vrhovski B., Weiss A. S., Biochemistry of tropoelastin, *Eur. J. Biochem.*, **258**, 1-18 (1998).

[6] Muiznieks L. D., Weiss A. S., Keeley F. W., Structural disorder and dynamics of elastin, *Biochem. Cell Biol.*, **88**, 239-250 (2010).

[7] Pepe A., Guerra D., Bochicchio B., Quaglino D., Gheduzzi D., Pasquali Ronchetti I., Tamburro A. M., Dissection of human tropoelastin: supramolecular organization of polypeptide sequences coded by particular exons, *Matrix Biol.*, **24**, 96-109 (2005).

[8] Yeo G. C., Keeley F. W., Weiss A. S., Coacervation of tropoelastin, *Adv. Colloid Interface Sci.*, **167**, 94-103 (2011).

[9] MacEwan S. R., Chilkoti A., Applications of elastin-like polypeptides in drug delivery, *J. Control Release*, **190**, 314-330 (2014).

[10] Nettles D. L., Chilkoti A., Setton L. A., Applications of elastin-like polypeptides in tissue engineering, *Adv. Drug Deliv. Rev.*, **62**, 1479-1485 (2010).

[11] Roberts S., Dzuricky M., Chilkoti A., Elastin-like polypeptides as models of intrinsically disordered proteins, *FEBS Lett.*, **589**, 2477-2486 (2015).

[12] Foster J. A., Bruenger E., Gray W. R., Sandberg L. B., Isolation and amino acid sequences of tropoelastin peptides, *J. Biol. Chem.*, **248**, 2876-2879 (1973).

[13] Urry D. W., Physical chemistry of biological free energy transduction as demonstrated by elastic protein-based polymers, *J. Phys. Chem. B*, **101**, 11007–11028 (1997).

[14] Ribeiro A., Arias F. J., Reguera J., Alonso M., Rodríguez-Cabello J. C., Influence of the amino-acid sequence on the inverse temperature transition of elastin-like polymers, *Biophys. J.*, **97**, 312-320 (2009).

[15] Chilkoti A., Christensen T., MacKay J. A., Stimulus responsive elastin biopolymers: Applications in medicine and biotechnology, *Curr. Opin. Chem. Biol.*, **10**, 652-657 (2006).

[16] Meyer D. E., Chilkoti A., Quantification of the effects of chain length and concentration on the thermal behavior of elastin-like polypeptides, *Biomacromolecules*, **5**, 846-851 (2004).

[17] Miao M., Bellingham C. M., Stahl R. J., Sitarz E. E., Lane C. J., Keeley F. W.,

Sequence and structure determinants for the self-aggregation of recombinant polypeptides modeled after human elastin, *J. Biol. Chem.*, **278**, 48553-48562 (2003).

[18] Quiroz F. G., Chilkoti A., Sequence heuristics to encode phase behaviour in intrinsically disordered protein polymers, *Nat. Mater*, **14***,* 1164-1171 (2015).

[19] Rauscher S., Baud S., Miao M., Keeley F. W., Pomès R., Proline and glycine control protein self-organization into elastomeric or amyloid fibrils, *Structure*, **14**, 1667-1676 (2006).

[20] Muiznieks L. D., Keeley F. W., Proline periodicity modulates the self-assembly properties of elastin-like polypeptides, *J. Biol. Chem.*, **285**, 39779-39789 (2010),

[21] Li B., Alonso D. O., Daggett V., The molecular basis for the inverse temperature transition of elastin, *J. Mol. Biol.*, **305**, 581-592 (2001).

[22] Urry D. W., Urry K. D., Szaflarski W., Nowicki M. Elastic-contractile model proteins: Physical chemistry, protein function and drug design and delivery, *Adv. Drug. Deliv. Rev.*, **62**, 1404-1455 (2010).

[23] Vrhovski B., Jensen S., Weiss A. S., Coacervation characteristics of recombinant human tropoelastin, *Eur. J. Biochem.*, **250**, 92-98 (1997).

[24] Urry D. W., The change in Gibbs free energy for hydrophobic association: Derivation and evaluation by means of inverse temperature transitions, *Chem. Phys. Lett.*, **399**, 177–183 (2004).

[25] Li N. K., García Quiroz F., Hall C. K., Chilkoti A., Yingling Y. G., Molecular description of the LCST behavior of an elastin-like polypeptide, *Biomacromolecules*, **15**, 3522-3530 (2014).

[26] Reiersen H., Clarke A. R., Rees A. R., Short elastin-like peptides exhibit the same temperature-induced structural transitions as elastin polymers: implications for protein engineering, *J. Mol. Biol.*, **283**, 255-264 (1998).

[27] Toonkool P., Regan D. G., Kuchel P. W., Morris M. B., Weiss A. S., Thermodynamic and hydrodynamic properties of human tropoelastin. Analytical ultracentrifuge and pulsed field-gradient spin-echo NMR studies, *J. Biol. Chem.*, **276**, 28042-28050 (2001).

[28] Bochicchio B., Aït-Ali A., Tamburro A. M., Alix A. J., Spectroscopic evidence revealing polyproline II structure in hydrophobic, putatively elastomeric sequences encoded by specific exons of human tropoelastin, *Biopolymers*, **73**, 484-493 (2008).

[29] Nuhn H., Klok H. A., Secondary structure formation and LCST behavior of short elastin-like peptides, *Biomacromolecules*, **9**, 2755-2763 (2008).

[30] Tamburro A. M., Guantieri V., Gordini D. D., Synthesis and structural studies of a pentapeptide sequence of elastin. Poly (Val-Gly-Gly-Leu-Gly), *J. Biomol. Struct. Dyn.*, **10**, 441-454 (1992).

[31] Maeda I., Fukumoto Y., Nose T., Shimohigashi Y., Nezu T., Terada Y., Kodama H., Kaibara K., Okamoto K., Structural requirements essential for elastin coacervation:

favorable spatial arrangements of valine ridges on the three-dimensional structure of elastin-derived polypeptide $(VPGVG)_n$, *J. Pept. Sci.*, **17**, 735-743 (2011).

[32] Kaibara K., Akinari Y., Okamoto K., Uemura Y., Yamamoto S., Kodama H., Kondo M., Characteristic interaction of Ca^{2+} ions with elastin coacervate: ion transport study across coacervate layers of alpha-elastin and elastin model polypeptide. $(Val\text{-}Pro\text{-}Gly\text{-}Val\text{-}Gly)_n$, *Biopolymers*, **39**, 189-198 (1996).

[33] Maeda I., Taniguchi S., Ebina J., Watanabe N., Hattori T., Nose T., Comparison between coacervation property and secondary structure of synthetic peptides, Ile-containing elastin-derived pentapeptide repeats, *Protein Pept. Lett.*, **20**, 905-910 (2013).

[34] Maeda I., Taniguchi S., Watanabe N., Inoue A., Yamasaki Y., Nose T., Design of Phenylalanine-Containing Elastin-Derived Peptides Exhibiting Highly Potent Self-Assembling Capability, *Protein Pept. Lett.*, **22**, 934-939 (2015).

[35] Taniguchi S., Watanabe N., Nose T., Maeda I., Development of short and highly potent self-assembling elastin-derived pentapeptide repeats containing aromatic amino acid residues, *J. Pept. Sci.*, **22**, 36-42 (2016).

[36] Suyama K., Taniguchi S., Tatsubo D., Maeda I., Nose T., Dimerization effects on coacervation property of an elastin-derived synthetic peptide $(FPGVG)_5$, *J. Pept. Sci.*, **22**, 236-243 (2016).

[37] Aladini F., Araman C., Becker C. F., Chemical synthesis and characterization of elastin-like polypeptides (ELPs) with variable guest residues, *J. Pept. Sci.*, **22**, 334-342 (2016).

[38] Dhandhukia J., Weitzhandler I., Wang W., MacKay J. A., Switchable elastin-like polypeptides that respond to chemical inducers of dimerization, *Biomacromolecules*, **14**, 976-985 (2013).

[39] Ghoorchian A., Cole J. T., Holland N. B., Thermoreversible Micelle Formation Using a Three-Armed Star Elastin-like Polypeptide, *Macromolecules*, **43**, 4340–4345 (2010).

[40] Ghoorchian A., Holland N. B., Molecular architecture influences the thermally induced aggregation behavior of elastin-like polypeptides, *Biomacromolecules*, **12**, 4022-4029 (2011).

[41] Ghoorchian A., Vandemark K., Freeman K., Kambow S., Holland N. B., Streletzky K. A., Size and shape characterization of thermoreversible micelles of three-armed star elastin-like polypeptides, *J. Phys. Chem. B.*, **117**, 8865-8874 (2013).

[42] Fukushima D., Sk U. H., Sakamoto Y., Nakase I., Kojima C., Dual stimuli-sensitive dendrimers: Photothermogenic gold nanoparticle-loaded thermo-responsive elastin-mimetic dendrimers, *Colloids Surf. B. Biointerfaces*, **132**, 155-160 (2015).

[43] Navon Y., Zhou M., Matson J. B., Bitton R., Dendritic Elastin-like Peptides: The Effect of Branching on Thermoresponsiveness, *Biomacromolecules*, **17**, 262-270

(2016).

[44] Zhou M., Shmidov Y., Matson J. B., Bitton R., Multi-scale characterization of thermoresponsive dendritic elastin-like peptides, *Colloids Surf. B. Biointerfaces*, **153**, 141-151 (2017).

[45] Muiznieks L. D., Reichheld S. E., Sitarz E. E., Miao M., Keeley F. W., Proline-poor hydrophobic domains modulate the assembly and material properties of polymeric elastin, *Biopolymers*, **103**, 563-573 (2015).

[46] Urry D. W., Characterization of soluble peptides of elastin by physical techniques, *Methods Enzymol.*, **82**, 673-716 (1982).

[47] Herrero-Vanrell R., Rincón A. C., Alonso M., Reboto V., Molina-Martinez I. T., Rodríguez-Cabello J. C., Self-assembled particles of an elastin-like polymer as vehicles for controlled drug release, *J. Control. Release*, **102**, 113-122 (2005).

[48] Osborne J. L., Farmer R., Woodhouse K. A., Self-assembled elastin-like polypeptide particles, *Acta Biomater.*, **4**, 49-57 (2008).

[49] Kim W., Thévenot J., Ibarboure E., Lecommandoux S., Chaikof E. L., Self-assembly of thermally responsive amphiphilic diblock copolypeptides into spherical micellar nanoparticles, *Angew. Chem. Int. Ed. Engl.*, **49**, 4257-4260 (2010).

[50] Kabsch W., Sander C., Dictionary of protein secondary structure: Pattern recognition of hydrogen-bonded and geometrical features, *Biopolymers*, **22**, 2577-2637 (1983).

[51] Lopes J. L., Miles A. J., Whitmore L., Wallace B. A., Distinct circular dichroism spectroscopic signatures of polyproline II and unordered secondary structures: applications in secondary structure analyses, *Protein Sci.*, **23**, 1765-1772 (2014).

[52] Lam S. L., Hsu V. L., NMR identification of left-handed polyproline type II helices, *Biopolymers*, **69**, 270-281 (2003).

[53] Tamburro A. M., Lorusso M., Ibris N., Pepe A., Bochicchio B., Investigating by circular dichroism some amyloidogenic elastin-derived polypeptides, *Chirality,* **22**, E56-66 (2010).

[54] Zhao B., Li N. K., Yingling Y. G., Hall C. K., LCST Behavior is Manifested in a Single Molecule: Elastin-Like polypeptide $(VPGVG)_n$, *Biomacromolecules*, **17**, 111-118 (2016).

Table 1. The self-assembling property of (CW3)2. [a]

Concentration (mg/mL)	T_t (˚C)	Maximum OD_{400}	Reversibility (%)
1.0	38.5 ± 1.5	0.63 ± 0.03	97.9 ± 1.0
0.50	40.3 ± 1.5	0.41 ± 0.03	99.1 ± 0.8
0.050	NA.	0.03 ± 0.02	NA.

[a] Assays at concentrations of 1.0 and 0.50 mg/mL were performed seven times. The assay at a concentration of 0.050 mg/mL was repeated three times. Data were shown with SE.

Table 2. Structure data of (CW3)2 obtained from MD simulation. [a]

Temperature (K)	R_g (nm)	Total SASA (nm^2)	Secondary structure		
			Random coil (%)	Turn (%)	Sheet (%)
278.0	0.909 ± 0.002	23.57 ± 0.07	75.6 ± 0.5	23.1 ± 0.5	1.2 ± 0.3
294.0	0.929 ± 0.007	23.93 ± 0.12	61.2 ± 0.4	20.7 ± 0.2	17.9 ± 0.5
310.0	1.081 ± 0.015	26.57 ± 0.22	75.6 ± 0.6	19.4 ± 0.4	4.9 ± 0.5
326.0	1.468 ± 0.018	32.30 ± 0.22	85.3 ± 0.7	13.1 ± 0.6	1.3 ± 0.2
343.0	1.510 ± 0.016	32.75 ± 0.18	84.5 ± 0.7	12.5 ± 0.5	2.9 ± 0.4

[a] The structure data were obtained from trajectory with SE. Contents of secondary structure was calculated by averaging the ratio of secondary structure in each frame.

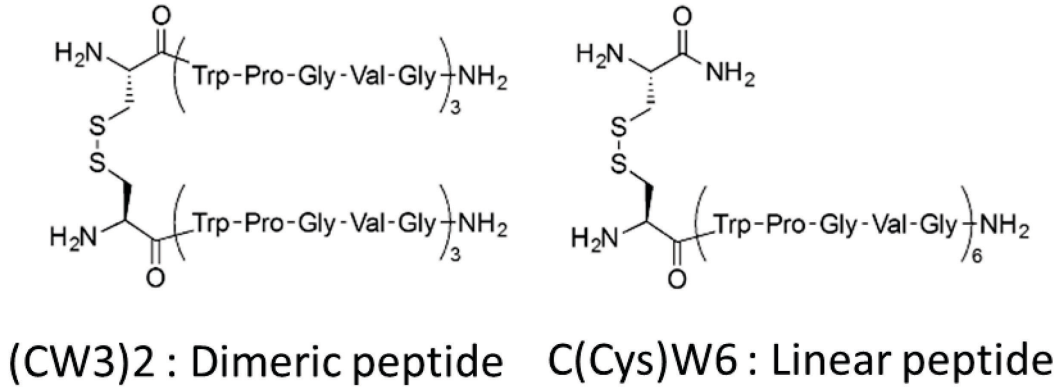

Figure 1. Chemical structures of (CW3)2 and C(Cys)W6.

C(Cys)W6 was synthesized as a reference for (CW3)2 dimer with a linear peptide chain.

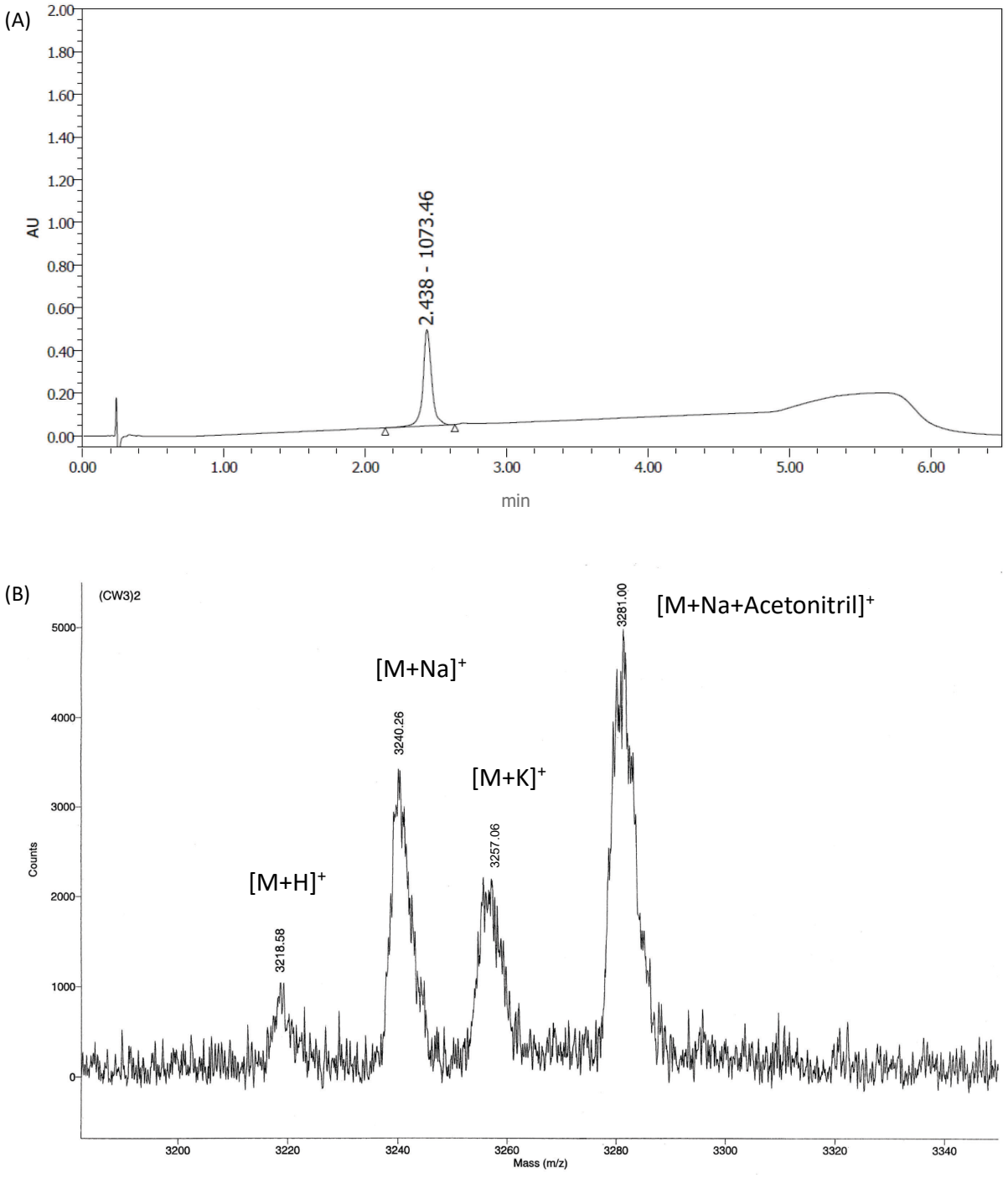

Figure 2. UPLC and MALDI-TOF MS analysis of (CW3)2.
(A) UPLC chart and (B) m/z values in MALDI-TOF MS of (CW3)2 were shown.

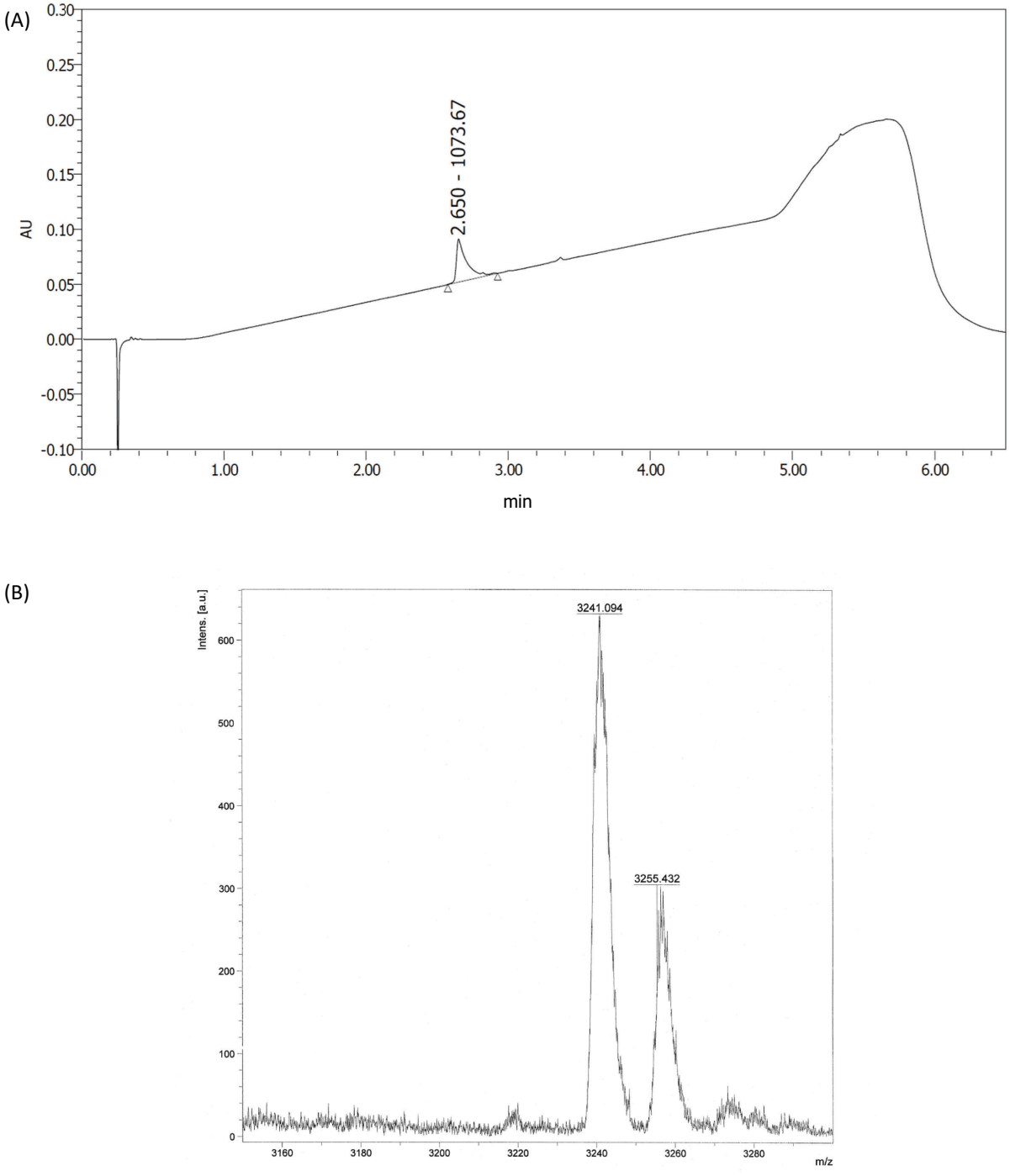

Figure 3. UPLC and MALDI-TOF MS analysis of C(Cys)W6.

(C) UPLC chart and (D) m/z values in MALDI-TOF MS of C(Cys)W6 were shown.

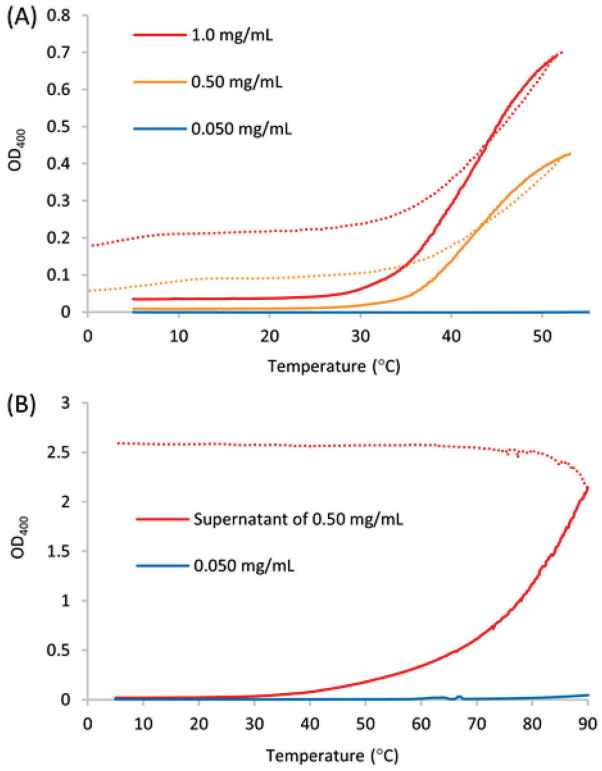

Figure 4. Turbidity profiles of (CW3)2 and C(Cys)W6.at each concentration.
Turbidity changes of (CW3)2 (A) and C(Cys)W6 (B) associated with heating (solid lines) and cooling (dashed lines) were shown.

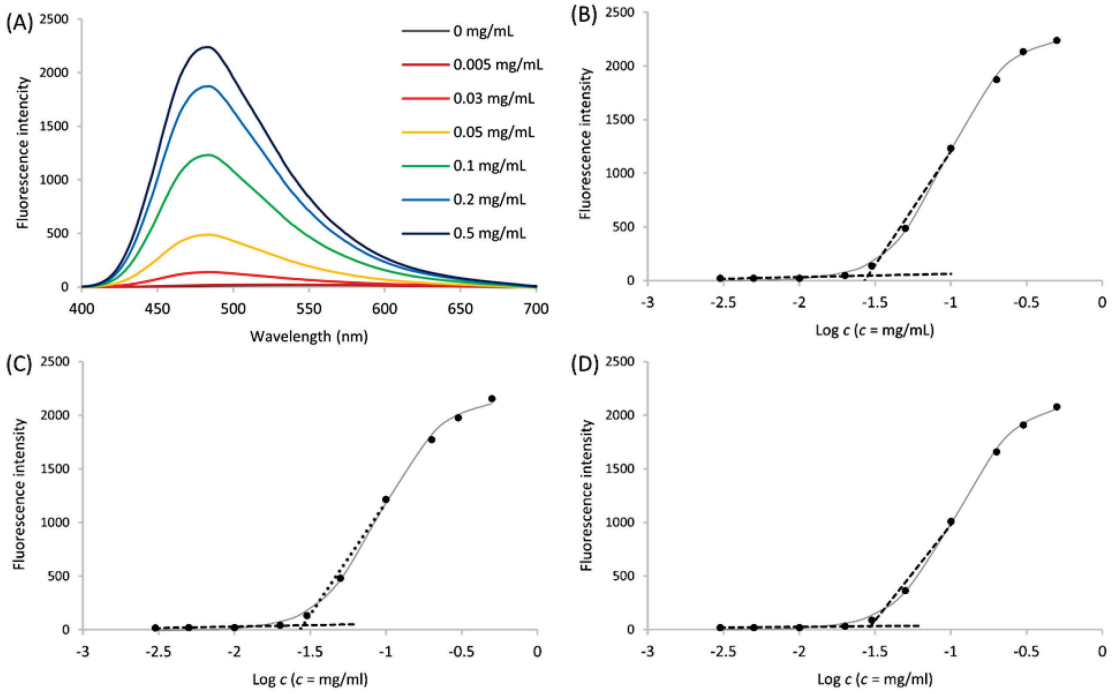

Figure 5. Fluorescence measurement with 1,8-ANS at various concentrations of (CW3)2. (A) Fluorescence spectra of 50 μM 1,8-ANS were measured at 5°C with the various concentrations of (CW3)2. Critical concentration of (CW3)2 at 5°C (B), 15°C (C), and 25°C (D) were determined from the maximum fluorescence intensity of the spectra by the two-line method.

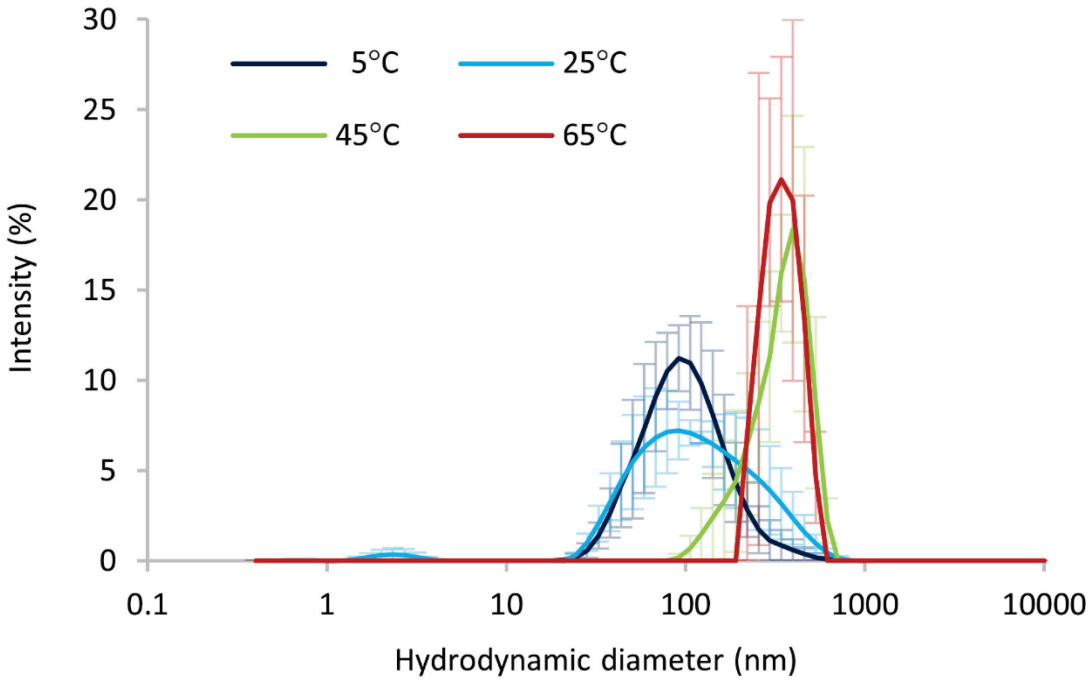

Figure 6. Particle size distribution of (CW3)2 at various temperatures.
Mean intensity at each temperature was shown with SE.

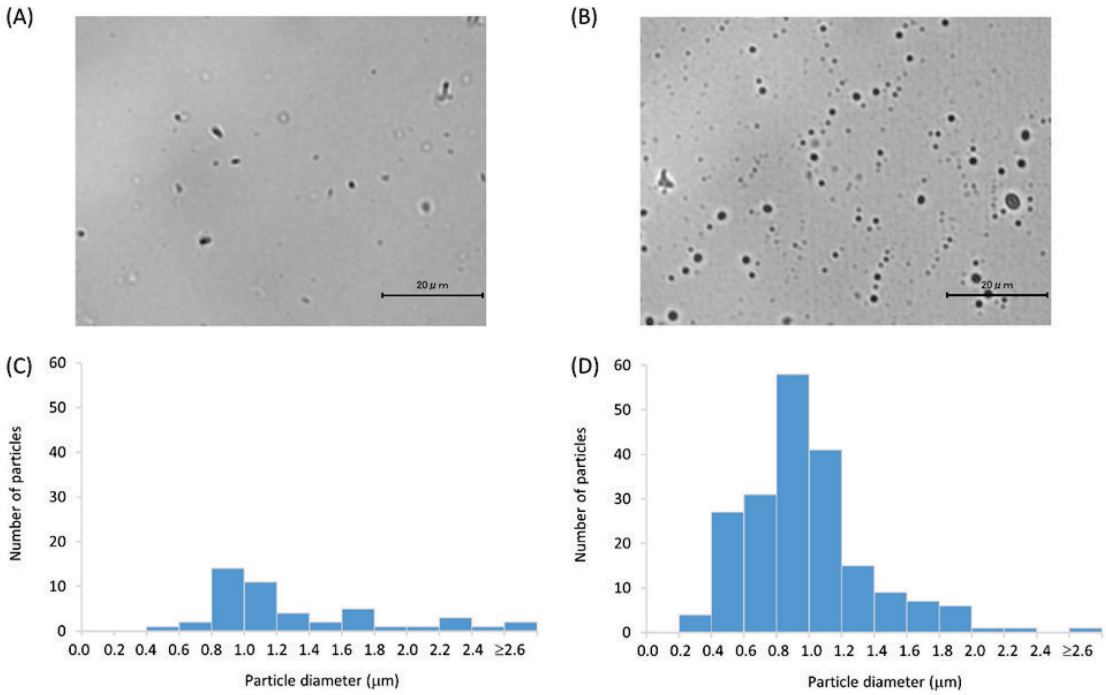

Figure 7. Phase-contrast microscopy images of (CW3)2 and histogram of particle diameter.

The images were obtained (A) at room temperature (25°C) and (B) after heating at 60°C. An aqueous solution of the peptide was prepared at a concentration of 1.0 mg/mL. (Scale bars indicate 20 μm.) Distribution of particle diameter in optical microscopy (A) at 25°C and (B) after heating at 60°C were also shown.

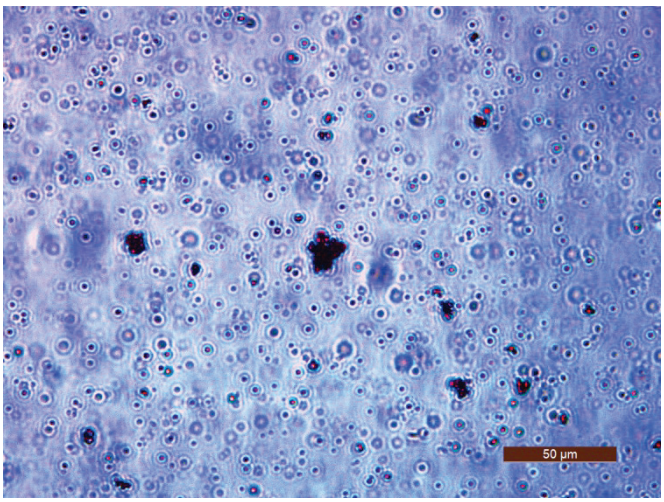

Figure 8. The light field microscopy images of (CW3)2 with Ponceau S.
(CW3)2 and ponceau S solution was heated at 60°C, centrifuged, and washed with 60°C water.

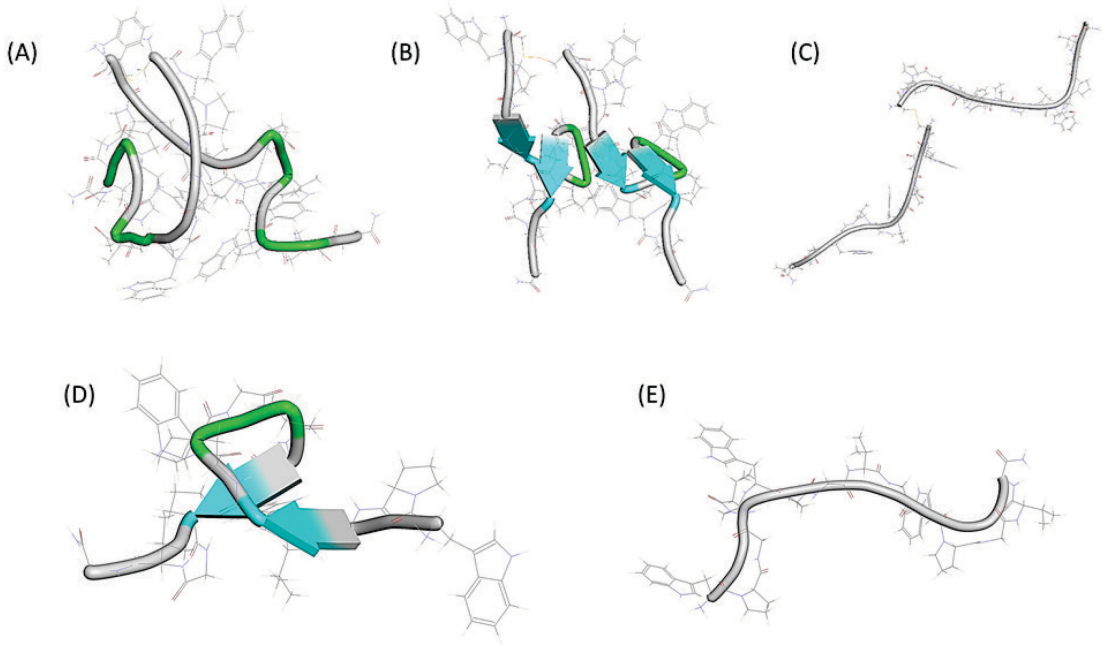

Figure 9. Representative structures of (CW3)2 and W3 estimated by MD simulation. Representative structures of (CW3)2 at (A) 278.0, (B) 294.0, and (C) 343.0 K. Representative structures of W3 at (D) 278.0 K and (E) 343.0 K were also shown. Each secondary structure was indicated as follows: light blue, sheet; green, turn; and white, random.

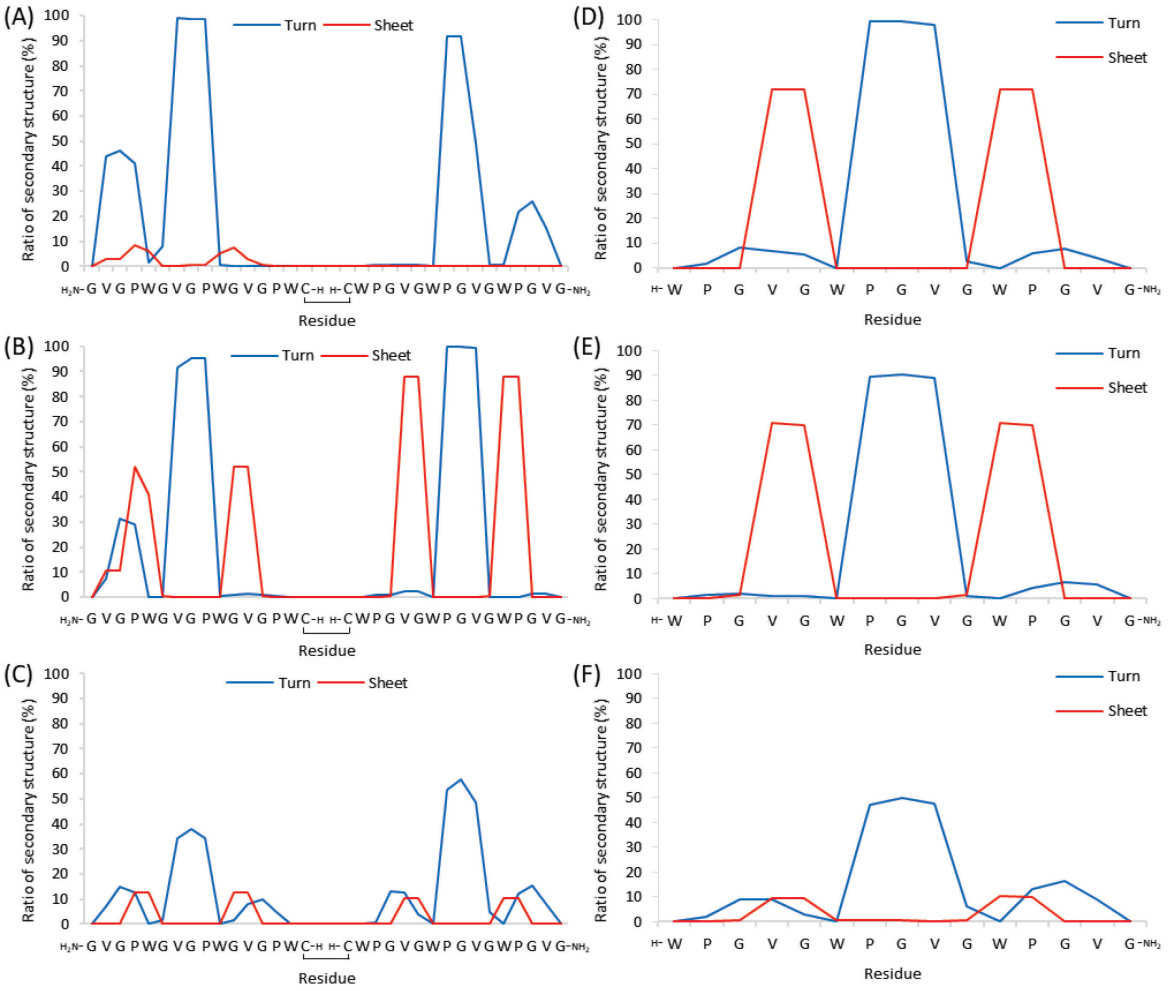

Figure 10. A ratio of secondary structures at certain residues in simulation time. The content of turn and sheet structure in each residue of (CW3)2 was estimated from the trajectory at (A) 278.0 K, (B) 294.0 K, and (C) 343.0 K. The content in W3 was also estimated at (D) 278.0 K, (E) 294.0 K, and (F) 343.0 K.

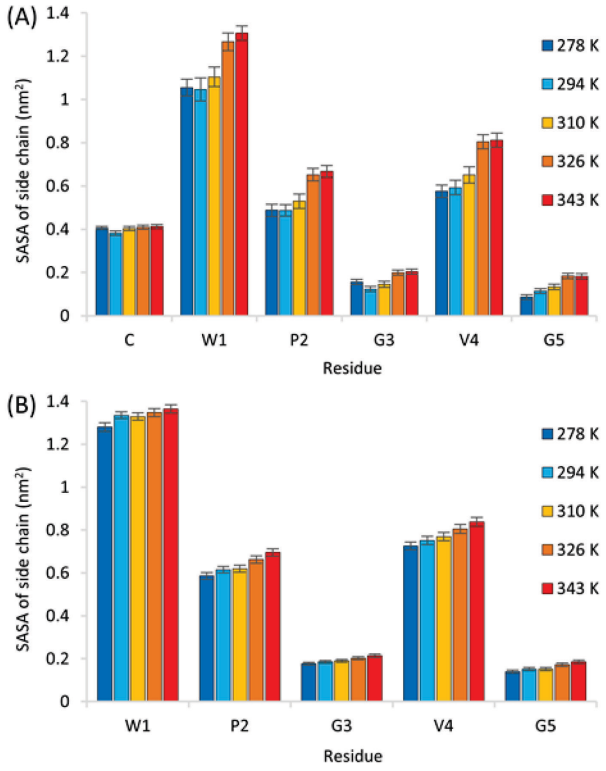

Figure 11. SASA of the side chain at each residue of (CW3)2 and W3.

SASA values of the (A) (CW3)2 and (B) W3 were obtained from trajectory analyses of the MD simulation. The means with SE were calculated by averaging the SASA of residues at each position (1st - 5th) in the repetitive unit sequence.

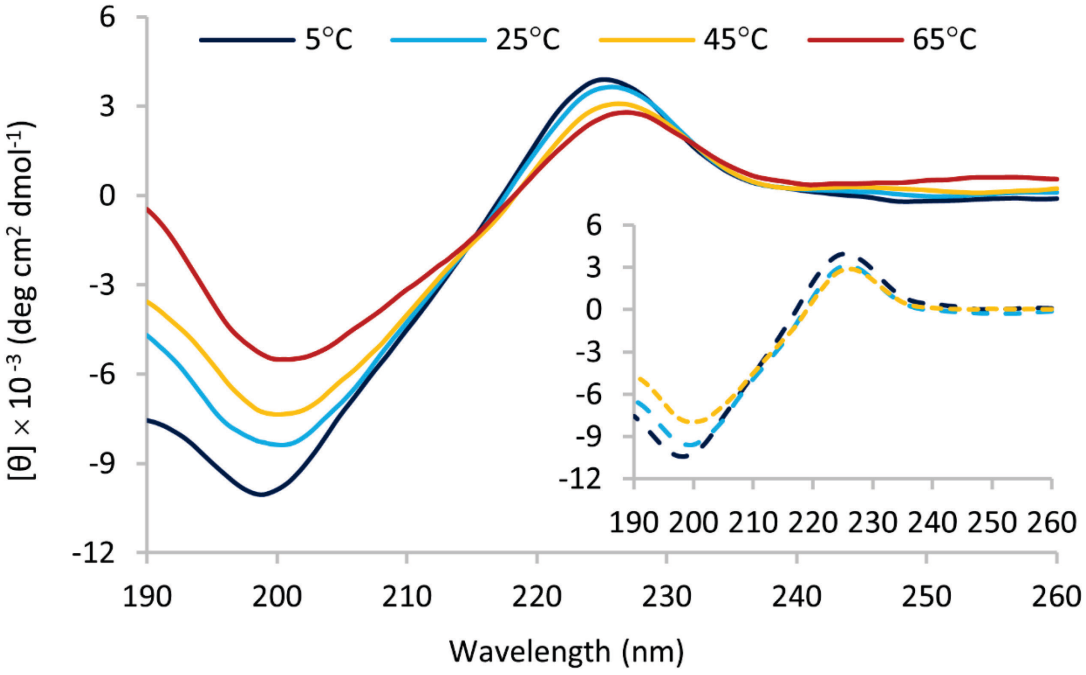

Figure 12. CD spectra of (CW3)2 at various temperatures.
Spectra were measured from 5 to 65°C with increasing temperatures. The inset shows spectra with decreasing temperatures.

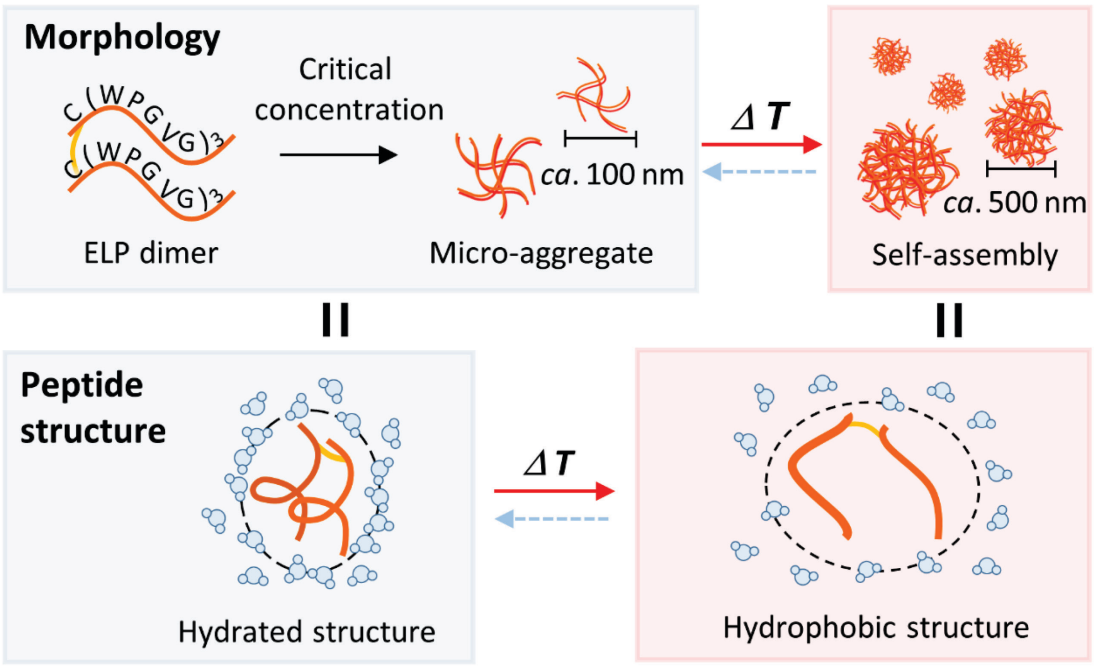

Figure 13. Images of the structural features and stepwise coacervation of (CW3)2. Morphology of (CW3)2 would change stepwise. The dimeric peptide seemed to be dissolved in water and formed micro-aggregation over a critical concentration. Then, the peptide was likely to take soluble structure. However, heating would cause destabilization of hydration and maturing of self-assembly.

CHAPTER 3

The effect of pH and salt on self-assembling property of short elastin-like peptides

Abstract

Elastin-like peptides (ELPs) are composed of hydrophobic repeats derived from elastin, such as $(VPGVG)_n$, and exhibits a temperature-dependent reversible self-assembly property. Although ELPs have been applied as biomaterials due to the characteristic property, they were often used in the form of long polypeptides provided by genetic engineering method. It was considered that synthesizable shorter peptide sequences are advantageous for bulk synthesis and industrial applications. Our previous study developed a short-length ELP, $(FPGVG)_5$ with self-assembling property. On the other hand, it is known that the self-assembling property of ELPs in solution are influenced by external factors such as pH and salt. This effect of pH and salt is well investigated with long ELP, but it is not sufficiently described how pH and salt affects self-assembly of short ELPs. Therefore, this study aimed to investigate the responsiveness of short ELPs to pH and salt. In this chapter, four peptide analogs derived from $(FPGVG)_5$, at which each terminus was protected or unprotected, were synthesized. Salt and pH responsiveness in their self-assembling property were analyzed by turbidity measurement and molecular dynamics (MD) simulation. As a results, the self-assembling properties of $(FPGVG)_5$ analogs depended on the ionized state of the termini. Ionization of the termini induced by the pH alteration decreased the self-assembly property, with the exception of $(FPGVG)_5$ in the zwitterionic state. Salts showed salting in and out effect according to Hofmeister series for non-ionized peptides. It was also indicated that the more chaotropic anions interacted with the charge at the ionized N-terminus. The self-assembling property of N-terminus-ionized peptide was significantly improved by more chaotropic anions. Furthermore, it was found that the self-assembling property of $(FPGVG)_5$ seemed to be sensibly influenced by pH and salt compared to the corresponding long-length ELPs. It was indicated that pH and salt efficiently worked as factors to control self-assembling property of short ELPs. These findings will be useful for future applications of ELPs as stimulus responsive materials.

1. Introduction

The use of biomolecule as materials has become widespread [1, 2]. It would be beneficial to elucidate their functions and molecular mechanisms, because it would bring precise controls and improvements of their valuable individual functions. Among biomolecules, elastin like peptides, abbreviated ELPs, are attractive as biomaterials [3-6].

Typical ELPs have repetitive sequence of VPGVG derived from elastin [5]. The hydrophobic repetitive sequence shows self-assembly at high temperature and dissociates at low temperature in solution. Such a reversible and LCST-like phase transition behavior is also called coacervation [7, 8]. Recently, the self-assembling property of ELPs was widely applied as a carrier of drug delivery systems or a scaffold of tissue engineering [3-6]. Thus, the elucidation of self-assembling mechanism in ELPs has become important research subjects in order to provide rational design of ELPs.

In the application of ELPs, it is often used long-length ELPs. This is because that more than 40 VPGVG repeating units are required to afford self-assembly in a physiological condition [9-11]. However, inexpensive and massive chemical synthesis of long polypeptides is difficult to carry out, and this difficulty was thought to be a bottle neck in the bulk application of ELPs at present. Here, previous studies developed chemically synthesizable short ELPs with self-assembling property [10, 12-16]. They revealed that substitution of valine residue at first position of each typical repetitive sequence of elastin, VPGVG, with hydrophobic one induced relatively strong self-assembling property. Among them, $(IPGVG)_7$, $(FPGVG)_5$, and $(WPGVG)_3$ showed self-assembly with shorter and more hydrophobic repetitive sequences than $(VPGVG)_{40}$. Peptides, when used as biomaterials, have some advantages over proteins [17, 18]. Therefore, this study also aimed to develop the novel short ELPs and evaluate characteristics of them in more detail.

The differences in pH and salt in solution affect the self-assembling properties of ELPs [19-23]. They have been considered as common environmental factors to use ELPs as base materials in solution. Moreover, some ELPs were designed and applied as biomaterials which showed responsibility to ion or pH by combining with other functional groups [24-28]. For the development of smart application of ELPs, it is important to know how ELPs respond to the differences in salt and/or pH condition(s). These responsiveness on self-assembly were well investigated in long ELPs [19-23]. On the contrary, it is not known whether self-assembling property of short ELPs is affected by pH and salt. In other words, for further functionalization of short ELPs, it is required to conduct fundamental studies to clarify the responsiveness.

This chapter investigated the responsiveness of short ELPs to pH and salt. Here, $(FPGVG)_5$ is abbreviated F5. Four F5 analogs with different terminal state, H-F5-OH, Ac-F5-OH, H-F5-NH_2, and Ac-F5-NH_2 were synthesized. These self-assembling properties were evaluated under different pH and salt conditions. As a result, it was shown that the ionization of termini interfered with the self-assembling property of the peptides. It was also revealed that chaotropic anions significantly improved the self-assembling property of the peptide with ionized N-terminus. Additionally, molecular dynamics simulation was performed to analyze hydration state of the peptide under pH buffered or salted condition. The results

suggested that pH and salt would change the self-assembling property by affecting the hydration state of the peptide termini. The findings obtained in this chapter would provide fundamental knowledge for further downsizing and functionalization of short ELPs.

2. Materials and methods

Chemicals

Fmoc-NH-SAL-MBHA resin (100–200 mesh) and Fmoc-Gly Alko Resin (100-200 mesh) were purchased from Watanabe Chemical Industries Ltd. (Hiroshima, Japan). Acetic anhydride for peptide synthesis was purchased from Wako Pure Chemical Industries, Ltd. (Osaka, Japan). 2-(1H-Benzotriazol-1-yl)-1,1,3,3-tetramethyluronium hexafluorophosphate (HBTU) and 1-hydroxybenzotriazole (HOBt) were purchased from Kokusan Chemical Co., Ltd. (Tokyo, Japan). Other reagents for peptide synthesis were also purchased from Watanabe Chemical Industries Ltd. Acetic acid, aluminum (III) chloride hexahydrate, calcium chloride, disodium hydrogen phosphate 12-water, sodium acetate, sodium carbonate, sodium chloride, sodium dihydrogenphosphate dihydrate, sodium fluoride, and sodium formate were purchased from Nacalai Tesque Co. Ltd. (Kyoto, Japan). Phosphoric acid, magnesium chloride hexahydrate, potassium chloride, sodium hydrogen carbonate, sodium nitrate, sodium perchlorate monohydrate, and sodium thiocyanate were purchased from Wako Pure Chemical Industries, Ltd. Sodium bromide and sodium iodide were purchased from Tokyo Chemical Industry Co., Ltd. (Tokyo, Japan). Formic acid was purchased from Kanto Chemical Co., Inc. (Tokyo, Japan). Water for sample preparation was purified by Milli-Q Integral 3 (Merck Millipore, Billerica, MA). Solvents for peptide synthesis and other reagents were also obtained from commercial suppliers and used without further purification.

Synthesis of the F5 analogs

F5 analogs were synthesized by following the synthesis method described in our previous studies with a few modifications [12, 13]. All peptides were synthesized with an ABI 433A peptide synthesizer (Applied Biosystems, Foster City, CA) using the 0.10 or 0.25 mmol scale solid phase method by Fmoc chemistry. 0.147 mg (0.10 mmol scale) and 0.370 mg (0.25 mmol scale) of Fmoc-NH-SAL-MBHA Resin (100–200 mesh) were used as the solid phase support for synthesis of Ac-F5-NH_2 and H-F5-NH_2, respectively. 0.111 mg (0.10 mmol scale) and 0.278 mg (0.25 mmol scale) of Fmoc-Gly Alko Resin (100-200 mesh) were used for synthesis of H-F5-OH and Ac-F5-OH, respectively. After peptide elongation, acetylation of the N-terminus was additionally performed in synthesis of Ac-F5-NH_2 and Ac-F5-OH. Each resin was suspended in dichloromethane (9 mL) with acetic anhydride (31.7 mmol, 3 mL) and DIEPA (62.0 μmol, 10.8 μl). The resulting mixture was stirred for 2 hours at room temperature. Deresination was performed by a reagent cocktail containing 95%

TFA/2.5% TIS/2.5% H_2O. After the reaction, the peptide was precipitated by di-ethyl ether and pre-purified by Sep-pak Vac 35cc C18 (Waters Co., Milford, MA) column. Subsequently, further purification was performed by RP-HPLC (The Breeze™ 2 HPLC System, Waters Co.) composed with a C8 column (μ-BONDASPHERE, 150 x 19 mmI.D., C8-AP 5 μm, 300 Å, Waters Co.) and a solvent system consisting of 0.1% TFA aqueous solution (v/v) and 0.1% TFA aqueous solution in 80% acetonitrile aqueous solution (v/v). The eluted fractions containing peptides were concentrated by evaporation and lyophilized. Consequently, all peptides were obtained as a colorless powder and yielding 266 mg of H-F5-OH (46.1%), 74.4 mg of Ac-F5-OH (31.7%), 212 mg of H-F5-NH_2 (36.8%), and 62.9 mg of Ac-F5-NH_2 (26.8%). Purity and molecular weights of the peptides were confirmed by ACQUITY UPLC H-Class (Waters Co.) equipped with an ACQUITY UPLC BEH C-18 column (100 mm, flow rate 0.6 mL/min) (Waters Co.) at 49 ˚C and the eluting product was detected by UV at 225 nm and a quadrupole mass spectrometer, ACQUITY QDa (Waters Co.). The solvent system for UPLC consisted of 0.1% formic acid aqueous solution (v/v, solvent A) and 0.1% formic acid in acetonitrile (v/v, solvent B), and elution was performed with a linear gradient of solvent B, 24% to 56% over 4.23 min.

H-F5-OH : H-(FPGVG)$_5$-OH

Retention time = 2.712 min. MS (ESI) m/z: calculated for $C_{230}H_{312}N_{50}O_{51}$ 1153.84 ([M + 2H]$^{2+}$), found 1153.87

Ac-F5-OH : Ac-(FPGVG)$_5$-OH

Retention time = 3.357 min. MS (ESI) m/z: calculated for $C_{232}H_{314}N_{50}O_{52}$ 1174.86 ([M + 2H]$^{2+}$), found 1174.77

H-F5-NH_2 : H-(FPGVG)$_5$-NH_2

Retention time = 2.496 min. MS (ESI) m/z: calculated for $C_{230}H_{313}N_{51}O_{50}$ 1153.35 ([M + 2H]$^{2+}$), found 1153.31

Ac-F5-NH_2 : Ac-(FPGVG)$_5$-NH_2

Retention time = 3.270 min. MS (ESI) m/z: calculated for $C_{232}H_{315}N_{51}O_{51}$ 1174.36 ([M + 2H]$^{2+}$), found 1174.40

Removal of TFA from H-F5-NH_2

To analyze effects of TFA anion which came along with the peptide as a counter ion derived from the purification solvent, TFA was removed from H-F5-NH_2 by VariPure IPE column (100 mg/3 mL, Agilent Technologies, Santa Clara, CA). At first, VariPure column

was preconditioned with 10 mL methanol. Subsequently, the column was feather conditioned by 10 mL of 80% acetonitrile aqueous solution. After that, the column was added the HPLC-purified H-F5-NH_2 (23.31 mg) solution prepared in 1 mL 80% acetonitrile aqueous solution and washed by 10 mL MeOH. All elution fractions were collected and the peptide containing fraction was concentrated by evaporation and lyophilized. Consequently, H-F5-NH_2 without TFA anion was obtained as colorless powder (21.21 mg, 91.0%).

Sample preparation

The effects of pH and salt on self-assembly of F5 analogs were evaluated by T_t values in pH buffered and/or salted solutions. The pH buffered samples were prepared by dissolving the peptides into five pH buffered solutions, that is, phosphate buffers (pH = 2.1 (NaH_2PO_4 50.0 mM, H_3PO_4, 49.9 mM) and pH = 7.0 (NaH_2PO_4 68.2 mM, Na_2HPO_4 10.6 mM), formate buffer (pH = 2.9, HCOONa 100 mM, HCOOH 468 mM), acetate buffer (pH = 4.8, CH_3COONa 100 mM, CH_3COOH 72.4 mM), and bicarbonate buffer (pH = 9.8, $NaHCO_3$ 41.2 mM, Na_2CO_3 19.6 mM). All buffers were prepared to ionic strength = 0.1 M and adjusted to each target pH with slight amount of aqueous solution of hydrochloric acid or sodium hydroxide. To observe effects of salts on self-assembly, peptide samples dissolved in eleven salt solutions, were also prepared. These samples were prepared at salt concentration of 0.10 M by adding aqueous stock solutions of 1.0 M NaCl, KCl, $MgCl_2$, $CaCl_2$, $AlCl_3$, NaBr, $NaNO_3$, NaI, $NaClO_4$, NaSCN, and 0.50 M NaF. Furthermore, samples of H-F5-NH_2 in 0.05, 0.1, 0.15, 0.2, 0.3 M NaCl solution were also prepared to confirm the effect of salt concentration. In addition to the condition described above, using a combination of pH and salt, each peptide solution was prepared to observe the effect of salts on ionized peptides. Four peptides were dissolved in phosphate buffer (pH = 2.1) or bicarbonate buffer (pH = 9.8), and added 1.0 M NaCl, KCl, NaBr, $NaNO_3$, or $NaClO_4$ stock solution to be 0.10 M of salt concentration. This preparation was only performed for neutral salts and stable salts in acidic or basic pH condition. Furthermore, salted or pH buffered samples of the H-F5-NH_2 excluding TFA were also prepared by following the method described above to validate effects of the counter ion on self-assembly. In all preparation, final concentrations of each peptide were fixed at 10 mg/mL for H-F5-OH and H-F5-NH_2, 1 mg/mL for Ac-F5-OH and Ac-F5-NH_2, and 2 mg/mL for the H-F5-NH_2 excluding TFA.

Turbidity Measurement

The temperature-dependent self-assembly was evaluated using a JASCO V-660 spectral photometer, (JASCO Co., Tokyo, Japan). Turbidity measurements were performed at 400 nm while the temperature was being increased or decreased at a rate of 0.5 °C/min from 6 °C or less. Each concentration of sample solution was measured at least three times.

Self-assembly was determined by the phase transition temperature (T_t). This is the temperature at which the turbidity of the solution reaches half the maximum value [12].

MD Simulation

The effect of pH and salt on molecule of F5 structure was simulated in GROMACS 5.1.4 software with OPLS/AA force field and TIP3P explicit solvent model. To take into account in the change of charges on functional groups that can be ionized according to pH, peptide structures with ionized or non-ionized terminus were constructed, respectively. We performed simulations of H_2^+-F5-OH (H_2^+- means H_3N^+-), H_2^+-F5-O^-, H-F5-O^-, Ac-F5-OH, Ac-F5-O^-, H_2^+-F5-NH_2, H-F5-NH_2, and Ac-F5-NH_2. Initial conformations were generated as an extended form by Discovery studio 4.0 software, and arranged its terminal state by *gmx pdb2gmx* command in GROMACS. These peptides ware solvated in 7.2 nm cubic box with explicit TIP3P water molecules by *gmx solvate*. Successively, 22 or 23 Na^+ and Cl^- ions were replaced with water molecules by *gmx genion* to provide the ionic strength of 0.1 M and to neutralize total charge of the system. In addition, we also generated structures of H_2^+-F5-NH_2 and H-F5-NH_2 with 0.1 M NaBr, NaI, $NaNO_3$, or $NaClO_4$ to estimate the effect of chaotropic anions against peptides having a charge at the N-terminus. Subsequently, topologies of NO_3^- and ClO_4^- were referred from Doherty's study [29]. Each simulation was performed at two temperatures of 310 K and 278 K to consider the change in molecular state due to difference of temperature. Each MD system also contained minimization, temperature annealing, equilibrium, and production stages. Solvent minimization was performed using steepest descent method for 10,000 steps and conjugate gradient algorithm for 20,000 steps. Then, the system was gradually heated for 100 ps and equilibrated for 100 ps in NPT ensemble using v-rescale thermostat and the berendsen barostat. Until this first equilibrium, all-peptide atoms except hydrogens ware restricted with 20 kcal/mol·nm^2. Second and third equilibrium were further conducted in same condition with first equilibrium except restraints. Restriction of 2 kcal/mol nm^2 and no constraint were also applied to them, respectively. After that, final production run was performed for 50 ns with a 2 fs time step and no constraint. V-rescale thermostat and Parrinello-Rahman barostat ware used for NPT ensemble. 10 Å cutoff radius was used for the short-range intermolecular interactions. Partial mesh Ewald (PME) summation was used for the long-ranged electrostatic interactions. The LINCS algorithm was used to convert the bonds with H-atoms to constraints. Trajectories were processed to analyze peptide hydration. Radius of gyration (R_g), solvent accessible surface areas (SASA), and ratios of secondary structure, were obtained by using *gmx gyrate*, *gmx sasa,* and *gmx do_dssp* [30], respectively. The number of hydrogen bonds between water and peptide N-terminus (N_{nw}) or C-terminus (N_{cw}), distance distribution of closest ions (DDCI), and Coulomb and van der Waals interaction energy between water or solvent and the peptide

[31] were also obtained by using *gmx hbond*, *gmx mindist,* and *gmx energy*, respectively.

3. Results and discussion

Synthesis of the Peptides

Four peptides with different terminal states were successfully synthesized by a conventional solid phase peptide synthesis procedure. The purity and molecular weight of each peptide were confirmed by RP-UPLC-MS. These data were shown in figure 1. All peptide showed single peak in RP-UPLC-MS and correct mass number. They were obtained with high purity.

(Figure 1)

The effects of pH and salt on H-F5-NH_2

The influence of pH and salt on H-F5-NH_2 was shown at first, because the self-assembling properties of short-ELPs with protected C-terminus were well studied [12, 13, 15, 16]. In case of H-F5-NH_2, it was previously revealed that the peptide required concentration of 30 mg/mL to show self-assembly in pure water [15]. As shown in figure 2, analysis on pH alteration revealed that H-F5-NH_2 did not exhibit self-assembly under the strongly acidic conditions (pH = 2.1). It was also shown that the phase transition temperature significantly decreased as the pH of the solution became basic. It cannot be separate the effect of pH and salt type in buffer on the phase transition, because the buffers is made from a combination of salts. However, it seemed that the non-ionized state of the peptide in neutral and basic buffers increased the hydrophobicity and induced the self-assembly driven by the hydrophobic effect.

(Figure 2)

The effect of salts on the self-assembly was observed in pure water. These data were shown in figure 3. Comparing the effect of cations in the chloride salt series, the T_t of H-F5-$NH_2$was linearly decreased as the valence of the cations increased (Figure 3A and 3B). This result was opposite to salting in and out effects according to Hofmeister series. In comparison with anions in the sodium salts series, chaotropic anions that generally show salting in effect, also reduced the T_t (Figures 3C and 3D). Especially, addition of NaI, $NaClO_4$, or NaSCN immediately made the peptide solution cloudy under ice cooling condition. Thus, anion type more significantly affected T_t of H-F5-NH_2 than cation type. Here, we thought that inverse and linear salting out effects of multivalent cations probably related to increase in concentration of their counter chloride anion. It was supported by the result that T_t of the peptide linearly decreased as the NaCl concentration increased from 0.1 to 0.3 M (Figure 4). In comparison with previous studies, self-assembling property of H-F5-NH_2

seemed to be significantly affected by salt type even at salt concentration of 0.1 M [19, 20]. It seemed to be different from the property of conventional long ELPs.

(Figures 3 and 4)

The specific anion sensitivity of H-F5-NH_2 was further analyzed. It was suspected that the anions and the peptide were electrically interacting with each other in solution. To analyze the effect of salt on H-F5-NH_2, the turbidity measurement was carried out using TFA removed peptides. Generally, HPLC-purified peptides contain TFA ion at N-terminal as a counter ion, because TFA was usually used in the HPLC eluents. TFA is a strong acid and is expected to ionize the peptide well. Here, H-F5-NH_2 removed TFA showed self-assembly at concentrations of 2 mg/mL (T_t = 39.3 ± 0.1°C) and 5 mg/mL (T_t = 19.1 ± 0.1°C). It was confirmed that removal of TFA from the peptide decrease T_t value. The effects of pH, cation and anion species on the TFA removed H-F5-NH_2 in pure water were shown in the figures 5 and 6. Due to relatively low concentration of 2 mg/mL in measurements, the peptide self-assembled only under neutral and basic conditions at T_t of 38.8 ± 0.5 and 34.1 ± 0.5°C, respectively. No change in T_t was observed except for $AlCl_3$ in the comparison with the effects depending on the types of cations. Since $AlCl_3$ is an acidic salt, it was thought that lower pH caused by $AlCl_3$ changed the ionization state of the peptide and prevented self-assembly. Additionally, no systematic differences in T_t according anion type were also observed. Therefore, it was confirmed that the T_t significantly decreased by the interaction of chaotropic anion with the positive charged N-terminus.

(Figures 5 and 6)

The influence of anions was also analyzed in acidic phosphate buffer (pH = 2.1) and basic bicarbonate buffer (pH = 9.8) (Figure 7). Although the peptide did not show self-assembly in the acidic phosphate buffer, the self-assembling property emerged in the acidic buffer with 0.1 M NaCl. NaBr or $NaNO_3$ decreased *T*t of the peptide more than NaCl. The addition of $NaClO_4$ stock solution also make the peptide solution cloudy even in ice cooling. These results indicated that more chaotropic anions likely induced stronger self-assembly of the peptide. It was similar to the case in pure water. On the other hand, in bicarbonate solution, addition of each salt lowered the T_t to 3 °C. There was no significant change depending on the kind of salts in basic condition. In addition to the findings described in the previous paragraph, it was strongly supported that chaotropic salts greatly reduce the T_t value of the N-terminus charged peptide.

(Figure 7)

The effects of pH and salt on Ac-F5-NH_2

In order to investigate influence of the N-terminal state on pH alterations, T_t of Ac-F5-NH_2 was measured in various pH conditions. In comparison with H-F5-NH_2, Ac-F5-NH_2 which possessed no chargeable functional group(s) at both termini showed self-assembly at a lower concentrations of 1 mg/mL (T_t = 45.8 ± 0.3°C) and 2 mg/mL (30.8 ± 1.0°C) in pure water. Interestingly, Ac-F5-NH_2 did not dissolve at concentration of 5 mg/mL in pure water. At the peptide concentration of 1 mg/mL in buffers with various pH, the T_t values of Ac-F5-NH_2 ranged between 36 and 40°C (Figure 8). The slight difference in T_t was thought to be induced by interaction of ions constituting the buffer with the peptide surface other than the terminal functional group(s). Consequently, it was found that the self-assembly of Ac-F5-NH_2 was not significantly affected by pH.

(Figure 8)

The effect of salt type in the self-assembly of Ac-F5-NH_2 was also confirmed. These data was shown in figure 9. In comparison between the cations, although the T_t tended to decrease as the valence of the cation was increased, it was not a significant change in T_t (Figures 9A and 9B). In comparison between the anions, the T_t values were ordered in the sequence: F^- <Cl^- < salt free < ClO_4^- < Br^- ≈ NO_3^- < SCN^- < I^- (Figures 9C, and Figure 9D). It was shown that cosmotropic/chaotropic anions tended to decrease/increase T_t at a salt concentration of 0.1 M, respectively. It was consistent with salting in and out effects described in previous studies about elastin-like polypeptides [20]. Surprisingly, it was found that Ac-F5-NH_2, which could not have generally charges in solution, was affected by salts in similar trend as same as the conventional ELPs that have at least one amino group at N-terminal.

(Figure 9)

The influence of anion species on T_t of Ac-F5-NH_2 was also confirmed in acidic and basic conditions (Figure 10). In each buffer, difference in salts did not bring large difference in T_t by 6°C or more (Figure 10). As a result, the salting in and out effects according to the Hofmeister series were found in bicarbonate buffer. Since multiple ionic species were present in these bicarbonate solutions, it is difficult to discuss further from the slight differences in T_t. Consequently, it was revealed that the salt responsiveness of T_t in Ac-F5-NH_2 did not depend strongly on pH.

(Figure 10)

The effects of pH and salt on Ac-F5-OH

Using the same procedure for the analyses on N-terminus, the influence of the C-

terminal state on the self-assembly of F5 was analyzed. As well as Ac-F5-NH_2, Ac-F5-OH showed phase transition in pure water at relatively low concentration of 1 mg/mL (T_t = 35.0 ± 0.4°C). As results of measurement in several pH buffers, the phase transition was shown in acidic phosphate and formic acid buffers (Figure 11). However, the peptide did not self-assemble in acetic, neutral phosphate, and bicarbonate buffers. Thus, there is a possibility that a pH value higher than the formic buffer made the C-terminus of Ac-F5-OH ionized, and it was expected that the increment of hydrophilicity of the peptide preventing the phase transition in the solution. As well as the N-terminus of the ELPs, it was suggested that the C-terminus also regulated the self-assembling property depending on its charged state.

(Figure 11)

The influence of salt on Ac-F5-OH was further analyzed in pure water and a series of buffers with various pH values. In the comparison between the cations in pure water, it was found that the T_t increased with the increment of the valence of the cation (Figure 12). Although this increasing behavior seemed to be according to Hofmeister series of cation, the difference in T_t by salt types was found to be within the range of 5°C. This small range of difference indicated that the magnitude of the influence by the cations was small in the self-assembling. Excluding NaF which was basic salt and promoted ionization of C-Terminus, the anions also behaved according to the Hofmeister series as well as the cation against the self-assembling of Ac-F5-OH (Figures 12C and 12D). This trend was consistent with that of unchargeable Ac-F5-NH_2. In addition to these results, no change in anion responsiveness of Ac-F5-OH was observed in acidic and basic condition. (Figure 13). In the acidic phosphate buffer, the difference of T_t between the anion species was ranged only 4°C. Consequently, salt addition did not bring phase transition at low peptide concentration (1 mg/mL) in basic condition at which ionized C-terminus of Ac-F5-OH existed. In comparison with the result on Ac-F5-NH_2, it was confirmed that the C-terminus protecting group only prevented ionizing of C-terminus, and the group itself did not affect significantly the salt responsiveness of F5 backbone.

(Figures 12 and 13)

The effects of pH and salt on H-F5-OH

Analysis of *T*t change was also conducted on H-F5-OH which had unprotected termini. Similar to H-F5-NH_2, H-F5-OH was expected to be obtained as a TFA salt via HPLC purification. As a result of the turbidity measurement in pure water, H-F5-OH showed self-assembly at a concentrations of 10 mg/ml (T_t = 53.3 ± 1.1°C) and 20 mg/ml (T_t = 29.2 ± 0.9°C). These peptide concentrations were lower than that of H-F5-NH_2 described above. It was thought that H-F5-OH could ionize at both termini in acetic buffer and neutral phosphate

buffer to be amphoteric ion (zwitterion). This zwitterion would be more hydrophilic than the peptide ionized at either one of termini. However, as shown in figure 14, H-F5-OH showed relatively low T_t in these neutral - weak acidic conditions compared with that in acidic phosphate buffer (pH = 2.1). In addition, no phase transition was observed in bicarbonate buffer. Thus, it was thought that H-F5-OH was possible to form a self-assembly with an aid of electrical interaction between homogeneous peptide molecules. The property of zwitterionic F5 raises interesting questions regarding self-assembling mechanism of H-F5-OH. Further verification is necessary in the future for examination of this hypothesis how an aid of electrical interaction between homogeneous peptide molecules induce and strengthen self-assembly of H-F5-OH, which can be a zwitterion form.

(Figure 14)

In pure water, self-assembly of H-F5-OH was affected by salts similar to that of H-F5-NH_2. As shown in figure 15, the T_t of H-F5-OH decreased with increasing valence of the cations in solution. The addition of more chaotropic anions also significantly reduced the T_t. The peptide solution with NaI, $NaClO_4$, or NaSCN showed self-assembly even under ice cooling condition. As shown in figure 16, the tendency of salt influence in acidic buffers was also similar to that of H-F5-NH_2. On the other hand, no self-assembly was induced by addition of any salts in bicarbonate buffer. Consequently, it was revealed that non-ionized C-terminus did not affect salt responsiveness of H-F5-OH. In addition, it was observed that the non-ionized N-terminus and the ionized C-terminus under basic conditions would prevent self-assembly properties of H-F5-OH.

(Figures 15 and 16)

Molecular dynamics simulation of hydration state of peptide

In vitro experiments demonstrated that the importance of the state of the termini of ELPs in self-assembly. To elucidate the influence of the state of the peptide terminus, the hydration state around the termini was estimated by *in silico* procedure using MD. The data on the structure at 278 K was listed in table 1. All eight peptides possessed bend, turn, and abundant coil structure at 278 K. Thus, it was thought that the influence of the change in the termini on the backbone structure was not significant. As analyses of the peptide hydration, the number of hydrogen bonds formed between water molecules and N-terminus (N_{nw}) or C-terminus (N_{cw}) was also shown in table 1 and figure 17. Here, the ionized N-terminus had more hydrogen bonds with water molecules as compared with the non-ionized or protected one. The ionized N-terminus possessed about 0.8 bond per one amino group. In addition, it was also shown that the ionization at the C-terminus increased *ca.* 4 hydrogen bonds with water molecules. The difference in the number of hydrogen bonds in C-terminal carboxyl

groups was larger than that in N-terminal amino groups. The radius distribution function (RDF) of the water molecules was also analyzed from the surface of each terminus. This result was also described in figure 17. At both termini, the ionized state caused large distribution peak of water in the region shorter than 0.2 nm from the surface of each terminus. It was revealed that the ionized terminus was more hydrated than the non-ionized or protected terminus. In comparison between ionized termini, C-terminus showed a higher intensity than N-terminus in the graph (Figure 17). It was also indicated that more water molecules were localized in the first hydration shell of the C-terminus. As shown in figure 18, the analysis of interaction energy indicated that the peptide having a well hydrated terminus tended to interact with water molecules. Understandably, it was suggested that ionization of termini gave high hydrophilicity to the peptides.

(Table 1, figures 17 and 18)

An analysis at 310 K was conducted using the trajectories. The date on the structure was listed in table 2. As well as the results at 278 K, secondary structure at 310 K was dominated by bend, turn, and abundant coil structure. In addition, β-sheet and β-bridge structures increased its proportion in comparison with the results at 278 K. These components were commonly found in the ELPs. Thus, it was suggested that the state of termini did not affect the whole peptide structure at 310 K similar to that at 278 K. The results of analysis of hydrogen bonds at each terminus at 310 K was shown in figure 19. The hydrogen bond distance between the N-terminus and water molecules tended to be slightly longer in the ionized state than that in non-ionized state. However, in analysis at the C-terminus, there was a trajectory in which number of hydrogen bonds with water did not increase even in the ionized state. This result was different from that at 278 K. It was thought that the hydrogen bonds at high temperatures became unstable due to thermal motion of the system. In the analysis of RDF, ionized state of both termini showed the peak which indicated first hydration shell. However, intensity of C-terminus tends to be lower than that at 278 K. These results indicated that the localization of water molecules near the C-terminus was decreased at high temperature. Moreover, as shown in figure 18, the interaction between the peptides and water molecules among almost all the peptides destabilized at 310 K. This result suggested that high temperature induced hydrophobic effect leading to self-assembly of the peptides.

(Table 2 and figure 19)

The influence of anions on the peptide hydration was also analyzed by MD. The date on the structure was listed in table 3. In this result, secondary structure of H_2^+-F5-NH_2 and H-F5-NH_2 was dominated by bend, turn, and abundant coil structure at 278 K. In addition, β-

sheet and β-bridge structures tended to increase its proportion at 310 K. On the other hand, no systematic change in the secondary structure of the peptides depending on the salt type was observed (Table 3). Analysis of DDCI that indicated how each anion was close to the N-terminus of the peptide was also conducted [31]. The data of the analysis was obtained by calculating the frequency of minimum distances between the N-terminus and an anion in trajectories. As shown in figure 20, it was confirmed that anions tended to localize in the region of 0.2 to 0.4 nm from the ionized N-terminus. Among them, temperature-dependent systematic change in distribution of the anion was not observed. Analysis of the intermolecular interaction between the peptide and molecules consisting of solvent and salt was also conducted. Analyzed data was shown in figure 21. Although the interaction tended to become unstable due to an increase in the temperature, difference in anion type did not bring systematic change in the interaction energy between peptide and solvent. Consequently, this MD results suggested that the localization of anion molecules around the ionized N-terminus could not properly explain the influence of anion types on the hydration state of the peptide. However, previous studies showed that chaotropic anions close to the ionized N-terminus acted on reverse Hofmeister series, interfered with hydration of the peptide [32] and reduced interaction between protein and water [31]. From these findings, it seemed plausible that anions close to the N-terminus had some influence even for the peptide hydration as well as the proteins. To confirm this hypothesis, further experiments are required, that is, selection of appropriate conditions in MD, such as simulation time, salt concentration, and the number of peptide, may bring more accurate description in self-assembly of shorter ELPs. As summary, it was estimated that the anions were localized around the charged N-terminus in this calculation condition.

(Figures 20 and 21)

Discussion from turbidity measurement and MD

To summarize the results of turbidity assay, obtained T_t values in pH buffer, in salt solution, and pH buffers with salt were listed with SEM. in table 4, 5, and 6, respectively. Comparison the results between the four peptide analogs suggested that the pH and salt significantly changed the T_t by influencing both termini of the peptide rather than the peptide backbone.

(Table 4, 5, and 6)

Previous research described that the effect of ionized termini on T_t was considered negligible in a long ELP, H-(VPGVG)$_{120}$-OH [19]. However, this study revealed that the low molecular weight ELP was sensitively affected by pH and salt in solution. In the turbidity measurement, H-F5-OH exhibited self-assembly with T_t value under acidic conditions but did

not show self-assembly in basic conditions. Thus, it was expected that the ionization of the carboxyl group more effectively interfered with the hydrophobic effect, which induce the self-assembly, than that of the amino group. This result was consistent with previous report indicating that ionized aspartic acid and glutamic acid brought lower T_t than ionized lysine in long ELP [22]. The results of MD simulation also showed that the peptide was more hydrated at the C-terminus than the N-terminus. Therefore, this study suggested a novel mechanism in hydration of short ELPs that the ionization at each terminus had different effects on T_t. On the other hand, H-F5-OH in weak acidic condition and neutral condition showed relatively lower T_t than that in strong acidic condition. From this result, it was hypothesized that the self-assembly of the peptide was promoted via electrical interactions occurring between zwitter ionized peptides. To verify this presumed self-assembling process, further verification is needed, in particular, MD simulation of zwitter ionized peptides are required.

This study also showed that the chaotropic anions significantly reduced the T_t of the peptide analogs which possessed ionized N-terminus. Anions showed salting in and out effects according to Hofmeister series against F5 analogs that possessed protected N-terminus or uncharged N-terminus under basic conditions (only in case of H-F5-NH_2). However, the effect was reversed on the F5 analogs with ionized N-terminus. The results of MD simulation revealed that anions were localized around the positive charge at N-terminus. Previous studies also showed that the chaotropic anion prevented the hydration of positive charges by masking [31, 32]. From these findings, anions in solution seemed to control the hydration of charged N-terminus in F5 analogs. It would be an important factor determining the self-assembling properties of short ELPs.

In conclusion, it would be possible to control the self-assembling property of short ELPs by presence or absence of charge on the peptide and anion interacting with the positive charge. This could be a simple and potent factor to switch self-assembling property of short ELPs. Because of their small molecular weight, short ELPs possess different responsiveness against environmental factors from long ELPs. In order to observe the responsiveness of short ELPs more effectively and in more detail, it is necessary to pursue the dependence of self-assembly on pH, type and concentrations of salts, and chemical state of peptides, multi-dimensionally.

4. Conclusion

This chapter showed that pH and salt worked as factors controlling self-assembling properties of short ELPs. Analyses of four $(FPGVG)_5$ analogs at which each terminus were protected or unprotected, indicated that pH-dependent ionization of each terminus promoted peptide hydration and interfered with self-assembling property of $(FPGVG)_5$. As an

exception, H-(FPGVG)$_5$-OH in the zwitterionic state showed self-assembly at a relatively low temperature. It was thought that there was a possibility of forming self-assembly via electrical interaction. Salts exhibited salting in and out effect according to the Hoffmeister series against non-ionized peptide. However, it was shown that chaotropic anions greatly decreased the T_t of the short ELP whose N-terminus was ionized. The chaotropic anions seemed to specifically interact with the charge at the ionized N-terminus. Such effect was not observed in long ELPs. Thus, this chapter revealed that short ELPs were affected partially differently by salts. As summary, this study showed that pH and salt could control self-assembling properties of short ELPs. These findings would help further downsizing of ELPs and application of ELPs as stimulus responsive materials.

5. References

[1] Willner I., Willner B., Biomolecule-based nanomaterials and nanostructures, *Nano Lett.*, **10**, 3805-3815 (2010).

[2] Bauri K., Nandi M., De, P., Amino acid-derived stimuli-responsive polymers and their applications. *Polymer Chemistry*, **9**, 1257-1287 (2018).

[3] MacEwan S. R., Chilkoti A., Applications of elastin-like polypeptides in drug delivery, *J. Control Release*, **190**, 314-330 (2014).

[4] Nettles D. L., Chilkoti A., Setton L. A., Applications of elastin-like polypeptides in tissue engineering, *Adv. Drug Deliv. Rev.*, **62**, 1479-1485 (2010).

[5] Despanie J., Dhandhukia J. P., Hamm-Alvarez S. F., MacKay J. A., Elastin-like polypeptides: Therapeutic applications for an emerging class of nanomedicines, *J. Control Release*, **240**, 93-108 (2016).

[6] Yeo G. C., Aghaei-Ghareh-Bolagh B., Brackenreg E. P., Hiob M. A., Lee P., Weiss A.S., Fabricated Elastin, *Advanced Healthcare Materials*, **4**, 2530-2556 (2010).

[7] Yeo G. C., Keeley F. W., Weiss A. S., Coacervation of tropoelastin, *Adv. Colloid Interface Sci.*, **167**, 94-103 (2011).

[8] Li N. K., García Quiroz F., Hall C. K., Chilkoti A., Yingling Y. G., Molecular Description of the LCST Behavior of an Elastin-Like Polypeptide, *Biomacromolecules*, **15**, 3522-3530 (2014).

[9] McDaniel J. R., Radford D. C., Chilkoti A., A unified model for de novo design of elastin-like polypeptides with tunable inverse transition temperatures, *Biomacromolecules*, **14**, 2866-2872 (2013).

[10] Maeda I., Taniguchi S., Ebina J., Watanabe N., Hattori T., Nose T., Comparison between coacervation property and secondary structure of synthetic peptides, Ile-containing elastin-derived pentapeptide repeats, *Protein Pept. Lett.*, **20**, 905-910 (2013).

[11] Kaibara K., Akinari Y., Okamoto K., Uemura Y., Yamamoto S., Kodama H., Kondo

M., Characteristic interaction of Ca^{2+} ions with elastin coacervate: ion transport study across coacervate layers of alpha-elastin and elastin model polypeptide, (Val-Pro-Gly-Val-Gly)$_n$, *Biopolymers*, **39**, 189-198 (1996).

[12] Suyama K., Taniguchi S., Tatsubo D., Maeda I., Nose T., Dimerization effects on coacervation property of an elastin-derived synthetic peptide (FPGVG)$_5$, *J. Pept. Sci.*, **22**, 236-243 (2016).

[13] Tatsubo D., Suyama K., Miyazaki M., Maeda I., Nose T., Stepwise Mechanism of Temperature-Dependent Coacervation of the Elastin-like Peptide Analogue Dimer, (C(WPGVG)$_3$)$_2$, *Biochemistry,* **57**, 1582-1590 (2018).

[14] Suyama K., Tatsubo D., Iwasaki W., Miyazaki M., Kiyota Y., Takahashi I., Maeda I., Nose T., Enhancement of Self-Aggregation Properties of Linear Elastin-Derived Short Peptides by Simple Cyclization: Strong Self-Aggregation Properties of Cyclo[FPGVG]$_n$, Consisting Only of Natural Amino Acids, *Biomacromolecules*, **19**, 3201-3211 (2018).

[15] Maeda I., Taniguchi S., Watanabe N., Inoue A., Yamasaki Y., Nose T., Design of phenylalanine-containing elastin-derived peptides exhibiting highly potent self-assembling capability, *Protein Pept. Lett.*, **22**, 934-939 (2015).

[16] Taniguchi S., Watanabe N., Nose T., Maeda I., Development of short and highly potent self-assembling elastin-derived pentapeptide repeats containing aromatic amino acid residues, *J. Pept. Sci.*, **22**, 36-42 (2016).

[17] Shin H., Jo S., Mikos A. G., Biomimetic materials for tissue engineering, *Biomaterials*, **24**, 4353-4364 (2003).

[18] Groß A., Hashimoto C., Sticht H., Eichler J., Synthetic Peptides as Protein Mimics, *Front. Bioeng. Biotechnol.*, **3**, 211 (2016).

[19] Aladini F., Araman C., Becker C. F., Chemical synthesis and characterization of elastin-like polypeptides (ELPs) with variable guest residues, *J. Pept. Sci.*, **22** (5), 334-342 (2016).

[20] Cho Y., Zhang Y., Christensen T., Sagle L. B., Chilkoti A., Cremer P. S., Effects of Hofmeister anions on the phase transition temperature of elastin-like polypeptides, *J. Phys. Chem. B*, **112**, 13765-13771 (2008).

[21] Rembert K.B., Paterová J., Heyda J., Hilty C., Jungwirth P., Cremer P. S., Molecular mechanisms of ion-specific effects on proteins, *J. Am. Chem. Soc.*, **134**, 10039-10046 (2012).

[22] Urry D. W., Physical Chemistry of Biological Free Energy Transduction As Demonstrated by Elastic Protein-Based Polymers, *J. Phys. Chem. B*, **101** (51), 11007–11028 (1997).

[23] Mackay J. A., Callahan D. J., Fitzgerald K. N., Chilkoti A., Quantitative model of the phase behavior of recombinant pH-responsive elastin-like polypeptides, *Biomacromolecules*, **11**, 2873-2879 (2010).

[24] Lao U. L., Chen A., Matsumoto M. R., Mulchandani A., Chen W., Cadmium removal from contaminated soil by thermally responsive elastin (ELPEC20) biopolymers, *Biotechnol. Bioeng.,* **98**, 349-355 (2007).

[25] Kostal J., Mulchandani A., Gropp K. E., Chen W., A temperature responsive biopolymer for mercury remediation, *Environ. Sci. Technol.*, **37**, 4457-4462 (2003),

[26] Zhao P., Xia G., Dong S., Jiang Z. -X., Chen M. An iTEP-salinomycin nanoparticle that specifically and effectively inhibits metastases of 4T1 orthotopic breast tumors, *Biomaterials*, **93**, 1-9 (2016).

[27] Veneti E., Tu R. S., Auguste D. T., RGD-Targeted Liposome Binding and Uptake on Breast Cancer Cells Is Dependent on Elastin Linker Secondary Structure *Bioconjugate Chem.*, **27**, 1813-1821 (2016).

[28] Hu J., Xie L., Zhao W., Sun M., Liu X., Gao W., Design of tumor-homing and pH-responsive polypeptide-doxorubicin nanoparticles with enhanced anticancer efficacy and reduced side effects, *Chem. Commun.*, **51**, 11405-11408 (2015).

[29] Doherty B., Zhong X., Gathiaka S., Li B., Acevedo O., Revisiting OPLS Force Field Parameters for Ionic Liquid Simulations, *J. Chem. Theory Comput.*, **13**, 6131-6145 (2017).

[30] Kabsch W., Sander C., Dictionary of protein secondary structure: pattern recognition of hydrogen-bonded and geometrical features, *Biopolymers*, **22**, 2577-2637 (1983).

[31] Násztor Z., Dér A., Bogár F., Ion-induced alterations of the local hydration environment elucidate Hofmeister effect in a simple classical model of Trp-cage miniprotein, *J. Mol. Model.*, **23**, 298 (2017).

[32] Paterová J., Rembert K. B., Heyda J., Kurra Y., Okur H. I., Liu W. R., Hilty C., Cremer P. S., Jungwirth P., Reversal of the hofmeister series: specific ion effects on peptides, *J. Phys. Chem. B*, **117**, 8150-8158 (2013).

Table 1. Structure data from MD trajectories at 278 K.[a]

Peptide	Charge	R_g (nm)	SASA (nm^2)	Coil (%)	β-bridge (%)	Bend (%)	Turn (%)	N_{nw}	N_{cw}
Ac-F5-OH	0	0.82 ± 0.02	22.07 ± 1.01	57	4	34	5	2.08 ± 0.66	2.07 ± 0.77
Ac-F5-NH_2		0.83 ± 0.01	21.70 ± 0.57	50	2	37	10	2.11 ± 0.70	1.18 ± 0.79
H-F5-NH_2		0.89 ± 0.03	23.24 ± 1.35	60	0	34	6	2.08 ± 0.80	2.91 ± 1.00
H_2^+-F5-OH	+1	0.78 ± 0.02	21.45 ± 0.93	44	2	37	17	2.82 ± 0.41	2.09 ± 0.76
H_2^+-F5-NH_2		0.82 ± 0.08	21.68 ± 1.18	37	0	51	11	2.81 ± 0.43	1.24 ± 1.14
Ac-F5-O^-	-1	0.81 ± 0.03	22.77 ± 0.87	47	3	39	10	2.03 ± 0.85	6.50 ± 0.86
H-F5-O^-		0.86 ± 0.04	23.24 ± 1.04	49	0	43	8	2.06 ± 0.84	6.43 ± 0.93
H_2^+-F5-O^-	+1, -1	0.85 ± 0.04	22.87 ± 0.93	53	3	36	7	2.81 ± 0.43	6.51 ± 0.90

[a] Ratios of each secondary structure were obtained via dividing the number of residues recognized as each secondary structure by the number of whole residues in a trajectory, 25 residues times 5,000 frames. Other data were described with SD.

Table 2. Structure data from MD trajectories at 310 K.[a]

Peptide	Charge	R_g (nm)	SASA (nm^2)	Coil (%)	β-sheet (%)	β-bridge (%)	Bend (%)	Turn (%)	N_{nw}	N_{cw}
Ac-F5-OH	0	0.81 ± 0.07	21.76 ± 1.15	43	1	7	27	22	1.53 ± 0.74	2.11 ± 0.79
Ac-F5-NH_2		0.82 ± 0.02	21.00 ± 0.72	46	13	1	26	13	2.14 ± 0.82	2.34 ± 0.81
H-F5-NH_2		0.85 ± 0.06	23.03 ± 1.09	36	6	8	33	17	1.71 ± 0.81	2.62 ± 1.04
H_2^+-F5-OH	+1	0.82 ± 0.02	21.72 ± 0.76	44	4	7	39	6	2.83 ± 0.41	1.94 ± 0.76
H_2^+-F5-NH_2		0.82 ± 0.01	21.15 ± 0.63	33	3	7	44	13	2.75 ± 0.49	3.06 ± 1.01
Ac-F5-O^-	-1	0.78 ± 0.03	20.92 ± 0.92	34	0	4	34	28	2.11 ± 0.78	6.19 ± 1.03
H-F5-O^-		0.76 ± 0.01	19.32 ± 0.52	29	1	12	30	28	2.11 ± 0.82	4.70 ± 0.91
H_2^+-F5-O^-	+1, -1	0.71 ± 0.01	19.35 ± 0.52	43	0	4	31	23	2.78 ± 0.46	2.99 ± 0.59

[a] Ratios of each secondary structure were obtained via dividing the number of residues recognized as each secondary structure by the number of whole residues in a trajectory, 25 residues times 5,000 frames. Other data were described with SD.

Table 3. Structure data from MD trajectories with various salts.[a]

Temperature (K)	Peptide	salt	R_g (nm)	SASA (nm^2)	Coil (%)	β-sheet (%)	β-bridge (%)	Bend (%)	Turn (%)	N_{nw}	N_{cw}
278	H_2^+-F5-NH_2	NaCl	0.82 ± 0.08	21.68 ± 1.18	37	0	0	51	11	2.81 ± 0.43	1.24 ± 1.14
		NaBr	0.81 ± 0.01	20.96 ± 0.58	61	0	2	35	2	2.82 ± 0.42	2.25 ± 0.82
		$NaNO_3$	0.84 ± 0.04	21.67 ± 0.92	38	0	3	48	10	2.77 ± 0.47	3.08 ± 0.98
		$NaClO_4$	0.90 ± 0.08	23.17 ± 1.65	52	0	6	20	22	2.75 ± 0.47	2.50 ± 1.07
	H-F5-NH_2	NaCl	0.89 ± 0.03	23.24 ± 1.35	60	0	0	34	6	2.08 ± 0.80	2.91 ± 1.00
		NaBr	1.13 ± 0.06	24.18 ± 1.03	62	3	7	19	10	1.40 ± 0.69	3.10 ± 0.88
		$NaNO_3$	0.90 ± 0.04	22.82 ± 1.24	49	3	8	32	8	2.04 ± 0.85	2.01 ± 1.51
		$NaClO_4$	0.79 ± 0.02	20.69 ± 0.63	52		1	35	12	2.07 ± 0.79	2.54 ± 0.88
310	H_2^+-F5-NH_2	NaCl	0.82 ± 0.01	21.15 ± 0.63	33	3	7	44	13	2.75 ± 0.49	3.06 ± 1.01
		NaBr	0.79 ± 0.02	21.28 ± 0.98	50	3	5	30	11	2.71 ± 0.50	2.89 ± 0.97
		$NaNO_3$	0.79 ± 0.04	20.00 ± 1.03	56	0	7	27	10	2.79 ± 0.45	2.70 ± 0.98
		$NaClO_4$	0.79 ± 0.02	21.50 ± 0.78	42	2	8	33	14	2.60 ± 0.58	2.92 ± 1.03
	H-F5-NH_2	NaCl	0.82 ± 0.02	21.00 ± 0.72	46	13	1	26	13	2.14 ± 0.82	2.34 ± 0.81
		NaBr	0.89 ± 0.05	22.82 ± 1.02	45	1	10	21	24	1.87 ± 0.82	2.54 ± 1.08
		$NaNO_3$	0.83 ± 0.08	21.86 ± 1.49	45	0	2	46	7	1.85 ± 0.86	2.30 ± 1.10
		$NaClO_4$	0.91 ± 0.06	23.17 ± 0.91	59	9	5	26	1	2.14 ± 0.82	2.80 ± 0.99

[a] Ratios of each secondary structure were obtained via dividing the number of residues recognized as each secondary structure by the number of whole residues in a trajectory, 25 residues times 5,000 frames. Other data were described with SD.

Table 4. T_t values of four $(FPGVG)_5$ analogs in different pH buffers.[a]

pH buffer	pH	T_t of each peptide (°C)				
		H-F5-OH (10 mg/mL)	Ac-F5-OH (10 mg/mL)	H-F5-NH_2 (10 mg/mL)	H-F5-NH_2 (2.0 mg/mL, TFA free)	Ac-F5-NH_2 (1.0 mg/mL)
Acidic phosphate buffer	2.1	34.1 ± 0.7	22.3 ± 0.1	NA.	NA.	35.8 ± 1.1
Formate buffer	2.9	24.9 ± 0.7	27.7 ± 0.1	51.8 ± 2.6	NA.	40.0 ± 0.5
Acetic buffer	4.8	25.8 ± 0.5	NA.	49.2 ± 0.1	NA.	40.1 ± 0.5
Neutral phosphate buffer	7.0	28.0 ± 0.5	NA.	23.0 ± 0.7	38.8 ± 0.5	38.4 ± 0.6
Bicarbonate buffer	9.8	NA.	NA.	16.1 ± 0.5	34.1 ± 0.5	39.1 ± 0.7

[a] Mean T_t values with SE. were shown in the table. The measurements were repeated at least three times. NA. meant that the sample did not show self-assembly between 5°C and 90°C.

Table 5. T_t values of four $(FPGVG)_5$ analogs in various salts solution.[a]

Salt type	T_t of each peptide (°C)				
	H-F5-OH (10 mg/mL)	Ac-F5-OH (10 mg/mL)	H-F5-NH_2 (10 mg/mL)	H-F5-NH_2 (2.0 mg/mL, TFA free)	Ac-F5-NH_2 (1.0 mg/mL)
NaCl	22.2 ± 0.3	34.3 ± 0.9	36.3 ± 1.1	34.8 ± 0.3	44.4 ± 0.6
KCl	22.5 ± 0.1	35.7 ± 0.3	36.7 ± 0.2	34.9 ± 0.3	43.9 ± 0.2
$MgCl_2$	16.7 ± 0.1	36.8 ± 1.3	27.0 ± 0.7	33.1 ± 0.5	43.3 ± 0.4
$CaCl_2$	18.5 ± 0.2	37.6 ± 1.2	28.4 ± 0.9	35.0 ± 0.6	43.7 ± 0.8
$AlCl_3$	18.8 ± 0.5	38.5 ± 0.5	20.9 ± 1.5	NA.	39.9 ± 0.7
NaF	23.1 ± 0.3	NA.	41.5 ± 1.0	29.6 ± 0.4	35.6 ± 1.0
NaBr	13.7 ± 0.1	38.2 ± 0.1	19.5 ± 0.1	36.1 ± 0.6	48.6 ± 1.1
$NaNO_3$	9.2 ± 0.2	38.6 ± 0.2	16.6 ± 0.2	36.1 ± 0.3	48.9 ± 0.5
NaI	Coacervated under 5°C	45.7 ± 1.4	Coacervated under 5°C	38.7 ± 0.7	54.6 ± 0.3
$NaClO_4$	Coacervated under 5°C	44.5 ± 0.6	Coacervated under 5°C	32.5 ± 0.3	46.2 ± 1.0
NaSCN	Coacervated under 5°C	47.5 ± 1.7	Coacervated under 5°C	35.4 ± 1.1	52.7 ± 1.3

[a] Mean T_t values with SE. were shown in the table. The measurements were repeated at least three times.

Table 6. T_t values of four $(FPGVG)_5$ analogs in two pH buffers with salts.[a]

pH buffer	Salt type	T_t of each peptide (°C)			
		H-F5-OH (10mg/mL)	Ac-F5-OH (1.0 mg/mL)	H-F5-NH_2 (10 mg/mL)	Ac-F5-NH_2 (1.0 mg/mL)
Acidic phosphate buffer (pH = 2.1)	NaCl	15.3 ± 0.9	20.5 ± 0.3	24.9 ± 0.5	31.9 ± 0.5
	KCl	15.8 ± 0.2	20.7 ± 0.3	24.5 ± 0.1	30.7 ± 0.5
	NaBr	7.2 ± 0.5	22.1 ± 0.7	14.0 ± 0.8	30.9 ± 1.0
	$NaNO_3$	Coacervated under 5° C	20.7 ± 0.3	10.1 ± 0.3	34.0 ± 1.8
	$NaClO_4$	Coacervated under 5° C	18.2 ± 0.7	Coacervated under 5° C	30.8 ± 0.5
Bicarbonate buffer (pH = 9.8)	NaCl	NA.	NA.	13.3 ± 0.6	38.7 ± 1.4
	KCl	NA.	NA.	14.0 ± 0.2	39.5 ± 1.1
	NaBr	NA.	NA.	15.5 ± 0.2	43.7 ± 1.5
	$NaNO_3$	NA.	NA.	15.6 ± 0.2	44.2 ± 1.9
	$NaClO_4$	NA.	NA.	14.2 ± 0.6	42.5 ± 1.0

[a] Mean T_t values with SE. were shown in the table. The measurements were repeated at least three times.

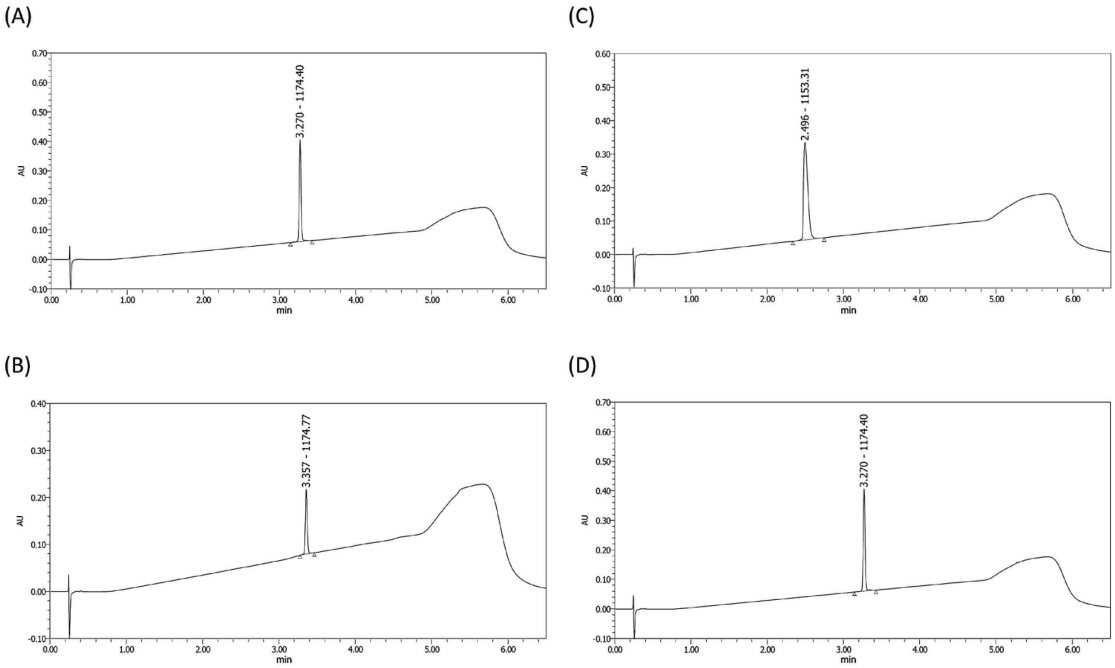

Figure 1. UPLC charts of four peptide analogs.

UPLC data of (A) H-F5-OH (B) Ac-F5-OH (C) H-F5-NH_2 (D) Ac-F5-NH_2 were shown.

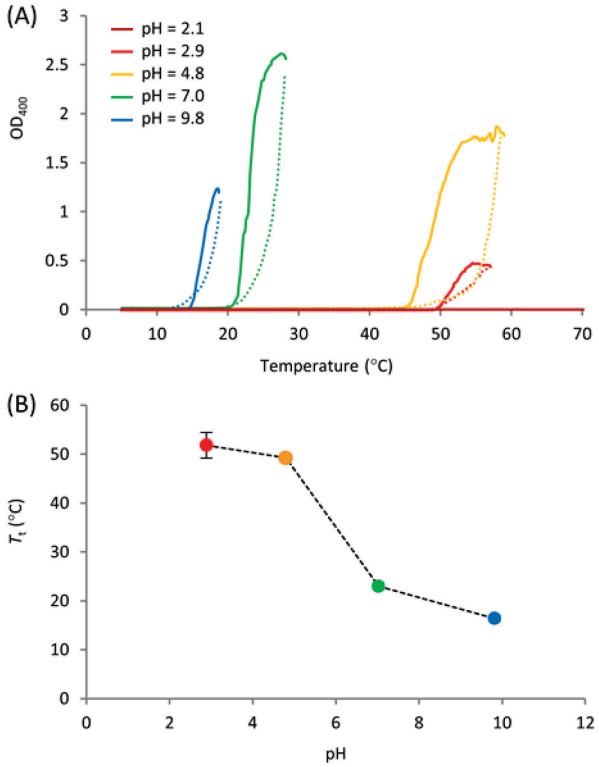

Figure 2. Turbidity profiles and T_t values of H-F5-NH_2 depending on pH values.
(A) Turbidity profiles and (B) T_t in each pH buffer were shown. In figure A, heating curve was shown by solid line and cooling curve was shown by dashed line.

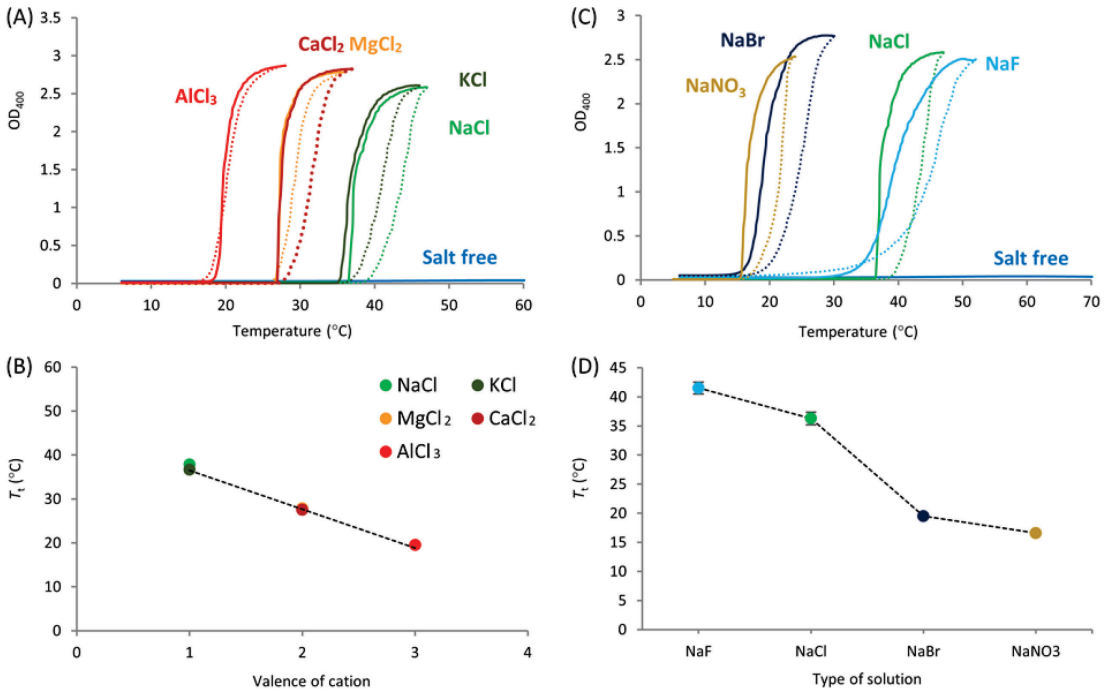

Figure 3. Turbidity profiles and T_t values of H-F5-NH$_2$ depending on salt types. Turbidity profiles and T_ts of H-F5-NH$_2$ in (A, B) solution of chloride salts and (C, D) solution of sodium salts were shown. In figure A and C, heating curve was shown by solid line and cooling curve was shown by dashed line.

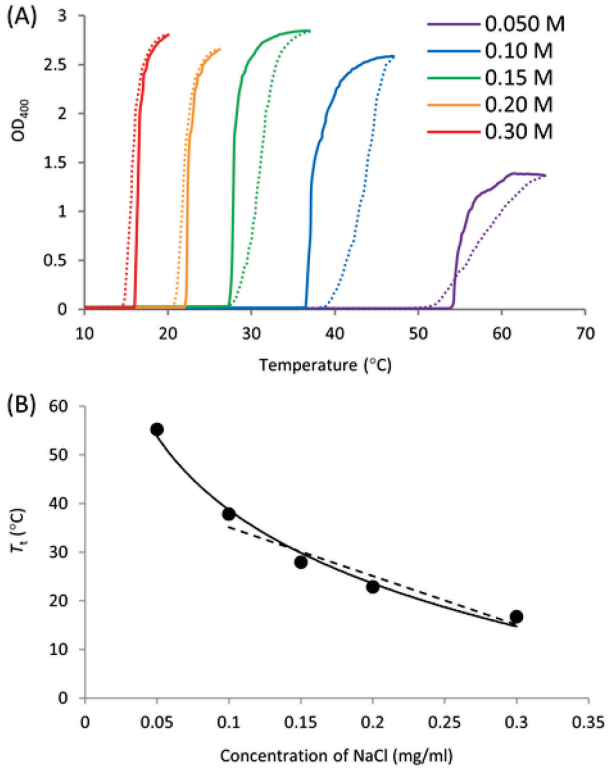

Figure 4. Turbidity profiles and T_t values of H-F5-NH_2 depending on concentration of NaCl.
(A) Turbidity profiles and (B) T_t values of H-F5-NH_2 depending on concentration of NaCl were shown. In figure A, heating curve was shown by solid line and cooling curve was shown by dashed line. Logarithm fitting between 0.05 and 0.3 mg/ml was described by solid line and linear fitting between 0.1 and 0.3 mg/ml was described by dashed line in (B).

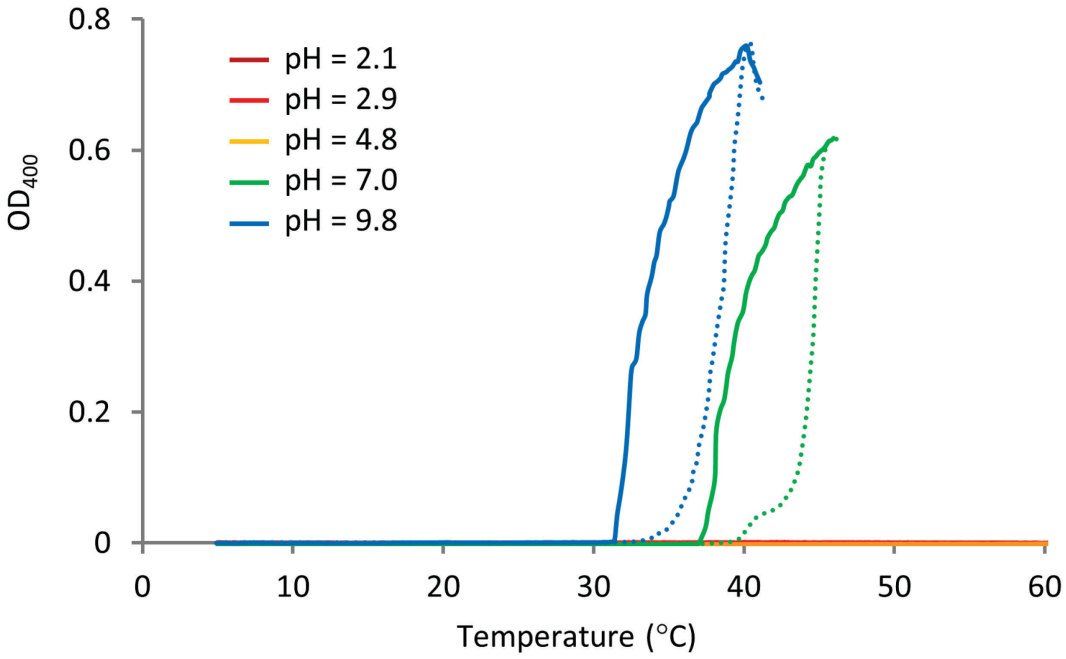

Figure 5. Turbidity profiles and T_t values of H-F5-NH_2 removed TFA depending on pH values.

H-F5-NH_2 showed self-assembly in phosphate buffer (T_t = 38.8 ± 0.5°C) and bicarbonate buffer (T_t = 34.1 ± 0.5°C). In figure A, heating curve was shown by solid line and cooling curve was shown by dashed line.

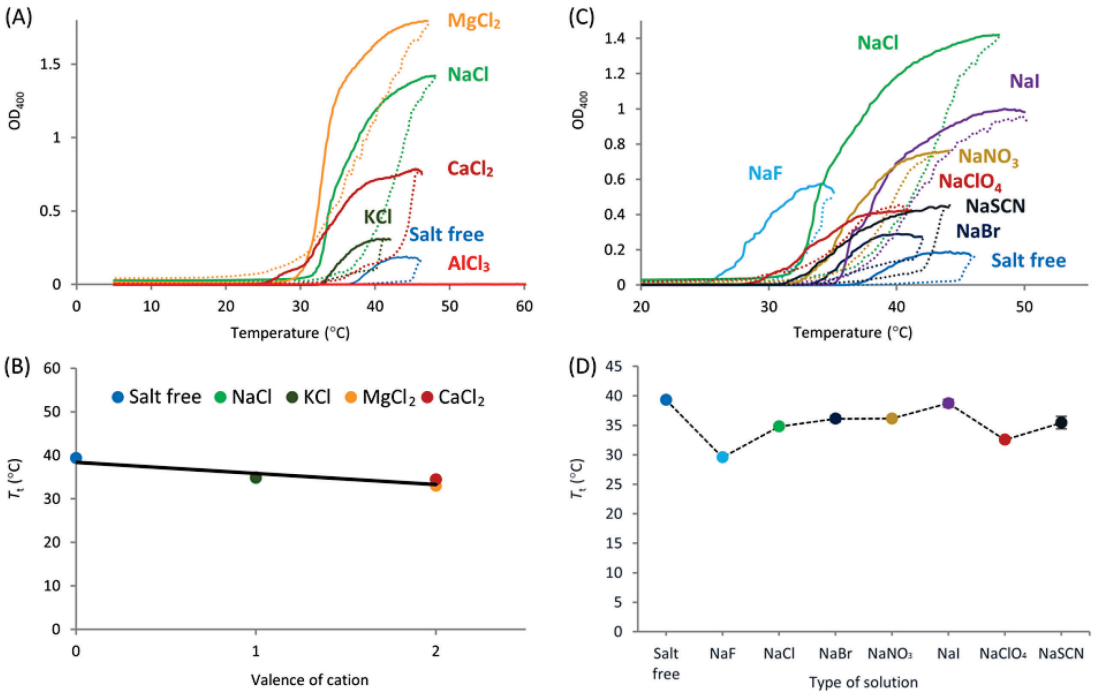

Figure 6. Turbidity profiles and T_t values of H-F5-NH_2 removed TFA depending on salt types.

Turbidity profiles and T_t values of H-F5-NH_2 removed TFA in (A, B) solution of chloride salts and (C, D) solution of sodium salts were shown. In figure A and C, heating curve was shown by solid line and cooling curve was shown by dashed line.

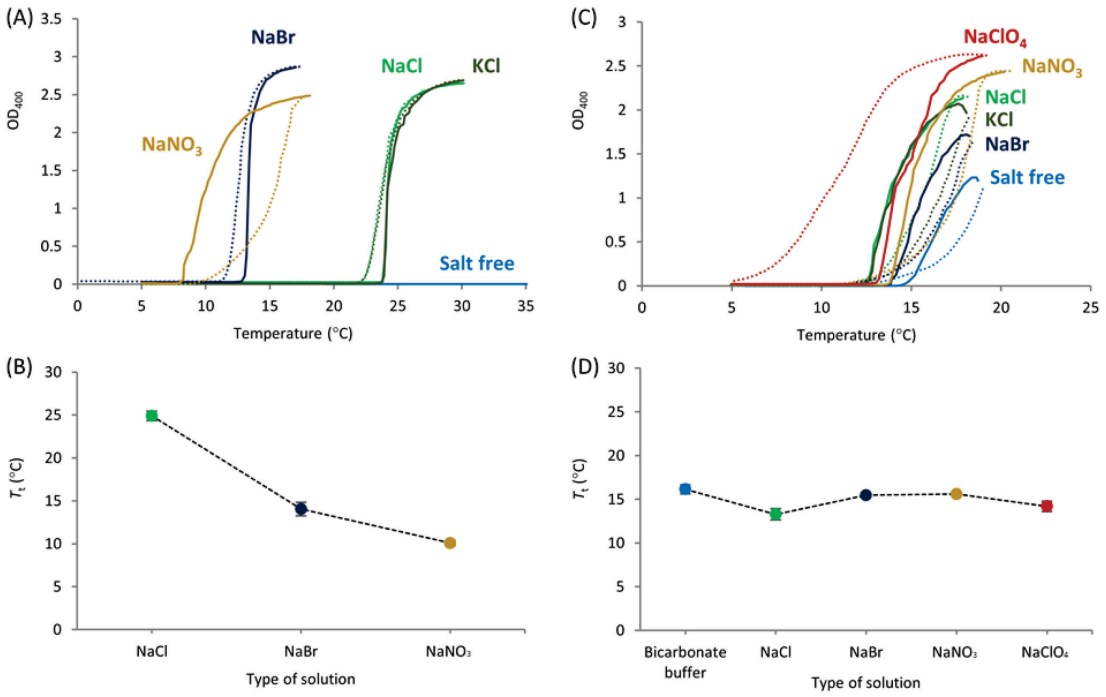

Figure 7. Turbidity profiles and T_t values of H-F5-NH_2 depending on salt types in acidic or basic condition.

Turbidity profiles and T_t values of H-F5-NH_2 in (A, B) acidic phosphate buffer and (C, D) bicarbonate buffer with various salt were shown. In figure A and C, heating curve was shown by solid line and cooling curve was shown by dashed line.

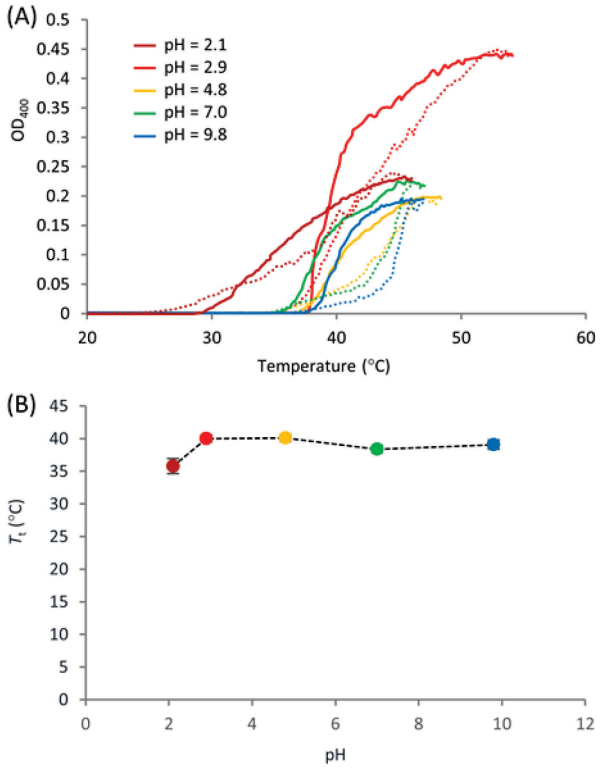

Figure 8. Turbidity profiles and T_t values of Ac-F5-NH_2 depending on pH values.
(A) Turbidity profiles and (B) T_t in each pH buffer were shown. In figure A, heating curve was shown by solid line and cooling curve was shown by dashed line.

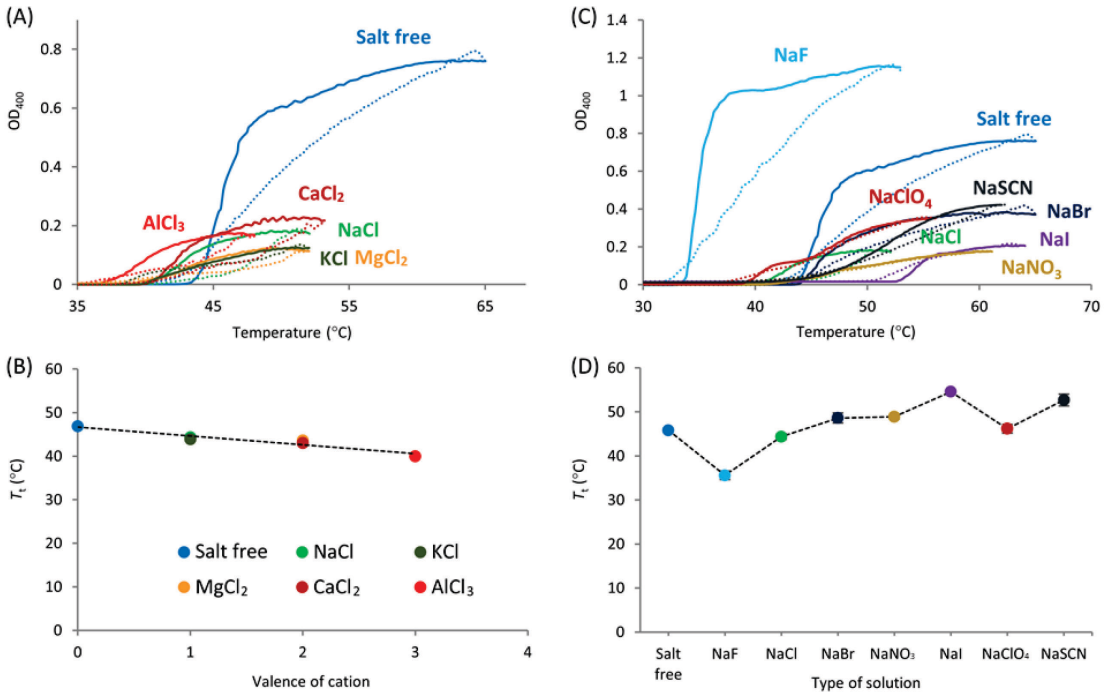

Figure 9. Turbidity profiles and T_t values of Ac-F5-NH_2 depending on salt types. Turbidity profiles and T_t values of Ac-F5-NH_2 in (A, B) solution of chloride salts and (C, D) solution of sodium salts were shown. In figure A and C, heating curve was shown by solid line and cooling curve was shown by dashed line.

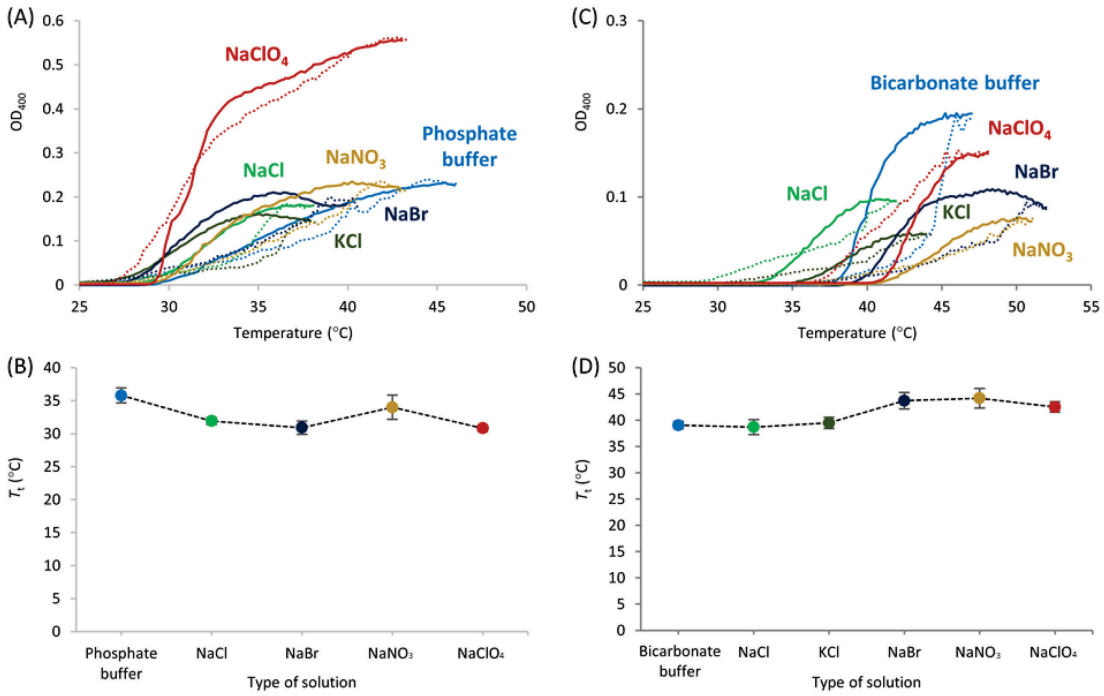

Figure 10. Turbidity profiles and T_t values of Ac-F5-NH_2 depending on salt types in acidic or basic condition.

Turbidity profiles and T_t values of Ac-F5-NH_2 in (A, B) acidic phosphate buffer and (C, D) bicarbonate buffer with various salts were shown. In figure A and C, heating curve was shown by solid line and cooling curve was shown by dashed line.

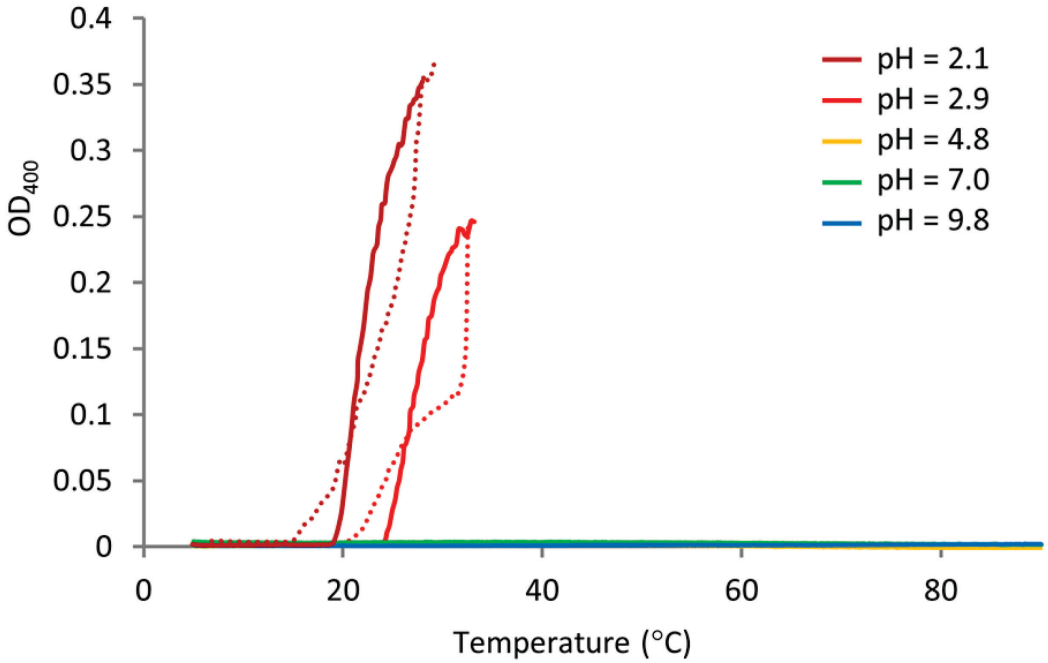

Figure 11. Turbidity profiles and T_t values of Ac-F5-OH depending on pH values. Ac-F5-OH show self-assembly in acidic phosphate buffer (T_t = 22.3 ± 0.1°C) and formate buffer (T_t = 27.7 ± 0.1°C). In figure A, heating curve was shown by solid line and cooling curve was shown by dashed line.

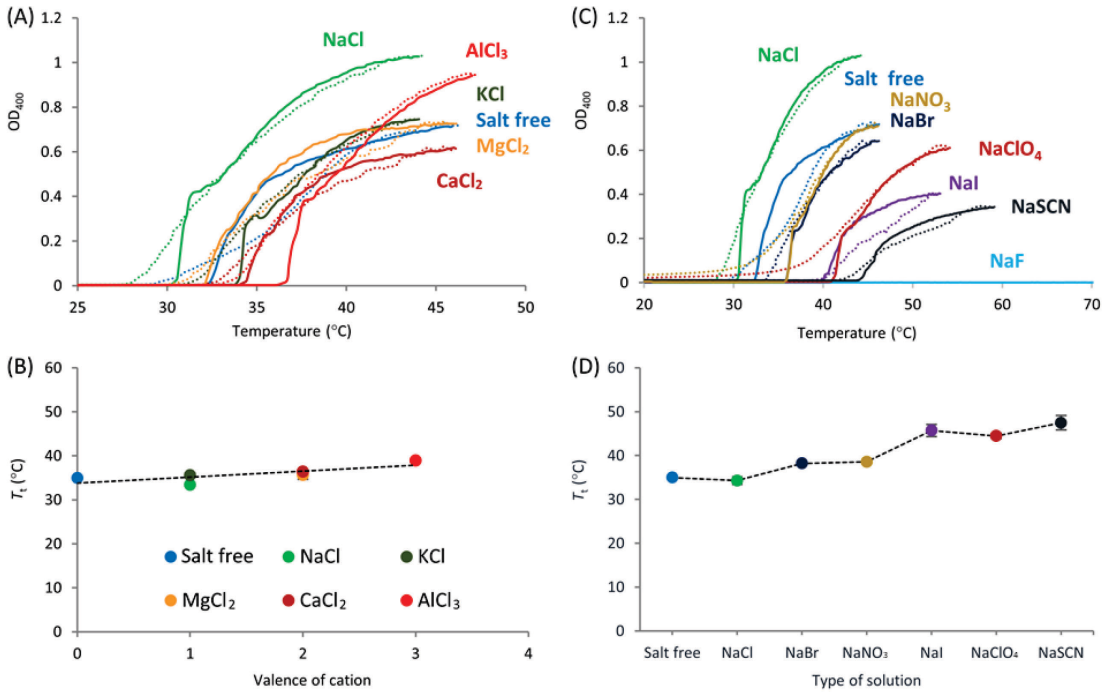

Figure 12. Turbidity profiles and T_t values of Ac-F5-OH depending on salt types. Turbidity profiles and T_t values of Ac-F5-OH in (A, B) solution of chloride salts and (C, D) solution of sodium salts were shown. In figure A and C, heating curve was shown by solid line and cooling curve was shown by dashed line.

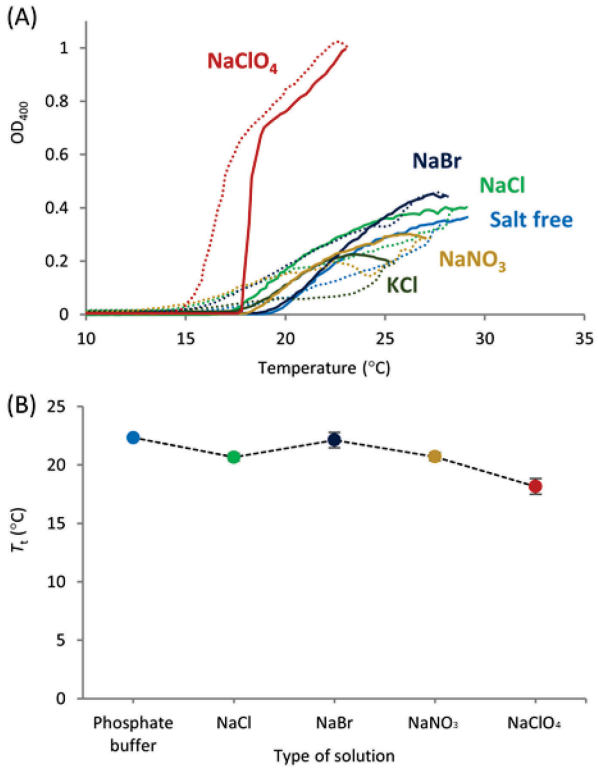

Figure 13. Turbidity profiles and T_t values of Ac-F5-OH depending on salt types in acidic condition.

(A) Turbidity profiles and (B) T_t values of Ac-F5-OH in acidic phosphate buffer with various salts were shown. In figure A, heating curve was shown by solid line and cooling curve was shown by dashed line.

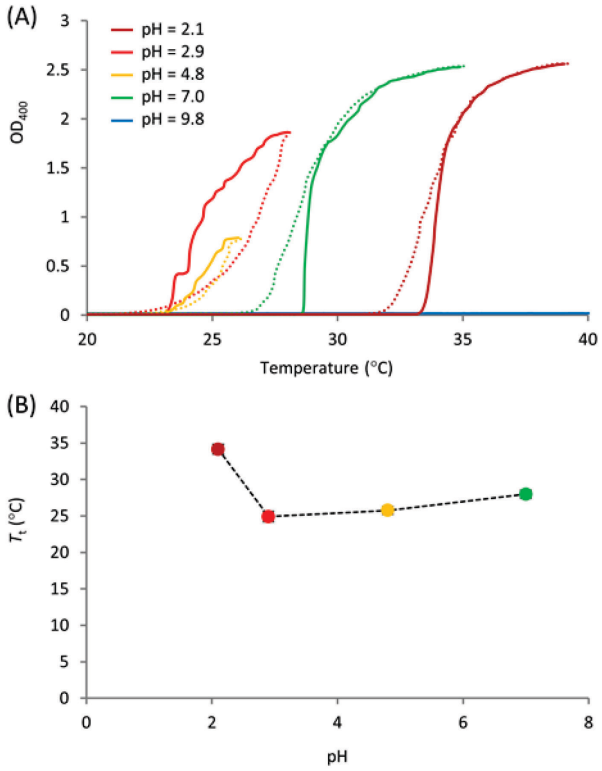

Figure 14. Turbidity profiles and T_t values of H-F5-OH depending on pH values.
(A) Turbidity profiles and (B) T_t in each pH buffer were shown. In figure A, heating curve was shown by solid line and cooling curve was shown by dashed line.

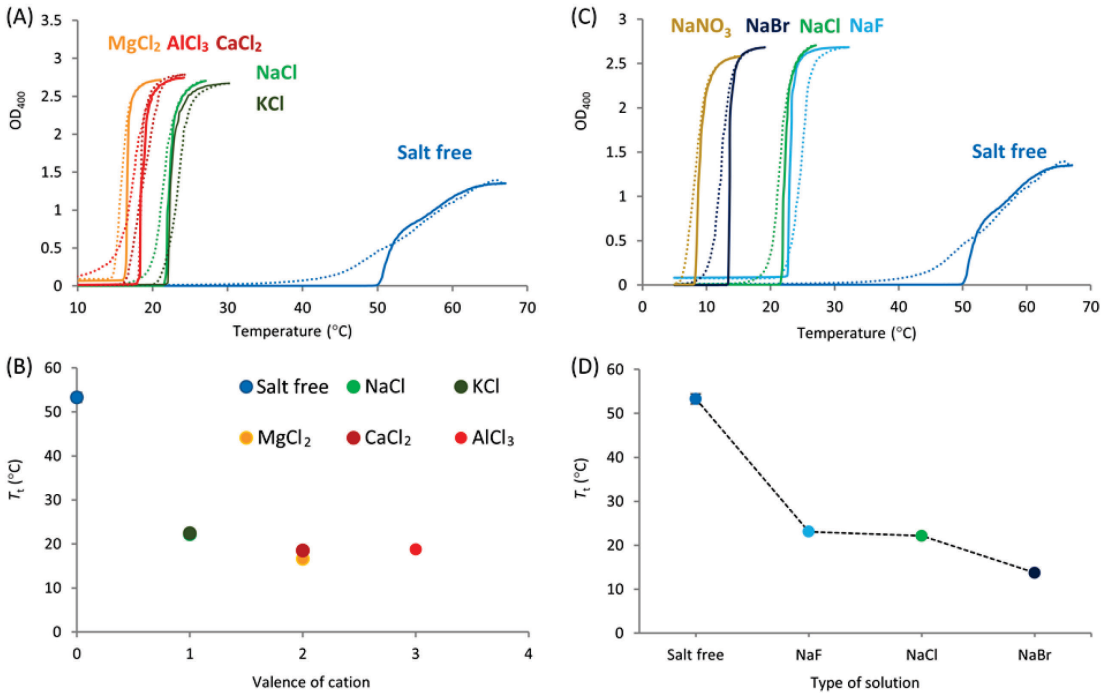

Figure 15. Turbidity profiles and T_t values of H-F5-OH depending on salt types. Turbidity profiles and T_t values of H-F5-OH in (A, B) solution of chloride salts and (C, D) solution of sodium salts were shown. In figure A and C, heating curve was shown by solid line and cooling curve was shown by dashed line.

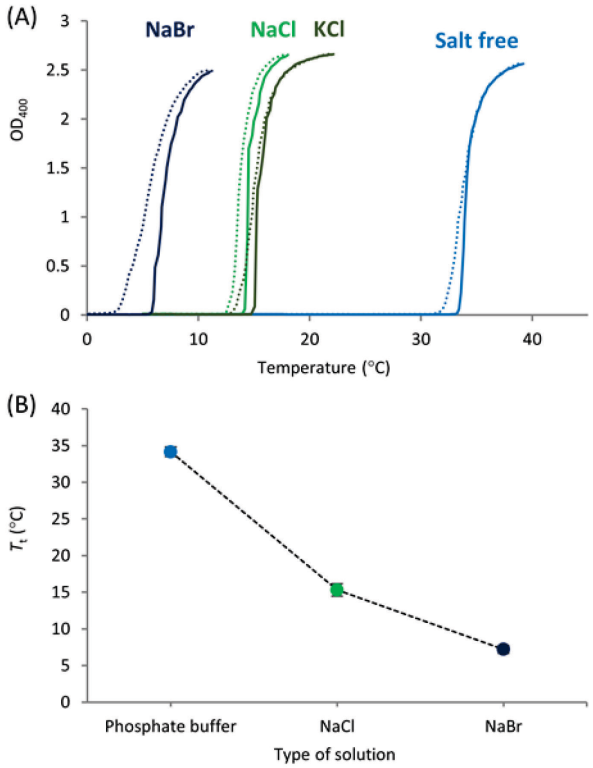

Figure 16. Turbidity profiles and T_t values of Ac-F5-OH depending on salt types in acidic condition.

(A) Turbidity profiles and (B) T_t values of Ac-F5-OH in acidic phosphate buffer with various salts were shown. In figure A, heating curve was shown by solid line and cooling curve was shown by dashed line.

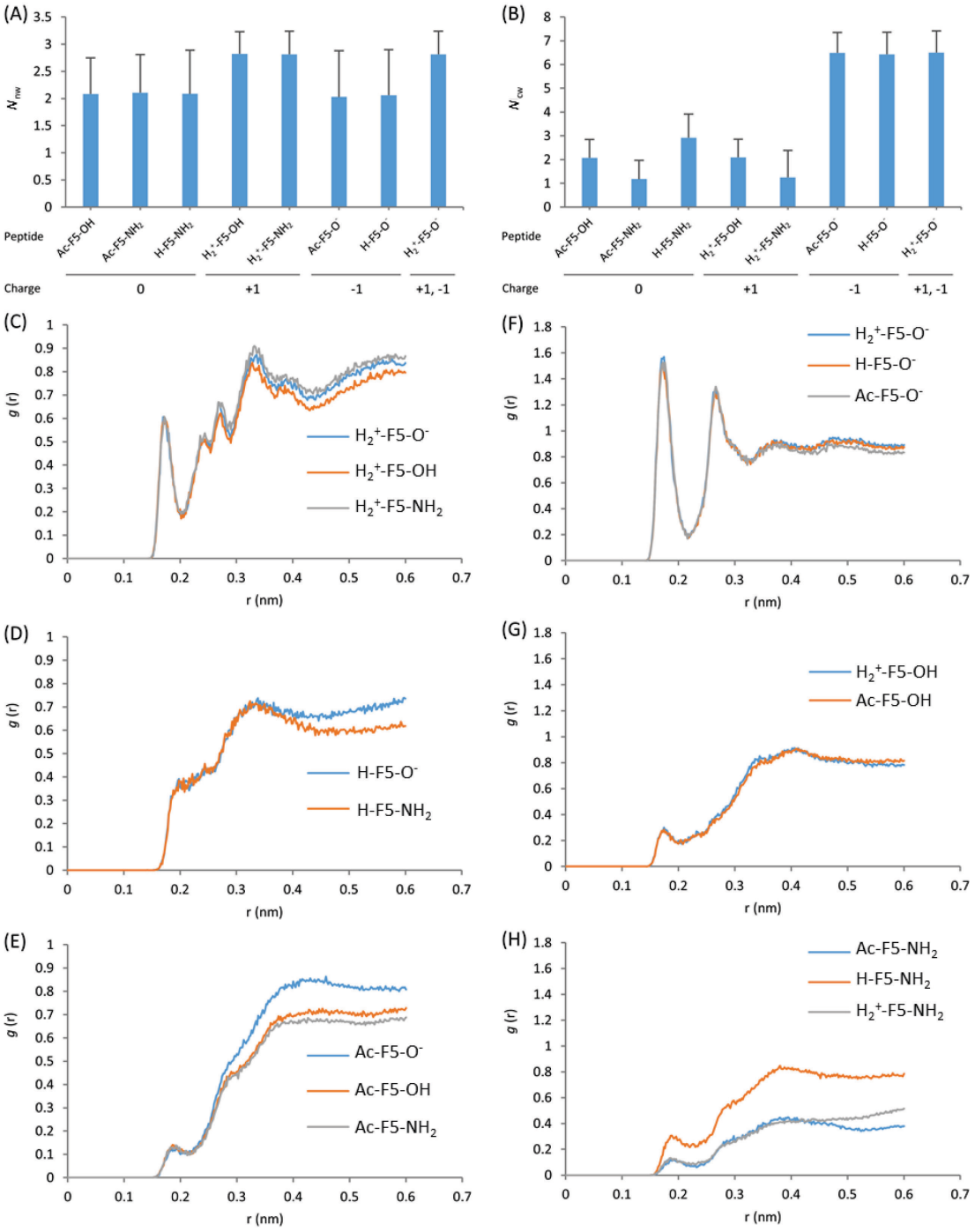

Figure 17. The analysis of hydration state of each peptide terminus in trajectories at 278 K. Average number of hydrogen bond between water molecules and (A) N-terminus and (B) C-terminus with SD. RDF of water from (C) ionized, (D) neutral, and (E) acetylated N-terminus were shown. RDF of water from (F) ionized, (G) neutral, and (H) amidated C-terminus were also described.

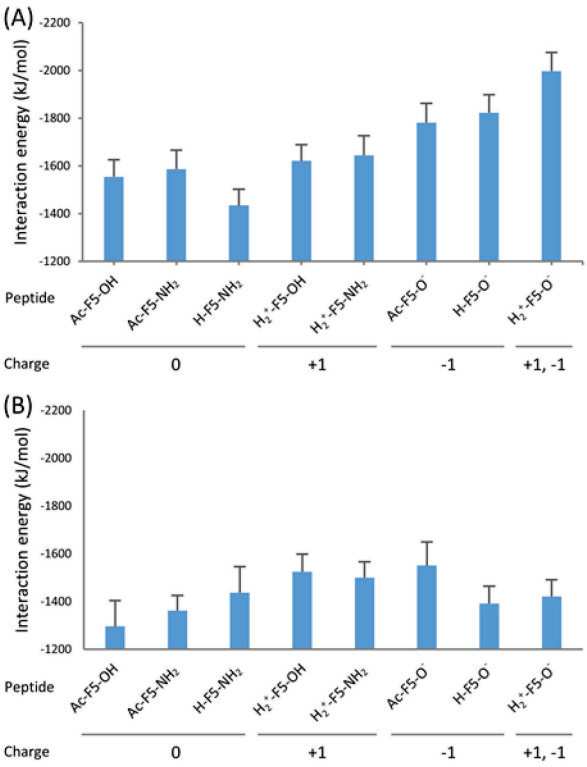

Figure 18. Interaction energy between water and each peptide.

Interaction energy was calculated from trajectories at (A) 278 K and (B) 310 K. These values were obtained with SD by time-averaging summations of Coulomb (Coul-SR) and van der Waals interaction (LJ-SR).

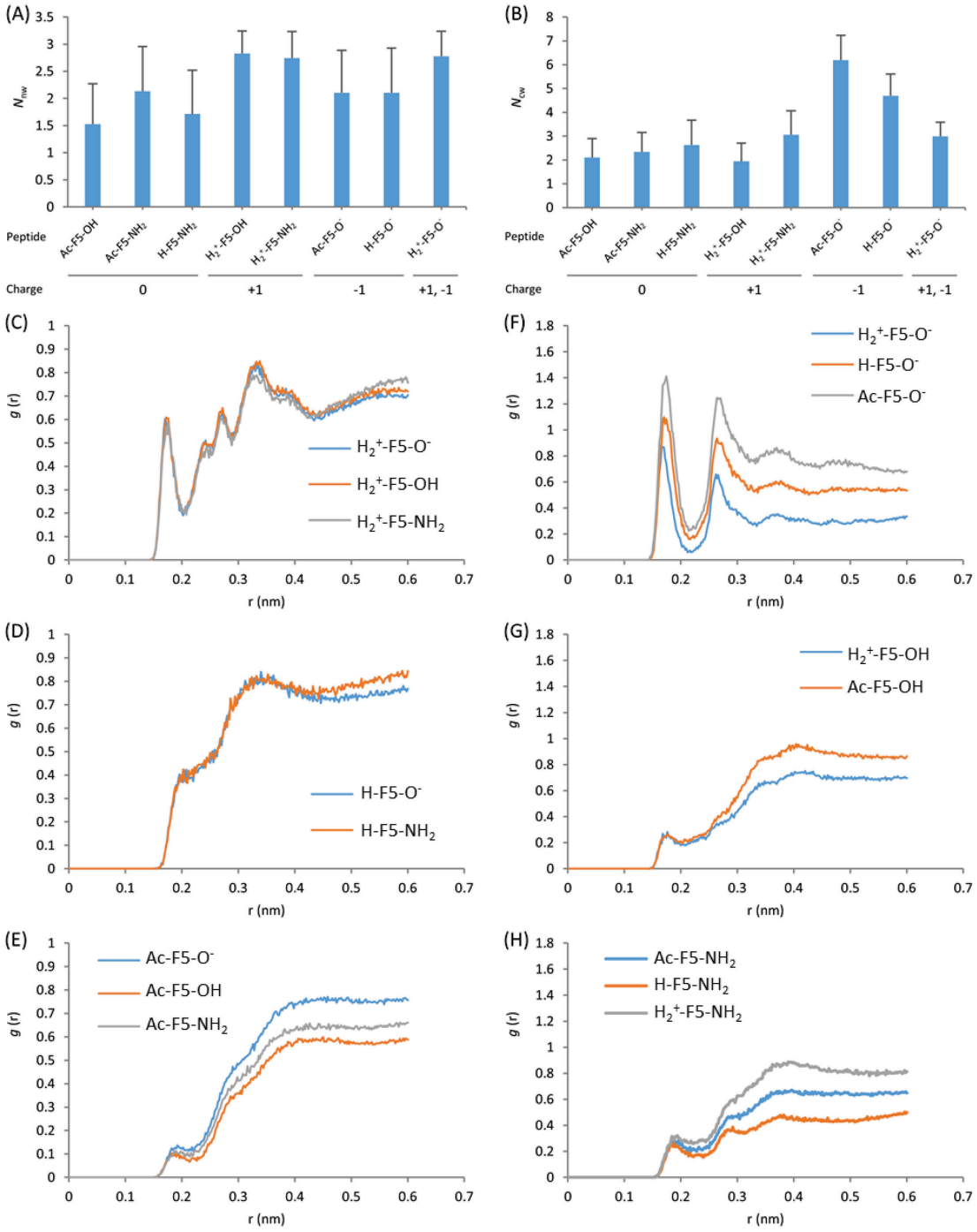

Figure 19. The analysis of hydration state of each peptide terminus in trajectories at 310 K

Average number of hydrogen bond between water molecules and (A) N-terminus and (B) C-terminus with SD. RDF of water from (C) ionized, (D) neutral, and (E) acetylated N-terminus were shown. RDF of water from (F) ionized, (G) neutral, and (H) amidated C-terminus were also described.

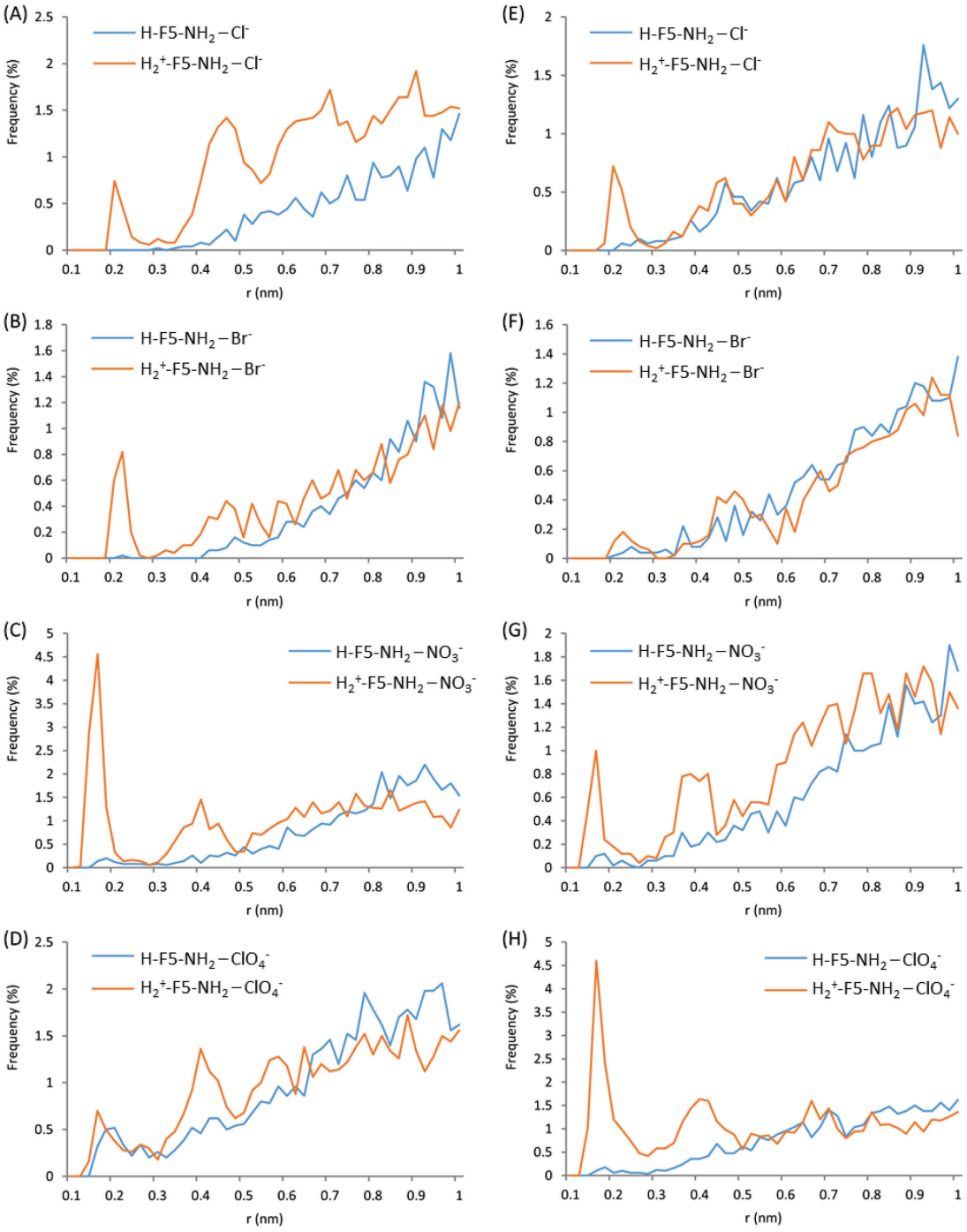

Figure 20. The DDCI analysis in H_2^+-F5-NH_2 and H-F5-NH_2

The frequency of the minimum distance is plotted at intervals of 0.02 nm. DDCI profile between the peptides and (A) Cl^-, (B) Br^-, (C) NO_3^-, and (D) ClO_4^- at 278K, and (E) Cl^-, (F) Br^-, (G) NO_3^-, and (H) ClO_4^- at 310 K were shown. Orange line described DDCI between H_2^+-F5-NH_2 and anions. Blue line described DDCI between H-F5-NH_2 and anions.

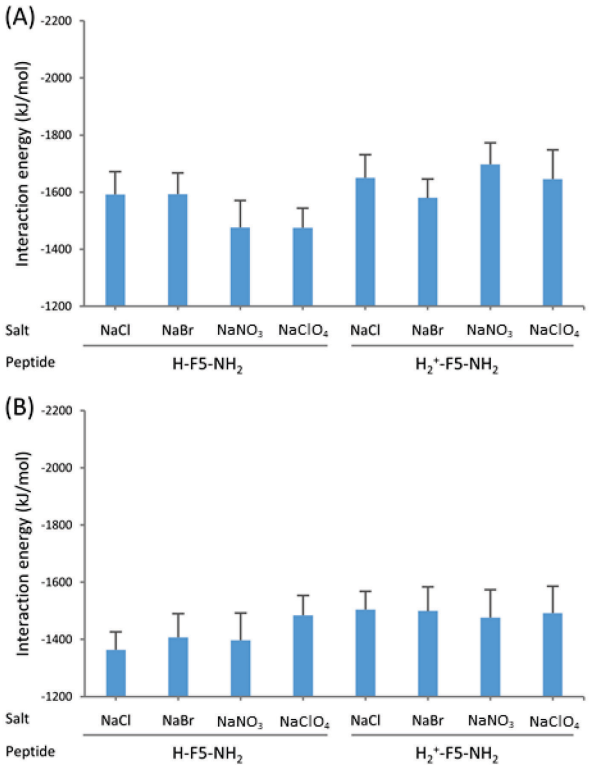

Figure 21. Interaction energy between solvent and each peptide.

Interaction energy was calculated from trajectories at (A) 278 K and (B) 310 K. Solvent included water molecules, cations and anions. These values were obtained with SD by time-averaging summations of Coulomb (Coul-SR) and van der Waals interaction (LJ-SR).

CHAPTER 4

Investigation of sequential and structural requirement for self-assembly using short elastin-like peptide analogs with shuffled unit sequences

Abstract

Elastin-like peptides (ELPs) that possess characteristic hydrophobic repetitive sequences, such as $(VPGVG)_n$, show temperature-dependent reversible self-assembling properties. Although the stimuli responsiveness of this self-assembling property was well studied, sequential and structural requirement for self-assembly is still ambiguous. In this chapter, based on $(FPGVG)_5$ that is a short ELP previously developed, 11 shuffled peptide analogs were designed to elucidate the sequential and structural requirement for self-assembly of ELPs. The sequence of the 11 shuffled peptide analogs were analyzed by turbidity measurement, circular dichroism, and molecular dynamics. As a result, it was shown that 8 peptides exhibited self-assembling property, while the 3 peptides were hard to dissolve in water and could not determine self-assembling property. In the structural analyses, they indicated different structural features. Among the peptide analogs possessing self-assembling potency, their secondary structures were different from each other. These results suggested that composition of amino acid in each repeating unit would cause phase transition behavior of the peptides, but potential of self-assembly and water solubility were dependent on primary structure of each repetition sequence. Moreover, this chapter also found 2 peptides which exhibited more potent self-assembling property than the original $(FPGVG)_5$, indicating that shorter ELPs could be obtained by using their novel and potential motifs as repetitive units. Although further analysis will be necessary to elucidate molecular mechanism in self-assembly of these repeating peptides, this study gives insight into structure-function relationship of the self-assembling peptides for application of ELPs.

1. Introduction

Elastin-like peptides (ELPs) which derived from elastin show temperature-dependent reversible self-assembling property [1]. In general, the ELPs possess repetitive sequences containing hydrophobic amino acids, such as $(GGVP)_n$, $(VPGVG)_n$, and $(GVGVAP)_n$, respectively [2]. These hydrophobic sequences were thought to induce the self-assembly by hydrophobic effect between them [3-5]. As shown in chapters 1 and 2, the self-assembling property showed responsiveness to various factors in addition to temperature. Thus, the ELPs have been applied to variety of biomaterials with the advantage of such responsiveness [6-9]. Previously, the dependencies of self-assembly on these factors, such as hydrophobicity of residues [10-15], repetition number (n) [10, 16-19], ions [12, 20-22], pH [12, 23], pressure

[24], osmolytes [25, 26], multimerization, and branching [12, 27-35], have been studied to elucidate molecular mechanism in the self-assembly and/or to obtain better molecular designs for application. However, further studies are needed in order to clarify the relationship between structure and function in ELPs.

In elastin that is the origin of ELPs, motifs including Pro-Gly (PG) sequence were well preserved in many animal species [36]. Notably, some studies mentioned that the turn structure occurring in the PG sequence was important for the self-assembly of ELPs [37-39]. On the other hand, it was reported that secondary structure of a self-assembling ELP showed different from that of the conventional ELP [40]. Consequently, the importance of secondary structures in self-assembling property seemed to be ambiguous at present. Recently, some repetitive peptides including P-X_n-G (X = arbitrary amino acid) motif that dominated by hydrophobic residues also indicated LCST-like phase transition behavior [41]. It was shown that primary structure in a repetition unit affected phase transition behavior of the peptide containing the repetitive sequence. However, detailed mechanisms driving self-assembly of ELPs do not clarified, further accumulation of such sequence libraries of the peptides with phase transition property and further specification of the structural factors driving the self-assembly are required currently. Moreover, these knowledge regarding self-assembling would also help efficient design of ELPs for application to develop new materials.

Design of ELPs in the applications possess scalability due to their various stimuli responsiveness and sequential varieties. Shortening of peptide-length had thought to be reduced the self-assembling property of ELPs [10, 19]. However, short ELPs keeping the self-assembling property were developed by substituting the first valine residue in the typical repetitive sequence, VPGVG, to more hydrophobic amino acids [13-15]. Although $(VPGVG)_n$ required 40 or more of repetition number to show self-assembly [10, 13, 38, 42], $(IPGVG)_7$, $(FPGVG)_5$, and $(WPGVG)_3$ showed self-assembly with relatively short peptide-lengths. Among them, the repetitive number, n, decreased in proportion to the hydrophobicity of the residues replaced [13, 14, 15]. These chemically synthesizable short ELPs could be advantageous in bulk preparation in comparison with the long polypeptides that had to be prepared by protein expression systems. In addition, as we described in chapter 2, $(FPGVG)_5$ tended to respond to pH and specific salt more sensitively as compared with the long ELPs. Perhaps, short ELPs may exhibit novel stimuli responsiveness different from the long ELPs by various kinds of chemical modifications. Such novel properties would give variety in the choice of the ELPs possessing different sequences and lengths at individual applications. On the other hand, the self-assembling property also depends on the order of amino acids in repeating units [41]. It was thought that the self-assembling property of ELPs could be controlled by the primary structure in the repetition sequences. As in previous studies [41], comparisons of the properties among the ELPs with different primary structures

would give valuable insights for identifying the factors that necessary for self-assembly. Moreover, such comparisons may bring novel sequential motifs exhibiting potent self-assembling property. By using such motifs, it may enable to provide shorter ELPs.

In this chapter, the relationship between the primary structure of PG-rich motifs derived from the short ELP and its various properties were investigated. To elucidate the influence of the primary structure of the motifs on the self-assembling property, 11 $(FPGVG)_5$ based-peptide analogs that were constructed by shuffling FPGVG sequences were designed by using the circular permutation method. The properties of these chemically synthesized peptides were analyzed by turbidity measurement, circular dichroism, and molecular dynamics. It was shown that the eight shuffled peptide motifs exhibited self-assembling property, and the other 3 peptides was hard to dissolve in water. In addition, they showed different structural features in the structure analyses. These results suggested that composition of amino acids in the repeating unit would bring phase transition behavior of the peptides, but potentials of self-assembly and solubility in water were dependent on primary structures in repetitive sequences. Furthermore, this study also disclosed new motifs that exhibited more potent self-assembling property than the original FPGVG. As a result, shorter ELPs could be obtained by using these novel and potential motifs as repetitive units.

2. Materials and methods

Chemicals

Fmoc-NH-SAL-MBHA resin (100–200 mesh) and Fmoc-Gly Alko Resin (100-200 mesh) were purchased from Watanabe Chemical Industries Ltd. (Hiroshima, Japan). 2-(1H-Benzotriazol-1-yl)-1,1,3,3-tetramethyluronium hexafluorophosphate (HBTU) and 1-hydroxybenzotriazole (HOBt) were purchased from Kokusan Chemical Co., Ltd. (Tokyo, Japan). Other reagents for peptide synthesis were also purchased from Watanabe Chemical Industries Ltd. Disodium hydrogen phosphate 12-water and sodium dihydrogenphosphate dehydrate were purchased from Nacalai Tesque Co. Ltd. (Kyoto, Japan). Water for sample preparation was purified by Milli-Q Integral 3 (Merck Millipore, Billerica, MA). Solvents for peptide synthesis and other reagents were also obtained from commercial suppliers and used without further purification.

Synthesis of $(FPGVG)_5$ and 11 shuffled $(FPGVG)_5$ analogs

All peptides were synthesized by following the synthesis method described in our previous study [27, 28]. They were synthesized on an ABI 433A peptide synthesizer (Applied Biosystems, Foster City, CA) in 0.10 mmol scale by using the solid phase method with Fmoc chemistry. 0.149 mg (equivalent to 0.1 mmol) of Fmoc-NH-SAL-MBHA Resin (100–200 mesh) were used as the solid phase support for peptide synthesis. After peptide

elongation, deresination was performed by a reagent cocktail containing 95% TFA/2.5% TIS/2.5% H_2O. The deresinated-peptide was pre-purified by Sep-pak Vac 35cc C18 (Waters Co., Milford, MA) column. Subsequently, further purification was performed by RP-HPLC (The Breeze^{TM} 2 HPLC System, Waters Co.) composed with a C8 column (COSMOSIL 5C8-AR300 20 mmI.D. x 150 mm, Nacalai Tesque Co. Ltd.) and a solvent system consisting of 0.1% TFA aqueous solution (v/v) and 0.1% TFA aqueous solution in 80% acetonitrile aqueous solution (v/v). The eluted fractions containing peptides were concentrated by evaporation and lyophilized. Consequently, all peptides were obtained as a colorless powder. Purity and molecular weights of the peptides were confirmed by ACQUITY UPLC H-Class (Waters Co.) equipped with an ACQUITY UPLC BEH C-18 column (100 mm, flow rate 0.6 mL/min) (Waters Co.) at 49 ˚C and the eluting product was detected by UV at 225 nm and a quadrupole mass spectrometer, ACQUITY QDa (Waters Co.). The solvent system for UPLC consisted of 0.1% formic acid aqueous solution (v/v, solvent A) and 0.1% formic acid in acetonitrile (v/v, solvent B), and elution was performed with a linear gradient of solvent B, 24% to 56% over 4.23 min. As listed below, H-(FPGVG)$_5$-NH_2 and 11 shuffled analogs based on H-(FPGVG)$_5$-NH_2 were designated for convenience.

Peptide A : H-(FPGVG)$_5$-NH_2

Yield = 120.2 mg / 52.2 %. Retention time = 2.578 min. MS (ESI) m/z: calculated for $C_{230}H_{313}N_{51}O_{50}$ 1153.35 ($[M + 2H]^{2+}$), found 1153.47.

Peptide B : H-(FGPVG)$_5$-NH_2

Yield = 72.0 mg / 31.3 %. Retention time = 2.493 min. MS (ESI) m/z: calculated for $C_{230}H_{313}N_{51}O_{50}$ 1153.35 ($[M + 2H]^{2+}$), found 1153.53.

Peptide C : H-(FGPGV)$_5$-NH_2

Yield = 104.3 mg / 45.3 %. Retention time = 2.491 min. MS (ESI) m/z: calculated for $C_{230}H_{313}N_{51}O_{50}$ 1153.35 ($[M + 2H]^{2+}$), found 1153.47.

Peptide D : H-(FGVGP)$_5$-NH_2

Yield = 69.2 mg / 30.0 %. Retention time = 2.819 min. MS (ESI) m/z: calculated for $C_{230}H_{313}N_{51}O_{50}$ 1153.35 ($[M + 2H]^{2+}$), found 1153.48.

Peptide E : H-(FGVPG)$_5$-NH_2

Yield = 110.7 mg / 48.0 %. Retention time = 2.721 min. MS (ESI) m/z: calculated for $C_{230}H_{313}N_{51}O_{50}$ 1153.35 ($[M + 2H]^{2+}$), found 1153.67.

Peptide F : H-(FGGPV)$_5$-NH$_2$

Yield = 47.7 mg / 20.7 %. Retention time = 2.377 min. MS (ESI) m/z: calculated for $C_{230}H_{313}N_{51}O_{50}$ 1153.35 ($[M + 2H]^{2+}$), found 1153.29.

Peptide G : H-(FGGVP)$_5$-NH$_2$

Yield = 110.8 mg / 48.1 %. Retention time = 2.531 min. MS (ESI) m/z: calculated for $C_{230}H_{313}N_{51}O_{50}$ 1153.35 ($[M + 2H]^{2+}$), found 1153.52.

Peptide H : H-(FPGGV)$_5$-NH$_2$

Yield = 52.3 mg / 22.7 %. Retention time = 2.395 min. MS (ESI) m/z: calculated for $C_{230}H_{313}N_{51}O_{50}$ 1153.35 ($[M + 2H]^{2+}$), found 1153.31.

Peptide I : H-(FPVGG)$_5$-NH$_2$

Yield = 56.2 mg / 24.4 %. Retention time = 2.391 min. MS (ESI) m/z: calculated for $C_{230}H_{313}N_{51}O_{50}$ 1153.35 ($[M + 2H]^{2+}$), found 1153.57.

Peptide J : H-(FVPGGG)$_5$-NH$_2$

Yield = 45.3 mg / 19.7 %. Retention time = 2.074 min. MS (ESI) m/z: calculated for $C_{230}H_{313}N_{51}O_{50}$ 1153.35 ($[M + 2H]^{2+}$), found 1153.47.

Peptide K : H-(FVGPG)$_5$-NH$_2$

Yield = 90.7 mg / 39.3 %. Retention time = 1.979 min. MS (ESI) m/z: calculated for $C_{230}H_{313}N_{51}O_{50}$ 1153.35 ($[M + 2H]^{2+}$), found 1153.48.

Peptide L : H-(FVGGP)$_5$-NH$_2$

Yield = 115.2 mg / 50.0 %. Retention time = 2.220 min. MS (ESI) m/z: calculated for $C_{230}H_{313}N_{51}O_{50}$ 1153.35 ($[M + 2H]^{2+}$), found 1153.51.

Turbidity Measurement

The temperature-dependent self-assembly of the peptides was evaluated using a JASCO V-660 spectral photometer (JASCO Co., Tokyo, Japan). Solution of the peptides were prepared at each concentration in phosphate buffer (pH = 7.4 at 25°C, I = 0.10 mol/L). Turbidity measurements were collected at 400 nm while the temperature was being increased or decreased at a rate of 0.5 °C/min from 5°C to turbidity plateau and the plateau to 5°C or less. Band width and response were set to L2.0 nm and medium, respectively. Self-assembly was determined by the phase transition temperature (T_t). This is the temperature at which the turbidity of the solution reaches half the maximum value [27]. Measurement at each peptide

and concentration was measured at least three times. T_t values were obtained as a mean with standard error.

CD measurement

CD measurement was performed in a JASCO J-725 spectropolarimeter (JASCO Co.). Peptides except D, F, and L were dissolved in the phosphate buffer at a concentration of 0.1 mg/mL. Spectra of the sample solution were measured from 260 to 190 nm at various temperatures between 5 and 65°C. Equilibration time was taken for 5 min after changing temperature. Response, band width, scan speed, sensitivity, and integration were set to 2 seconds, 1 nm, 100 nm/min, 50 mdeg, and 6 times, respectively. A 1.0 mm path-length cuvette was used for all measurements. All spectra of the peptide solution were obtained by subtracting the solvent spectra obtained under the same conditions and smoothing with Savitzky–Golay smoothing filters.

MD Simulation

Structural features of 12 peptides were analyzed in GROMACS 5.1.4 software with charmm36 force field and TIP4P explicit solvent model. Sampling simulation was performed after 50 ns pre-simulation for structural equilibration. Initial conformations in pre-simulation were generated as an extended form by Discovery studio 4.0 software. Ionization of N-terminus and amidation of C-terminus was performed by using *gmx pdb2gmx* command with *–ter* option in GROMACS. These peptide ware solvated in 6.93 nm cubic box with explicit TIP4P water molecules by *gmx solvate*. Successively, 19 or 20 Na^+ and Cl^- ions were replaced with water molecules by *gmx genion* to provide the ionic strength of 0.1 M and to neutralize total charge of the system. The pre-simulation was performed at 278 K for 50 ns. Final coordinates in pre-simulation was trimmed and resized to 5.1 nm cubic box for long MD simulation. After that, ionic strength was adjusted to 0.1 M again by *gmx insert-molecules* command with *-replace* option. GROMACS 2018 was used only in this adjustment. The resized coordinates were used as an initial structure of sampling simulation. Sampling simulation for 100 ns was performed at three temperatures of 278 K, 310 K, and 343 K to consider the change in molecular state due to difference of temperature. A sequence and parameters in pre- and sampling simulation were described in following paragraph.

Pre- and sampling simulation contained minimization, temperature annealing, three equilibrium, and production stages. Solvent minimization was first performed using steepest descent method for 10,000 steps and conjugate gradient algorithm for 20,000 steps. Then, the system was gradually heated for 100 ps in NVT ensemble using v-rescale and equilibrated for 100 ps three times in NPT ensemble using v-rescale thermostat and the berendsen barostat. Until this first equilibrium, all-peptide atoms except hydrogens were

restricted with 20 kcal/mol nm^2. Second and third equilibrium simulations were further conducted in the same condition with first equilibrium except the restraint setting, that is, 2 kcal/mol nm^2 and no constraint were applied to them, respectively. After that, production run with no constraint was performed for 50 ns in pre-simulation and 100 ns in sampling simulation. V-rescale thermostat and Parrinello-Rahman barostat ware used for NPT ensemble in production run. Time step was set to 2 fs. 10 Å cutoff radius was used for the short-range intermolecular interactions. Partial mesh Ewald (PME) summation was used for the long-ranged electrostatic interactions. The LINCS algorithm was used to convert the bonds with H-atoms to constraints. Last 50 ns trajectories were processed to analyze peptide structure. Radius of gyration (R_g), solvent accessible surface areas (SASA), ratios of secondary structure observed, were obtained by using *gmx gyrate*, *gmx sasa*, and *gmx do_dssp* [43].

3. Results and discussion

Peptide syntheses

To investigate the influence of the primary structure of the unit sequences of the ELPs on the self-assembling property, 11 shuffled analogs based on $(FPGVG)_5$ were designed by using the circular permutation. In repetitive sequences, each amino acid residue of the unit sequence was circulating in whole of the sequence. Therefore, it was considered that all patterns with respect to shuffling of the primary structure in the unit sequence can be obtained by fixing one residue with replacing the other residues, respectively, like circular permutation. In this study, the shuffled repetitive peptides which possessed same composition of amino acids as $(FPGVG)_5$ were designed by fixing phenylalanine at first position of the pentapeptide unit. As shown in table 1, they were designated as A to L for convenience. They were successfully synthesized by a conventional solid phase peptide synthesis procedure. The purity and molecular weight of each peptide were confirmed by RP-UPLC–MS. These data were shown in figure 1. As a result, all peptide showed single peak in RP-UPLC–MS with an accurate molecular weight. They were obtained with high purity.

(Figure 1)

The self-assembling property of $(FPGVG)_5$ and 11 shuffled peptides

The self-assembling properties of the peptides were analyzed by the turbidity measurement. Peptide concentration dependency on self-assembly was also investigated using the concentration rage 0.5 to 10 mg/mL. As a result, 8 shuffled analogs exhibited self-assembly (Figure 2). The obtained phase transition temperatures (T_t) were shown in table 1 and the peptide concentration-dependency of T_t values was plotted and shown in figure 3.

These results indicated that a certain order of amino acids (an amino acid sequence) in repetition was not required for self-assembly. Notably, novel repetitive motifs showing potent self-assembly were discovered. The peptides B and C showed lower T_t than original $(FPGVG)_5$ at a concentration of 1 mg/mL. T_t was often used as an indicator of self-assembling ability, and low T_t could be translated into potent self-assembling ability [15, 28, 29]. Although it was known that shortening the peptide-length reduced the self-assembling property of ELPs, shorter ELPs ($n < 5$) keeping self-assembling property could be obtained by using these potential motifs as a repetitive unit. In addition to this finding, irreversible self-assembling property was observed in peptides B and K. In the turbidity measurement, turbid solution of these peptides could return to clear solution when the solution temperature was immediately decreased after reaching a turbidity plateau. However, they formed irreversible self-assembly when the temperature continued to increase after reaching the turbidity plateau. Turbidity profiles in this irreversible aggregation formation was shown in the figure 4. Interestingly, this irreversible self-assembly occurred at relatively low peptide concentration of B and K where the reversible self-assembly did not observed. Furthermore, the approximate temperature at which irreversible self-assembly occurred, appeared to be independent of peptide concentration. These results suggested that the two different self-assemblies of reversible and irreversible reactions occurred in separate individual processes. In our knowledge, short ELPs showing such two-way reversible/irreversible self-assembly were probably the first report. Consequently, novel self-assembling properties were obtained by shuffling the primary structure of already-known short ELP, $(FPGVG)_5$.

(Table 1)

(Figures 2, 3, and 4)

The properties of shuffled peptides were further examined. In addition to the properties of self-assembled peptides described above, 3 shuffled analogs showed a typical property that they were hardly dissolved in phosphate buffer. Thus, it was shown that solubility of the repetitive peptides to aqueous solvents varied with the primary sequence. It was observed that the dependence of T_t on peptide concentrations were also different in the primary structures. To analyze the relationship between peptide concentration and T_t, a fitting analysis was carried out. In this analysis, they were well fit to the logarithm function of concentration described below [10, 19].

$$T_t = m \ln c + b \quad \ldots \text{Equation 1.}$$

The slope and intercept of equation 1 were shown in table 2 and correlation of them was plotted in figure 3. It was indicated that the slope and intercept of the fitting were differently depending on the hydrophobicity and the peptide length of each ELP. However,

these parameters of $(FPGVG)_5$ were different, in particular intercept *b*, from that of shuffled analogs which possessed same peptide length and amino acid composition. Consequently, this analysis indicated that the primary structure in repetitions changed the dependency of T_t on peptide concentration. As a summary of the turbidity measurement, we found that the water solubility and dependency of T_t on the peptide concentration were controlled by primary structure in the repetitions composed of F: P: G: V = 1: 1: 2: 1. In addition, it should be stated that a specific amino acid sequence in the repetitions would not be always required for the expression of phase transition, because all synthesized peptides showing relative high water solubility showed self-assembly in this study.

(Table 2)

Structure analysis of $(FPGVG)_5$ and 11 shuffled peptides

In order to investigate the importance of the structural factor in the self-assembly, CD spectrum measurement of the synthesized peptides was carried out. CD measurement is known to be one of popular means in structural analysis of ELPs. The relationship between structure and function of ELPs was often discussed by using results of CD spectrum measurement. In this study, CD spectra of $(FPGVG)_5$ and water soluble shuffled analogs were measured. These data were shown in figure 5. At low temperature, $(FPGVG)_5$ had a minimal peak near 198 nm and a maximal peak near 220 nm. The intensities of these peaks reversibly decreased with increasing temperature, suggesting an alteration in the structure occurred. The results that obtained in phosphate buffer were almost consistent with the previous result obtained in pure water [15]. This minimal peak near 198 nm suggesting the existence of turn structure was commonly found in many ELPs [11, 15, 38, 41, 44]. Therefore, it was considered that the turn structure was necessary for self-assembling properties of ELPs [37-39]. Here, the spectra of $(FPGVG)_5$ and shuffled analogs had local maximums around 220 nm. Their features were also common in decline in the peak intensities with increasing temperature. However, spectral shape around 200 nm differed among the peptides. Thus, it was suggested that some shuffled analogs were different from $(FPGVG)_5$ and conventional ELPs in terms of structural features. In a comparison among these results obtained in this study, CD spectra of peptides B and K were similar to that of $(FPGVG)_5$, but the local minimum of peptide B was slightly red-shifted. Spectra of the peptide C, G, H, I, and J were different from that of $(FPGVG)_5$ as to whether or not they had a maximum peak at 200 nm. In addition, peptide E showed no apparent minimal peak between 220 nm and 190 nm. As a result, it was observed that 8 soluble shuffled peptides exhibited different features in CD spectra. Therefore, their structures were thought to be different in solution. Since these 8 peptides exhibited self-assembly in common, it was thought that specific secondary structure was not required to express self-assembling properties.

(Figure 5)

The structure of the shuffled analogs was further analyzed by MD. Structure data, such as R_g, SASA, and proportion of secondary structure at each temperature were listed in tables 3, 4, and 5. No systematic change in values correlating with peptide self-assembling properties was found in R_g and SASA. Regarding the secondary structure, all peptides were dominated by bend, turn, and abundant random coil structures at low temperature of 278 K. The peptides tended to possess many turns, bend, and disorder structures in the peptide backbone. Although the tendency was maintained at 310 K and 343 K, β structures such as β-bridge and β-sheet were observed in addition to the preexisting bend, turn, and random coil structures. Overall, it was suggested that conformation of the peptides changed with increasing temperature. This changes in structure were common to almost all peptides used in this study, but the regions where each secondary structure appeared were different between the peptides. The ratio of these secondary structures at each amino acid residue in the full-length sequence was shown in figure 6, 7, and 8. Each secondary structure tended to appear periodically in the repeat sequence, and the average ratio of these secondary structure at each residue in the repetition was also shown in figure 9, 10, and 11. Among them, the place where each secondary structure was likely to appear depended on the peptide. In summary, the structures of shuffled peptides were commonly dominated by bend, turn, β-structures and abundant random coil, but each peptide possessed different folding in their structure.

(Table 3, 4, and 5)

(Figure 6, 7, 8, 9, 10, and 11)

Discussion of the influence of primary structure in self-assembly

Peptides with different repeating primary sequences, which had same amino acid composition, exhibited self-assembly in the turbidity measurement. Their structural features were different from each other in the structural analysis performed in this study. These results suggested that the composition of the amino acids in the repetition and highly bend and turned structures that commonly observed in the peptides were important for the expression of self-assembling properties. However, the dependences of T_t on the peptide concentration and the water solubility of the peptides differently depended on the primary structure of peptides. More detailed consideration regarding T_t change was necessary to discuss molecular mechanisms evoking self-assembly of ELPs. Among the repeating peptides, there were pairs of sequences that they had similar hydrophobic residues in relative positions of each repetitive penta-peptide (Table 6). Both peptide in pair were in a relationship with exchanging the positions of hydrophobic residues. Peptide B and D, and F and L were in this pair of relationship, respectively. As shown in table 6, these pairs commonly had relative

poor water solubility. Additionally, these peptides were also common in that they had the dipeptide sequence of GP. It was considered that existence of GP sequence, XGPYG (X = F or V) or XGGPY in the repetition made the repeating peptide insoluble in water. On the other hand, the peptides having PG sequences were relatively soluble in water and exhibited self-assembling properties, even possessing the GP sequence, simultaneously. Therefore, it was considered that the PG sequence was important for hydration of the peptide. Moreover, the pair of peptide G and I which proline residues located between the hydrophobic residues were also soluble in water and exhibited self-assembly. Thus, it was thought that the PG sequence was not necessary, but sufficient for hydration of the peptide. Interestingly, the self-assembling properties (i.e. T_t values) of shuffled analogs were different even in the pair relationship. Therefore, depending on the position of bulky hydrophobic residue(s) in the repetitive sequence, the dependence of T_t on peptide concentration were different.

(Table 6)

Structural analyses suggested that the shuffled peptides that had the same amino acid composition had commonly bent and turned structures, but different in where they occur one another (Figures 5, 9, 10, and 11). Due to the difference in local structures, how the hydrophobic ELPs and the shuffled analogs hydrate and self-assemble was an interesting subject to be solved. Hence, it was thought that the differences in higher order structures influenced the hydration state of the peptides and the hydrophobic effect around the peptides that drove self-assembly. Since it was difficult to differentiate highly bended and flexible structures on the peptides, the influence of secondary structure on self-assembly could not be analyzed directly. Despite the difficulty, the ideas that the shuffled peptides with PG sequence were relatively soluble in water and exhibited self–assembly was revealed by the comparison among primary structures. Further analysis of hydration and dehydration change around the PG sequence is required to clarify the mechanism of self-assembly.

In summary, this study gave insight into the importance of PG sequences in these self-assembly peptides. One of the remarkable finding of this study is that peptide B and C have potent self-assembling properties than the original $(FPGVG)_5$. By using these potential motifs, shorter ELPs keeping the reversible self-assembling property could be obtained.

4. Conclusion

This chapter analyzed the self-assembling property and structural features of the 11 shuffled peptide analogs based on $(FPGVG)_5$. As a result, 3 peptides were hard to dissolve in phosphate buffer, while 8 peptides were soluble in water and showed self-assembly in turbidity measurement. In this measurement, it was found that $(FGPVG)_5$ and $(FGPGV)_5$ possessed potent self-assembling ability than $(FPGVG)_5$. Furthermore, $(FPGVG)_5$ and

shuffled peptides showing self-assembly indicated different structural features in CD measurement and MD simulation. Thus it was also suggested that specific secondary structure was not necessary for expression of the self-assembling property. On the other hand, the dependences of T_t on the peptide concentration and the water solubility were differently affected by the primary structures. It was suggested that primary and higher order structures would complexly affected these properties of the repeating peptides. As summary of this chapter, this study revealed the importance of composition of amino acid and primary sequence in the repetition in the self-assembly of the peptides. We also found that the repeating peptides consisting of hydrophobic pentapeptide unit which composed of F: P: G: V = 1: 1: 2: 1 clearly exhibited self-assembly. Although further analysis will be required to elucidate precise molecular mechanism in self-assembly of these repeating peptide, this study gave insights into structure-function relationships of the self-assembling peptides and the concept to design of novel ELPs for application.

5. References

[1] Miao M, Bellingham C. M., Stahl R. J., Sitarz E. E., Lane C. J., Keeley F. W., Sequence and structure determinants for the self-aggregation of recombinant polypeptides modeled after human elastin. *J. Biol. Chem.*, **278**, 48553–48562 (2003).

[2] Despanie J., Dhandhukia J. P., Hamm-Alvarez S. F., MacKay J. A., Elastin-like polypeptides: Therapeutic applications for an emerging class of nanomedicines, *J Control Release*, **240**, 93-108 (2016).

[3] Luan C. H., Parker T. M., Prasad K. U., Urry D. W., Differential scanning calorimetry studies of NaCl effect on the inverse temperature transition of some elastin-based polytetrapeptides, polypentapeptides, and polynonapeptides, *Biopolymers*, **31**, 465-475 (1991).

[4] Luan C. H., Harris R. D., Prasad K. U., Urry D. W., Differential scanning calorimetry studies of the inverse temperature transition of the polypentapeptide of elastin and its analogs, *Biopolymers*, **29**, 1699–1706 (1990).

[5] Urry D. W., The change in Gibbs free energy for hydrophobic association - derivation and evaluation by means of inverse temperature transitions, *Chem. Phys. Lett.*, **399**, 177-183 (2004).

[6] MacEwan S. R., Chilkoti A., Applications of elastin-like polypeptides in drug delivery, *J. Control Release*, **190**, 314-330 (2014).

[7] Nettles D. L., Chilkoti A., Setton L. A., Applications of elastin-like polypeptides in tissue engineering, *Adv. Drug Deliv. Rev.*, **62**, 1479-1485 (2010).

[8] Despanie J., Dhandhukia J. P., Hamm-Alvarez S. F., MacKay J. A., Elastin-like polypeptides: Therapeutic applications for an emerging class of nanomedicines, *J Control Release*, **240**, 93-108 (2016).

[9] Yeo G. C., Aghaei-Ghareh-Bolagh B., Brackenreg E. P., Hiob M. A., Lee P., Weiss A.S., Fabricated Elastin, *Advanced Healthcare Materials*, **4**, 2530-2556 (2010).

[10] McDaniel J. R., Radford D. C., Chilkoti A., A unified model for de novo design of elastin-like polypeptides with tunable inverse transition temperatures, *Biomacromolecules*, **14** (8), 2866-2872 (2013).

[11] Nuhn H., Klok H. A., Secondary structure formation and LCST behavior of short elastin-like peptides, *Biomacromolecules*, **9** (10), 2755-2763 (2008).

[12] Aladini F., Araman C., Becker C. F., Chemical synthesis and characterization of elastin-like polypeptides (ELPs) with variable guest residues, *J. Pept. Sci.*, **22** (5), 334-342 (2016).

[13] Maeda I., Taniguchi S., Ebina J., Watanabe N., Hattori T., Nose T., Comparison between coacervation property and secondary structure of synthetic peptides, Ile-containing elastin-derived pentapeptide repeats, *Protein Pept. Lett.*, **20**, 905-910 (2013).

[14] Maeda I., Taniguchi S., Watanabe N., Inoue A., Yamasaki Y., Nose T., Design of phenylalanine-containing elastin-derived peptides exhibiting highly potent self-assembling capability, *Protein Pept. Lett.*, **22**, 934-939 (2015).

[15] Taniguchi S., Watanabe N., Nose T., Maeda I., Development of short and highly potent self-assembling elastin-derived pentapeptide repeats containing aromatic amino acid residues, *J. Pept. Sci.*, **22**, 36-42 (2016).

[16] Li N. K., García Quiroz F., Hall C. K., Chilkoti A., Yingling Y. G., Molecular Description of the LCST Behavior of an Elastin-Like Polypeptide, *Biomacromolecules*, **15**, 3522-3530 (2014).

[17] Zhao B., Li N. K., Yingling Y. G., Hall C. K., LCST Behavior is Manifested in a Single Molecule: Elastin-Like polypeptide $(VPGVG)_n$, *Biomacromolecules*, **17**, 111-118 (2016).

[18] Miao M, Bellingham C. M., Stahl R. J., Sitarz E. E., Lane C. J., Keeley F. W., Sequence and structure determinants for the self-aggregation of recombinant polypeptides modeled after human elastin. *J. Biol. Chem.*, **278**, 48553–48562 (2003).

[19] Meyer D. E., Chilkoti A., Quantification of the effects of chain length and concentration on the thermal behavior of elastin-like polypeptides, *Biomacromolecules*, **5**, 846-851 (2004).

[20] Cho Y., Zhang Y., Christensen T., Sagle L. B., Chilkoti A., Cremer P. S., Effects of Hofmeister anions on the phase transition temperature of elastin-like polypeptides, *J. Phys. Chem. B*, **112**, 13765-13771 (2008).

[21] Rembert K. B., Paterová J., Heyda J., Hilty C., Jungwirth P., Cremer P. S., Molecular mechanisms of ion-specific effects on proteins, *J. Am. Chem. Soc.*, **134**, 10039-10046 (2012).

[22] Urry D. W., Physical Chemistry of Biological Free Energy Transduction As

Demonstrated by Elastic Protein-Based Polymers, *J. Phys. Chem. B*, **101** (51), 11007–11028 (1997).

[23] Mackay J. A., Callahan D. J., Fitzgerald K. N., Chilkoti A., Quantitative model of the phase behavior of recombinant pH-responsive elastin-like polypeptides, *Biomacromolecules*, **11**, 2873-2879 (2010).

[24] Yamaoka T., Tamura T., Seto Y., Tada T., Kunugi S., Tirrell D. A., Mechanism for the phase transition of a genetically engineered elastin model peptide $(VPGIG)_{40}$ in aqueous solution, *Biomacromolecules*, **4** (6), 1680-1685 (2003).

[25] Ferreira L. A., Cole J. T., Reichardt C., Holland N. B., Uversky V. N., Zaslavsky B. Y., Solvent properties of water in aqueous solutions of elastin-like polypeptide, *Int. J. Mol. Sci.*, **16**, 13528-13547 (2015).

[26] Liao Y. -T., Manson A. C., DeLyser M. R., Noid W. G., Cremer P. S., Trimethylamine N-oxide stabilizes proteins via a distinct mechanism compared with betaine and glycine, *P. Natl. Acad. Sci. USA*, **114**, 2479-2484 (2017).

[27] Tatsubo D., Suyama K., Miyazaki M., Maeda I., Nose T., Stepwise Mechanism of Temperature-Dependent Coacervation of the Elastin-like Peptide Analogue Dimer, $(C(WPGVG)_3)_2$, *Biochemistry-US*, **57**, 1582-1590 (2018).

[28] Suyama K., Taniguchi S., Tatsubo D., Maeda I., Nose T., Dimerization effects on coacervation property of an elastin-derived synthetic peptide $(FPGVG)_5$, *J. Pept. Sci.*, **22**, 236-243 (2016).

[29] Dhandhukia J., Weitzhandler I., Wang W., MacKay J. A., Switchable elastin-like polypeptides that respond to chemical inducers of dimerization, *Biomacromolecules*, **14** (4), 976-985 (2013).

[30] Ghoorchian A., Cole J. T., Holland N. B., Thermoreversible Micelle Formation Using a Three-Armed Star Elastin-like Polypeptide, *Macromolecules*, **43** (9), 4340–4345 (2010).

[31] Ghoorchian A., Holland N. B., Molecular architecture influences the thermally induced aggregation behavior of elastin-like polypeptides, *Biomacromolecules*, **12** (11), 4022-4029 (2011).

[32] Ghoorchian A., Vandemark K., Freeman K., Kambow S., Holland N. B., Streletzky K. A., Size and shape characterization of thermoreversible micelles of three-armed star elastin-like polypeptides, *J. Phys. Chem. B.*, **117** (29), 8865-8874 (2013).

[33] Fukushima D., Sk U. H., Sakamoto Y., Nakase I., Kojima C., Dual stimuli-sensitive dendrimers: Photothermogenic gold nanoparticle-loaded thermo-responsive elastin-mimetic dendrimers, *Colloids Surf. B. Biointerfaces*, **132**, 155-160 (2015).

[34] Navon Y., Zhou M., Matson J. B., Bitton R., Dendritic Elastin-like Peptides: The Effect of Branching on Thermoresponsiveness, *Biomacromolecules*, **17** (1), 262-270 (2016),

[35] Zhou M., Shmidov Y., Matson J. B., Bitton R., Multi-scale characterization of

thermoresponsive dendritic elastin-like peptides, *Colloids Surf. B. Biointerfaces*, **153**, 141-151 (2017).

[36] He D., Chung M., Chan E., Alleyne T., Ha K. C., Miao M., Stahl R. J., Keeley F. W., Parkinson J., Comparative genomics of elastin: Sequence analysis of a highly repetitive protein. *Matrix Biol.*, **26**, 524-540 (2007).

[37] Tamburro A. M., Guantieri V., Gordini D. D., Synthesis and structural studies of a pentapeptide sequence of elastin. Poly (Val-Gly-Gly-Leu-Gly), *J. Biomol. Struct. Dyn.*, **10**, 441– 454 (1992) .

[38] Maeda I., Fukumoto Y., Nose T., Shimohigashi Y., Nezu T., Terada Y., Kodama H., Kaibara K., Okamoto K., Structural requirements essential for elastin coacervation: favorable spatial arrangements of valine ridges on the three-dimensional structure of elastin-derived polypeptide $(VPGVG)_n$, *J. Pept. Sci.*, **17**, 735–743 (2011).

[39] Zhang Y., Zai-Rose V., Price C. J., Ezzell N. A., Bidwell G. L., Correia J. J., Fitzkee N. C., Modeling the Early Stages of Phase Separation in Disordered Elastin-like Proteins, *Biophys. J.*, **114**, 1563-1578 (2018).

[40] Chen Y., Guan Z., Bioinspired modular synthesis of elastin-mimic polymers to probe the mechanism of elastin elasticity, *J. Am. Chem. Soc.*, **132**, 4577-4579 (2010).

[41] Quiroz F. G., Chilkoti A., Sequence heuristics to encode phase behaviour in intrinsically disordered protein polymers, *Nat. Mater.*, **14**, 1164–1171 (2015).

[42] Kaibara K., Akinari Y., Okamoto K., Uemura Y., Yamamoto S., Kodama H., Kondo M., Characteristic interaction of Ca^{2+} ions with elastin coacervate: ion transport study across coacervate layers of alpha-elastin and elastin model polypeptide, $(Val\text{-}Pro\text{-}Gly\text{-}Val\text{-}Gly)_n$, *Biopolymers*, **39**, 189–198 (1996).

[43] Kabsch W., Sander C., Dictionary of protein secondary structure: pattern recognition of hydrogen-bonded and geometrical features, *Biopolymers*, **22**, 2577-2637 (1983).

Table 1. Phase transition temperature of the peptides.[a]

Code	Sequence	Phase transition temperatures (T_t) at each peptide concentration (°C)				
		0.5 mg/mL	1 mg/mL	2 mg/mL	5 mg/mL	10 mg/mL
A	H-(FPGVG)$_5$-NH$_2$	NA.	59.3 ± 1.9	39.0 ± 0.2	25.6 ± 1.2	20.5 ± 0.1
B	H-(FGPVG)$_5$-NH$_2$	NA.	31.5 ± 1.6		Not dissolved	
C	H-(FGPGV)$_5$-NH$_2$	NA.	36.2 ± 0.1	24.1 ± 0.5	13.8 ± 0.5	Not dissolved
D	H-(FGVGP)$_5$-NH$_2$			Not dissolved		
E	H-(FGVPG)$_5$-NH$_2$	NA.	44.8 ± 0.9	32.7 ± 0.4	20.5 ± 0.7	13.5 ± 0.5
F	H-(FGGPV)$_5$-NH$_2$			Not dissolved		
G	H-(FGGVP)$_5$-NH$_2$	NA.	59.9 ± 1.0	39.4 ± 1.4	25.3 ± 0.2	19.0 ± 0.5
H	H-(FPGGV)$_5$-NH$_2$		NA.	51.4 ± 1.6	29.5 ± 0.1	20.0 ± 0.6
I	H-(FPVGG)$_5$-NH$_2$		NA.	55.1 ± 1.0	36.3 ± 0.3	27.2 ± 0.4
J	H-(FVPGG)$_5$-NH$_2$		NA.	38.6 ± 0.8	21.9 ± 0.8	Not dissolved
K	H-(FVGPG)$_5$-NH$_2$		NA.	52.1 ± 0.7	32.7 ± 0.6	24.4 ± 0.6
L	H-(FVGGP)$_5$-NH$_2$			Not dissolved		
Code	Sequence	0.5 mg/mL	0.7 mg/mL	1 mg/mL	1.2 mg/mL	1.5 mg/mL
B	H-(FGPVG)$_5$-NH$_2$	NA.	36.2 ± 2.2	31.5 ± 1.6	25.5 ± 0.9	22.0 ± 1.0

[a] T_t of the peptides were measured at each peptide concentration in phosphate buffer (pH = 7.4). Peptide D, F, and L were not dissolved at concentration of 0.1 mg/mL.

Table 2. Slopes and intercepts in fitting of the dependence of T_t on peptide concentration.[a]

Code	Sequence	*m* (°C)	*b* (°C)
A	H-(FPGVG)$_5$-NH$_2$	-16.5	55.1
B	H-(FGPVG)$_5$-NH$_2$	-19.3	29.9
C	H-(FGPGV)$_5$-NH$_2$	-13.8	35.3
D	H-(FGVGP)$_5$-NH$_2$	Not dissolved	
E	H-(FGVPG)$_5$-NH$_2$	-13.6	43.5
F	H-(FGGPV)$_5$-NH$_2$	Not dissolved	
G	H-(FGGVP)$_5$-NH$_2$	-17.4	56.0
H	H-(FPGGV)$_5$-NH$_2$	-19.8	64.0
I	H-(FPVGG)$_5$-NH$_2$	-17.5	66.4
J	H-(FVPGG)$_5$-NH$_2$	-18.2	51.2
K	H-(FVGPG)$_5$-NH$_2$	-17.4	63.2
L	H-(FVGGP)$_5$-NH$_2$	Not dissolved	

[a] Slopes and intercepts in equation 1 : $T_t = m \ln c + b$, were calculate from each peptide concentration dependence of T_t. *m* value represents the amount of change in T_t with respect to the logarithm of concentration. *b* value represents the estimate of T_t at 1 mg/mL.

Table 3. Structure data from trajectories at 278 K.[a]

Temperature (K)	Code	Peptide	R_g (nm)	SASA (nm^2)	Ratio of each secondary structure				
					Coil (%)	β-bridge (%)	Bend (%)	Turn (%)	3_{10}-Helix (%)
278	A	H-(FPGVG)$_5$-NH_2	1.33 ± 0.22	28.49 ± 1.88	65	0	32	3	0
	B	H-(FGPVG)$_5$-NH_2	0.89 ± 0.05	25.35 ± 1.38	52	5	43	0	0
	C	H-(FGPGV)$_5$-NH_2	1.07 ± 0.10	26.97 ± 1.41	51	1	39	8	1
	D	H-(FGVGP)$_5$-NH_2	1.05 ± 0.07	26.29 ± 1.09	61	0	24	14	1
	E	H-(FGVPG)$_5$-NH_2	0.87 ± 0.02	23.98 ± 0.93	50	7	36	7	0
	F	H-(FGGPV)$_5$-NH_2	0.80 ± 0.01	22.41 ± 1.01	53	4	38	6	0
	G	H-(FGGVP)$_5$-NH_2	0.78 ± 0.03	21.19 ± 0.93	58	0	30	12	0
	H	H-(FPGGV)$_5$-NH_2	0.81 ± 0.03	22.31 ± 1.26	59	4	35	2	0
	I	H-(FPVGG)$_5$-NH_2	1.16 ± 0.14	27.35 ± 1.72	59	0	34	7	0
	J	H-(FVPGG)$_5$-NH_2	1.10 ± 0.12	26.61 ± 1.09	73	0	17	10	0
	K	H-(FVGPG)$_5$-NH_2	1.55 ± 0.18	29.13 ± 1.52	64	0	21	15	0
	L	H-(FVGGP)$_5$-NH_2	0.88 ± 0.04	24.33 ± 1.32	51	0	39	10	0

[a] Ratios of each secondary structure were obtained via dividing the number of residues recognized as each secondary structure by the number of whole residues in the trajectory. Other data were described with SD.

Table 4. Structure data from trajectories at 310 K.[a]

Temperature (K)	Code	Peptide	R_g (nm)	SASA (nm^2)	Ratio of each secondary structure						
					Coil (%)	β-sheet (%)	β-bridge (%)	Bend (%)	Turn (%)	α-helix (%)	3_{10}-Helix (%)
310	A	H-(FPGVG)$_5$-NH_2	0.96 ± 0.15	25.32 ± 2.51	51	0	2	37	10	0	0
	B	H-(FGPVG)$_5$-NH_2	0.89 ± 0.07	24.08 ± 1.77	47	1	9	29	9	0	6
	C	H-(FGPGV)$_5$-NH_2	0.88 ± 0.11	22.84 ± 2.33	39	0	2	26	26	5	2
	D	H-(FGVGP)$_5$-NH_2	1.00 ± 0.10	25.51 ± 1.75	50	10	5	25	11	0	0
	E	H-(FGVPG)$_5$-NH_2	1.11 ± 0.21	27.45 ± 2.76	63	0	1	27	9	0	0
	F	H-(FGGPV)$_5$-NH_2	0.88 ± 0.08	22.94 ± 1.64	44	14	1	32	9	0	0
	G	H-(FGGVP)$_5$-NH_2	0.89 ± 0.04	23.09 ± 1.03	51	0	3	20	23	0	2
	H	H-(FPGGV)$_5$-NH_2	0.83 ± 0.05	21.77 ± 1.21	54	1	2	32	11	0	0
	I	H-(FPVGG)$_5$-NH_2	0.96 ± 0.08	25.38 ± 1.69	64	1	2	23	11	0	0
	J	H-(FVPGG)$_5$-NH_2	1.06 ± 0.18	25.89 ± 2.24	67	0	0	24	10	0	0
	K	H-(FVGPG)$_5$-NH_2	0.98 ± 0.20	25.43 ± 2.72	63	0	0	29	8	0	0
	L	H-(FVGGP)$_5$-NH_2	0.87 ± 0.03	22.99 ± 1.20	53	15	3	29	0	0	0

[a] Ratios of each secondary structure were obtained via dividing the number of residues recognized as each secondary structure by the number of whole residues in the trajectory. Other data were described with SD.

Table 5. Structure data from trajectories at 343 K.[a]

Temperature (K)	Code	Peptide	R_g (nm)	SASA (nm^2)	Ratio of each secondary structure						
					Coil (%)	β-sheet (%)	β-bridge (%)	Bend (%)	Turn (%)	α-helix (%)	3_{10}-Helix (%)
343	A	H-(FPGVG)$_5$-NH$_2$	0.90 ± 0.12	24.00 ± 2.16	53	2	2	33	11	0	0
	B	H-(FGPVG)$_5$-NH$_2$	0.98 ± 0.18	25.24 ± 2.82	47	0	2	31	17	2	2
	C	H-(FGPGV)$_5$-NH$_2$	0.88 ± 0.05	22.73 ± 1.16	36	29	1	22	12	0	0
	D	H-(FGVGP)$_5$-NH$_2$	0.92 ± 0.11	24.05 ± 2.12	50	0	2	33	10	1	4
	E	H-(FGVPG)$_5$-NH$_2$	0.91 ± 0.13	24.41 ± 2.37	47	0	4	32	16	0	0
	F	H-(FGGPV)$_5$-NH$_2$	0.91 ± 0.12	23.96 ± 3.09	48	4	2	35	10	0	1
	G	H-(FGGVP)$_5$-NH$_2$	0.94 ± 0.24	23.95 ± 3.25	56	0	4	32	8	0	0
	H	H-(FPGGV)$_5$-NH$_2$	0.87 ± 0.08	22.80 ± 1.61	48	0	8	22	19	0	2
	I	H-(FPVGG)$_5$-NH$_2$	0.91 ± 0.09	24.14 ± 1.83	57	1	2	30	10	0	0
	J	H-(FVPGG)$_5$-NH$_2$	0.93 ± 0.16	23.83 ± 2.38	67	0	1	27	6	0	0
	K	H-(FVGPG)$_5$-NH$_2$	0.83 ± 0.06	22.40 ± 1.60	59	0	0	33	7	0	0
	L	H-(FVGGP)$_5$-NH$_2$	0.81 ± 0.04	21.62 ± 1.11	49	0	0	50	1	0	0

[a] Ratios of each secondary structure were obtained via dividing the number of residues recognized as each secondary structure by the number of whole residues in the trajectory. Other data were described with SD.

Table 6. Phase transition temperature of the paired peptides.[a]

Code	Motif	T_t (°C)		Code	Motif	T_t (°C)
A	FPGVG	39.0 ± 0.2	↔	E	FGVPG	32.7 ± 0.4
B	FGPVG	22.0 ± 1.0	↔	D	FGVGP	Not dissolved
C	FGPGV	24.1 ± 0.5	↔	K	FVGPG	52.1 ± 0.7
F	FGGPV	Not dissolved	↔	L	FVGGP	Not dissolved
G	FGGVP	39.4 ± 1.4	↔	I	FPVGG	55.1 ± 1.0
H	FPGGV	51.4 ± 1.6	↔	J	FVPGG	38.6 ± 0.8

[a] The peptides in the pair relationship are written in same line. Hydrophobic residues were colored in red, and PG sequence was in blue. Except for peptide B, T_t or solubility of each peptide at a peptide concentration of 2 mg/mL were shown. T_t at 1.5 mg/mL was shown in peptide B due to insolubility.

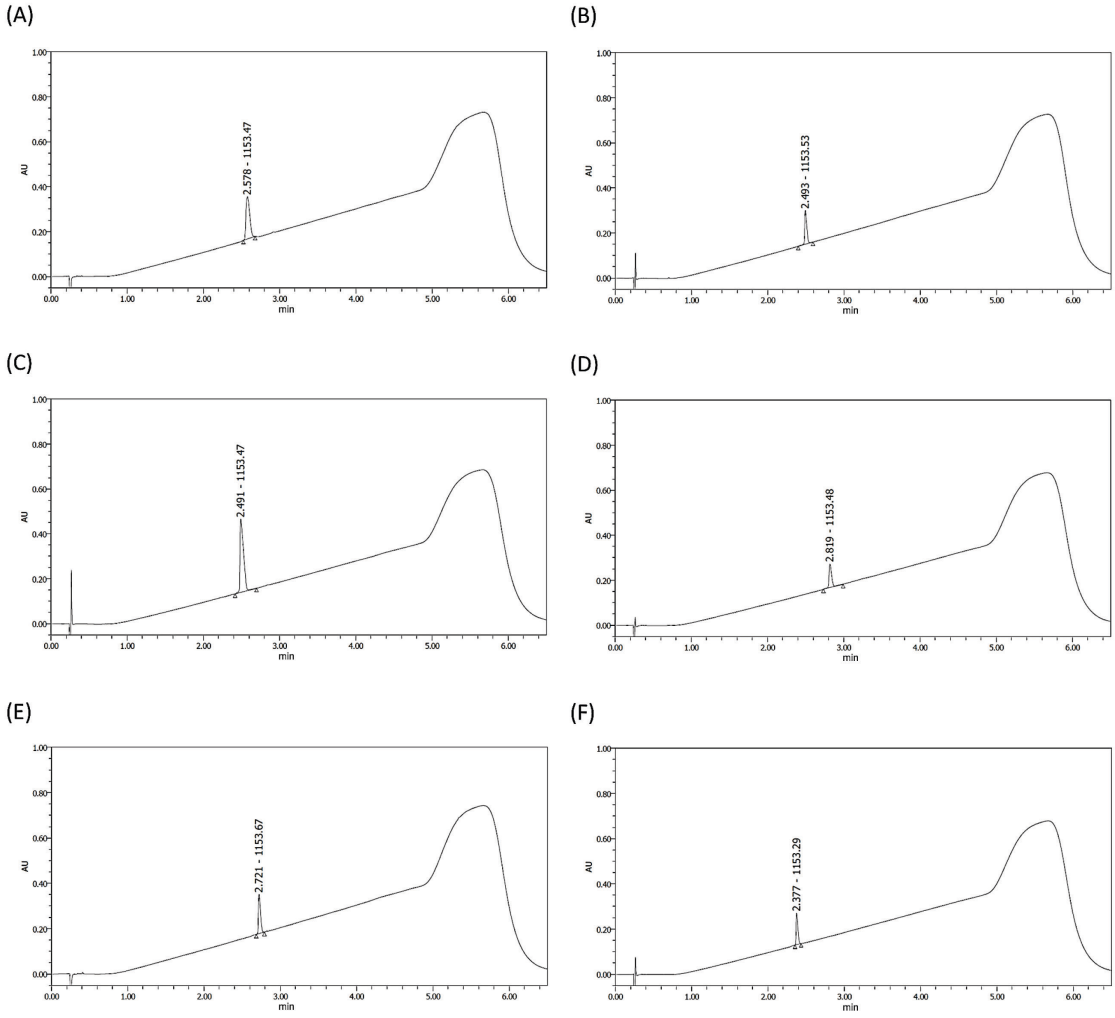

Figure 1. UPLC-MS analysis of $(FPGVG)_5$ and 11 shuffled peptide analogs.
UPLC data of (A) H-$(FPGVG)_5$-NH_2, (B) peptide B, (C) peptide C, (D) peptide D, (E) peptide E, (F) peptide F, (G) peptide G, (H) peptide H, (I) peptide I, (J) peptide J, (K) peptide K, and (L) peptide L were shown.

Continued

(G)

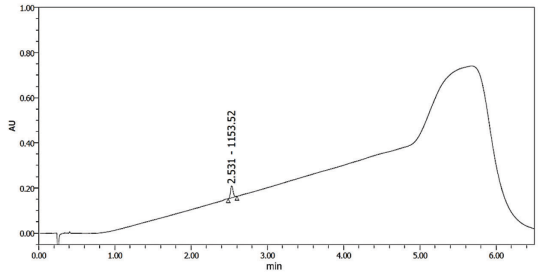

(H)

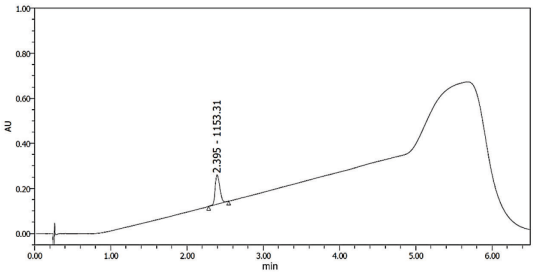

(I)

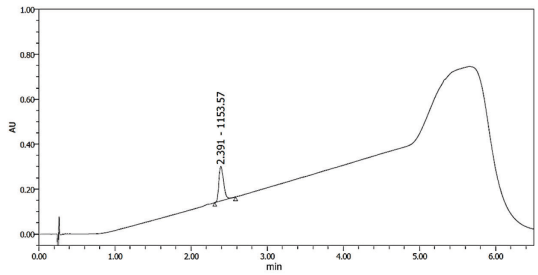

(J)

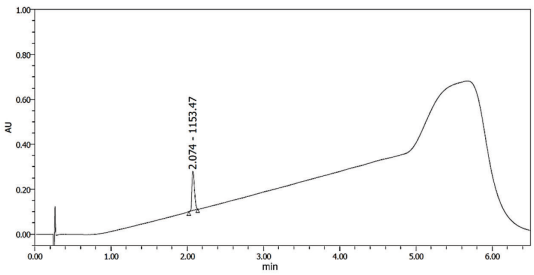

(K)

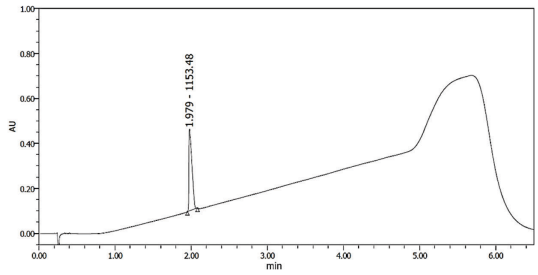

(L)

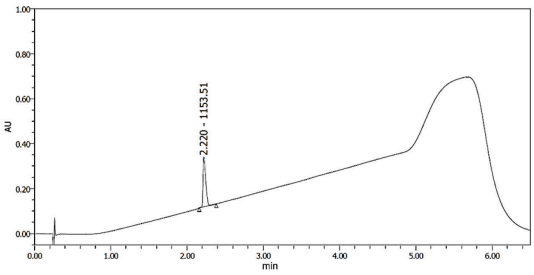

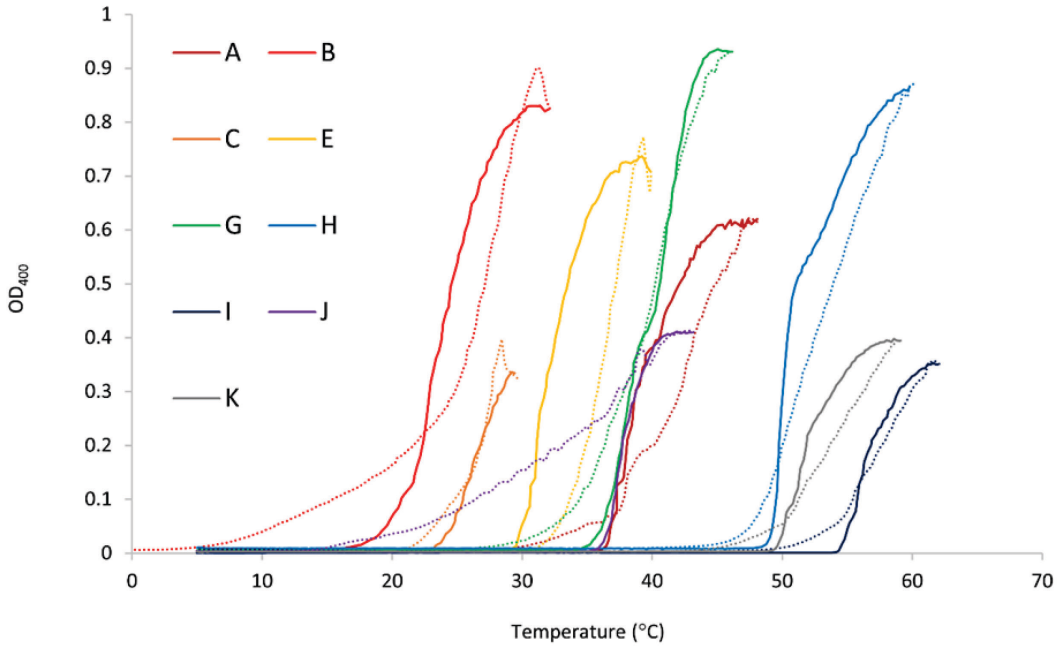

Figure 2. Turbidity profile of $(FPGVG)_5$ and 11 shuffled peptide analogs.
Representative turbidity profile of the $(FPGVG)_5$ and soluble shuffled peptides at peptide concentration of 2.0 mg/mL were shown. Only in the date of peptide B, the turbidity change at concentration of 1.5 mg/mL was shown.

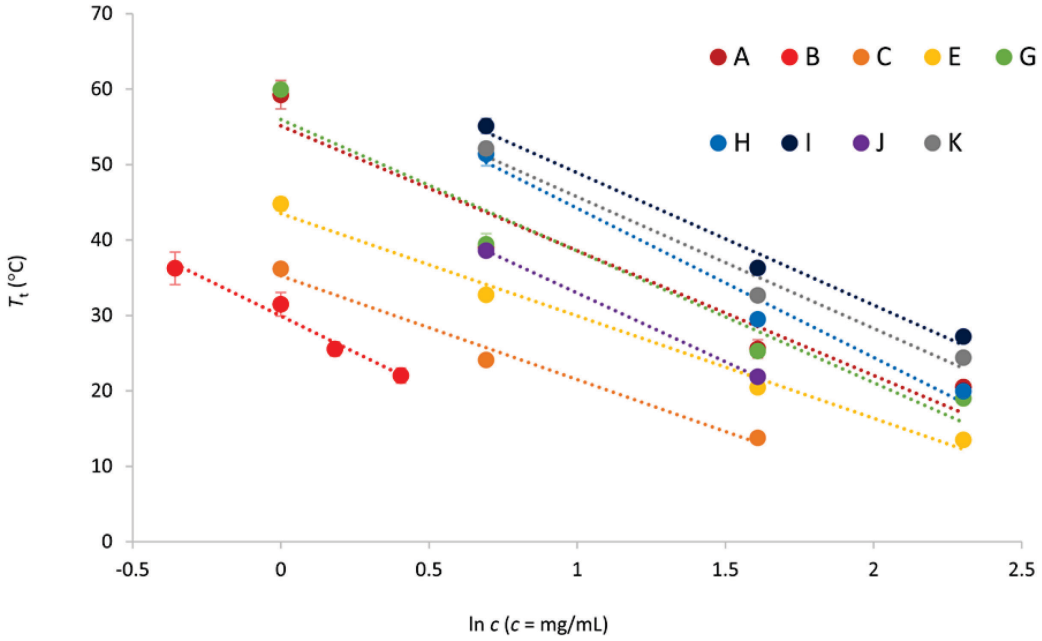

Figure 3. The dependence of T_t on peptide concentration in each peptide.
T_t at each peptide concentration was shown. These plot was fit to the logarithm function and described as dashed line.

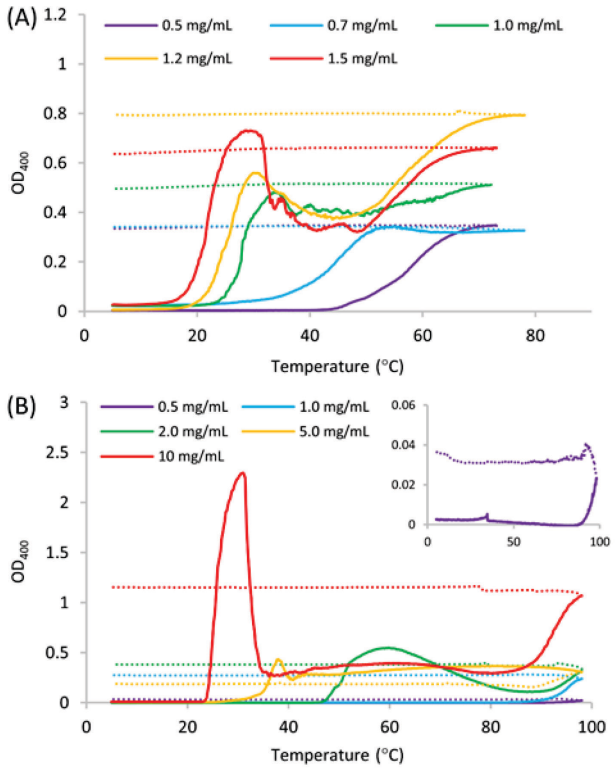

Figure 4. Turbidity profiles in irreversible self-assembly of peptide B and K.
(A) Peptide B and (B) peptide K showed irreversible self-assembly over 50°C and 90°C, respectively.

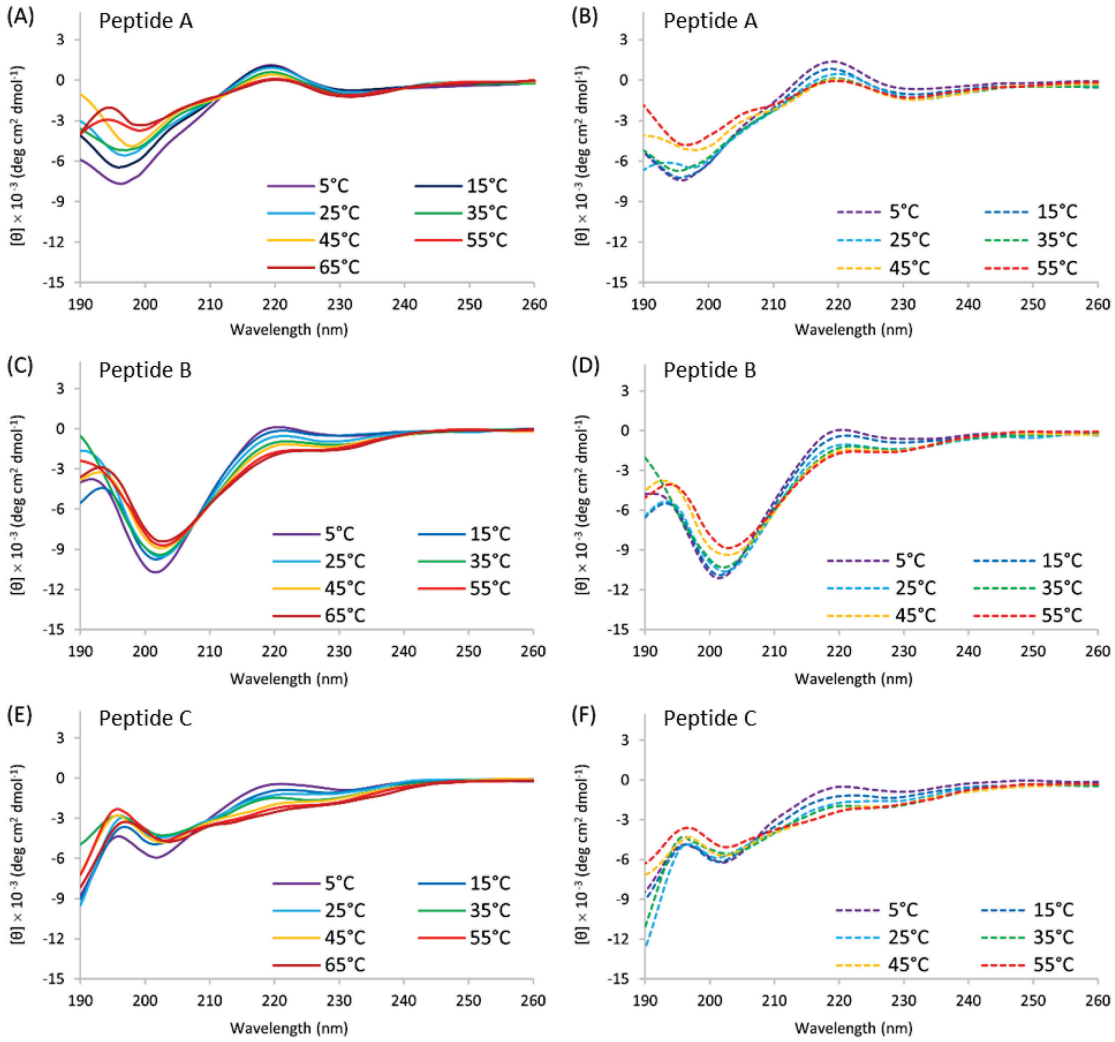

Figure 5. CD spectra of $(FPGVG)_5$ and shuffled analogs.

CD spectra of $(FPGVG)_5$ and shuffled peptides B, C, E, G, H, I, J, and K were shown. The spectra with increasing temperature were described in solid line. The spectra with decreasing temperature were described in dashed line.

Continued

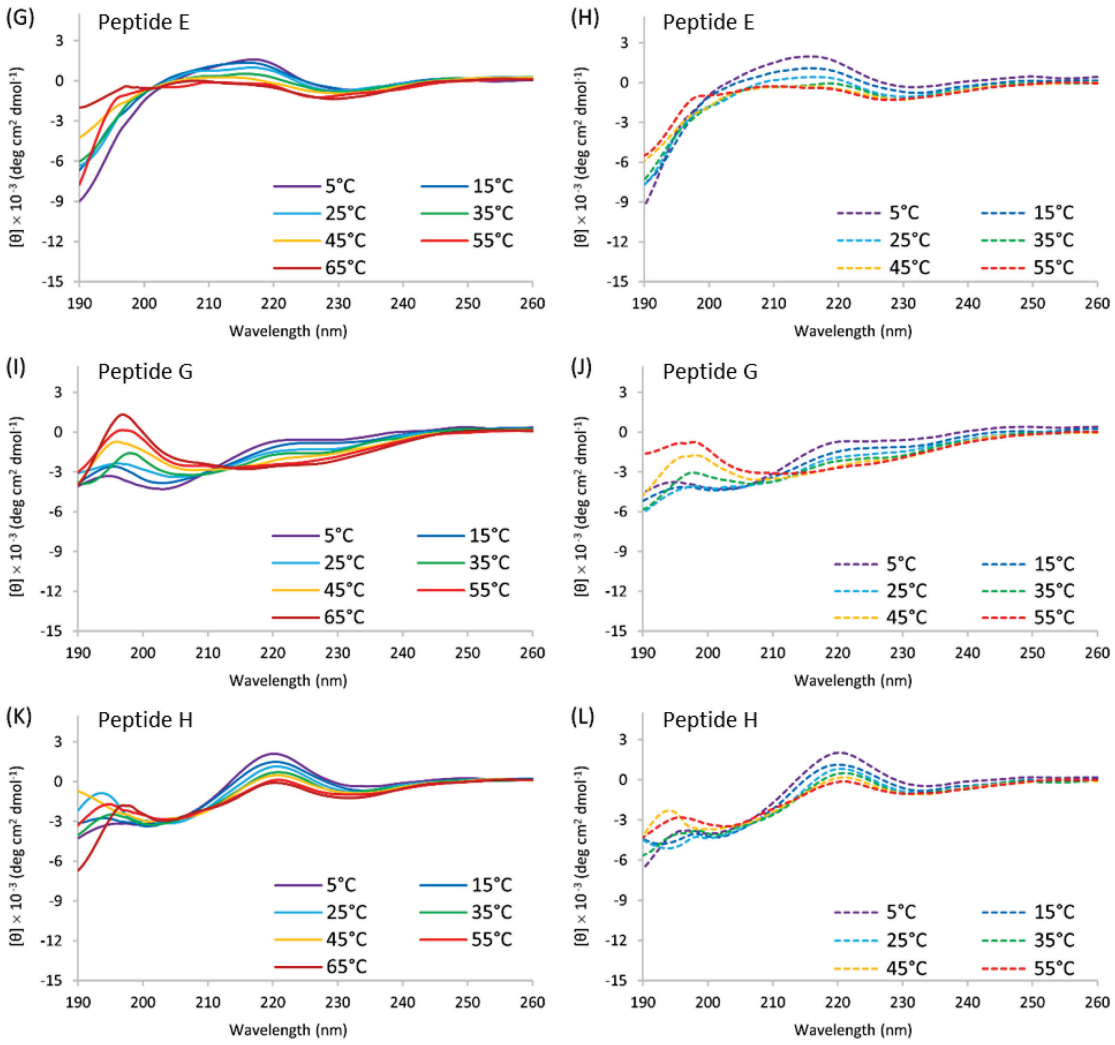
(G)
Peptide E
(H)
Peptide E
(I)
Peptide G
(J)
Peptide G
(K)
Peptide H
(L)
Peptide H
[θ] × 10⁻³ (deg cm² dmol⁻¹)
Wavelength (nm)
5°C
15°C
25°C
35°C
45°C
55°C
65°C

Continued

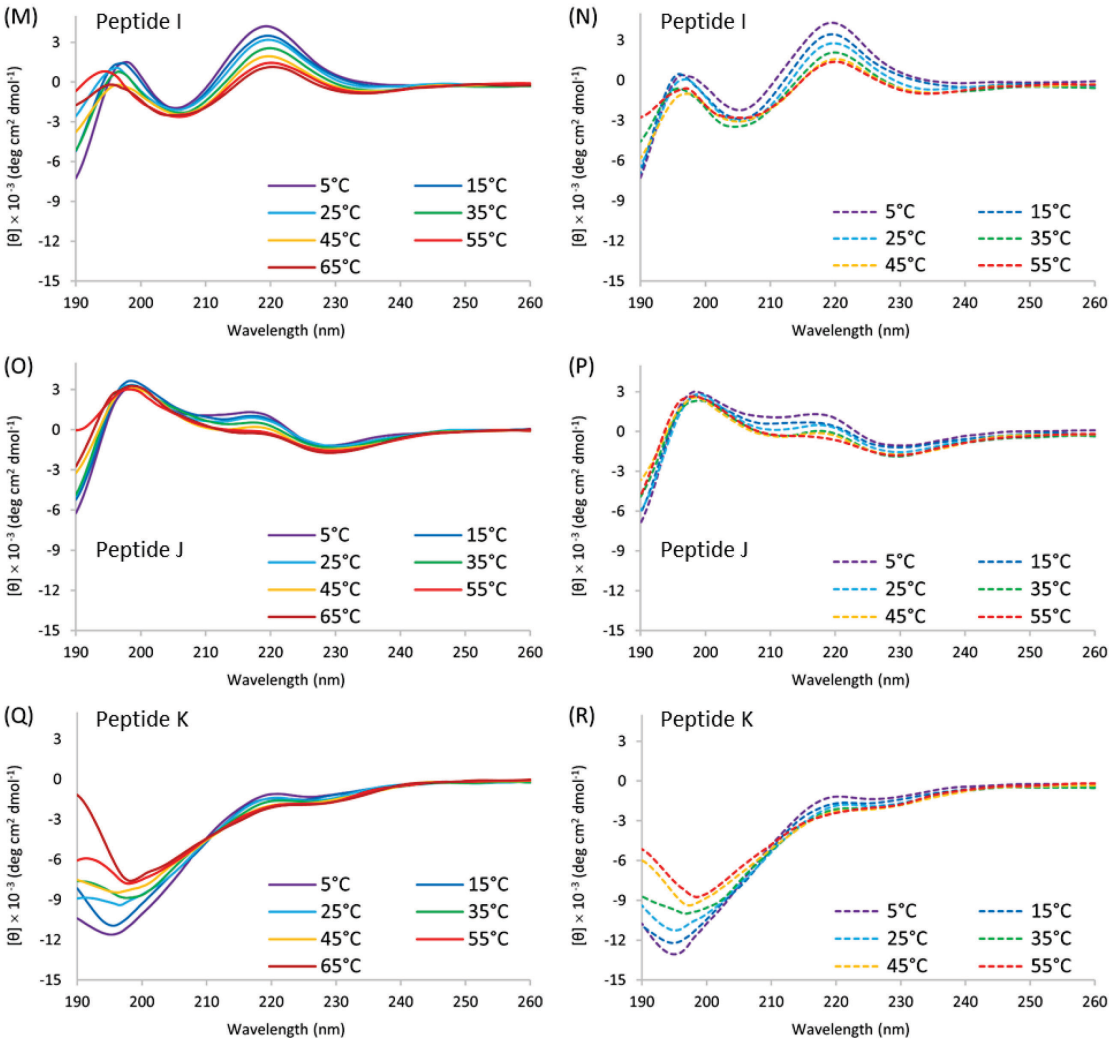
(M)
Peptide I
(N)
Peptide I
(O)
Peptide J
(P)
Peptide J
(Q)
Peptide K
(R)
Peptide K
[θ] × 10⁻³ (deg cm² dmol⁻¹)
Wavelength (nm)
5°C
15°C
25°C
35°C
45°C
55°C
65°C

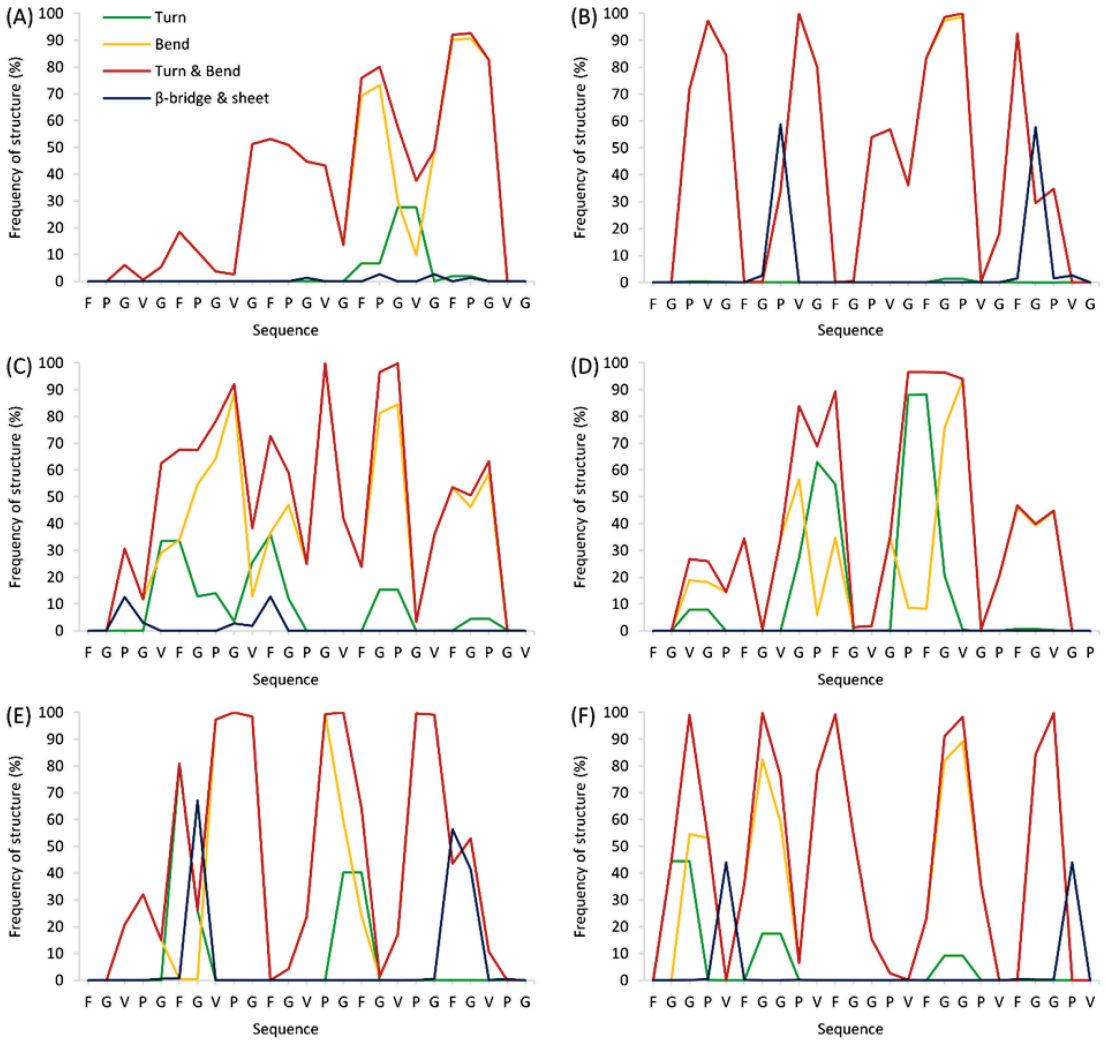

Figure 6. Ratios of secondary structures at each residue in whole peptide sequence at 278 K. The data in (A) peptide A, (B) peptide B, (C) peptide C, (D) peptide D, (E) peptide E, (F) peptide F, (G) peptide G, (H) peptide H, (I) peptide I, (J) peptide J, (K) peptide K, and (L) peptide L were shown. Each ratio was calculated by dividing the number of secondary structure at each residue in whole of trajectory by the number of trajectory frame.

Continued

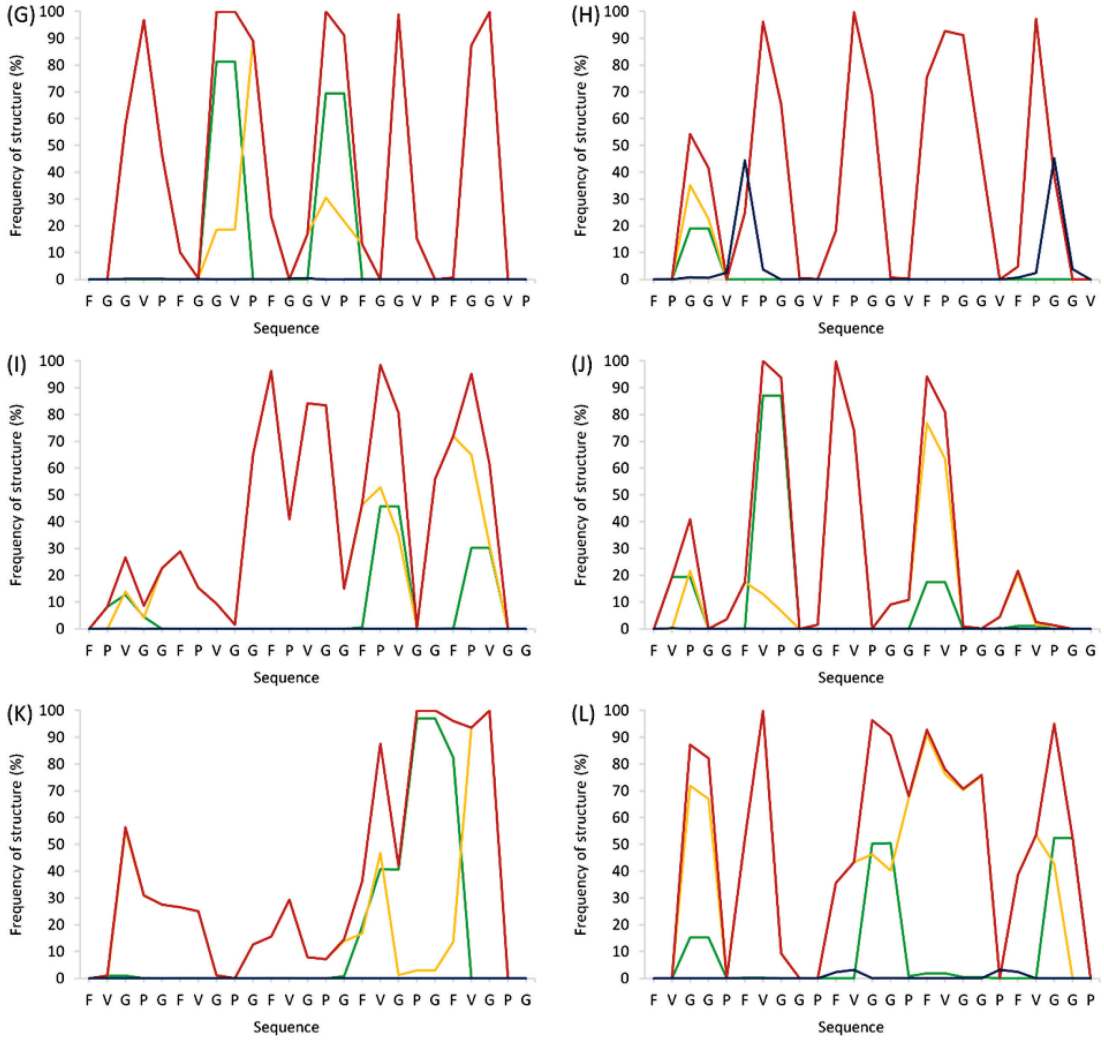
(G)
(H)
(I)
(J)
(K)
(L)
Frequency of structure (%)
Sequence
F G G V P F G G V P F G G V P F G G V P F G G V P
F P G G V F P G G V F P G G V F P G G V F P G G V
F P V G G F P V G G F P V G G F P V G G F P V G G
F V P G G F V P G G F V P G G F V P G G F V P G G
F V G P G F V G P G F V G P G F V G P G F V G P G
F V G G P F V G G P F V G G P F V G G P F V G G P

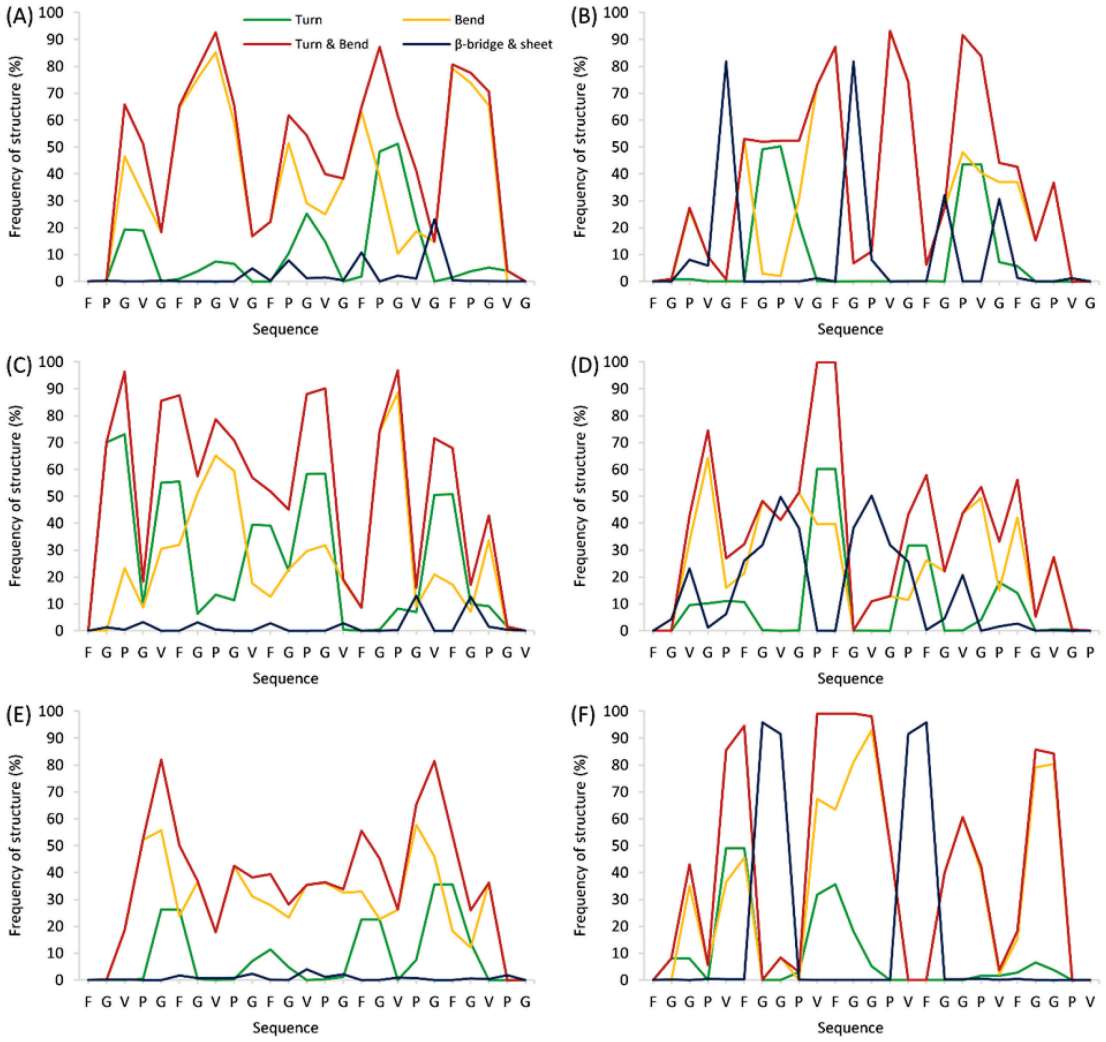

Figure 7. Ratios of secondary structures at each residue in whole peptide sequence at 310 K. The data in (A) peptide A, (B) peptide B, (C) peptide C, (D) peptide D, (E) peptide E, (F) peptide F, (G) peptide G, (H) peptide H, (I) peptide I, (J) peptide J, (K) peptide K, and (L) peptide L were shown. Each ratio was calculated by dividing the number of secondary structure at each residue in whole of trajectory by the number of trajectory frame.

Continued

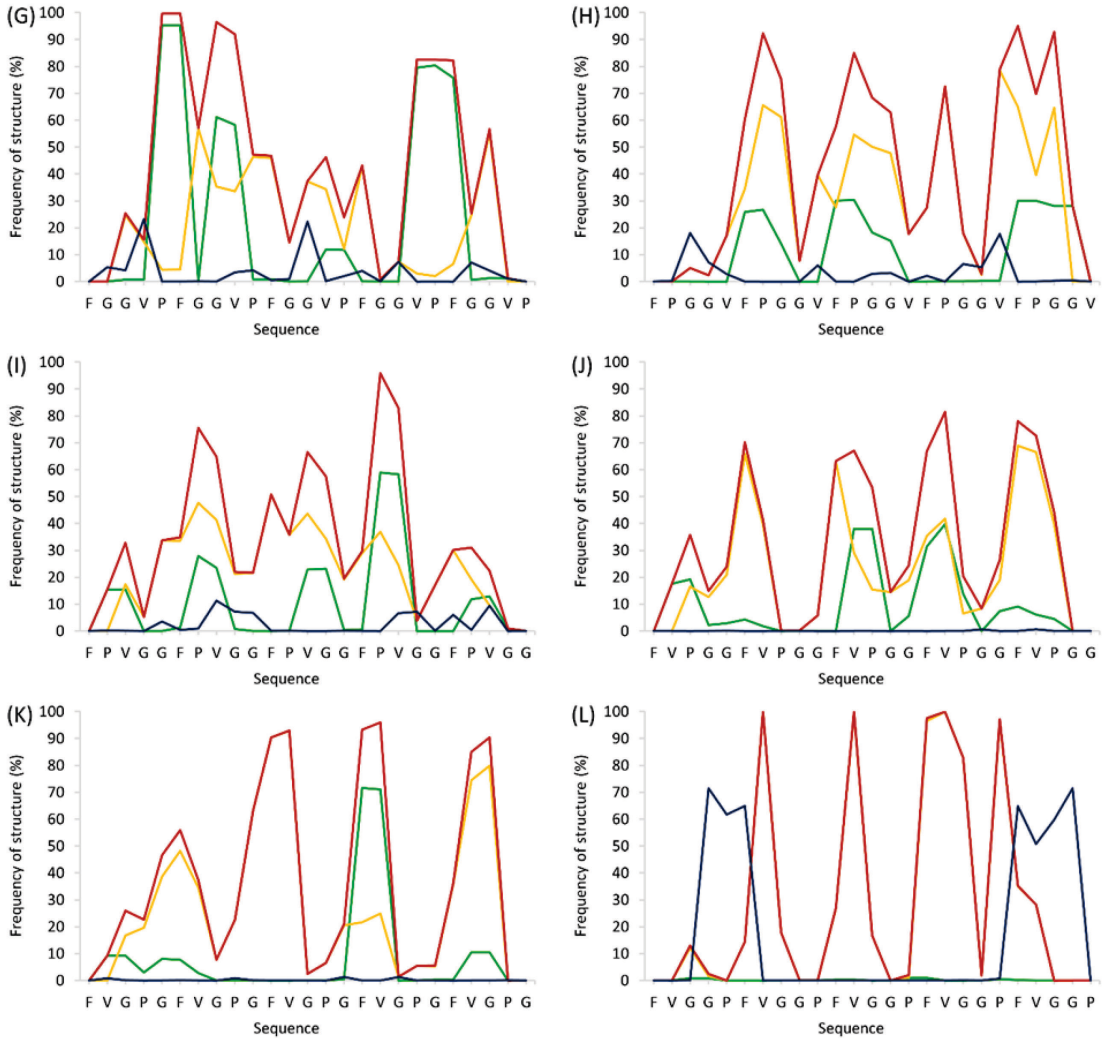
(G)
(H)
(I)
(J)
(K)
(L)
Frequency of structure (%)
Sequence
F G G V P F G G V P F G G V P F G G V P
F P G G V F P G G V F P G G V F P G G V
F P V G G F P V G G F P V G G F P V G G
F V P G G F V P G G F V P G G F V P G G
F V G P G F V G P G F V G P G F V G P G
F V G G P F V G G P F V G G P F V G G P

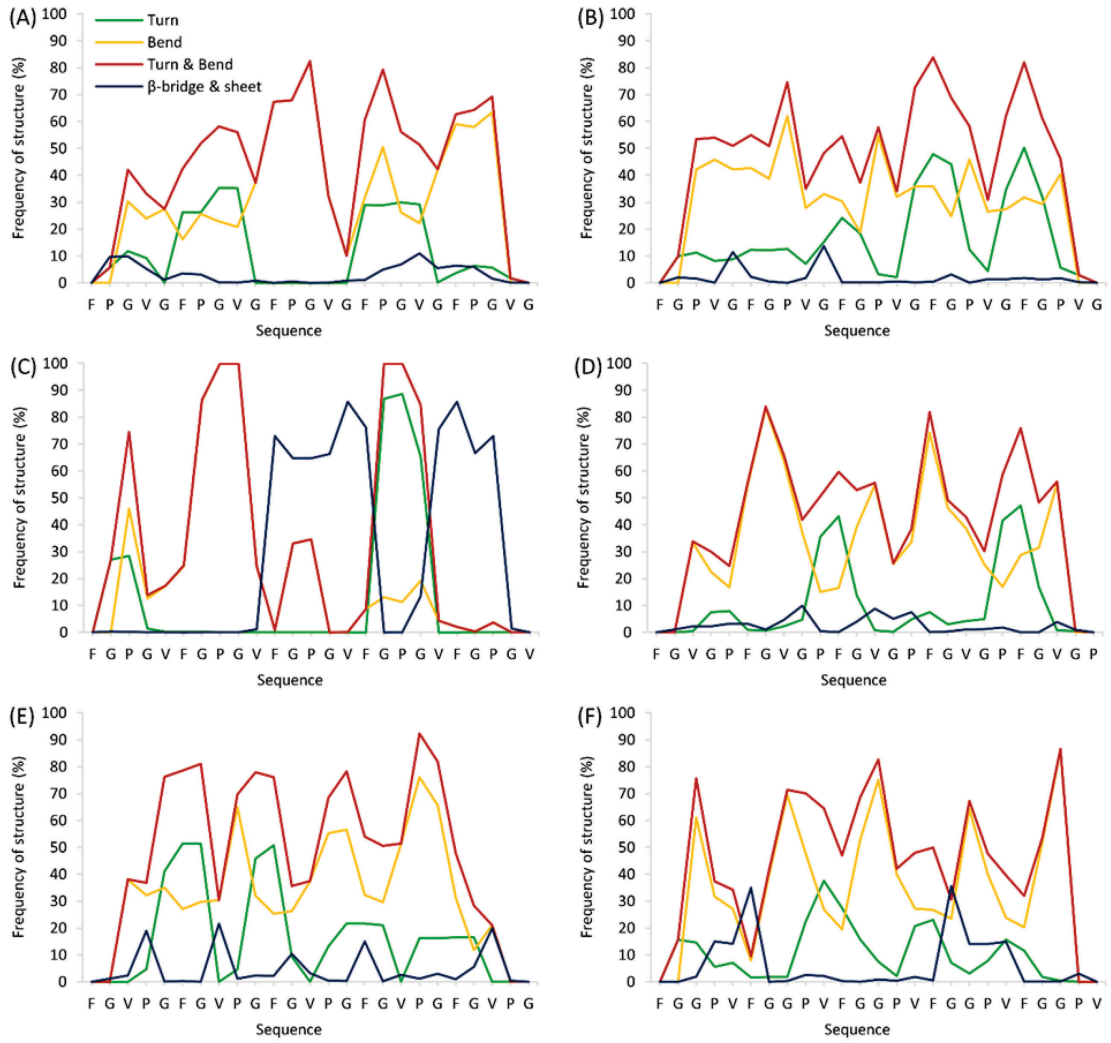

Figure 8. Ratios of secondary structures at each residue in whole peptide sequence at 343 K. The data in (A) peptide A, (B) peptide B, (C) peptide C, (D) peptide D, (E) peptide E, (F) peptide F, (G) peptide G, (H) peptide H, (I) peptide I, (J) peptide J, (K) peptide K, and (L) peptide L were shown. Each ratio was calculated by dividing the number of secondary structure at each residue in whole of trajectory by the number of trajectory frame.

Continued

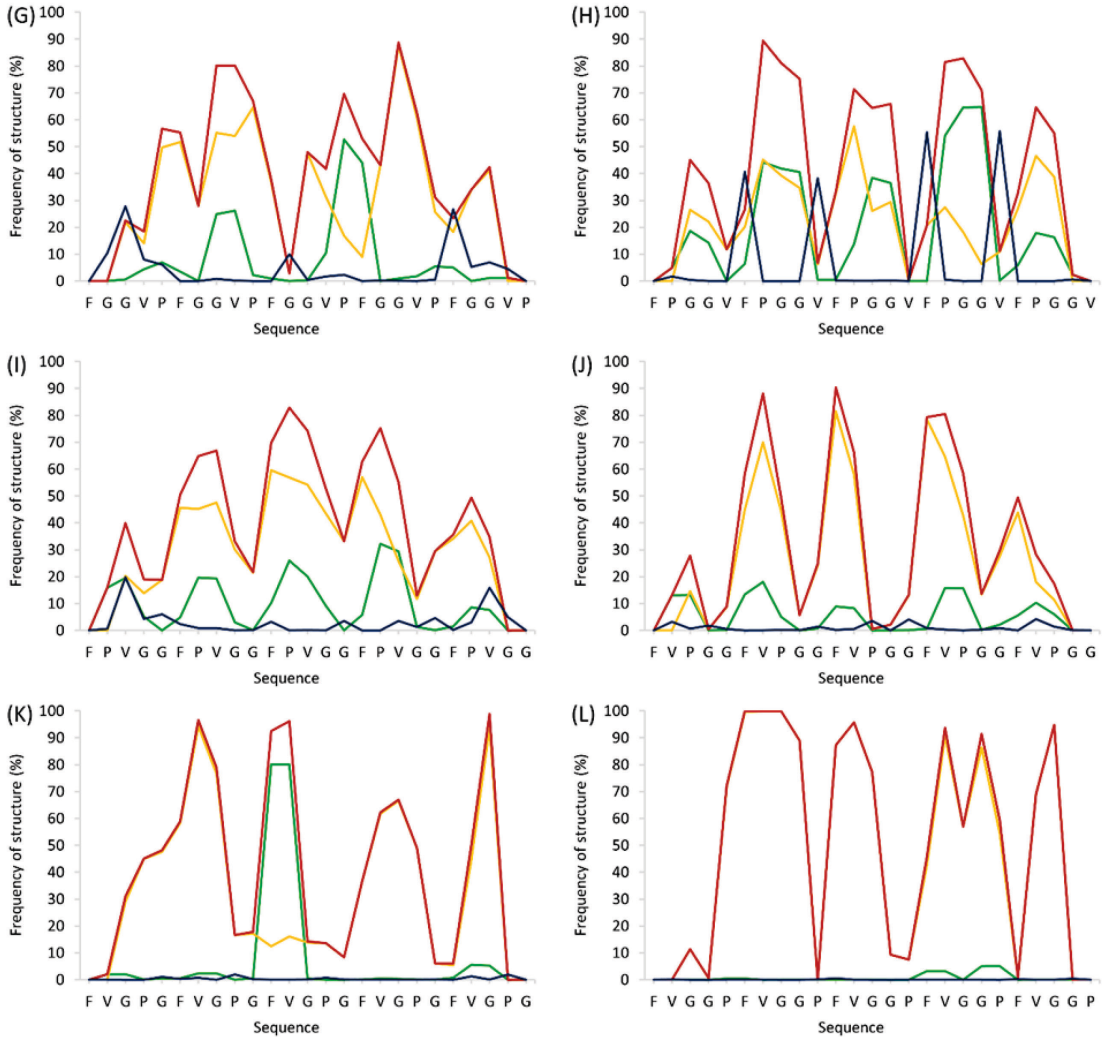
(G)
(H)
(I)
(J)
(K)
(L)
Frequency of structure (%)
Sequence
F G G V P F G G V P F G G V P F G G V P
F P G G V F P G G V F P G G V F P G G V
F P V G G F P V G G F P V G G F P V G G
F V P G G F V P G G F V P G G F V P G G
F V G P G F V G P G F V G P G F V G P G
F V G G P F V G G P F V G G P F V G G P

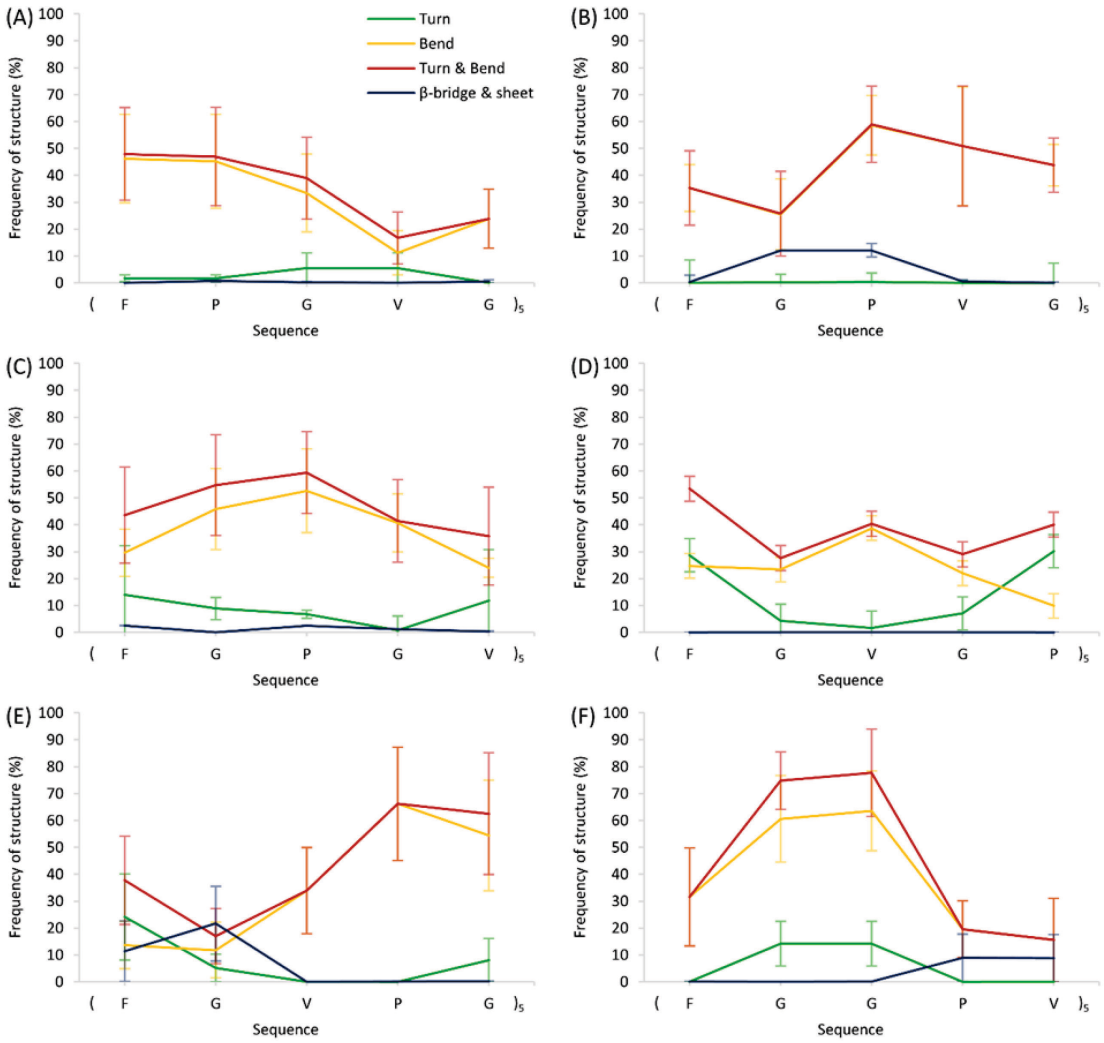

Figure 9. Mean ratios of secondary structure at each residue in repetition at 278 K. The data in (A) peptide A, (B) peptide B, (C) peptide C, (D) peptide D, (E) peptide E, (F) peptide F, (G) peptide G, (H) peptide H, (I) peptide I, (J) peptide J, (K) peptide K, and (L) peptide L were shown. The mean was calculated with SE by averaging the ratio of secondary structure at five residues which periodically appeared at each position (1st - 5th) in the repetitive unit.

Continued

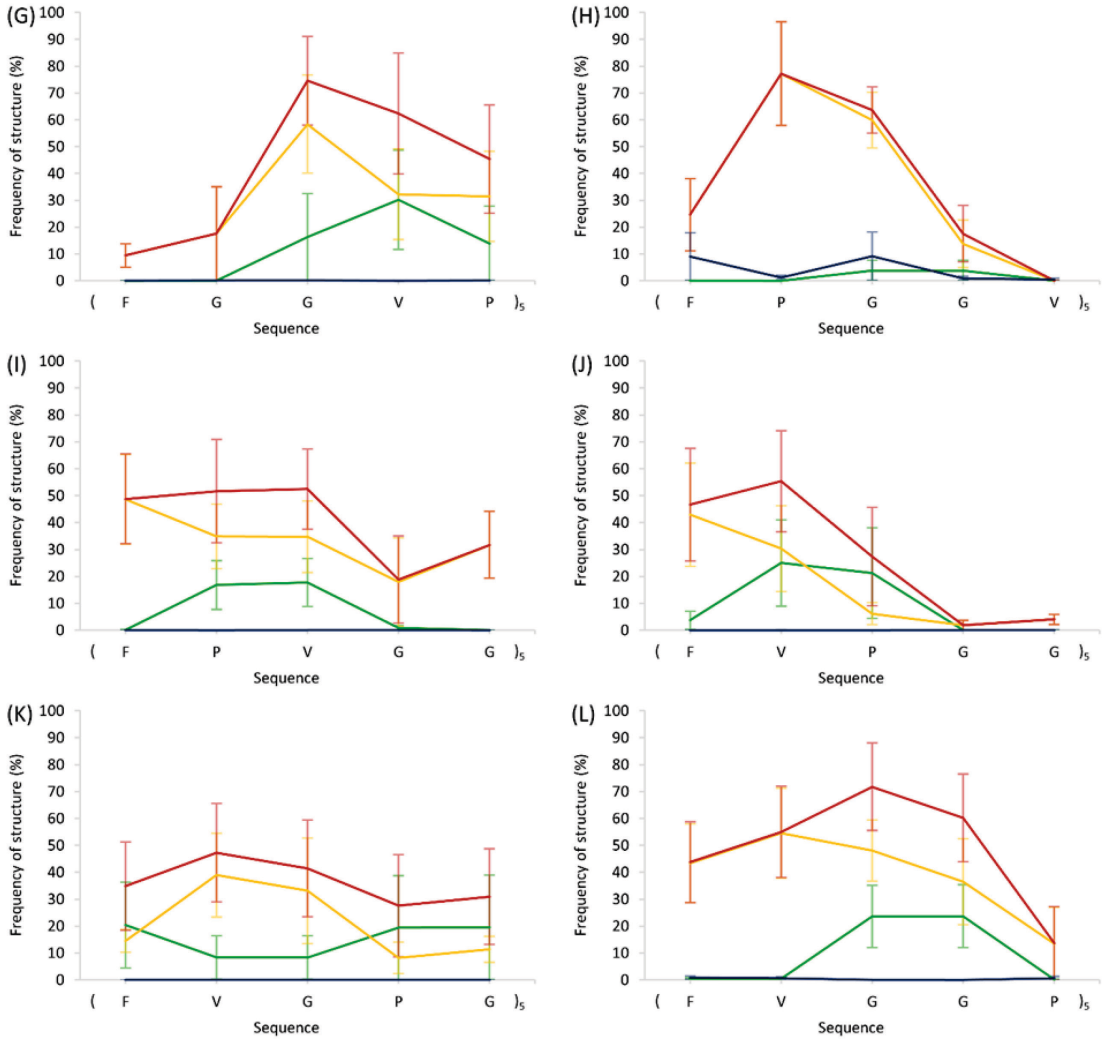
(G)
(H)
(I)
(J)
(K)
(L)
Frequency of structure (%)
Sequence
(F G G V P)5
(F P G G V)5
(F P V G G)5
(F V P G G)5
(F V G P G)5
(F V G G P)5

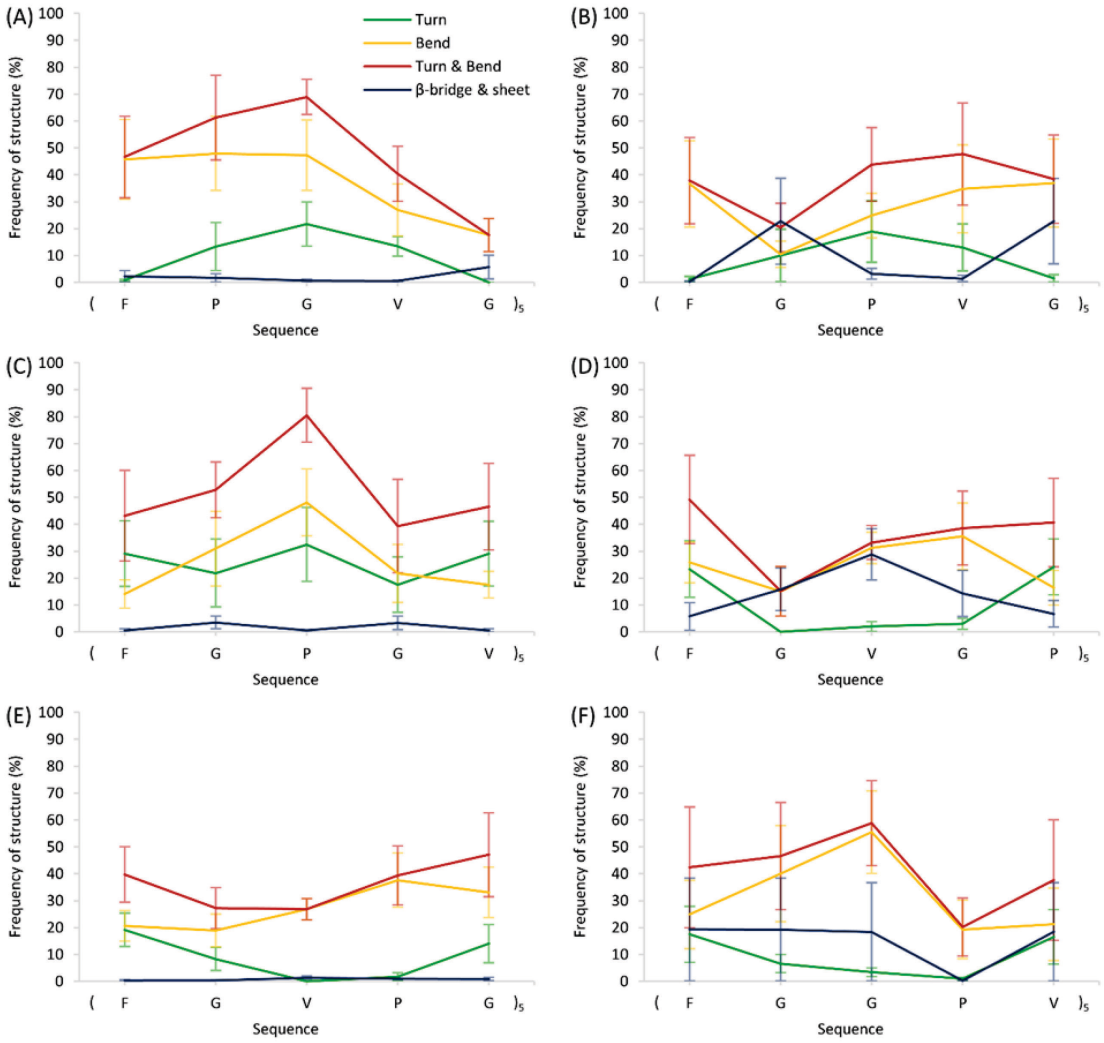

Figure 10. Mean ratios of secondary structure at each residue in repetition at 310 K. The data in (A) peptide A, (B) peptide B, (C) peptide C, (D) peptide D, (E) peptide E, (F) peptide F, (G) peptide G, (H) peptide H, (I) peptide I, (J) peptide J, (K) peptide K, and (L) peptide L were shown. The mean was calculated with SE by averaging the ratio of secondary structure at five residues which periodically appeared at each position (1st - 5th) in the repetitive unit.

Continued

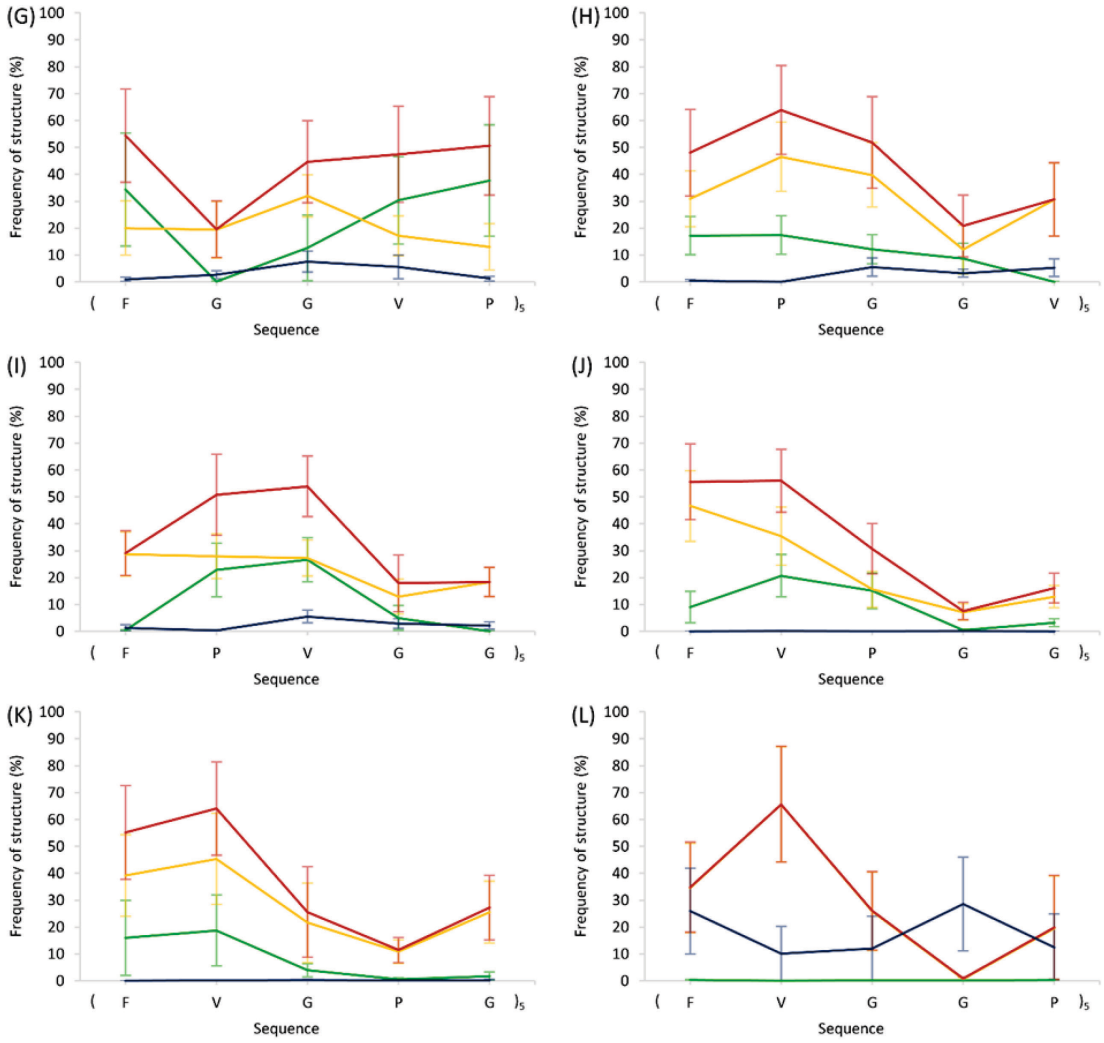
(G)
(H)
(I)
(J)
(K)
(L)
Frequency of structure (%)
Sequence
(F G G V P)5
(F P G G V)5
(F P V G G)5
(F V P G G)5
(F V G P G)5
(F V G G P)5

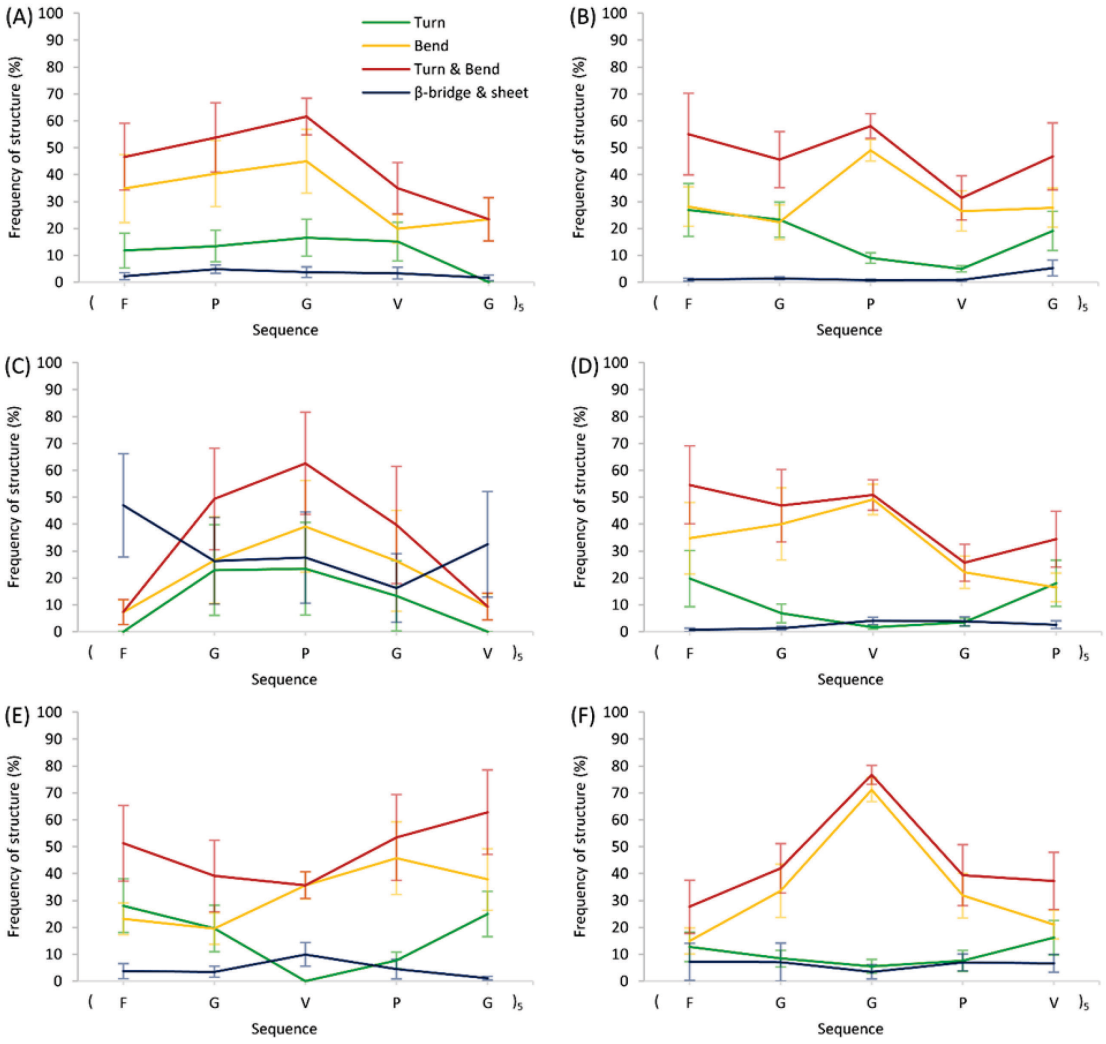

Figure 11. Mean ratios of secondary structure at each residue in repetition at 343 K. The data in (A) peptide A, (B) peptide B, (C) peptide C, (D) peptide D, (E) peptide E, (F) peptide F, (G) peptide G, (H) peptide H, (I) peptide I, (J) peptide J, (K) peptide K, and (L) peptide L were shown. The mean was calculated with SE by averaging the ratio of secondary structure at five residues which periodically appeared at each position (1st - 5th) in the repetitive unit.

Continued

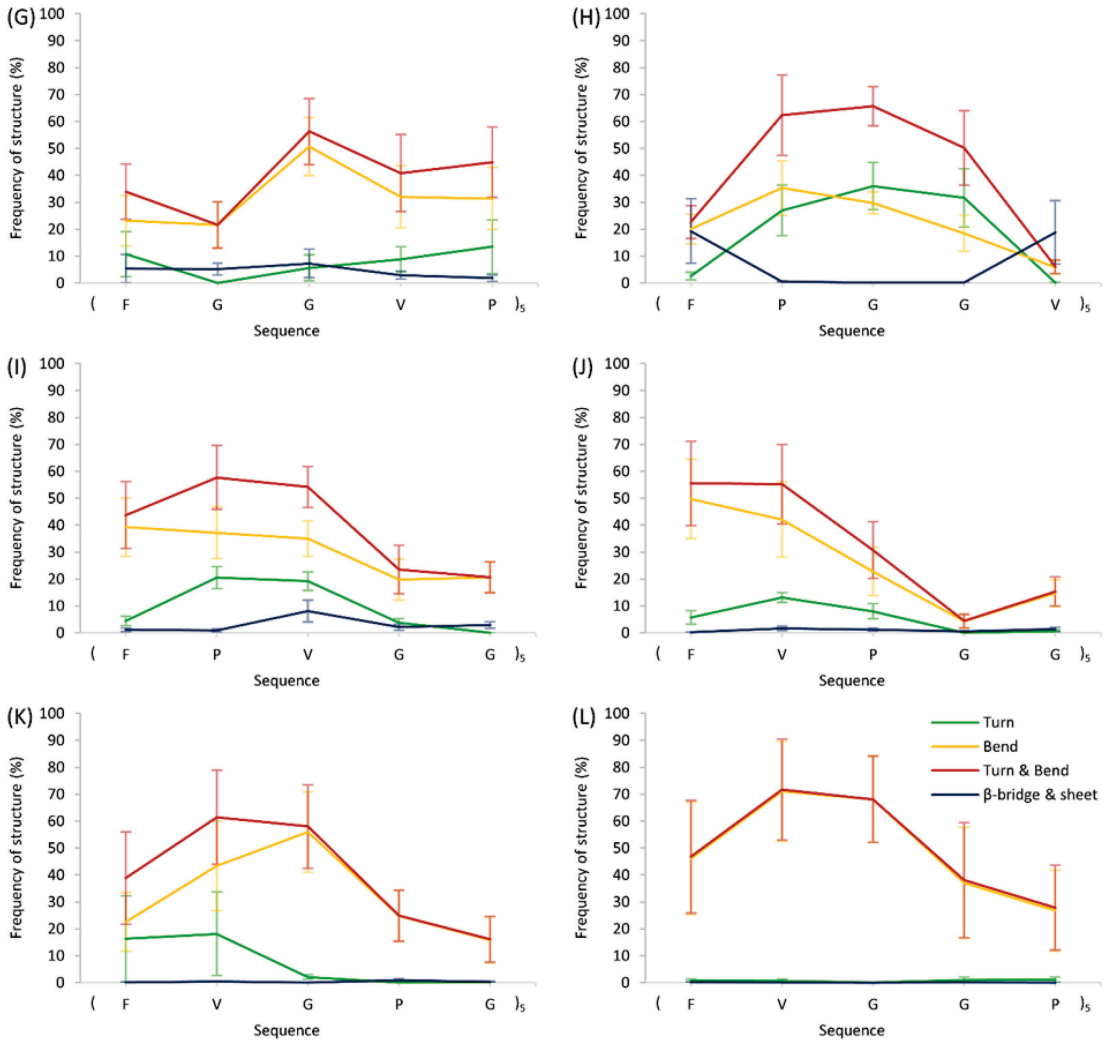
(G)
(H)
(I)
(J)
(K)
(L)
Frequency of structure (%)
Sequence
(F G V P)5
(F P G G V)5
(F P V G G)5
(F V P G G)5
(F V G P G)5
(F V G G P)5
Turn
Bend
Turn & Bend
β-bridge & sheet

Acknowledgements

The author, Daiki Tatsubo wishes to express his most sincere thanks to Professor Takeru Nose, Kyushu University, for his supervision with invaluable suggestion and insightful discussion throughout this work. The author is one of those who have felt his vivific influence as a member of the Laboratory of Biomolecular chemistry of Kyushu University.

The author is sincerely grateful to Assistant Professor Suyama Keitaro, Kyushu University, for his excellent research assistance throughout the study. In particular the author would like to express his special thanks to Dr. Suyama for his teaching of various experimental methods and techniques. The author is greatly thankful to Assistant Professor Keisuke Tomohara, Kyushu University, for his excellent suggestion. The author is also grateful to Dr. Iori maeda, Kyushu Institute of Technology, for her advice and encouragements.

The author is very thankful to Dr. Masaya Miyazaki and Dr. Wataru Iwasaki of National Institute of Advanced Industrial Science and Technology (AIST) for teaching the ways to perform the DLS measurement. His sincere thanks also goes to Associate Professor Ayami Matsushima and Assistant Professor Xiaohui Liu, Kyushu University, for their precious help in CD measurement. The author is sincerely grateful to Dr. Suguru Taniguchi for his benign support in turbidity measurement and MALDI-TOF MS. The author wishes to express his sincere thanks to Mr. Keiji Sato and Ms. Misako Kodama for his and her assistances in synthesis and analysis of peptide analogs

Finally, the author greatly appreciates to all of colleagues of the laboratory, Mr. Hitoshi Kesamaru, Mr. Shuhei Kaneko, Mr. Takashi Okubo, Ms. Mika Mawatari, Mr. Kazumi Kasatani, Mr. Naoki Sakamoto, Ms. Haruka Kuriki, and Mr. Shogo Sumiyoshi, for their assist, cooperation, and heart-warming encouragements.